# Investigation of two respiratory monitoring systems used for 4D CT and respiratory gating

Joanne McNamara
University of Wollongong

# INVESTIGATION OF TWO RESPIRATORY MONITORING SYSTEMS USED FOR 4D CT AND RESPIRATORY GATING

**JOANNE MCNAMARA**
BCA BSc

A thesis submitted in partial fulfilment of the
requirements for the award of the degree of

## MASTER OF SCIENCE

**By Research**

**from**

## UNIVERSITY OF WOLLONGONG

## FACULTY OF ENGINEERING

**March 2008**

## CERTIFICATION

I, Joanne L. McNamara, declare that this thesis, submitted in partial fulfilment of the requirements for the award of Master of Science by Research, in the faculty of Engineering, University of Wollongong, is wholly my own work unless otherwise referenced or acknowledged. The document has not been submitted for qualifications at any other academic institution.

Signed.....

Date.....

**ACKNOWLEDGEMENTS**

Thank you to my supervisor, Professor Peter Metcalfe, for all his help and invaluable advice. To the staff at the Illawarra Cancer Care Centre, who so generously gave up their time and resources to assist in the project; I am very grateful. Special thanks to Dr. Matthew Williams for taking the time to discuss ideas with me, and to Dr. Martin Carolan, who built the infrared time stamp. Thank you to Professor Anatoly Rosenfeld for his assistance in attending conferences, and to the physics team at the Austin for their encouragement. I appreciate the support of my brother, Jon, who was willing to help me with data entry and thank my family, and my partner, Sam, for always reminding me of what is most important.

**CONTENTS**

## LIST OF TABLES

## LIST OF FIGURES

## ABSTRACT

Respiratory gating enables breathing synchronised activation of CT image acquisition and linear accelerator radiation output. Two commercially available respiratory gating systems used for planning and treatment of thoracic and abdominal cancer are investigated. The strain gauged AZ-733V respiratory gating system (Anzai Medical Systems, Tokyo, Japan) was used concurrently with the infrared Real-time Position Management system (Varian Medical Systems, Palo Alto, CA) to measure the respiratory cycle of 15 volunteers. Correlation between systems was measured in six locations and the optimum position of the external surrogates determined based on signal amplitude, reproducibility of breathing waveforms and the coefficient of determination between Anzai and RPM signals. The mean value of $R^2$ between the two systems was found to be 0.611, 0.788 and 0.925 when both markers were positioned at the xiphoid, midway between the xiphoid process and umbilicus, and at the umbilicus respectively. When positioned in separate locations results were varied, $R^2$ values ranging from 0.345-0.965. Results highlighted the importance of external surrogate position to the respiratory signal obtained, and indicated that the external marker position on the chest wall needs to be reproducible between 4D CT scanning and treatment. Recommendations are made that external surrogates must always be positioned at the umbilicus for the most clinically useful scans.

Image distortion and artifacts were studied using the Anzai AZ-733V respiratory gating system in combination with the Siemens Sensation Open CT scanner. A moving respiratory phantom was constructed and the volumetric accuracy of retrospectively reconstructed 4D CT images for three moving test objects, across five frequencies and four amplitudes of movement was compared. Volumetric accuracy was found to be within 10% for retrospectively reconstructed gated objects moving with a period of 4 s, amplitude 1 cm. Large deviations of 19.4-51.6% from the static volume of the objects were observed in gated images for periods of 3 s or less. Significant distortion and under sampling was observed in gated images of the objects moving with a period of 10 s. Artifacts were related to the partial projection effect and data sufficiency conditions outlined in literature (Keall 2004, Pan 2004, Dinkel 2007).

## GLOSSARY AND ABBREVIATIONS

*3DCRT:* Three-dimensional conformal radiation therapy

*4D CT:* Four-dimensional computed tomography

*ABC:* Active Breathing Control

*ACPSEM:* Australasian College of Physical Scientists and Engineers in Medicine

*AP:* Anterior-Posterior

*CCD:* Charge coupled device

*CTV:* Clinical Target Volume

*DIBH:* Deep Inspiration Breath Hold

*DICOM*: Digital Imaging and Communications in Medicine.

*DRR:* Digitally Reconstructed Radiograph

*Duty cycle:* Ratio of the beam on time to the total treatment time.

*EPID:* Electronic Portal Imaging Device

*EOE:* End of Exhale

*EOI*: End of Inhale

*External surrogate:* Traceable reference point exterior to the patient

*Exhalation:* Resting expiratory level (Keall 2006)

*Fiducials:* Reference points located within the patient

*Gating window*: Range of the surrogate signal to which image acquisition or treatment is restricted.

*GTV*: Gross Tumour Volume

*Hysteresis*: The lagging of an effect behind its cause

*ICCC*: Illawarra Cancer Care Centre

*Interfraction motion*: Motion which occurs between fractions

*Intrafraction motion*: Motion which occurs during a fraction (treatment session).

*IGRT:* Image-guided radiation therapy

*IMRT*: Intensity Modulated Radiation Therapy

*MLC:* Multi-leaf collimator

*Phase sorting:* The phase angle specifies a percentage of the period of the breathing cycle

*Pitch:* The ratio of distance that the table moves during one complete rotation of the x-ray tube to slice thickness.

*PTV:* Planning Target Volume

*Prospective 4DCT gating:* Data acquisition is triggered by events in the respiratory signal

*Range of motion:* Displacement between inhalation and exhalation (Keall 2006)

*Respiratory gated:* The synchronisation of image acquisition and treatment with respiration such that the image is acquired/radiation delivered only during a specified portion of the breathing cycle (Keall 2006).

*Retrospective 4DCT gating:* CT and respiratory signal are acquired simultaneously. Post scan, CT images are sorted into respiratory phases based on phase or amplitude of the respiratory trace.

*RPM system:* Real-time Position Management respiratory gating system (Varian Medical Systems, Palo Alto, Ca)

*rpm:* Respirations per minute

*SI:* Superior-Inferior

*Spirometer:* A device measuring the volume of air entering and leaving the lungs.

*Tumour residual motion:* Tumour motion when the surrogate signal is in the gating window.

## PREFACE

This thesis compares the waveforms obtained from two different respiratory gating systems, the Anzai AZ-733V and the Real-time Position Management (RPM) infrared marker system. The primary aim was to determine if the two respiratory gating systems can be used interchangeably for radiotherapy planning and treatment. The design required observation and quantification of variations in signal ascribed to difference in monitoring methods or sensor placement.

The secondary aim of this thesis was to observe and quantify artifacts in 4D CT images and to determine if a relationship exists between severity of artifacts in 4D CT, duration of breathing cycle, and amplitude of tumour movement. The intention was to make recommendations, based on findings and literature, for optimum 4D CT respiratory gating parameters to be adhered to during 4D CT patient scans.

Chapter One contains a literature review. Issues associated with respiratory gating both in 4D CT and dose delivery, and previous work that has been reported which addresses these issues is summarised. The principles of 4D CT and the implications of gated CT acquisition on treatment planning are outlined. Artifacts in 4D CT and their cause are considered. Chapter one also describes the two respiratory gating systems to be used in this work; the Anzai AZ-733V respiratory gating system and the RPM system.

Chapter Two focuses on the measurement of respiration by two commercially available respiratory gating systems utilising external surrogates. Method and experimental set-up for the comparison of respiratory waveforms obtained from the Anzai AZ-733V system, consisting of a belt with a strain gauge, and an infrared camera-based motion-tracking system (RPM), is provided. The respiratory waveforms recorded simultaneously by the RPM and Anzai systems for a cohort of 15 staff volunteers are compared. For each volunteer, six anatomic marker locations are studied. The coefficient of determination between the two systems in each case is determined. Results are both tabulated and presented graphically. The external marker positioning has an impact on the respiratory signal obtained by the external surrogate. The influence of this was made apparent and the implications to radiotherapy planning and treatment are discussed.

In Chapter Three, artifacts are explored in 4D CT images. The Anzai AZ-733V respiratory gating system is coupled with the Siemens Sensation Open CT scanner and the accuracy of reconstructed images of a commercially available moving respiratory phantom (Anzai) assessed. An in-house respiratory phantom capable of variable frequency and amplitude of movement was constructed. Results compare volumetric accuracy of retrospectively reconstructed 4D CT images for three moving test objects, across five frequencies and four amplitudes of movement. Distortions in 4D CT images are related to the partial projection effect and data sufficiency conditions determined by scan parameters. Chapter four provides a conclusion and possibilities for future work in respiratory gating.

This work has been presented in part at the following conferences/ meetings:

McNamara, J., Metcalfe, P., Williams, M. "Comparison of two radiotherapy respiratory gating devices**" Engineering and Physical Sciences in Medicine and The Australian Biomedical Engineering Conference 2007**, Fremantle, Western Australia, 14-18 October 2007 (Abstract) *Aust. Phys. Eng. Sci. Med*. 30 (4) 373

McNamara, J., Metcalfe, P., Williams, M. "Comparison of two radiotherapy respiratory gating devices" Austin Health, Melbourne, 12th October 2007

McNamara, J., Metcalfe, P., Williams, M. "Comparison of two radiotherapy respiratory gating devices" **Vic/Tas branch of the ACPSEM Annual General Meeting**, Peter MacCallum Cancer Centre, Melbourne, 3rd December 2007 *Awarded Best Postgraduate Speaker*

Experiments were performed at the Illawarra Cancer Care Centre and results should be translatable to other centres using the combined system i.e. Anzai AZ-733V respiratory gating system with Siemens 4D CT and Real-time Position Management system coupled with Varian linear accelerators. As such two papers are in preparation for

submission to journals. These include one paper dealing with the comparison of the two gating systems and another paper outlining findings from the artifact study.

# CHAPTER 1

# LITERATURE REVIEW

## 1.1 Introduction

Lung cancer is the most common cause of death by cancer in Australia (www.abs.gov.au 2004). Only 12% of people with lung cancer in Australia will live 5 years after diagnosis (www.cancer.org.au 2005). Optimum targeting of lung tumours in radiotherapy has been hindered due to respiratory motion; lung tumours have been reported to move up to 5 cm (Li et al 2006, Keall et al 2006, Ramsey et al 1999). Large margins are necessary in the planning treatment volume to cover the limits of tumour motion. These limits include excess normal tissue, which causes increased risk to normal tissue and a reduction in prescribed dose (Yorke et al 2005). During radiation delivery, it is suggested breathing leads to a spreading out of the dose distribution, which results in a deviation between the intended dose and the dose delivered (Li et al 2006). Methods which specifically account for respiratory motion include breath holds (Hadley et al 1999, Nelson et al 2005), breathing synchronised planning and delivery (Borgert et al 2006) and respiratory gating. Gated scans allow selected portions of the breathing waveform to be reconstructed, between specified time intervals, or specified amplitudes. Gated delivery only treats in a specified portion of the breathing cycle, thus reducing tumour movement when the beam is on. Gating is optimal at the present time as not all patients can maintain a breath hold for a useful length of time (Vedam 2001) and accurate tracking systems rely on exact positioning of the target through advanced tumour motion prediction models which are currently still in development (Borgert et al 2006, Hoisak et al 2006, Timinger et al 2005).

Real time knowledge of the tumour position is necessary for all methods accounting for tumour motion (Lu et al 2006). Respiration monitoring techniques include internal-fiducial based methods, (Imura et al 2003, Seppenwoolde et al 2002, Rietzel et al 2004) and external surrogate-based methods. Internal-fiducial-based methods have the advantage of directly measuring tumour position by fluoroscopic imaging however

internal gating is challenging with lung tumours due to the risk of pneumothorax during the implantation of internal fiducials in the lung (Jiang et al 2006). Fixation of markers in the bronchial tree also poses problems due to the relationship between the markers and the tumour shifting over time (Beddar et al 2007, Imura et al 2005). External surrogates rely on the correlation between internal organ motion and an external marker such as a strain gauge (Li et al 2006) video camera, (Vedam et al 2003) or air flow (Hoisak et al 2006, Stepaniak et al 2005, Riedel 2006). Two external respiratory gating methods will be investigated in this thesis, a strain gauge, the AZ-733V respiratory gating system (Anzai Medical Systems, Japan) and the Real-time Position Management (RPM) system (Varian Medical Systems, Palo Alto, CA) which utilises a video camera and infrared markers placed on the patient's chest.

### 1.2 Motivation for this work

Due to the movement of lung and abdominal tumours with respiration, respiration-gated radiotherapy has potential to reduce the clinical target volume and the planned target volume (CTV and PTV). The extent of tumour movement over one respiratory cycle can be assessed for each patient and treatment margins applied appropriately. The Illawarra Cancer Care Centre (ICCC) is currently the only clinic in Australia to possess the AZ-733V respiratory gating system. This system, coupled with the Siemens Sensation Open 20 slice CT, will be used for treatment planning. Due to the relative "newness" of gated helical CT acquisition and the Anzai system there are still problems associated with imaging moving objects, even when gating is applied. An investigation into the origin of artifacts produced by gating, and the extent of any deformities will be performed. The accuracy of imaging a moving volume with and without gating will be assessed.

Radiation therapy departments are often multi-vendor environments. At ICCC there is a Siemens CT, a Varian Linac and a Philips Pinnacle Radiation Therapy planning system. A separate gating system, the Real-time Position Management system (RPM), is to be coupled with the Varian linear accelerator in the Wollongong clinic. It is often the role of the Radiation Oncology Medical Physicist to marry up these vendor systems so the patient can be successfully treated. To ensure accurate dose delivery, it is paramount that gated planning with the Anzai system corresponds to the same gated treatment on

the Varian RPM system. Hence a comparison of the two systems and the reproducibility of respiratory waveforms between patients must be performed.

### 1.3 Four-Dimensional Computed Tomography (4D CT)

The image quality of conventional 3D computed tomography of the abdomen and thoracic region is degraded by respiratory motion. Severe motion artifacts can occur as a result of the interplay effects between the advancing scan plane and object motion (Rietzel et al 2005). This leads to deformation and displacement of internal organs on the CT images. Four-dimensional computed tomography (4D CT) creates separate CT images at discrete phases of the respiratory cycle, which allows volumetric changes over time to be observed (Lu et al 2006b). 4D CT is produced by over sampled data acquisition at each slice. Such continuous data acquisition can be acquired by scanning in axial cine mode or in helical mode at a very low pitch, where pitch is defined as the ratio of table increment per rotation to slice thickness (Jiang et al 2006). The patient's abdominal surface motion is measured at the same time by the external surrogate e.g. strain gauge or infrared markers. Projection data is acquired over the duration of the patient's respiratory cycle plus the duration of one full gantry rotation. Multiple images are then reconstructed per slice and evenly distributed over the acquisition time (Rietzel et al 2005). Each of the images collected represent a different anatomical state during the breathing cycle. To obtain CT volumes at different states of the breathing cycle, reconstructed images are sorted into spatio-temporally coherent volumes based on respiratory phase as found by the external surface marker (Rietzel et al 2005). While binning, phase tolerances are chosen to obtain complete volumetric reconstruction. 4D CT thus helps reduce motion artifacts and blurring and aids in better delineating target structures. Underberg et al (2004) demonstrated that 4D CT accounts for motion caused by respiration better than the average of six conventional computed tomography scans.

## 1.4 Artifacts in Computed Tomography

An artifact is any distortion or error in an image that is unrelated to the subject being studied (Luo 1999). For CT, artifacts are any discrepancy between the CT numbers present in the image and the CT numbers expected based on the linear attenuation coefficient of the material. Motion causes artifacts that blur target location and limit the ability to precisely delineate the region of interest (Wink et al 2005, Rietzel et al 2005, Allen et al 2004, Wilting et al 1999). Although motion artifacts are somewhat reduced in 4D CT, they are still present. Each phase of retrospective re-binning 4D CT is a snapshot of regular respiration and is subject to artifacts due to an irregular breathing pattern or incorrect phase determination (Lu et al 2006b). Pan et al (2005) investigated artifacts caused by phantom movement, using 2 cm amplitude of movement, 2.5 mm slice, a gantry rotation time of 0.8 s and a reconstruction interval of 0.15 s. They found that of the eight phases chosen for registration (using the RPM system) the spheres were better registered at 0% and 50% of the entire breathing cycle where sinusoidal motion was the least. It was also noted by Pan et al (2005) that the larger sphere measured (5.5 cm diameter) was more preserved in shape than the smaller sphere (1.5 cm diameter). This was attributed to the partial volume effect of using 2.5 mm slice thickness which has a greater impact on the smaller sphere. Pan et al hypothesised that the helical artifacts produced are similar to those produced with un-gated studies in helical mode with a pitch of 1.3, and that the distortion is a function of time when the scan intersects the phantom.

Rietzel et al (2005) observed the same artifacts when moving a sphere in and out of the imaging plane (refer to figure 1.1). Rietzel et al (2005) attributed the variation in cross section of the spheres to the partial projection effect. CT projection data are a measure of the integral absorption across fan beam lines during data acquisition for all angles. The sphere moves in and out of the imaging plane as the tube rotates therefore the cross-section of the phantom in the beam varies as the tube rotates. Rietzel et al explains that as the reconstruction algorithm redistributes densities based on line projections, this results in an angular dependency of the reconstructed densities. This is more pronounced at the end of the sphere as the cross-section in the imaging plane changes more rapidly. Volumetric differences were also found to be more pronounced at higher velocities.

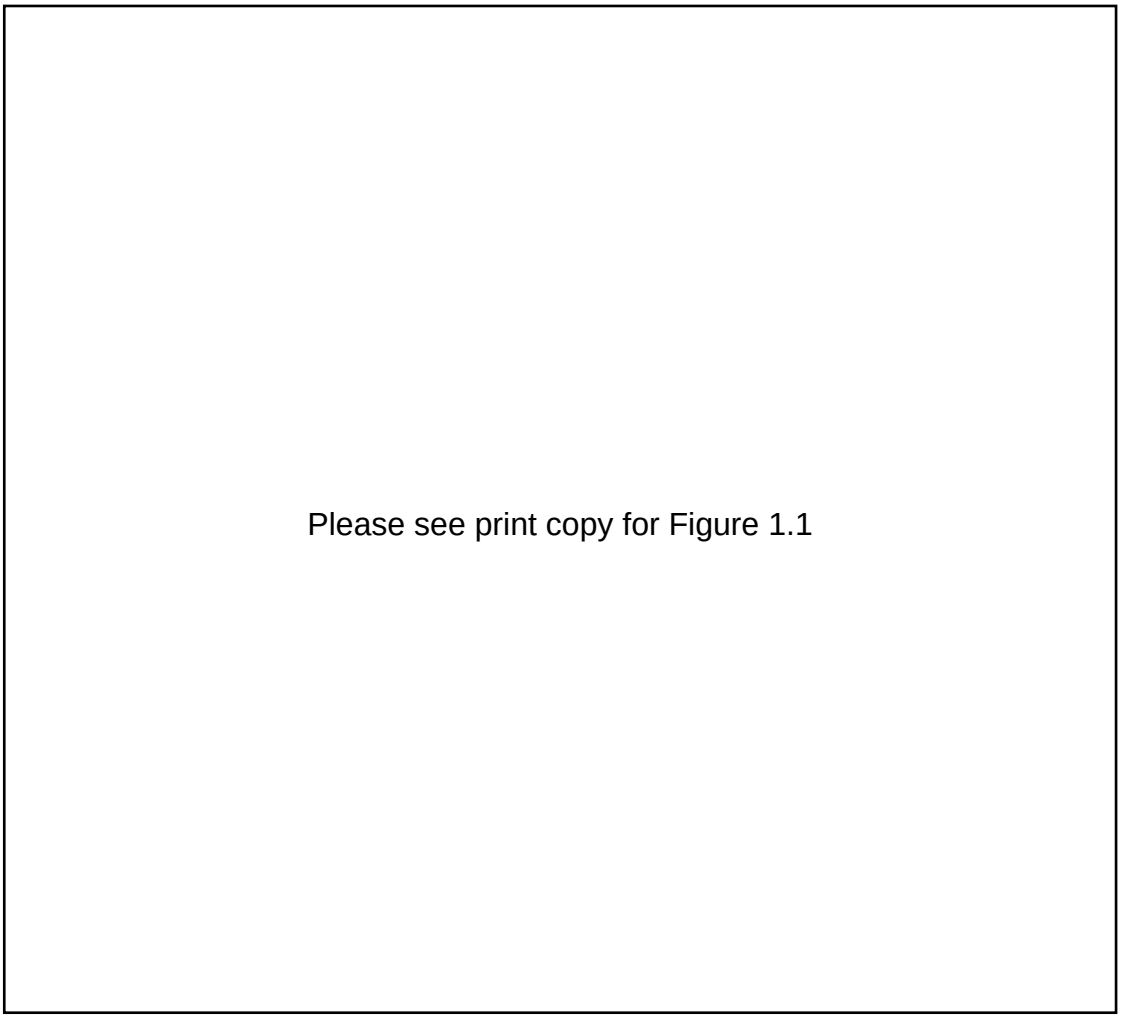


Figure 1.1 Axial slices of a spherical object (radius 3.2 cm) 4D CT scanned while periodically moving parallel to couch movement. Image reconstruction averages over a full rotation (0.8 s) resulting in spiral images of a spherical object with decreasing reconstructed density from inside to outside (Rietzel et al 2005).

Wink et al (2005) also investigated the effect of scanning parameters such as gantry rotation and scanning speed on image quality. Similarly it was found that distortion increased with decreasing object size.

For helical scanning, it has been found that gaps in the image set occur when the detector rows move past the phantom before an entire respiratory cycle plus one fan angle is complete (Wink et al 2005). Keall et al (2004) suggests that this can be avoided by ensuring that the gantry rotation time multiplied by the inverse of the pitch plus the fan angle per 360 degrees is greater to or equal to the breathing period.

$$\text{Gantry rotation time}\left(\frac{1}{pitch}+\frac{fan\_angle}{360^{o}}\right)\geq\text{Breathing period} \qquad (1.0)$$

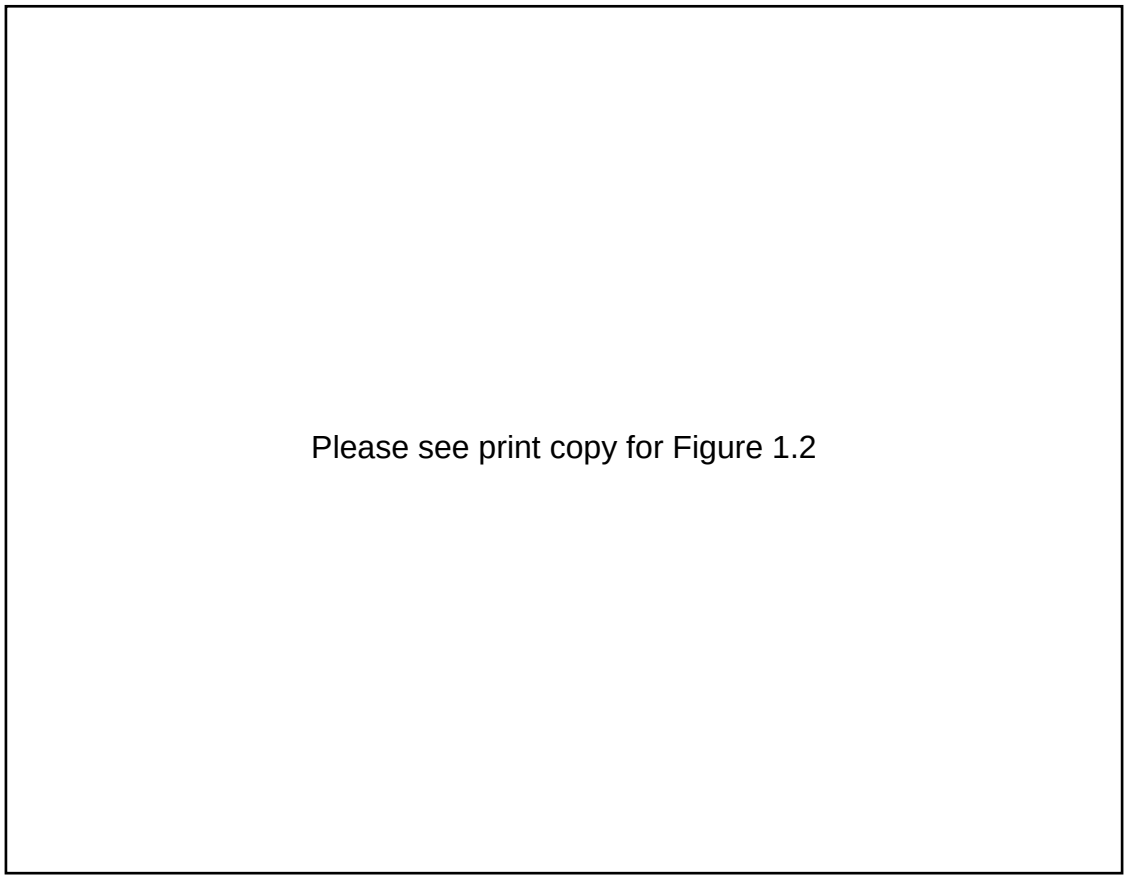


Figure 1.2: Scanning trajectories of (a) helical and (b) cine 4D-CTs for a breathing cycle of 4 s (Pan 2004). Note that to scan one breathing cycle in helical mode the scan will take 8.3 s but for cine only 4.3 s. Each solid trajectory line corresponds to the centre of the detector. (c) is an interpolation of the helical data around point 2 in (a). The parallel dotted lines show the outside of the detectors. Data point 1 will be interpolated from the data of the 1$^{st}$ detector by (1-a) and the 2$^{nd}$ by a. Similarly, data point 3 is interpolated from the data of the second detector as b and the third detector as (1-b).

Pan (2004) also introduced a data sufficiency condition such that a 4D CT acquisition has to collect data at each location for the duration of a breathing cycle plus the duration of data acquisition for an image reconstruction. The duration of data acquisition for an image reconstruction is one gantry rotation cycle if using a full-scan reconstruction or 2/3 gantry rotation if using the half-scan reconstruction. This is to ensure there are images covering the entire breathing cycle (refer to figure 1.2). In figure 1.2, both cine and helical scans will provide 4D CT images in the range $z_1$-$z_2$ however the helical scan switches on the x-ray earlier and switches off later than the cine scan. The shaded area in figure 1.2 is the possible image reconstruction where all phases of respiration are available. Each image is time-stamped with the average acquisition time which is used to register the images with the respiratory signal. Cine images are reconstructed from data in a single respiratory cycle however helical images can be obtained from a number

of breathing cycles. In figure 1.2 (a) it can be seen that the images at 3 s and 7 s correspond to the same phase in a breathing cycle of 4 s duration. Images in segment 1 overlap in the z location with images in segment 2. Either of the two images in the same z location could be chosen, or an average of the two images can be taken to produce a single z image (Pan 2004).

Wink et al (2005) demonstrated that the spatial resolution of a gated scan at 0.15 pitch with 1 second rotation time are equivalent to non-gated scans of objects in motion (3.96 mm vs. 3.95 mm) indicating that there is little benefit of gating in regard to resolution if long scan times are used. This is due to the fact that for gated scans of moving objects, a longer rotation will produce more movement per phase bin as more data is used. With a rotation time 0.5 s however, it was found all volume and deformation studies showed improvement in image quality parameters when gating was applied.

### 1.5 Implications of 4D CT on treatment planning

ICRU report 50 defines a set of target volumes to be used for treatment planning. The *gross tumour volume* (GTV) is the malignant tumour that is visible to the eye by palpation or imaging techniques. Lymph nodes with a short axis diameter > 1 cm should be included in the GTV. Surrounding the GTV is a zone in which tumour cells infiltrate, and across which tumour cell density decreases (Williams et al 2000). The *clinical target volume* (CTV) includes the GTV plus a margin to account for the microscopic spread of tumour. Regional lymph nodes should also be part of the CTV (Williams et al 2000). The *planning target volume* (PTV) includes the CTV plus an additional margin to account for set up errors and intrafraction organ movement (refer to figure 1.2). The magnitude of these margins must be added in a quadratic combination approach such that

$$IMSM_{combined} = \sqrt{IM^2 + SM^2} \qquad (1.1)$$

(Metcalfe et al 2007). This is due the combination of random and systematic uncertainties these margins are designed to compensate for.

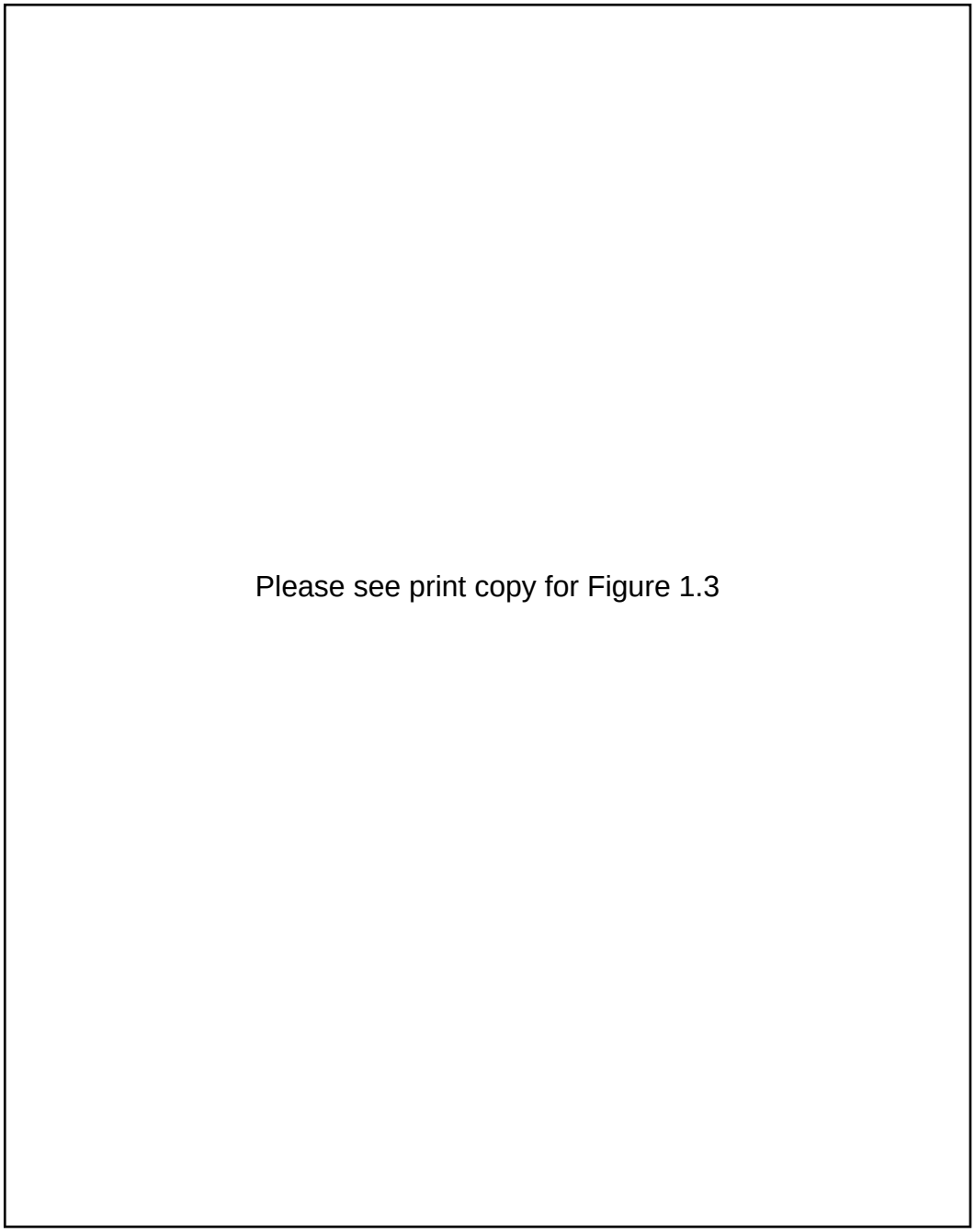


Figure 1.3: Schematic displaying ICRU target volumes and margins (ICRU Report 62, 1999).

For significant respiratory motion, a large PTV may be required to ensure accurate dose to the target (Gierga et al 2005). Tumour control can be improved by increasing the dose however in the case of lung tumours the oesophagus and surrounding healthy lung are dose limiting structures. To enable dose escalation, the volume of the irradiated surrounding healthy tissue should be reduced (Wolthaus et al 2006). One approach to achieving this aim is through reducing the PTV margin. The introduction of 4D CT scanning has made possible a distinction between the internal margin and the set-up

margin, allowing the concept of *internal target volume* (ITV). The ITV represents the volume encompassing the CTV and the internal margin (ICRU 62). The additional spatial and temporal motion information provided by 4D CT could be used to optimise treatment planning, leading to a reduced clinical tumour volume to planning target volume (CTV to PTV) margin and escalated dose (Kanoulas 2007). Wolthaus et al (2006) compared mid-ventilation 4D CT scans to conventional free-breathing CT scans and found that the treatment volume could be reduced up to 50%. Rietzel et al (2006) found that, assuming 4D CT images respiratory motion accurately, internal margins could be reduced from 10.0 mm to 5.0 mm and for the ten patients studied, the PTV could be reduced by 23% on average. Nøttrup et al (2007) warn that reducing planning treatment volume margins due to one planning session is unsafe due to the large variations in fraction baseline which exceed the intrafraction variation in exhale points (up to 10 times). Ionascu et al (2007) suggested an increase in the treatment margin of 5 mm in the AP and SI directions for gated studies using an external surrogate due to the phase shifts and amplitude mismatches introduced between external surrogate motion and internal tumour motion. Daily imaging is suggested for all patients (Nøttrup et al 2007).

### 1.6 The AZ-733V respiratory gating system

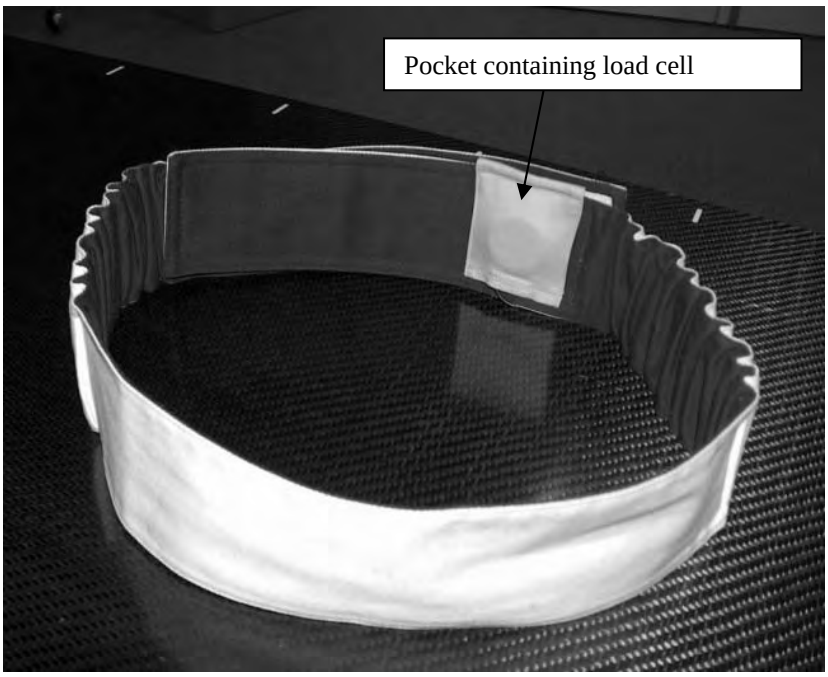


Figure 1.4: The Anzai belt showing pocket with load cell attached.

The AZ-733V by Anzai medical (http://www.anzai-med.co.jp/eigo/az733v.htm.) is a commercially available respiratory gating system. The system consists of an elastic belt containing a load cell as depicted in figure 1.4 (pressure sensor 30 mm in diameter, 9.5 mm thickness). The load cell detects external respiratory motion in real time through changes in abdominal motion at a frequency of 40Hz. The signal from the load cell is amplified and fed into the scanner. As the patient breathes in, the belt tightens and pressure is exerted on the load cell, thus a higher amplitude signal is produced. A decreasing in amplitude of the signal corresponds to the exhalation respiratory phase. The belt is connected to the sensor port which is in turn connected to the wave deck. The system is then run by a notebook computer with the az773v.exe windows program, which offers a graphical user interface for monitoring, processing and recording the signal (Riedel 2006). The system has two modes, sequential and spiral. During the spiral mode, respiratory data is acquired during a whole helical CT scan and stored. The *Syngo* software (Siemens Medical Solutions) is used to perform retrospective gating. Projections are integrated over a 250 ms window starting from a given phase. The AZ-733V recognises the lowest amplitude phase point (0% inhalation) and the highest amplitude phase point (100% inhalation).In-between phases for inhalation are calculated by linear scaling (Kleshneva et al 2006). Similarly the peak of the curve (maximum amplitude) is recognised as 0% exhalation, and the trough, 100% exhalation with phases in-between calculated by linear scaling. The Anzai system offers manual adjustment of both the maximum inhale and maximum exhale points.

The belt is fastened around the patient's waist. It has been suggested that the positioning of the belt in the cranial-caudal direction has a direct correlation to the quality of the signal and that the optimum position of the sensor is 7-8 cm below the end of the xiphoid (Kleshneva et al 2006). Siemens recommends placing the belt just below the diaphragm, but outside of the scan range. If the belt is in the scan range it can cause image artifacts due to small metallic components in the sensor (Bredenholler et al 2006).

In terms of the optimum phase for un-gated treatment, Stepaniak et al (2005) found that the lung volume in a single-phase CT scan within 20-30% of maximum inhale is approximately equal to the average volume of the breathing cycle. The time-averaged tumour position has been reported to be closer to the exhale position (Seppenwoolde

2002). The exhale phase was also found to be more stable by Seppenwoolde et al, although in treatment, shifts in the exhale position were observed to be more prominent both intra and inter-fractionally due to shifts in patient relaxation, gravity(posterior direction) movement and setup errors. Vedam et al (2001) made the point that despite the point of exhale being a more stable portion of the cycle, there was also an increased fraction of lung tissue exposed to higher doses if using maximum exhale for gated treatment. Inspiration provides a larger lung volume which means that the fractional treated lung volume is smaller, and also inspiration can provide a greater separation between the tumour and the critical structures, such as the spinal cord (Hanley et al 1999). Disagreements relating to optimal phase for planning and treatment are yet to be resolved.

There are several approaches to acquiring 4DCT image data sets. The Anzai gating system has two modes, sequential and spiral. In the sequential mode, several CT scans are performed, each of them in a certain phase window. The acquisition process is gated by the synchronisation signal. This mode allows the user to define the gating window width.

In the spiral mode, the image data is acquired through one longer scan which encompasses several respiratory cycles. The data is then sorted and retrospective gating can then be performed using the synchronisation signal (Kleshneva et al 2006). The retrospective gating window width is fixed at 250ms. Similarly the pitch and table speed cannot be changed using this mode. Reconstruction of images in any part of the respiratory cycle is possible hence a complete set of image data throughout the respiratory cycle can be viewed.

### 1.7 Correlation and reproducibility of the respiratory signal.

The external gating methods currently available are dependent upon the exterior skin-surface movement and the anterior-posterior motion being analogous to the internal tumour movement. Several studies have shown that gating based on anterior-posterior motion is not optimal. Koch et al (2004) used magnetic resonance imaging to demonstrate that the best correlation of skin movement with lung vessel motion was in the superior-inferior direction (correlation coefficient of between 0.87 and 0.89)

compared to anterior-posterior (correlation co-efficient between $0.44 \pm 0.27$ for patients and $0.72 \pm 0.23$ for volunteers.) Seppenwoolde et al (2002) found that average tumour movement in the cranial caudal direction was greatest (average amplitude 1.2 cm $\pm$ 0.6 cm) while in the anterior-posterior direction movement for tumours in both upper and lower lung lobes was on average $2 \pm 1$ mm. The important issue in determining if external anterior-posterior gating is suitable is not the amplitude of movement in the direction being measured, rather the correlation of tumour movement and positioning to the signal obtained from this anterior-posterior movement. Several studies (Vedam et al 2003, Yorke et al 2005) have reported that the RPM system correlates reasonably well with diaphragm motion. By using 63 fluoroscopic lung procedures acquired simultaneously with respiratory gated CT images, a linear relationship was discovered. Using model parameters from previous sessions diaphragm motion could be predicted to within 0.1 cm using gated radiotherapy (Vedam et al 2003). Ionascu et al (2007) also found good internal-external correlation along the superior-inferior direction however along the anterior-posterior direction it was found relatively large time shifts (0.4-0.6 s) and amplitude mismatches (2.5-4.7 mm) existed.

The reproducibility of the patient's breathing pattern between CT scanning and day-to-day treatment is also imperative. Studies have shown that respiratory training and visual and audio feedback improves respiratory reproducibility. Jiang et al (2006) utilised audio instructions which tell the patient when to breathe in and out coupled with a visual feedback function which guides the patient to a constant end-of-exhale position and end-of-inhale position by enabling the patient to see their own respiratory waveform in real time. This was found to be more successful than without breath-coaching (Kini et al 2003, Yorke et al 2005, Jiang et al 2006). Problems arose in the study by Jiang et al however as half of 38 patients could not follow audio and visual instructions simultaneously suggesting that although comprehensive, the method is too complicated. The solution proposed was to use amplitude gating, where the variation of the breathing period has no effect on treatment. The patients can then simply be given a visual prompt and asked to place their end-of–exhale position between two lines when breathing out.

The average length of the breathing cycle was found to be between $3.6 \pm 0.8$ s (Seppenwoolde et al (2002), Pan et al 2005) and 4.6 s by Lu et al (2006). Keall et al

(2006) suggested that patients with breathing cycles of over 20 cycles per minute were not suitable candidates for respiratory gating.

Several attempts have been made to relate respiratory signal and tumour motion. The position of the tumour as a function of time *t* can be defined as follows (Seppenwoolde et al 2002, Dietrich et al 2006):

$$s(t) = s_0 - S\cos^{2n}(\pi t/\tau - \phi), \tag{1.2}$$

where $s_o$ is the tumour's position at exhale, S is the amplitude of tumour harmonic movement, $\tau$ is the period of the breathing cycle in seconds, and $\phi$ is the starting phase. The factor n alters the shape of the breathing cycle, with n>1 the time in the exhale phase is greater than the inhale phase. Keall et al (2006) described an equation to express the relationship between respiratory motion as measured by movement of the abdominal wall and tumour motion. The respiratory signal, R, at a time *t* can be related to the tumour motion, T, by:

$$R(t) = I + M[T(t + \Delta\vartheta)] + \varepsilon(t)\ , \tag{1.3}$$

where I is the interfraction internal motion due to anatomic changes, M is the motion of the respiratory signal to the tumour, $\varepsilon$(t) is the error term which ideally should be 0, and $\Delta\vartheta$ is the phase difference (t) between tumour and respiratory signal. The correlation between R and T has been quantified and varying results achieved. Hoisak et al (2004) found a very good correlation (0.99) while others (Tsunashima et at 2004, Mageras et al 2004), discovered phase shifts of up to 1 second. Seppenwoolde et al (2002) also found heartbeat causing measurable tumour motion (1-4 mm LR) in 7 of the 20 patients measured. The distance of the fiducial marker to the cardiac wall was less than 3 cm in these cases. Kleshneva et al (2006) proposed an offline reconstruction algorithm for the determination of respiratory phase to account for the complicated nature of the signal due to heartbeat, patient movement, low signal-to-noise and respiratory irregularities. The use of this algorithm in a clinical setting would allow accurate determination of the phase points necessary for reconstruction of 4DCT without manual editing after scanning.

### 1.8 Real time Position Management system (RPM)

The RPM system (Varian Medical Systems, Palo Alto, CA) uses a CCD camera to detect the motion of external infrared reflecting markers placed on the patient's chest or abdomen. The CCD camera is a collection of light sensitive cells arranged in a 2D array. When light strikes a cell, electron production is proportional to the intensity of light incident on the cell (Wagner 2007). A 2D image is produced with brighter pixels in the array corresponding to higher light intensity, and darker array pixels corresponding to lower light intensity. The digital image can be analysed to select the pixels of highest intensity, (the reflective markers) and these pixels can then be tracked. The markers are illuminated by infrared light emitting diodes and images of the markers are captured by the camera at 30 frames per second (Pan et al 2005). The number of expected pixels per marker is specified. The markers are a calibrated distance apart, thus absolute motion in the plane perpendicular to the camera is obtained (Vedam 2001). The camera output is directed to a PC running the RPM software, a tracking algorithm establishes the period and amplitude and the motion is recorded (Yorke et al 2005). The software detects the peaks of the respiratory traces and assigns relative phases in between by linear interpolation (Rietzel et al 2005). Motion phases are reported in percentage values, 0% corresponds to end-inhalation. 50% does not necessarily correspond to end-exhalation as the breathing cycle is split evenly in time (Beddar 2007). The percentage values differ from the Anzai system which splits inhalation (phases 0% to 100%) and exhalation (phases 0% to 100 %). The RPM system has been investigated in a number of clinics (Beddar et al 2007, Jiang et al 2006, Yorke et al 2005).

### 1.9 Gated dose verification and delivery time.

Respiration during treatment delivery can lead to dosimetric errors of up to 4%, volumetric errors in dose volume histograms of up to 46% and positional errors (Ramsey et al 1999). As patients breathe the amount of dense tissue in the beam path may alter, and this has been found to give path length changes of up to 1.5 cm along the central axis. This can lead to improper beam weightings and monitor unit calculations (Balter et al 1996). This can be rectified with gated delivery. Li et al (2006) measured depth doses and profiles for gated delivery using the Anzai system with duty cycles of

25% and 50% and found them to agree to within 1% of those measured with un-gated delivery indicating that gating did not significantly alter beam characteristics. Measurements also verified MU linearity and beam output to within 0.3%.

Respiratory gating changes the delivery from continuous to periodic, thus increasing the treatment time. The duty cycle is a measure of the treatment efficiency and is defined as the beam on time to the total treatment time (Jiang et al 2006). Non-gated treatment has a duty cycle of 100%. For typical gated treatment the duty cycle can range from 30-50% however for Intensity Modulated Radiation Therapy (IMRT), when using step and shoot, the duty cycle is often less than 30% due to time needed for MLC leaf movement. The larger the duty cycle the larger the tumour residual motion. Jiang et al (2006) emphasise the importance of the gating window (range of the surrogate marker signal which designates beam on time). In external gating, the gating window is defined either by two anterior-posterior positions (amplitude) or 2 phase values of the surface marker. In phase gating the imaging and treatment are triggered when the calculated breathing phase is at a certain angular phase, say 30 degrees inhalation (Vedam 2001). The preferable method is yet to be determined. It is always a compromise between reducing tumour residual motion while maintaining/increasing the duty cycle. Jiang et al (2006) produced a preliminary study including 4 patients which found that amplitude gating was preferable over phase gating. Similarly, Berbeco et la (2005) found less residual motion of the tumour for amplitude-based gating in five of the eight patients studied. Lu et al, (2006) after monitoring 35 patients, also found amplitude gating to be superior however for a different reason. Using a spirometer, tidal volume was compared with both phase and amplitude gating. It was found the discrepancies were significantly smaller ($P<0.001$) with amplitude sorting than those with phase angle sorting, thus suggesting a stronger relationship between internal motion and amplitude. The major advantage of phase sorting is that relative phases can be determined for each respiratory cycle independent of amplitude variation (Rietzel et al 2005). Phase-sorting is still more widely used than amplitude sorting for 4DCT and is the only option available on the Anzai AZ-773V respiratory gating system. The RPM system gives a choice of which gating method the user prefers. The correlation between phase and amplitude gating on the RPM system and phase gating using the Anzai system needs further investigation.

Residual tumour motion is defined as the movement of the tumour within the gating window i.e. when the beam is on (Jiang et al 2006). It is important to keep residual tumour motion to a minimum while maximising the percentage of time per cycle the beam can be on. The residual tumour movement for duty cycles of 40%, 30% and 20% was calculated by Berbeco et al (2005) within six gating windows using stereoscopic imaging and the Anzai laser system. It was found that the residual motion ($95^{th}$ percentile) was between 0.7 and 5.8 mm, 0.8 and 6 mm and 0.9 and 6.2 mm for 20%, 30% and 40% gating windows respectively. Variations in the beam from previous treatment were 37% and 42% for amplitude and phase gating respectively. It was suggested therefore that although external gating reduced the total tumour motion, the residual motion still behaved unpredictably and treatment plans still need to account for this

## 1.10 Gated IMRT

IMRT provides the capacity to deliver highly conformal radiation dose to a complex static target volume. Internal organ motion however, provides treatment errors, and can pose a problem for image-guide radiation therapy (Jiang 2006). Respiratory gating can reduce the effects of intra-fractional tumour motion and combined with Intensity Modulated Radiation Therapy dose homogeneity can be increased and dose to critical structure reduced (Keall et al 2006).

Using a phantom on a motion platform, Keall et al (2006) performed ionisation and film measurements to compare the output of a gated IMRT beam using the RPM system to a non-gated IMRT beam. It was found using film dosimetry that the magnitude of the dosimetric difference between the static delivery and gated delivery is less than the magnitude of the difference between the free breathing and static delivery. IMRT increases the treatment time. Keall et al (2006) reported an increase of approximately 2 minutes for gated IMRT treatment; however this will be influenced by duty cycle, the leaf algorithm for the collimators, and treatment dose rate. Jiang et al (2006) used step-and shoot IMRT with the RPM system and found the delivery time for gated delivery to be 1.5 times more than non-gated delivery.

Without gating, the combination of MLC motion and target motion can cause hot/cold spots in the target volume (Bortfield et al 2002, Jiang et al 2006). This effect is in the order of 10% for one treatment however it is reduced to 1% for more than 30 fractions due to the randomness of the beam start relative to patient phase (Jiang et al 2006). For gated treatment, this averaging over fractions would be greatly reduced as the beam is only turned on at a certain phase thus hot spots/cold spots may not be cancelled out (Nioutsikou et al 2006). This issue needs further research.

### 1.11 Comparative study

Due to the availability and set-up in the Wollongong clinic, the AZ-733V gating system will be used with the Siemens Sensation Open and the Varian RPM system will be utilised in the future for gated delivery on a Varian Linear accelerator. It is necessary to produce a comparative study to ensure correlation between the two gating systems to ensure accurate planning and treatment. Li et al (2006) compared the respiratory signals produced by three volunteers and two patients on the Anzai AZ733V and RPM systems. The breathing waveforms were recorded by both systems simultaneously by placing both the pressure sensor and the infrared marker block on the same location, and the correlation was found to be 98.2-99.6%. A more comprehensive study between the gating systems for a larger patient sample is yet to be completed.

# CHAPTER II

# COMPARISON OF RESPIRATORY WAVEFORMS FROM TWO RADIOTHERAPY RESPIRATORY GATING SYSTEMS

## 2.1 Introduction

Intrafraction organ motion is due to a change in patient geometry during dose delivery within a treatment fraction (Metcalfe et al 2007). Skeletal, gastrointestinal, and cardiac systems all contribute to intrafraction motion however it is respiratory motion towards which significant research and development has been directed (Keall et al. 2006). Respiration is a complex mechanism, and organ motion is often unpredictable. Breathing waveforms vary between patients, but also between breaths for a single patient; baseline shifts, frequency modulation and amplitude changes are common both interfraction and intrafraction (Nøttrup et al 2007). Some patients may be predominately abdominal breathers while others may breathe with large chest excursions (Geirga et al 2005). For every person, each breath is unique and the challenge in respiratory gating is accurately measuring patient breathing and utilising the link between tumour motion and the respiratory cycle.

External surrogates are a non-invasive way to measure internal target motion. They presume that an external marker placed on the patient is primarily correlated with the respiratory component of the patient's internal motion (Beddar et al 2007), however this may not always be the case. Phase shift between external wall and diaphragm has been investigated. Mageras et al through fluoroscopy studies found that despite external monitor movement correlating well with diaphragm movement in four of the six patients measured, a phase shift was introduced in two of the patients. Yan et al (2006) found through using multiple external markers that correlation errors between internal and external signals could be reduced by correcting for phase shift. Yan et al highlighted the fact that it is critical to maintain a stable synchronisation between the internal target and the external surrogate and that an external single marker, such as that used by the RPM system, has limited capabilities due to the variability of marker location and breathing patterns.

The chest wall has more than one degree of freedom, and independent motion of chest wall and abdomen has been acknowledged for some time (Konno 1968). Several respiratory gating studies are concerned with correlation of internal tumour motion and the external surrogate but little research has focused on the role of the position of the external marker in this situation. Vedam et al (2001) noted that reproducibility of the marker position on the skin was important while Gierga et al (2005) stated that "the position of the external marker on the patient surface may impact on the underlying variation in tumour position." Chi et al (2006) found by using the RPM system and comparing a point on the chest wall in 10 4D CT phases that there was a significant variation depending on marker location, seven of the eight patients showing abdominal motion leading chest wall motion. The limitation of this method was that only 10 points were obtained per respiratory cycle in order to reconstruct an entire waveform. A recent paper (Killoran et al 2008) published close to the submission of this thesis measured the waveforms of 10 patients using the RPM system in two locations (xiphoid and isocentre). Killoran et al (2008) found that for some patients the xiphoid and isocentre markers were completely out of phase and when comparing the two retro-reflective markers for 4D CT treatment based on ten images per cycle, 4D reconstructions would be influenced depending on which marker was used by at least one bin 34.9% of the time due to phase shift. The only study thus far to compare the Anzai respiratory gating system and the RPM respiratory gating system waveform was completed by Li et al (2006). Two volunteers and three patients had their waveforms monitored while both systems were placed at the same location on the chest wall and the correlation between systems was discovered to be 98.2-99.6%. This study did not account for variations in marker location and did not address any phase shifts which may exist between thoracic and abdominal movements.

Positioning of the external markers may also impact on the respiratory signals obtained due to the way the chest wall expands. De Groote et al (2000) explored the discrepancies of sensors due to sensitivity with regards to variations of cross-sectional perimeter and area variations of the chest wall. A basic 2D model was formed by De Groote as shown in Figure 2.1. An ellipse with axes representing transverse and dorsoventral movement was constructed with a fixed point representing the spine. The centre of the ellipse moves in the anterior-posterior direction during breathing.

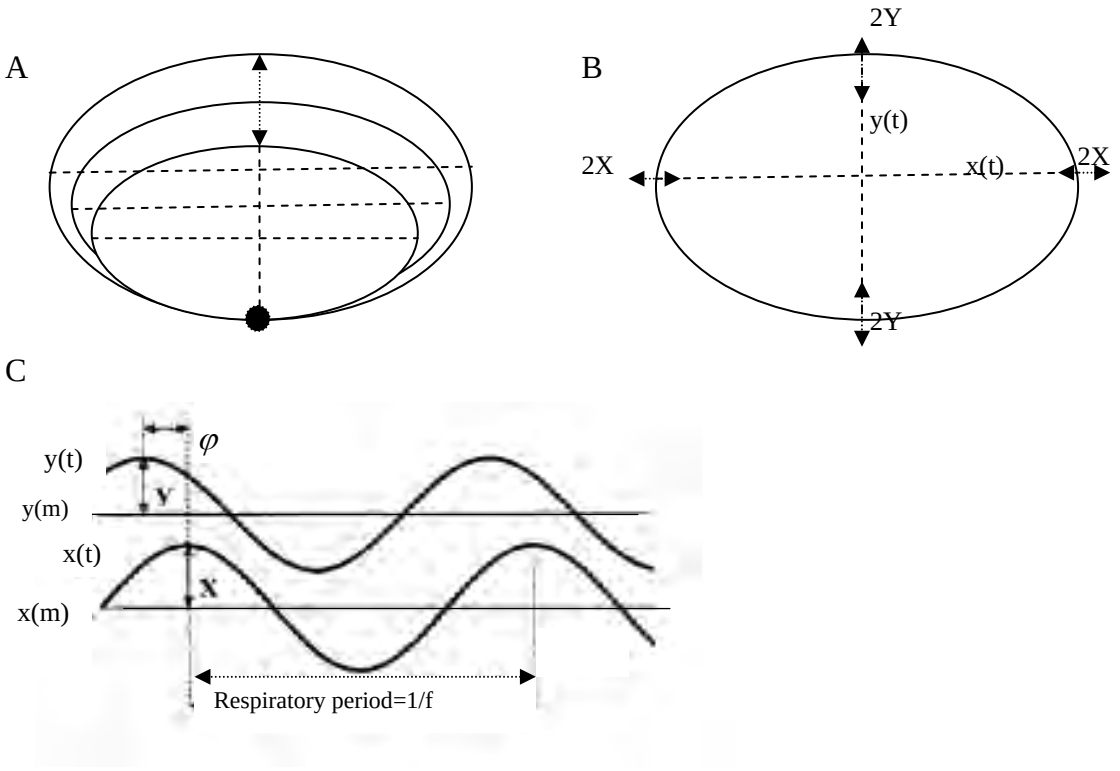


Figure 2.1: A: Elliptic model of the thoracic and abdominal cross section during breathing (De Groote et al 2000). The principal axes are dorsoventral and transverse diameter. The spinal cord is fixed. B is mathematically equivalent model to A, with the centre of the ellipse considered fixed. C is the simulation of respiratory movements by sinusoidal variations of each semi axis, x(t) and y(t). $\varphi$ is a phase shift between x and y movements, f respiratory frequency, X and Y the mean amplitudes and $x_m$ and $y_m$ the mean positions.

Respiratory movements are simulated by sinusoidal variations of x(t) and y(t), such that

$$x(t) = x_m + X\sin(2\pi ft)\ , \tag{2.1}$$

$$y(t) = y_m + Y\sin(2\pi ft + \varphi)\ , \tag{2.2}$$

where X and Y are the mean amplitudes, $x_m$ and $y_m$ are the mean values of the semiaxes, f is the respiratory frequency, t is time, and $\varphi$ is the phase shift between lateral and ventral movement. The perimeter of the ellipse can then be found by:

$$P(t) = 4y(t)E\left\{1-[x(t)/y(t)]^2\right\}\ , \tag{2.3}$$

Where the function E(m) is the elliptic integral of the second kind, calculated between 0 and $\pi/2$ given by:

$$E(m) = \int_0^{2\pi}\sqrt{1-m\sin^2(\theta)}d\theta\ \cdot \tag{2.4}$$

Strain gauges such as that used by the Anzai respiratory gating system are sensitive to perimeter changes whereas the RPM system is dependent solely on tracking AP movement. If equation 2.3 formulated by De Groote is expanded we have

$$P(t) = 4(y)E\left\{1 - \left[\frac{x_m + X\sin(2\pi ft)}{y_m + Y\sin(2\pi ft + \varphi)}\right]^2\right\},$$

$$P(t) = 4(y)E\left\{1 - (x_m / y_m)^2[1 + X / x_m \sin(2\pi ft)]^2 / [1 + Y / y_m \sin(2\pi ft + \varphi)^2\right\}. \quad (2.5)$$

Taylor expansion of the first order around (0,0) gives

$$\Delta P(t) = C_2(X / x_m)\sin(2\pi ft) + C_3(Y / y_m)\sin(2\pi ft + \varphi)$$

$$= C_4 \sin(2\pi ft + \phi_p) \quad (2.6)$$

where $\Delta P(t)$ represents the variation in perimeter, $C_2, C_3$ and $C_4$ are constants. $\phi_p$ is the phase shift of the perimeter with respect to the original movement y(t). It can be seen that a phase shift may be introduced between anterior-posterior movement and perimeter changes dependent on X/Y, $x_m / y_m$ and $\varphi$.

Thus if a phase shift is introduced between transverse and dorsoventral movements, a phase shift will be introduced between perimeter expansion (Anzai signal) and anterior-posterior movement (RPM signal).

### 2.2 Aim

The aim of this study was to compare the waveforms obtained from the Anzai AZ733V respiratory gating system and the RPM system when

i) markers are placed in the same location on the chest wall
ii) markers are placed in separate locations on the chest wall

To observe and quantify variations in signal, if any, ascribed to difference in monitoring methods or sensor placement.

### 2.3 Method and materials

The Anzai and RPM systems record respiratory waveforms as .daf files. The files do not contain in them a time stamp, so in order for a direct comparison to be performed a time

stamp was constructed. Maxima and minima of respiratory waveforms could not simply be 'aligned' as this would mask a phase shift, if one existed. A sharp cough at the beginning and end of data collection was trialled but this method did not provide a definitive point and any inherent delay between locations, although reduced, would still be present. An infrared diode was connected to the anterior surface of the RPM marker box as shown in figure 2.7. When the infrared diode was pulsed, the RPM system loses track of one of the markers momentarily and tracks the pulse. This produced a spike in the data of 0.20 s. A simple switch was constructed such that the infrared diode could be pulsed at the same time as a loss of signal to the Anzai sensor port. The loss of signal to the Anzai system was a deliberate trigger to enable alignment of the waveforms obtained from the two systems The first infrared pulse observed by the RPM system could then be manually aligned with the loss of signal observed by the Anzai system, and the second infrared pulse was aligned with the return of the signal to the sensor port (refer to figure 2.2). This process was completed at the beginning of obtaining the subject's waveform and also after a 2 minute period to provide an additional point to align the data. Subjects for the study were all volunteers working at the Illawarra Cancer Care Centre.

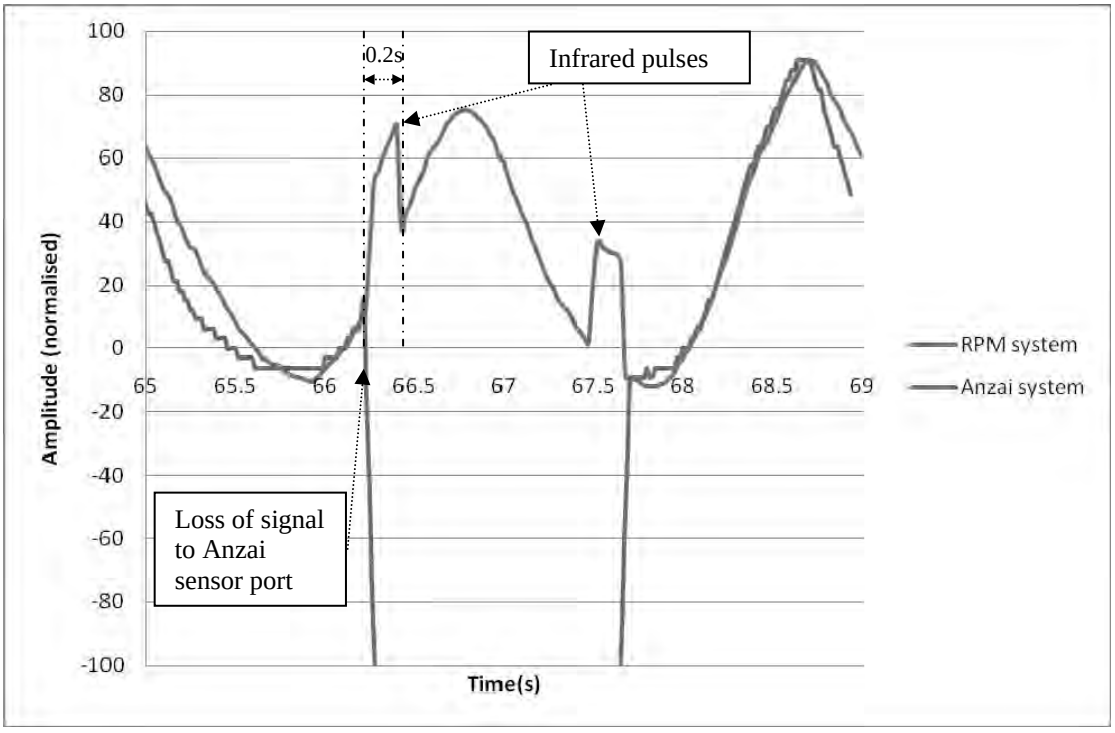


Figure 2.2: Graph illustrating time stamp method to align Anzai system and RPM system.

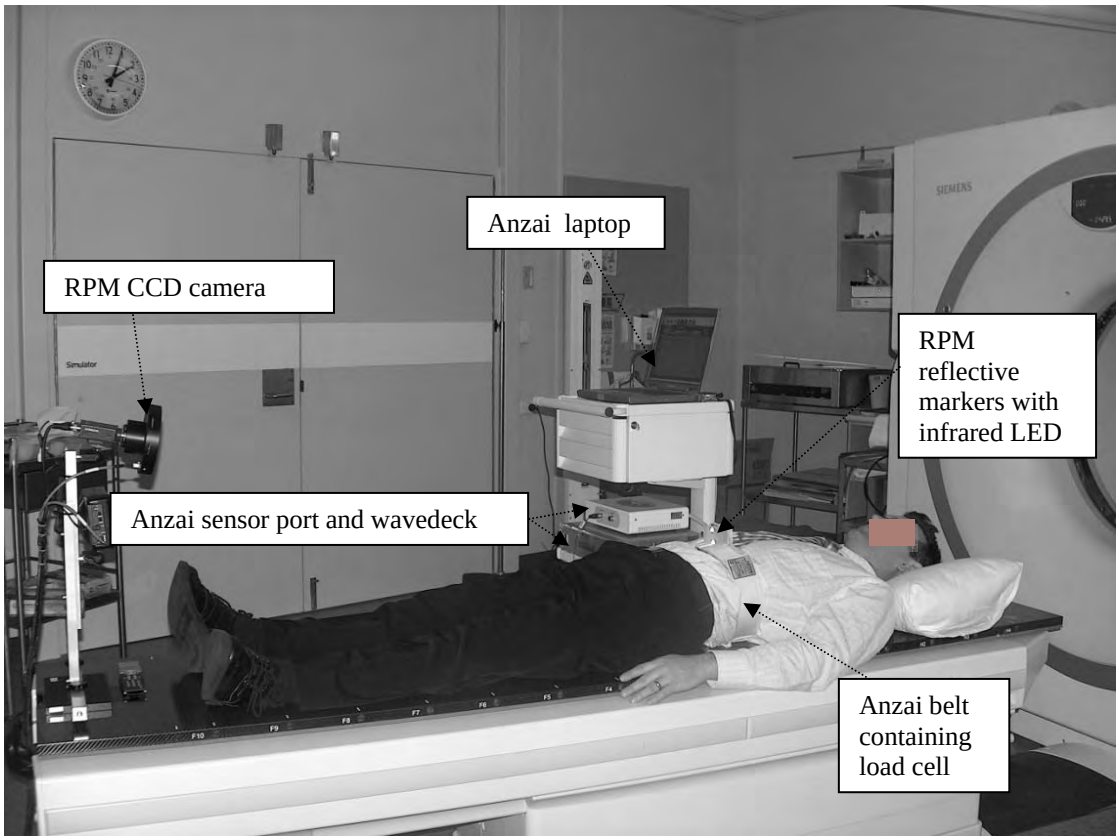


Figure 2.3 Experimental set-up showing volunteer connected to both respiratory gating systems for waveform measurement.

Subjects were asked to lie on the CT couch and breathe freely while their respiratory waveforms were monitored by both the Anzai respiratory gating system and the RPM respiratory gating system (refer to figure 2.3 for experimental set-up).

The Anzai respiratory gating system, consisting of an elastic belt (there are three sizes, small medium and large) and a pressure sensor (refer to figure 1.4) was fastened by Velcro around the subject's abdomen or thorax. As the subject breathes in, the chest wall expands, putting pressure on the load cell located in the pocket between the belt and the patient's skin. The "HIGH" pressure sensor was connected to the sensor port and the load sensor placed in the chosen belt. The sensor port was in turn connected to a wave deck, which was attached to a laptop. The system was placed in sequential mode. It was ensured that the sensor port displayed a green light indicating the signal was in range.

Figure 2.4 is the display window from the Anzai gating system showing the respiratory waveform obtained from a subject and the predicted waveform. No gating data is

available such as beam on/beam off as this mode was not in use while collecting waveforms.

Manual calibration was performed before readings were taken: the gain and position of the waveform were adjusted such that the respiratory signal always falls in a range between -25 to 125 (arbitrary values). If calibration is not performed, data outside the prescribed values will be lost (refer to figure 2.4).

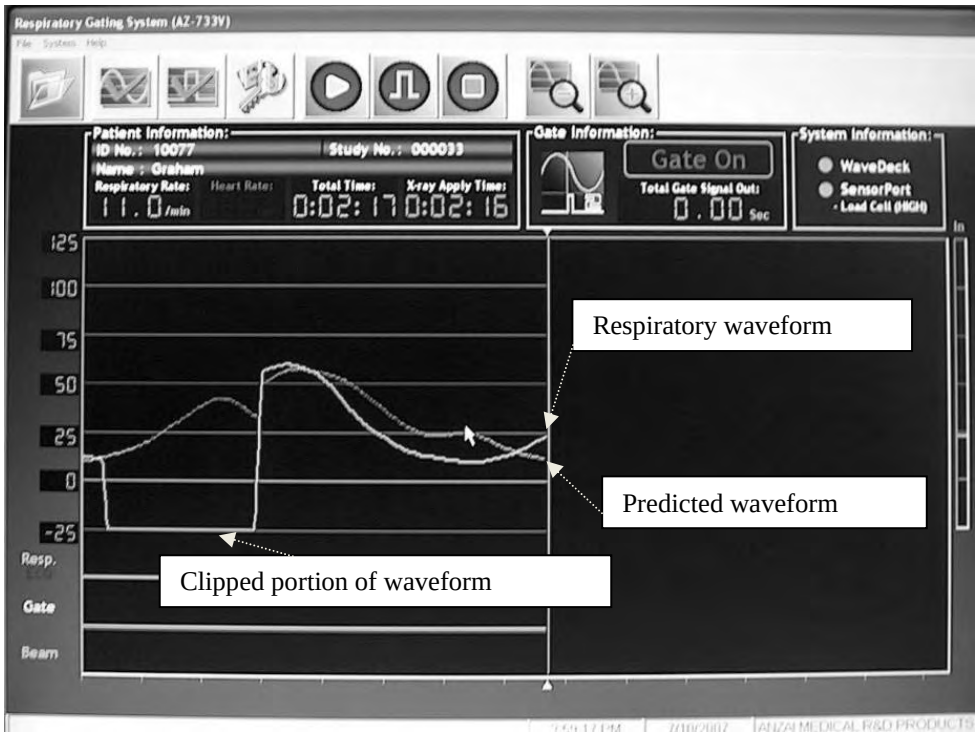


Figure 2.4: Anzai user interface showing subject's breathing waveform and predicted waveform.


Figure 2.5: RPM CCD camera surrounded by infrared LEDs, and display monitor.

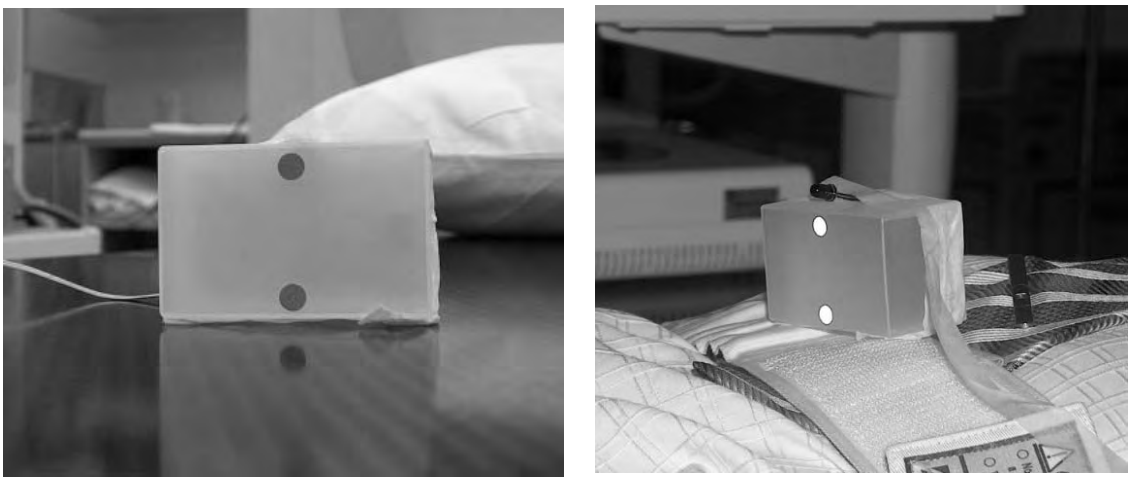

Figure 2.6: (a) RPM retro-reflective marker box (b) modified RPM box with added infrared LED.

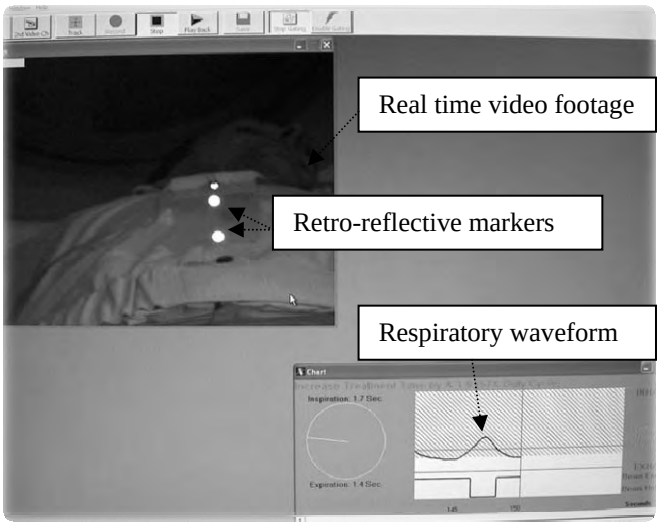


Figure 2.7: Real time Position Management system user interface showing subject's respiratory waveform.

The Real-time Position Management system was positioned on the Siemens Sensation Open couch. The camera, surrounded by infrared LEDs, and display monitor were attached to the foot of the bed, as shown in figure 2.5. The hollow, plastic RPM box (dimensions 6.5 cm x 3.5 cm x 4 cm) with two retro-reflective markers was placed on the subject's chest or abdomen. When setting up the RPM system it was ensured that no other reflective items were in view of the camera, such as the table top, to which the tracking point may have been relocated. The anterior-posterior movement of the two passive reflective markers was tracked, and converted to a one dimensional motion signal as seen in figure 2.7. The data and phase information was recorded as a .daf file in the computer system.

Respiratory waveforms were collected over 2 minute intervals for each patient. In the first instance both the RPM marker and the Anzai belt were placed at the umbilicus. The infrared LED attached to the RPM marker box was pulsed and the signal to the Anzai sensor port terminated simultaneously. The infrared LED was then pulsed a second time as the signal was reinstated to the Anzai system. The respiratory waveform was collected by both systems over a two minute interval with the subject breathing freely. The infrared LED was pulsed again as the Anzai sensor port was switched off. The LED was pulsed a final time as signal to the Anzai system was reinstated. This process was completed six times for each subject.

The systems were placed in the following locations (refer to figure 2.8)

- Both RPM marker and Anzai belt positioned at the umbilicus
- Both RPM marker and Anzai belt positioned midway between the umbilicus and xiphoid process
- Both RPM marker and Anzai belt positioned at the xiphoid process
- RPM marker positioned at the xiphoid process, Anzai belt positioned at the umbilicus
- RPM marker positioned at the umbilicus, Anzai positioned at the xiphoid process
- RPM marker positioned midway between xiphoid process and umbilicus, Anzai positioned at the umbilicus

These locations were chosen as they are indicative of the extent of chest wall movement as measured by both systems. Patient compliance (refer to figure A169) and a suitable time frame for measurement acquisition were also factors. The two sets of data were imported to Microsoft Excel 2007 and the time stamps aligned. The graphs were normalised; the average signal amplitude peak being assigned the value 100.

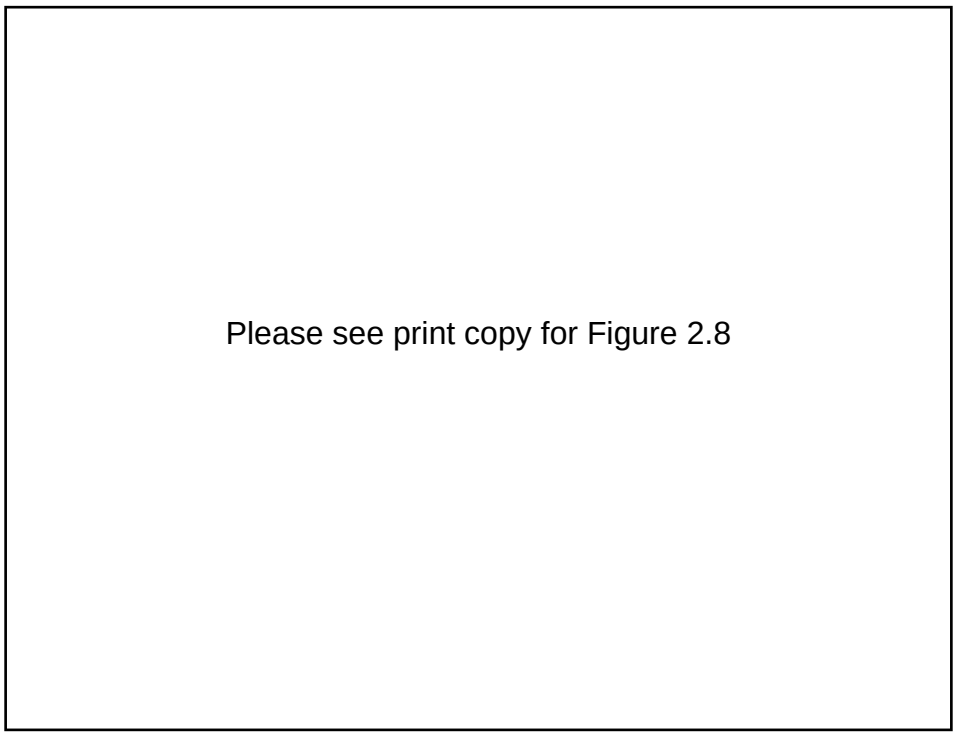


Figure 2.8: Schematic showing marker locations (Image: NCE State University).

The Anzai system samples at a rate of 40Hz, while the RPM system samples at a rate of 25Hz. The data sets were binned to account for this, and a graph of the signal amplitude given by the Anzai system (normalised) versus the amplitude of displacement given by the RPM system (normalised) was plotted. The amplitude of the Anzai signal was arbitrary: manual calibration of the gain and position of the waveform was performed such that the respiratory signal always fell in a range between -25 to 125. The RPM system gave displacement values however both the Anzai signal and the RPM displacement values were normalised so that the average peak-to-peak value of the breathing waveforms was 100. This enabled the breathing waveforms to be easily compared and the magnitude of a phase shift between the two systems to be determined, in the cases where a phase shift is present. The normalisation of the graphs has no effect on the correlation coefficient as it is completely invariant to linear transformations.

If we take a set of data with n data points then the correlation, r, of two random variables, x and y, can be found through linear regression where:

$$r = \frac{n\sum_{i=1}^{n}(x_i y_i) - (\sum_{i=1}^{n} x_i)(\sum_{i-1}^{n} y_i)}{\sqrt{\left[n\sum_{i=1}^{n}(x_i^2) - (\sum_{i=1}^{n} x_i)^2\right]\left[n\sum_{i=1}^{n}(y_i^2) - (\sum_{i=1}^{n} y_i)^2\right]}} \qquad (2.7)$$

The square of the correlation coefficient, $r^2$ ($R^2$ as defined by Excel) is a measure of the reliability of the linear relationship between y and x values. The closer $R^2$ is to 1, the smaller the unexplained variation between x and y, and the better the fit. The variables (x and y) in this case are the Anzai signal amplitude and the RPM marker displacement. Ideally, to be used interchangeably in the clinic, the RPM and Anzai systems should respond to motion of the chest wall and abdomen caused by respiration identically. If this were the case, signals would be in-phase, a plot of the Anzai signal vs. the RPM signal would display a straight line and values of r and $r^2$ would be 1.

A dataset of 2 minutes would consist of 3000 points measured by the RPM system and 4800 points measured by the Anzai system. After binning for determination of the correlation coefficient, a sample size of two minutes is reduced to 600 points. Due to the

size of the dataset there was no concern for normality assumptions (Bobko 2005) and $R^2$ was not adversely affected by sample size.

The correlation coefficient is highly sensitive to phase shifts between the data sets. Error is introduced in the correlation coefficient by the alignment of the time stamps, which can be no more than 0.2s. Care was taken to align the start of the pulse with the loss of signal. There are also potential physical time delays inherent in the gating system electronics. The RPM system infrared camera has a limited sampling rate of 30Hz thus a random delay is introduced here of up to 33ms. Similarly, the Anzai system samples at a rate of 40 Hz, introducing a possible delay of up to 25ms however these delays were considered negligible.

100% inspiration peaks were chosen to measure phase shifts between signals. This was chosen as it is a sine-wave independent value; it is the point chosen for determination of the start of a respiratory period for both the Anzai and RPM systems and the sharp inhalation peak means it is an easily comparable, definitive point as opposed to expiration. The mean respiratory period of subjects over the two minute interval was also calculated from the Anzai respiratory waveform and the results tabulated.

**2.4 Results**

The coefficient of determination ($R^2$) was found for the set of six marker positions in a sample of 15 staff volunteers and the results summarised in table 2.1. The mean coefficient of determination when both external surrogates were placed at the umbilicus was 0.925. When positioned at this location the signals from the two systems responded similarly to abdominal movement due to respiratory movement. When both external surrogates were positioned midway between xiphoid process and umbilicus, the mean coefficient of determination was found to be 0.788. When the RPM and Anzai systems were positioned at the xiphoid process the mean coefficient of determination was found to be 0.611. The mean $R^2$ value between signals when the Anzai load cell was positioned at the umbilicus and the RPM retro-reflective marker was positioned at the xiphoid process was found to be 0.776. When the Anzai marker was positioned at the xiphoid process, and the RPM marker positioned at the umbilicus, the mean coefficient of determination between the signals was found to be 0.752. The Anzai positioned at the

umbilicus and the RPM system placed midway between xiphoid process and umbilicus produced a mean correlation coefficient between signals of 0.878.

**Table 2.1: Coefficient of Determination ($R^2$) between Anzai and RPM signals measuring the same respiratory waveform**

| Subject ID | Coefficient of determination: both systems placed at umbilicus | Coefficient of determination: both systems placed midway between umbilicus and xiphoid process | Coefficient of determination: both systems placed at xiphoid process | Coefficient of determination : RPM placed at umbilicus, Anzai at xiphoid process | Coefficient of determination: RPM placed at xiphoid process, Anzai placed at umbilicus | Coefficient of determination : Anzai at umbilicus, RPM midway between umbilicus and xiphoid process |
|---|---|---|---|---|---|---|
| 1 | 0.931 | 0.953 | 0.827 | 0.962 | 0.789 | 0.932 |
| 2 | 0.845 | 0.511 | 0.765 | 0.888 | 0.720 | 0.965 |
| 3 | 0.968 | 0.769 | 0.204 | 0.807 | 0.900 | 0.889 |
| 4 | 0.913 | 0.81 | 0.831 | 0.896 | 0.860 | 0.916 |
| 5 | 0.968 | - | - | 0.945 | 0.884 | 0.897 |
| 6 | 0.981 | 0.523 | 0.195 | 0.521 | 0.401 | 0.823 |
| 7 | 0.918 | 0.784 | 0.517 | 0.665 | 0.624 | 0.817 |
| 8 | 0.912 | 0.899 | 0.897 | 0.676 | 0.737 | 0.955 |
| 9 | 0.950 | 0.935 | 0.774 | 0.912 | 0.936 | 0.960 |
| 10 | 0.944 | 0.805 | 0.816 | 0.806 | 0.924 | 0.938 |
| 11 | 0.984 | 0.852 | 0.735 | 0.345 | 0.788 | 0.91 |
| 12 | 0.917 | 0.896 | 0.610 | 0.501 | 0.633 | 0.699 |
| 13 | 0.879 | 0.645 | 0.519 | 0.847 | 0.815 | 0.851 |
| 14 | 0.844 | 0.830 | 0.414 |  | 0.854 | 0.735 |
| 15 | 0.930 | 0.804 | 0.494 | - | - | - |
| Mean | 0.925 | 0.788 | 0.611 | 0.752 | 0.776 | 0.878 |

**Table 2.2: Respiratory periods obtained for 15 staff volunteers using the waveform generated by the Anzai respiratory gating system.**

| Subject ID | Breathing period ($s \pm 1$ SD)both systems placed at umbilicus | Breathing period ($s \pm 1$ SD) both systems placed midway between umbilicus and xiphoid process | Breathing period ($s \pm 1$ SD) both systems placed at xiphoid process | Breathing period ($s \pm 1$ SD)RPM placed at umbilicus, Anzai at xiphoid process | Breathing period ($s \pm 1$ SD) RPM placed at xiphoid process, Anzai placed at umbilicus | Breathing period ($s \pm 1$ SD) Anzai at umbilicus, RPM midway between umbilicus and xiphoid process |
|---|---|---|---|---|---|---|
| 1 | 7.5 (0.3) | 6.0 (0.7) | 6.5 (0.6) | 10.0 (0.8) | 10.6 (0.8) | 8.7 (0.4) |
| 2 | 4.1 (0.5) | 4.9 (1.6) | 4.6 (0.6) | 5.3 (0.9) | 6.3 (1.5) | 5.9 (2.9) |
| 3 | 2.6 (0.4) | 4.4 (0.4) | 3.9 (0.5) | 3.7 (0.4) | 3.3 (0.4) | 3.7 (0.5) |
| 4 | 4.2 (0.7) | 3.9 (0.3) | 4.2 (0.4) | 5.7 (0.4) | 5.3 (0.5) | 5.9 (0.5) |
| 5 | 4.0 (0.4) | - | - | 7.5 (0.4) | 6.9 (0.5) | 5.4 (1.2) |
| 6 | 6.3 (0.4) | 7.3 (0.6) | 6.6 (1.9) | 6.0 (1.2) | 6.0 (1.1) | 6.2 (0.7) |
| 7 | 8.9 (3.3) | 5.8 (0.4) | 8.7 (2.3) | 6.3 (1.8) | 6.6 (2.5) | 7.2 (1.3) |
| 8 | 6.6 (2.2) | 8.1 (1.0) | 5.7 (0.7) | 6.6 (2.2) | 5.4 (1.2) | 4.6 (0.9) |
| 9 | 7.8 (1.3) | 9.5 (1.3) | 14.9 (1.3) | 15.4 (1.6) | 13.2 (3.2) | 18.0 (1.9) |
| 10 | 6.2 (1.0) | 5.2 (1.4) | 6.5 (1.3) | 4.8 (1.4) | 5.0 (2.0) | 5.2 (1.0) |
| 11 | 4.3 (0.2) | 4.1 (0.5) | 3.6 (0.5) | 4.2 (1.1) | 4.0 (0.7) | 4.0 (0.3) |
| 12 | 3.2 (0.5) | 3.6 (0.5) | 3.7 (0.4) | 3.6 (0.6) | 3.7 (0.7) | 3.7 (0.5) |
| 13 | 5.4 (0.9) | 5.6 (2.3) | 5.9 (1.2) | 5.3 (0.8) | 5.7 (1.0) | 5.3 (0.9) |
| 14 | 3.1 (0.4) | 3.0 (0.6) | 2.9 (0.3) | 3.0 (0.4) | 2.7 (0.3) | 3.1 (0.4) |
| 15 | 3.1 (0.3) | 2.9 (0.2) | 3.5 (0.2) | - | - | - |

The period for all respiratory waveforms collected was found by using the Anzai signal and summarised in table 2.2. One standard deviation from the mean is also quoted.
The results for each subject are described below.

*Subject 1*

The signals from the Anzai belt respiratory gating system and the RPM system with both external surrogates placed at the umbilicus agree well at inspiration, however at exhalation the RPM marker placed at the umbilicus lags behind the Anzai marker (refer to figure A1). The $R^2$ value was found to be 0.931. The average period was found to be 7.5 ± 0.7 s. The maximum lag time at mid-exhalation was found to be 0.7 s. When both systems were placed midway between xiphoid process and umbilicus for subject 1 (figure A3), the average respiratory cycle was found to be 6.0 s±0.7 s. The coefficient of determination, $R^2$ was found to be 0.953 and the signals agree well. When both external markers were moved to the xiphoid process (figure 2.9/A5), the $R^2$ value was reduced to 0.827 (figure 2.10/A6). The average respiratory cycle was 6.53±0.6 s. The Anzai signal can be seen to respond slightly before the RPM signal. At 100% inspiration, a time lag was observed of the RPM system behind the Anzai system of 0.5±0.1 s.The average respiratory cycle when the Anzai system was placed at the xiphoid process and the RPM system was placed at the umbilicus was found to be 10.0±0.8 s (figure A7). The signals correlate well at this position; the coefficient of determination was found to be 0.962 (figure A8). When the Anzai belt was positioned at the umbilicus and the RPM infrared reflective marker was positioned at xiphoid process (figure A9), the average respiratory cycle was found to be 10.6±0.8 s. The $R^2$ value was found to be 0.788 (figure A10). The signals correlated significantly better at inspiration than exhalation, the maximum time difference between exhalation signals at 50% amplitude was found to be 1.5 s (14% of period). When the RPM marker was placed midway between xiphoid process and umbilicus and the Anzai belt containing the load cell was placed at the umbilicus, the average respiratory cycle was found to be 8.7±0.4 s. The coefficient of determination was calculated to be 0.932 (figure A12). The signals were observed to agree better on the inhale phase than the exhale phase (refer to figure A11). Upon exhalation the Anzai signal drops away steeply while the RPM signal is slower to respond. The average respiratory period over all six samples was found to be 8.2±1.9 s. The respiratory period was seen to increase with time spent lying on the couch.

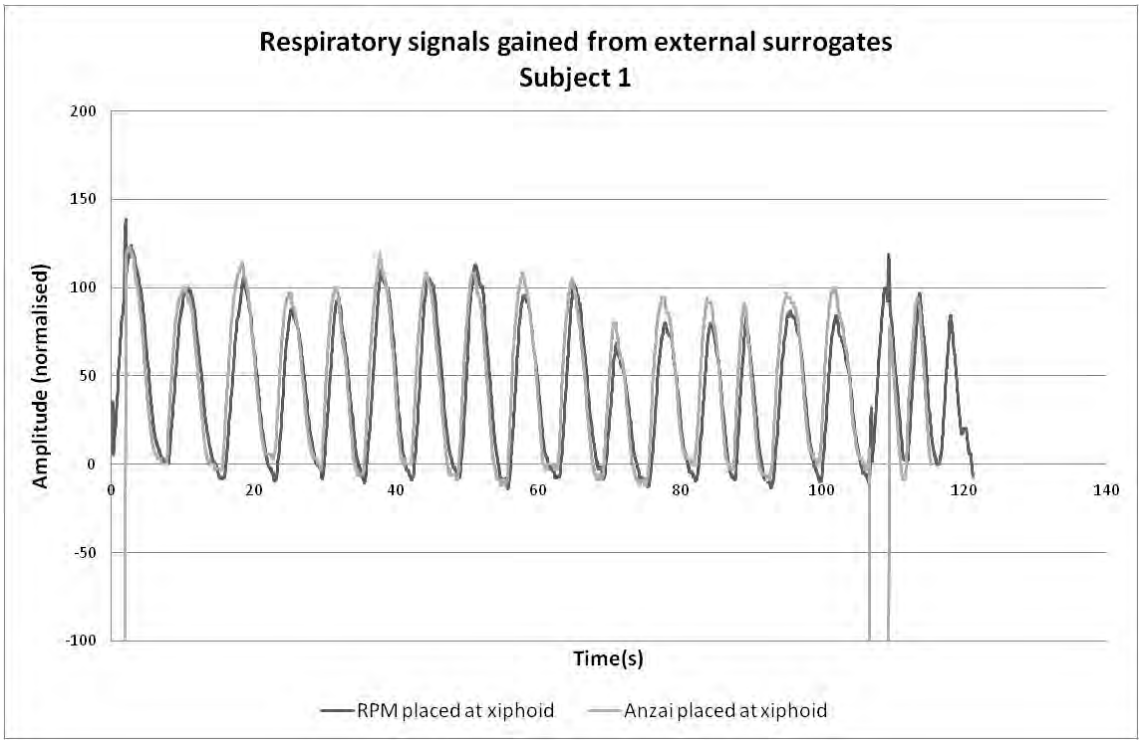


Figure 2.9: Respiratory waveforms gained using both RPM marker and Anzai belt positioned at xiphoid for subject 1 showing a phase shift between signals.

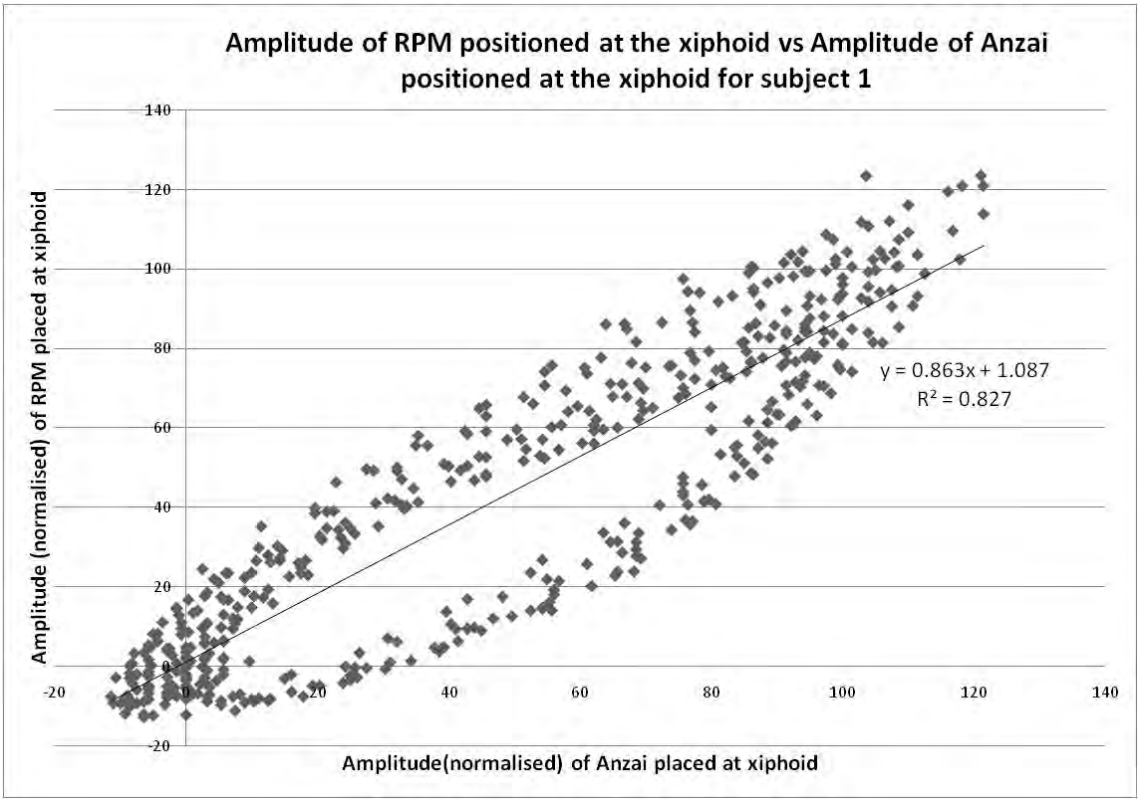


Figure 2.10: Determination of coefficient of determination for both RPM and Anzai positioned at xiphoid, subject 1.

*Subject 2*

When both respiratory markers were placed at the umbilicus for subject 2, the coefficient of determination was found to be 0.845 (figure A14). The average respiratory period was found to be 4.1±0.5 s (figure A13). The Anzai signal was found to lead the RPM signal (Anzai responds quicker). A shift in baseline can was observed after 40 s. Before the shift in baseline a slight phase shift was apparent. At 100% inspiration, the Anzai signal leads the RPM signal by 0.2±0.1 s. When both respiratory markers were moved to midway between the umbilicus and xiphoid process, $R^2$ was found to be 0.511 (figure A16). The average respiratory period was found to be 4.9±1.6 s. Irregular breathing was observed (refer to figure A15) as indicated by the large standard deviation in the respiratory period and the low correlation coefficient. The RPM system experienced a shift in baseline which was not mirrored by the Anzai system. The Anzai system responded to change quicker than the RPM system. When both respiratory markers were placed at the xiphoid process, a coefficient of determination of 0.765 was calculated (refer to figure 2.12/A18). The average respiratory cycle was found to be 4.6±0.6 s. The baseline of the RPM system was observed to drift while the Anzai system remained constant (figure 2.13/A17). No phase shift was apparent here. When the Anzai system was placed at the umbilicus and the RPM system was positioned at the xiphoid process, the signals were observed to agree well (figure A19), and a $R^2$ value was calculated to be 0.888 (figure A20). The average respiratory cycle was discovered to be 5.3±0.9 s. When the Anzai belt was positioned at the xiphoid process, and the RPM marker positioned at the umbilicus, the correlation ($R^2$) between systems was seen to decrease to 0.719 (figure A22).The average respiratory cycle was found to be 6.3±1.5 s. The Anzai exhalation curves are seen to be much steeper than the RPM exhalation curves (figure A21). This leads to a maximum time difference mid-exhalation of the RPM behind the Anzai system of 2.8 s in the largest peak (44% of breathing cycle). When the Anzai belt was placed at the umbilicus and the RPM retro-reflective marker was placed midway between xiphoid process and umbilicus, the coefficient of determination was found to be 0.965 (figure A24). The graphs correlate well despite shifts in baseline and frequency (figure A23).

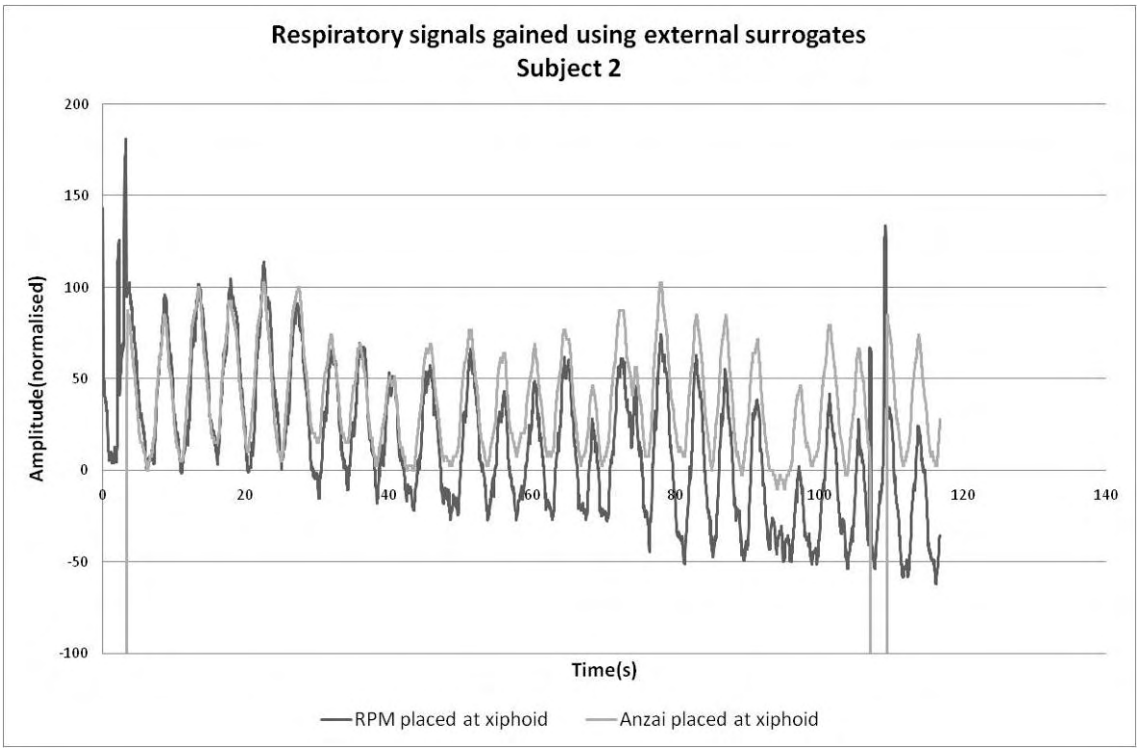


Figure 2.11: Respiratory signals gained using both RPM marker and Anzai belt positioned at xiphoid for subject 2. A shift in baseline is apparent for the RPM waveform.

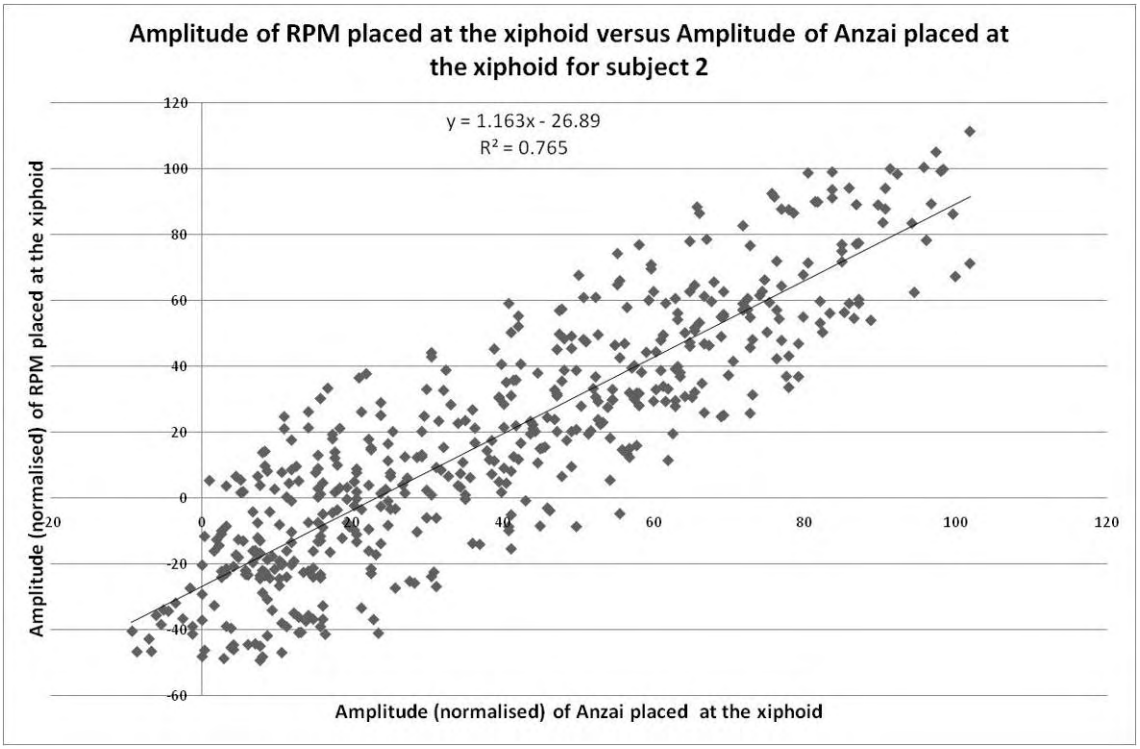


Figure 2.12: Determination of coefficient of determination for both RPM and Anzai positioned at xiphoid, subject 2.

The average respiratory period was found to be 5.9±2.9 s. The average respiratory period measured over the six waveforms for subject two was found to be 5.2±0.8 s.

*Subject 3*

The calculated coefficient of determination for both the Anzai external surrogate and the RPM marker positioned at the umbilicus was found to be 0.907 (figure A26). The average breathing cycle was found to be 2.6±0.7 s (figure A25). When both markers were moved to midway between the xiphoid process and umbilicus, $R^2$ was found to be 0.769 (figure A28). The RPM signal was observed to respond slower to changes in external wall movement, and an overall phase shift was apparent in the data (figure A27). At 100% inspiration, the RPM signal lagged behind the Anzai signal by 0.3±0.1 s. The average respiratory cycle was found to be 4.4±0.4 s. When both the Anzai marker and the RPM system were moved to the xiphoid process, the coefficient of determination was reduced to 0.165 (figure A30) and a very poor correlation was observed. The average respiratory cycle was found to be 3.9±0.5 s (figure A29). When the RPM marker was positioned at the xiphoid and the Anzai belt was positioned at the umbilicus the $R^2$value was found to be 0.900 (figure A32). The average respiratory cycle here was 3.3 s±0.4 s.The RPM marker positioned at the umbilicus while the Anzai belt was positioned at the xiphoid process produced a coefficient of determination of 0.807 (figure A34), and an average respiratory cycle was found of 3.7±0.4 s (figure A33).When the RPM was placed midway between the xiphoid process and umbilicus and the Anzai marker was placed at the umbilicus the respiratory waveforms obtained by the systems agreed fairly well, with an $R^2$ value of 0.889 (figure A36). The average respiratory period was found to be 3.7±0.5 s (figure A35). The average respiratory period for all sessions measured, as calculated from the Anzai data, was found to be 3.6±0.6 s. The relatively low standard deviation indicates that breathing period was regular across the six breathing sessions despite them being split over two separate days.

*Subject 4*

When both the Anzai and RPM markers are placed at the umbilicus for subject 4 the coefficient of determination was found to be 0.913 (figure A37). At inspiration, the

Anzai signal leads and a time shift is introduced between the Anzai and RPM respiratory signal which is not present at exhalation (refer to figure A38). The average respiratory period was found to be 4.2±0.7 s. When both systems were relocated to midway between the xiphoid process and umbilicus, $R^2$ was found to be 0.810 (figure A40). The average breathing cycle was found to be 3.9±0.3 s (figure A39). A phase shift was between systems was measured at 100% inspiration of 0.3±0.1 s (Anzai leads). The coefficient of determination when both the RPM respiratory marker and the Anzai belt were placed at the xiphoid process was found to be 0.830 and the average respiratory cycle, 4.2±0.2s (figures A41 and A42).The Anzai signal was seen to lead slightly that from the RPM marker. When the Anzai belt was placed at the xiphoid process and the RPM marker placed at the umbilicus, the coefficient of determination was found to be 0.896 (figure A44) and the average respiratory period, 5.7 s±0.4 s. Despite signals being in-phase, mid-inhalation demonstrated a lag in the RPM signal behind that of the Anzai signal of up to 0.7±0.1 s (figure A43). The RPM system placed at the xiphoid process and the Anzai system positioned at the umbilicus resulted in an $R^2$ value of 0.860 and a phase shift was observed between signals of 0.2±0.1 s based on 100% inspiration values (Anzai signal leads). The mean respiratory cycle was found to be 5.4 s±0.5 s (figure A46). The RPM marker placed midway between xiphoid process and umbilicus and the Anzai placed at the umbilicus also resulted in a slight phase shift with a time lag evident on exhalation phases (figure A48). The value of $R^2$ calculated from linear regression was found to be 0.916 (figure A47) and the average respiratory cycle was found to be 5.9±0.5 s. The average respiratory cycle for subject 4 over six sessions was determined to be 4.9±0.9 s.

*Subject 5*

When the Anzai respiratory marker and the RPM respiratory marker were positioned at the umbilicus for subject 5 the signals appeared to respond to respiratory motion in unison (figure A49). The signals were found to correlate well with an $R^2$ value of 0.967 (figure A50). The average respiratory cycle was found to be 4.0±0.4 s. Once the RPM was positioned at the umbilicus and the Anzai was positioned at the xiphoid process, the coefficient of determination was reduced slightly to 0.945. Figure A51 shows the two signals to be in-phase; however the RPM signal displays sharper peaks. The average respiratory cycle was found to be 7.5±0.4 s. The RPM positioned at the xiphoid process

and the Anzai belt positioned at the umbilicus displayed a phase shift between signals obtained (refer to figure A53). The RPM signal at the xiphoid process was seen to respond to changes slower than the Anzai signal. The coefficient of determination was found to be 0.884 (figure A54) and the average respiratory period was found to be 6.9±0.5 s. The Anzai system placed at the umbilicus and the RPM system positioned midway between the umbilicus and xiphoid process produced a coefficient of determination of 0.896 (figure A56). The RPM signal placed midway between xiphoid process and umbilicus lagged slightly behind the Anzai signal placed at the umbilicus (0.2±0.1 s) (figure A55). The average respiratory cycle was found to be 5.3±1.2 s. The average respiratory cycle across the four waveforms measured was found to be 5.9±1.5 s. The respiratory period was seen to increase with time spent lying on the couch.

*Subject 6*

When both the Anzai belt with load cell and the RPM reflective marker were placed at the umbilicus for subject 6, the signals responded to respiration in unison (figure 2.13/A57) and the lissajous plot displayed a straight line (figure 2.14/A58). The coefficient of determination was found to be 0.981.The average respiratory cycle was found to be 6.3±0.4 s. When markers from both systems were relocated to midway between the xiphoid process and umbilicus, the value of $R^2$ was significantly reduced to 0.523(figure A64). A time lag was evident of the RPM system behind the Anzai system of 0.7±0.1 s determined from peak positions. Exhalation at this location was interpreted differently by the systems, the Anzai system displaying a sharp drop followed by short pulse, while the RPM decreased in amplitude more uniformly (figure A63). The average respiratory cycle was found to be 7.3±0.6 s. The Anzai system and the RPM marker both placed at the xiphoid process produced a correlation of determination between systems of 0.195 (figure A66). 100% inspiration peaks can be seen to agree reasonably well (figure A65) however upon exhalation, the Anzai signal drops almost vertically before a spike while the RPM system measures exhalation as a gradual decline. Baseline and amplitude discrepancies are evident between the two systems.

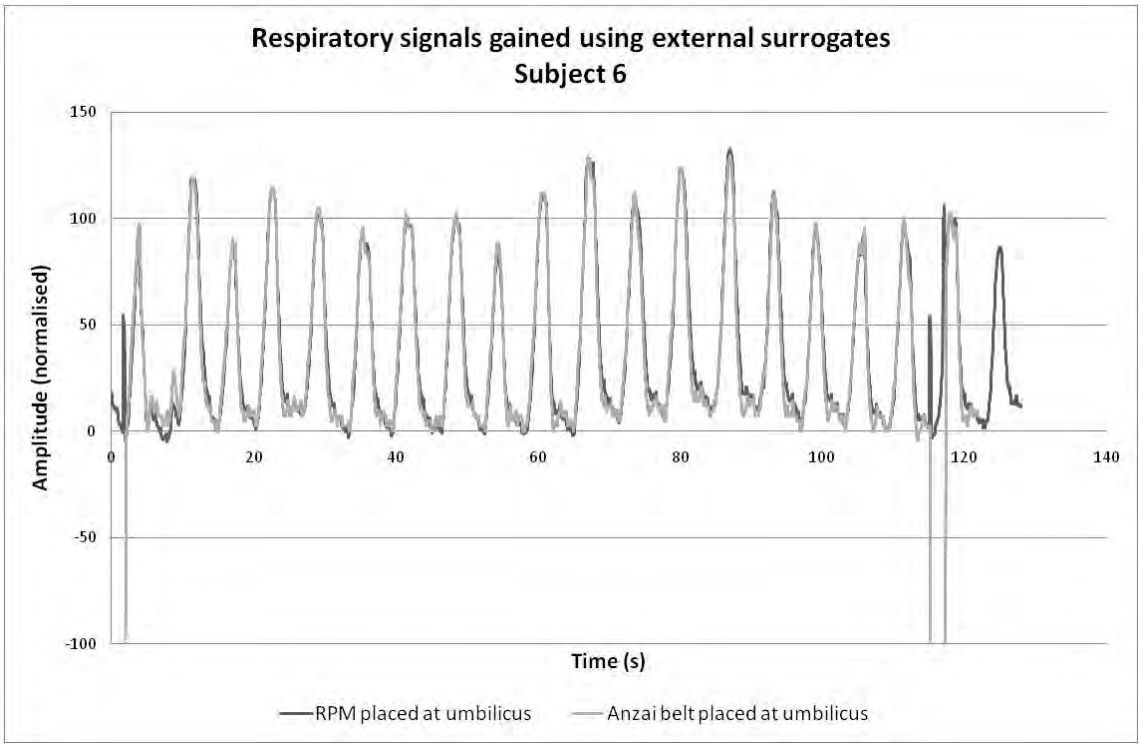


Figure 2.13: Respiratory signals gained using both RPM marker and Anzai belt positioned at umbilicus for subject 6. Motion is very similar and in phase.

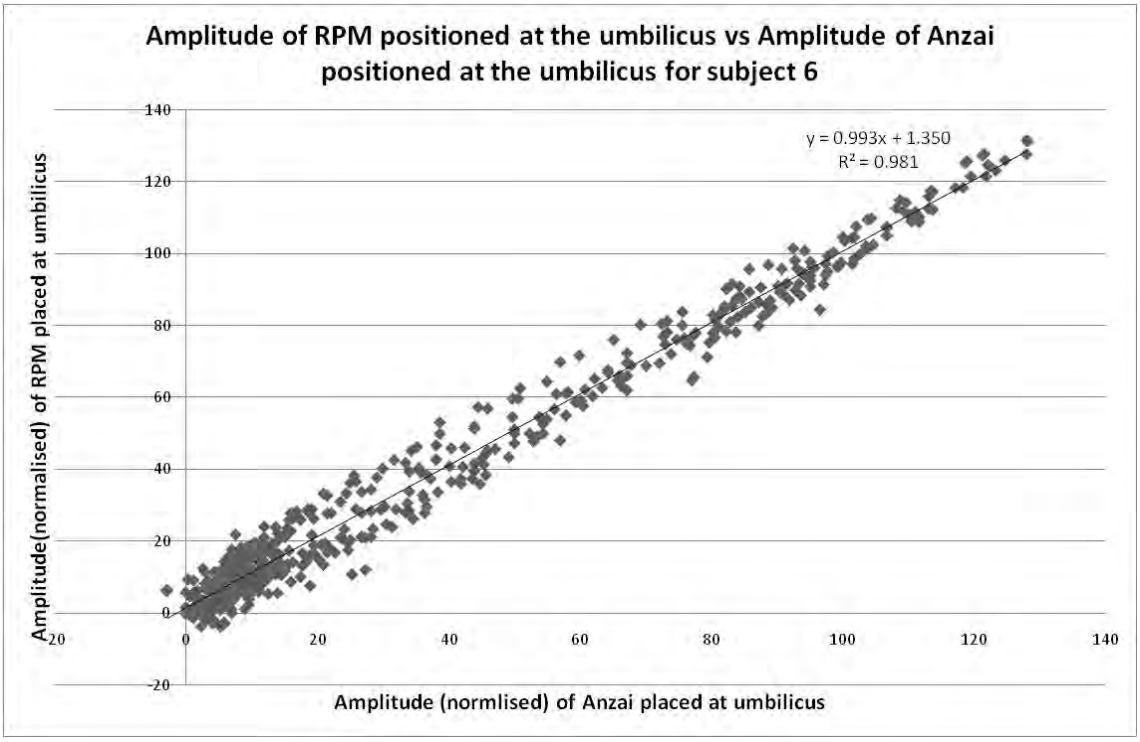


Figure 2.14: Determination of coefficient of determination for both RPM and Anzai positioned at umbilicus, subject 6.

The average respiratory signal was found to be 6.6±1.9 s. The RPM placed at the umbilicus and the Anzai placed at the xiphoid process resulted in an $R^2$ value of 0.523 (figure A60). Large discrepancies can be seen between the two systems in amplitude between 100% exhalation and 100% inhalation due to a secondary peak after the main breathing peak. There is also a lag in exhalation of the RPM signal placed at the umbilicus behind the xiphoid process. The average respiratory cycle was found to be 6.0±1.2 s. The large standard deviation also indicates changes in frequency across the sample. When the RPM marker was positioned at the xiphoid process and the Anzai marker was positioned at the umbilicus, the value of $R^2$ was found to be 0.408 (refer to figure A68). There were several outlying points observed on the lissajous plot. The signals respond differently to exhalation, the Anzai waveform drops steeply upon exhalation while the RPM signal shows a gradual decline. The average respiratory period was found to be 6.0±1.1 s. The signals obtained from the RPM retro-reflective marker placed midway between xiphoid process and umbilicus, and the Anzai belt with load cell placed at the umbilicus correlated well, with a coefficient of determination of 0.823 (figure A62). The average respiratory cycle was found to be 6.2±0.7 s (figure A61). Across the six sessions measured, the mean breathing cycle was found to be 6.4±0.5 s.

*Subject7*

The signals obtained from the Anzai marker and the RPM marker positioned at the umbilicus for subject 7 correlate well with an $R^2$ value of 0.918 (figure A70).Mid exhalation exhibits a lag of the RPM signal behind the Anzai signal of up to 0.9±0.1 s (figure A69). The average respiratory signal was found to be 8.9±3.4 s When both systems were relocated to midway between the xiphoid process and umbilicus the coefficient of determination between them was found to be reduced to 0.784 (figure A71). There is a lag of the RPM system behind the Anzai system at 100% inspiration of 0.3±0.1 s. The average respiratory signal was found to be 5.8±0.4 s. When both the Anzai and RPM systems were located at the xiphoid process, the signals showed reduced correlation; $R^2$ was found to be 0.516 (figure A74). The large spike in the data (figure A73) is reflected by outliers in figure A74. The average respiratory cycle was measured from the Anzai data to be 8.7±2.4 s. The large standard deviation indicates frequency modulations in the data set. The RPM retro-reflective marker placed at the

umbilicus and the Anzai belt positioned at the xiphoid process produced signals which when compared had a coefficient of determination of 0.624 (figure A76). Shifts in baseline reflected by the Real-time Position Management system were not mirrored by the Anzai system (figure A75). The average breathing period was found to be 6.2±1.8 s. When the RPM marker was positioned at the xiphoid process and the Anzai marker was positioned at the umbilicus an $R^2$ value between the two signals was found of 0.665 (figure A78). The large peak in the data was omitted from the determination of the coefficient of determination. The Anzai signal displays a shift in baseline of the respiratory waveform which was not measured by the RPM placed at the xiphoid process (figure A77). The average respiratory cycle was found to be 6.6±2.3 s. When the RPM marker was placed midway between umbilicus and xiphoid process and the Anzai was placed at the umbilicus a phase shift was observed between the signals (figure A79). The Anzai signal leads the RPM signal by 0.5±0.1 s at 100% inspiration. The value of $R^2$ found between signals was 0.817 (figure A80). The average respiratory cycle was found to be 7.2±1.4 s. Over the six sessions measured the mean breathing period was found from the Anzai system to be 7.2±1.3 s.

*Subject 8*

When both the Anzai and RPM markers were placed at the umbilicus for subject 8 the signals were found to correlate well, and a value of 0.912 was found for $R^2$(refer to figure A82).The average respiratory period was found to be 6.6±2.2 s using the Anzai respiratory waveform (figure A81). When both external surrogates were relocated to midway between the umbilicus and xiphoid process, the waveforms still correlated reasonably well and a coefficient of determination was found of 0.899 (figure A84). The RPM signal peaks were found to lag 0.4±0.2 s behind the Anzai peaks (figure A83). The average respiratory period was found to be 8.0±1.0 s. When both markers were relocated to the xiphoid process, signals obtained from the Anzai and the RPM markers were found to correlate reasonably well. The coefficient of determination was calculated to be 0.897 (figure A86). The average respiratory period was found to be 5.7±0.7 s.When the RPM retro-reflective marker was positioned at the umbilicus and the Anzai was placed at the xiphoid process a phase shift was observed between systems (figure A87). At 100% inspiration this resulted in a time lag of 0.6±0.3 s of the RPM signal behind the Anzai signal. Discrepancies were observed between systems for maximum

amplitude values. The coefficient of determination between the waveforms obtained by the two systems was found to be 0.676 (figure A88). The average breathing cycle was found to be 6.6±2.2 s. When the RPM was positioned at the xiphoid process and the Anzai marker was positioned at the umbilicus an $R^2$ value between signals was found of 0.737 (figure A90). Signals appeared to agree well on inhalation however a time lag of the RPM signal behind the Anzai signal was present on exhalation (figure A89). The average respiratory cycle was found to be 5.4±1.2 s. The signals obtained when the Anzai system was placed at the umbilicus and the RPM system was positioned midway between the xiphoid process and umbilicus correlated well (figure A92) The coefficient of determination was discovered to be 0.955. The average respiratory period was found to be 4.6±0.9 s from the Anzai signal (figure A91). Over the six sessions measured the mean breathing period was found to be 6.2±1.2 s.

*Subject 9*

The signals obtained from the Anzai and RPM respiratory gating systems when markers were placed at the umbilicus were found to correlate well (figure A93). A coefficient of determination between systems was found of 0.949 (figure A94). The average respiratory cycle was found to be 7.8±1.3 s. Both external markers were relocated to midway between xiphoid process and umbilicus and the signals were found to agree well with an $R^2$ value of 0.934 (figure A96). The average respiratory period for both markers placed midway between the xiphoid process and umbilicus was found to be 9.5±1.3 s (figure A95). The RPM retro-reflective marker and the Anzai belt located at the xiphoid process produced signals that had a coefficient of determination of 0.774 (refer to figure A98). The Anzai waveform demonstrated steeper gradients on both inhale and exhale (figure A97) than the RPM signal and there was a noticeable difference in waveform shape. The average respiratory period, determined from the Anzai waveform, was found to be 14.9±1.2 s. When the RPM marker was placed at the umbilicus and the Anzai marker was placed at the xiphoid process, the signals correlated well. A coefficient of determination was found between the signals of 0.911 (figure A100). Inhalation phase demonstrated a lag of the RPM signal behind the Anzai signal, however peaks and troughs from the two respiratory systems agreed well (figure A99). The average respiratory period was found to be 15.4±1.6 s. When the RPM marker was relocated to the xiphoid process, and the Anzai marker positioned at the

umbilicus the waveforms generated from the two gating systems correlated well with a coefficient of determination of 0.936 (figure A102). A slight phase shift was observed between the signals; at 100% inspiration a lag of the RPM system behind the Anzai of 0.4±0.2 s was measured (figure A101). The average respiratory cycle was found to be 13.2±3.2 s. The Anzai marker located at the umbilicus and the RPM marker located midway between umbilicus and xiphoid process also produced signals which correlated well with an $R^2$ value of 0.960 (figure A104). Exhalation phases determined by the RPM system demonstrated a lag behind the Anzai system (figure A103). The average breathing period was found to be 18.0 s ±1.9 s. The average breathing period across the six sessions was found to be 13.1±3.8 s. The large standard deviation is indicative of the fact that the breathing period increased gradually over time while the subject was lying on the couch.

*Subject 10*

The signals obtained from the Anzai respiratory gating system and the RPM system when external markers were placed at the umbilicus for subject 10 correlated well, having a coefficient of determination of 0.944 (figure A106). The average respiratory period was found to be 6.2±1.0 s. When both external surrogates were relocated to midway between the xiphoid process and umbilicus, the coefficient of determination between signals was reduced to 0.805 (figure A108). The large breathing irregularity which resulted in a sharp spike in the data (figure A107) was omitted from the determination of $R^2$. Large irregularities such as this would be omitted from any data used for gating by the software. The average respiratory cycle was found to be 5.1±1.3 s. When both the Anzai and the RPM markers were relocated to the xiphoid process a phase shift was observed between the Anzai and RPM signals. A time lag of the RPM signal behind the Anzai signal was found of 0.3±0.1 s at 100% inspiration. The coefficient of determination between systems was found to be 0.816 (figure A109). The average respiratory period was found to be 6.5±1.3 s (figure A110). When the Anzai system was placed at the xiphoid process and the RPM retro-reflective marker placed at the umbilicus, a coefficient of determination between signals was found to be 0.806 (figure A112). Irregularities can be seen throughout the data due to the subject speaking while measurements were being taken (figure A111). The average respiratory period was found to be 4.8±1.4 s. When the Anzai marker was placed at the umbilicus and the

RPM marker was positioned at the xiphoid process, the signals from the two systems can be seen to agree very well, and $R^2$ was determined to be 0.924 (figure A114). Figure A113 shows a loss of signal for the RPM system at 57.5 s. Information utilised for the regression curve was only after the signal was regained. The average respiratory signal was found to be 5.0 s±2.0 s. When the Anzai was placed at the umbilicus and the RPM marker was placed midway between the umbilicus and xiphoid process, the signals were observed correlate well. The $R^2$ value obtained between signals was 0.938 (figure A116). The average respiratory cycle was found to be 5.2±1.0 s. The mean breathing period across all sessions measured for subject 10 was found to be 5.5±0.7 s.

*Subject 11*

When both the Anzai marker and the RPM marker were positioned at the umbilicus, the signals obtained from the respiratory gating systems correlate well and an coefficient of determination between signals was found of 0.984 (figure A118). The average respiratory period was found to be 4.3±0.2 s. When both external surrogates were relocated to midway between xiphoid process and abdomen the signals appeared to agree well (figure A119). The value of $R^2$ between systems was discovered to be 0.852 (figure A120). Irregular breathing may have contributed to the reduced correlation coefficient here. The average respiratory cycle, as determined from the Anzai system, was found to be 4.1±0.5 s. A phase shift was observed between systems when both were positioned at the xiphoid process (figure A121). At 100% inspiration the RPM signal lagged behind the Anzai signal by 0.3±0.1 s. The coefficient of determination found between both systems located at the xiphoid process was 0.735 (figure A122). The mean breathing cycle was found to be 3.6±0.5 s. When the RPM was positioned at the umbilicus and the Anzai was placed at the xiphoid process, the signals did not correlate well and the waveform appeared erratic (figure A123). The $R^2$ value found between the Anzai and RPM was 0.345 (figure A124). The average respiratory cycle here was found to be 4.2±1.1 s. The RPM marker positioned at the xiphoid process and the Anzai external marker positioned at the umbilicus demonstrated a phase shift between signals (figure A125). The RPM signal lagged behind the Anzai signal by 0.3±0.1 s at 100% inspiration. The $R^2$ value determined between systems was 0.788 (figure A126). The average respiratory cycle was found to be 4.0±0.7 s. When the Anzai belt was placed at the umbilicus and the RPM retro-reflective marker was placed midway between the umbilicus and xiphoid process, the signals were observed to

correlate well and a coefficient of determination between signals of 0.910 was found (figure A129). The mean respiratory period was found to be 4.0±0.3 s. The average respiratory period, as determined by the Anzai waveform, over all six sessions measured was found to be 4.0±0.3 s

*Subject 12*

The respiratory waveforms measured simultaneously from both the Anzai and RPM systems when positioned at the umbilicus agree well (figure A129). The frequency of data sampling for the RPM system was adjusted automatically in this session which resulted in larger bins for determination of the correlation coefficient. The value of $R^2$ was found to be 0.917 (figure A130). The mean breathing cycle was found to be 3.2±0.5 s. The signals gained from both the Anzai and the RPM markers when placed midway between xiphoid process and umbilicus correlate well. The coefficient of determination between the signals was found to be 0.896 (figure A132). The mean respiratory period was found to be 3.6±0.5 s (figure A131). The Anzai belt and the RPM retro-reflective marker positioned at the xiphoid process resulted in a reduced correlation between signals. The value of $R^2$ was found to be 0.610 and shifts in baseline and frequency were observed (figure A133). The mean respiratory period at this location was found to be 3.7±0.4 s. When the RPM retro-reflective marker was positioned at the umbilicus and the Anzai was placed at the xiphoid process, the breathing cycle appeared erratic and an $R^2$ value was found between signals of 0.501 (figure A136). The mean respiratory period was found to be 3.6±0.6 s. Similarly, when the RPM system was placed at the xiphoid process and the Anzai marker was placed at the umbilicus a reduced correlation between signals was observed, and an $R^2$ value was found of 0.633 (figure A138). The mean breathing period, as determined from the Anzai waveform at this location was found to be 3.7±0.7 s. The respiratory signals obtained from subject 12 when the RPM marker was positioned midway between umbilicus and xiphoid process and the Anzai belt placed at the umbilicus did not correlate well. Initially, the RPM signal is observed to lag behind the Anzai signal (figure A139). At the 50 s mark, the signals begin to agree well, while at 100 s the Anzai signal is lagging behind the RPM signal. The mean respiratory period at this location as determined from the Anzai signal was 3.7±0.5 s. The subject's breathing period did not significantly alter throughout the

six sessions, and the mean respiratory period across the sessions was found to be 3.6 ±0.2 s.

*Subject 13*

The waveforms obtained from the two respiratory gating systems when both the Anzai and RPM external markers were positioned at the umbilicus agreed well (figure A140). The coefficient of determination found between the Anzai and RPM systems was 0.879 (figure A141). The large peak observed in the centre of the dataset was omitted from calculation of $R^2$. The average respiratory waveform was found to be 5.4±0.9 s.When both systems were relocated to midway between the umbilicus and xiphoid process, a phase shift was observed between signals (figure A142). At 100% inspiration, a lag of 0.4±0.2 s was observed of the RPM signal behind the Anzai signal. The coefficient of determination between signals was found to be 0.645 (figure A143). The mean respiratory period was found to be 5.6±2.3 s. When both external markers were relocated to the xiphoid process the correlation between signals was further reduced. The coefficient of determination between the Anzai and RPM signals when located at the xiphoid process was found to be 0.519 (figure 2.17/A145). A phase shift between signals was observed; at 100% inspiration the RPM system lagged behind the Anzai signal 0.4±0.2 s (figure 2.16/A144). Inhalation phases were observed to agree better than exhalation. The mean breathing period was found to be 5.9±1.2 s The RPM retro-reflective marker positioned at the umbilicus and the Anzai marker positioned at the xiphoid process produced signals which correlated well (figure A146). $R^2$ was found to be 0.847 (figure A147). The mean respiratory period was found to be 5.3±0.8 s. When the RPM marker was positioned at the xiphoid process and the Anzai marker was positioned at the umbilicus a slight phase shift was observed between the Anzai and RPM signal (figure A148). The coefficient of determination found between signals was 0.815 (figure A148). The mean respiratory period was found to be 5.7±1.0 s. When the Anzai external surrogate was placed at the umbilicus and the RPM marker was placed midway between xiphoid process and umbilicus, the signals also correlated well. $R^2$between the Anzai and RPM signal was found to be 0.851 (figure A151).

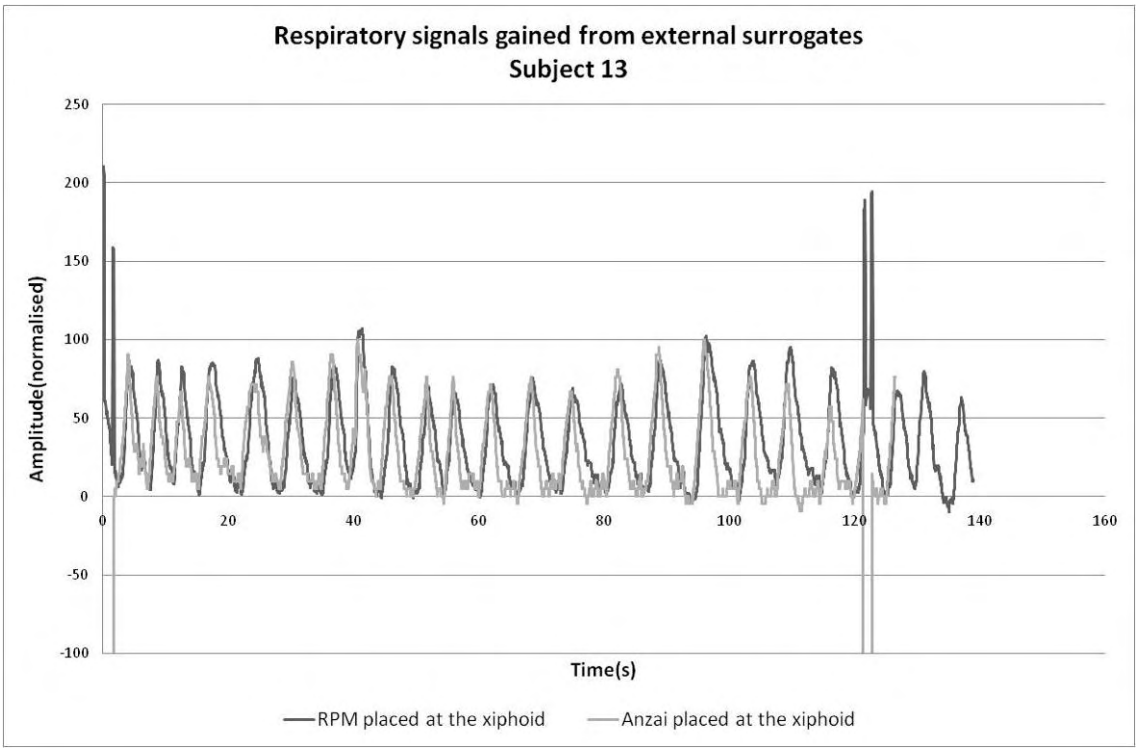


Figure 2.16: Respiratory signals gained using both RPM marker and Anzai belt positioned at xiphoid for subject 13. Signals agree better on inhalation than exhalation.

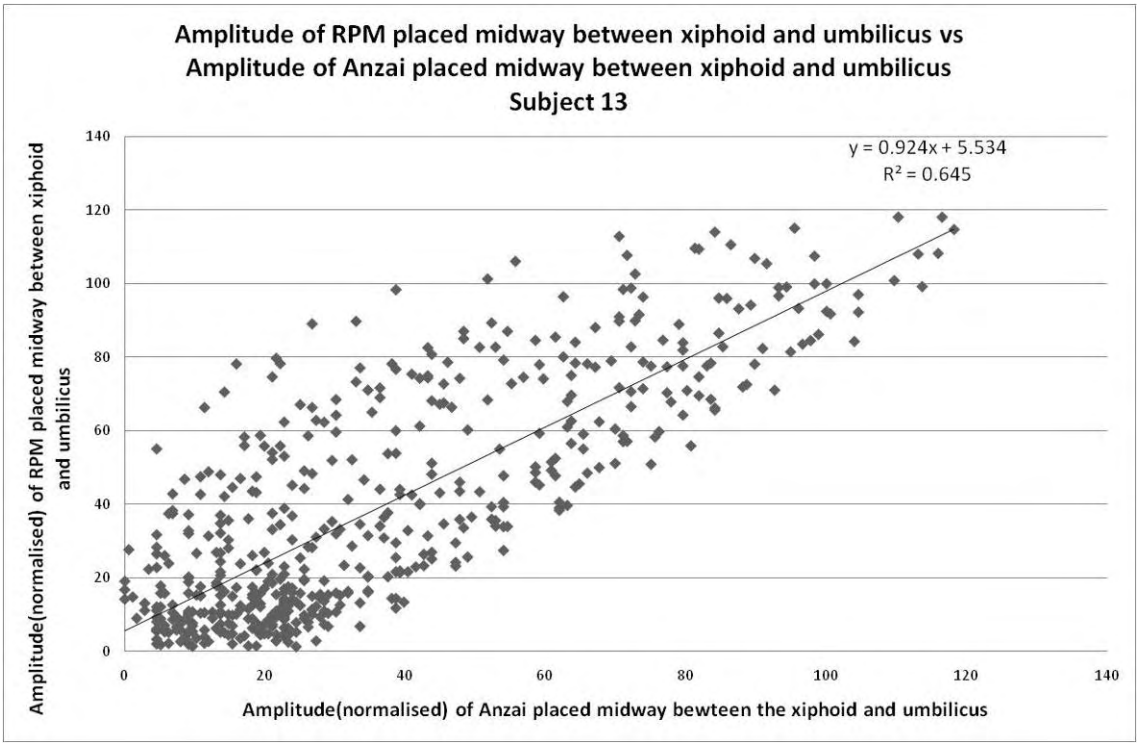


Figure 2.17: Determination of coefficient of determination for both RPM and Anzai positioned midway between xiphoid and umbilicus, subject 13.

The Anzai signal was observed to lead slightly the RPM signal. The mean respiratory period was found to be 5.3±0.9 s. The subject's breathing period varied very little over sessions, the mean period was found to be 5.5±0.2 s.

*Subject 14*

Both the Anzai and RPM systems positioned at the umbilicus for subject 14 produced a coefficient of determination between signals of 0.844 (figure 153). Shifts in baseline contributed to the reduced agreement between signals here (figure A152). The mean respiratory period was found to be 3.0±0.4 s. When both the Anzai and RPM marker were relocated to the xiphoid process the correlation between signals was significantly reduced. $R^2$was found to be 0.414 (figure A155). The Anzai signal here was small which meant limited values upon normalisation and large shifts in baseline were observed (figure A154). The average breathing period was found to be 2.9±0.3 s. The Anzai retro-reflective marker and the RPM marker positioned midway between the xiphoid process and umbilicus produced signals which were in phase (figure A156). Responses of the two external surrogates to shifts in baseline and maximum amplitude led to a $R^2$ value between signals of 0.830 (figure A157). The mean respiratory cycle was found to be 3.0±0.6 s. The Anzai external marker positioned at the umbilicus and the RPM marker positioned at the xiphoid process led to a coefficient of determination between signals of 0.854 (figure A159). The mean breathing period was found to be 2.7±0.3 s (figure A158). The Anzai belt and load cell placed at the xiphoid process and the RPM marker placed midway between the umbilicus and xiphoid process produced an $R^2$ value between signals of 0.735 (figure A161). Outliers caused by the large spike in the breathing waveform (figure A160) contributed to the reduced correlation. If the large spike in the data is removed the coefficient of determination between signals is improved to 0.839. The Anzai marker positioned at the xiphoid process and the RPM marker placed at the umbilicus produced signals which appeared to not correlate at all (figure 162). This can be attributed to the lack of breathing signal and high signal-to-noise measured by the Anzai system at the xiphoid process for this subject. The mean breathing period, as measured by the RPM system, at this location was found to be 3.0±0.4 s. The average respiratory period, across all six sessions, for subject 14 was found to be 3.0±0.2 s.

*Subject 15*

The Anzai external respiratory marker and the RPM external respiratory marker positioned at the umbilicus for subject 15 produced signals which correlated well (figure A163). The coefficient of determination between signals was found to be 0.930 (figure A164). The mean respiratory cycle was found to be 3.1±0.3 s. When the RPM and Anzai markers were relocated to midway between the xiphoid process and umbilicus, the coefficient of determination was reduced to 0.804 (figure A166).The average respiratory period was found to be 2.9±0.2 s. When both the RPM and Anzai external markers were positioned at the xiphoid process, a phase shift was observed between signals. At 100% inspiration, there was a lag of the RPM signal behind the Anzai signal of 0.5±0.1 s. The coefficient of determination was found to be 0.494(figure A168). The average respiratory period was found to be 3.5±0.2 s. The average respiratory period over the three sessions measured was 3.2±0.3 s

## 2.4 Discussion

The signals obtained from the two respiratory gating systems were found to agree best when external markers were both positioned at the umbilicus (mean $R^2$=0.925). Signals from the two systems measuring respiratory waveforms simultaneously were in-phase, and Lissajous plots displayed a straight line. The high $R^2$ value was expected and agreed with data from Li et al (2006), who found the two gating systems to correlate between 98.2-99.6%. The largest amplitude signal in both the RPM and Anzai cases was from the umbilicus, giving a higher signal-to-noise ratio. This larger amplitude at this location agreed with data from Beddar et al (2007) and Kleshneva (2006) who suggested that the positioning of the belt in the cranial-caudal direction is directly related to the quality of the signal and that the optimum position of the sensor is 7-8 cm below the end of the xiphoid process. The study by Chi et al (2006) also suggested that the marker placed at the umbilicus correlated best with diaphragm motion.

The coefficient of determination between the Anzai and RPM signal was reduced when both markers were positioned midway between xiphoid process and umbilicus (mean $R^2$=0.787). Phase shifts greater than 0.3 s between the Anzai and RPM signals were

measured in 6 of the 15 subjects at this location. A phase shift introduced between the signal used for planning and that used for gating the linear accelerator will be detrimental to patient treatment. Variations in tumour motion not accounted for when designing the gating window will impact the dose coverage of the tumour. Figure 2.18 shows data from subject 15 (both markers positioned at the umbilicus) where a phase shift was present between signals of 0.5±0.1 s. The division of the respiratory cycle by the Anzai system is shown. Inspiration and exhalation are divided into 10 phases each (20% intervals are shown). Expiration phases are larger than those for inspiration due to the larger portion of the breathing cycle taken up by expiration.

The planned treatment based on the images gained from the Anzai 4D CT in this case is from 70% exhale to 30% inhale as indicated by the light grey bar (duty cycle of 30%). During treatment, if the external marker is placed in an identical location, the RPM signal demonstrates a time lag behind the Anzai signal used for planning. 30% inhale using the RPM signal (65% RPM phase due to phase definition between 0-100percent of cycle) corresponds to including the 60% inspiration phase on the Anzai signal.

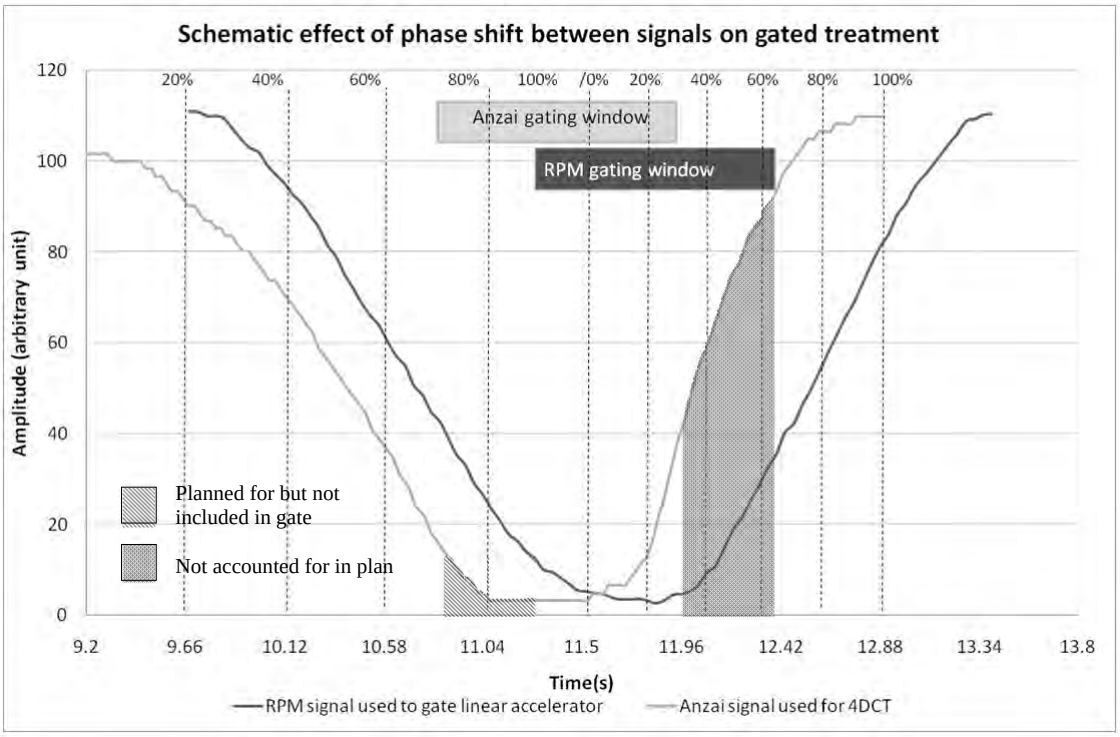


Figure 2.18: The effect of phase shift between signals on gated treatment: subject 15, both markers at xiphoid process, 0.5 s phase shift, and 3.5 s period. Ten phases used for 4DCT are shown. The gating is for a 30% duty cycle between 35-75%. The light and dark grey bars indicate the gating windows for the Anzai and RPM systems respectively based on the respiratory waveform obtained.

Treatment of the Anzai 60% inspiration phase which was not included in planning would occur in this situation. A reduction in the CTV to PTV margin due to confidence in gating technology in this instance may lead to potentially irradiating healthy tissue and under-treating the target volume (Ionascu 2007).

The agreement between signals was reduced further when both the Anzai and RPM external surrogates were positioned at the xiphoid process (mean $R^2$=0.611). Phase shifts were observed between data sets of up to 0.5±0.1 s. Physiological irregularities, low amplitude peaks caused by heartbeat, distortion and loss of signal were all observed at this location. At the xiphoid process, these irregularities are accentuated due to the smaller signal. This was noted by Kleshneva et al (2006) who found that if the external surrogate was placed superior to the end of the xiphoid process a low signal-to-noise would result, and the amplitude of respiratory peaks in cases greater than 9 cm superior were comparable with heartbeat peaks. The volunteer staff cohort used as subjects were all healthy, with good compliance and it would be expected that correlation would be further reduced for patients with breathing difficulties. Liu et al (2007) noted that due to the influence of lung tumours and the co-existence of pulmonary disease, lung cancer patients were likely to have altered breathing patterns to compensate for the loss of pulmonary function.

The Anzai signal was found to lead on all occasions where a phase shift was observed. When markers are positioned in the same location, this can only be attributed to the monitoring method. In the Anzai system, the load cell is enclosed in an elastic belt fastened around the patient's abdomen or chest. Pressure is exerted from belt expansion, be it transverse or AP motion. The lack of phase shift observed at the umbilicus indicates that, at this location, the majority of movement caused by respiration is in the anterior-posterior direction. The phase shifts between systems observed midway between the umbilicus and xiphoid process, and at the xiphoid process indicates that chest wall expansion at these locations contains both transverse and anterior-posterior motion and that a phase shift may exist between transverse and dorsoventral movements. For example, if the chest began expanding laterally before rising then it would be expected that the Anzai system would respond first, and a lag would be observed between the two systems.

When external markers were positioned at separate locations, results varied across subjects (coefficient of determination values between signals ranging from 0.401-0.965). Due to the nature of the sensors, phase shifts related to chest wall expansion and phase shifts introduced by a difference in thoracic and abdominal movement are difficult to distinguish. Subject 8 is an example where a phase shift is present between abdomen and thorax. When markers were placed in the same location, coefficient of determination values ranged from 0.897-0.912. When the Anzai external marker was placed at the xiphoid process and the RPM marker was placed at the umbilicus, the coefficient of determination was reduced to 0.676 and a phase shift was observed of 0.6±0.1 s. The Anzai signal at the xiphoid process led the RPM at the umbilicus. When the Anzai belt was positioned at the umbilicus and the RPM marker was positioned at the xiphoid process, the coefficient of determination was found to be 0.737. The signal from the RPM marker placed at the xiphoid process now appears in unison with the Anzai signal. A shift between thorax and abdomen was expected and concurs with results gained by Chi et al (2007) and Killoran et al (2008).

Breathing periods were found to range from 2.6 s-18 s. The average respiratory period was found to be 5.7±2.6 s. The average period was longer than expected, however this could be attributed to the sample which were all healthy volunteers. The average respiratory cycle found by Lu et al was 4.6 s (2006). Periods were found to be patient-specific and did not alter greatly inter or intra-fraction for the majority of subjects as indicated by the small standard deviations in the mean breathing cycle length (table 2.2). The breathing periods increased noticeably with time spent lying on the couch for three of the fifteen subjects indicating that allowing time for the breathing waveform to regulate before 4D CT may be beneficial. Waveforms such as those obtained from subject 2 in figure A23 would not be ideal candidates for respiratory gating as the irregular breathing pattern may cause binning artifacts in 4D CT.

The Anzai AZ-733V system is only capable of phase-gating thus amplitude variations were not addressed in this work. Variations in inspiration and expiration amplitudes between systems and locations were apparent in the waveforms measured, regardless of if the signals were in phase. Graphs such as figure A21 which have a lag in exhalation but not inspiration, and where the peaks and troughs are aligned would not be effected by phase gating however would be greatly affected by amplitude gating (an amplitude

of 40 (normalised) at mid-exhalation had a maximum time lag of 2.8 s here). This is 44% of the breathing cycle.

It is recommended, based on the results obtained in this thesis, that if the Anzai respiratory gating system be used for planning, and the RPM system used for gated treatment at the Illawarra Cancer Care Centre, that the external surrogate used to monitor respiratory motion be positioned only at the umbilicus. Placement of the external marker at this location does not ensure reproducibility of breathing traces, nor that internal and external motion correlate; it ensures errors due to variations in the marker position are not introduced.

This work has further implications to external marker positioning. Experimental results concur with Chi et al (2006) that a phase shift is introduced depending on the location of the external marker. The phase shift between internal tumour motion and external surrogate motion therefore may not only be dependent on viscoelastic properties of the lung and the position of the tumour, but also directly influenced by external set-up. Further work is needed to determine the adequacy of external surrogates to model internal tumour movement.

# CHAPTER III
# ARTIFACTS IN 4D CT

## 3.1 Introduction

Artifacts result in the spatial extent of a moving object becoming altered from its true shape and location. The density of the reconstructed object becomes altered from that derived under motionless conditions and the densities of surrounding structures can also become distorted from their true values (Gagne et al 2004). To understand the origin of artifacts in computed tomography, we can consider a stationary sphere, radius R, centred at (x=A, y=B, z=k from z slice) (refer to figure 3.1).

At the moment of acquisition, at a given table index and time, the scan plane will intersect the sphere and numerous projections of the static object containing transmission data will be obtained. These projections can then be represented in

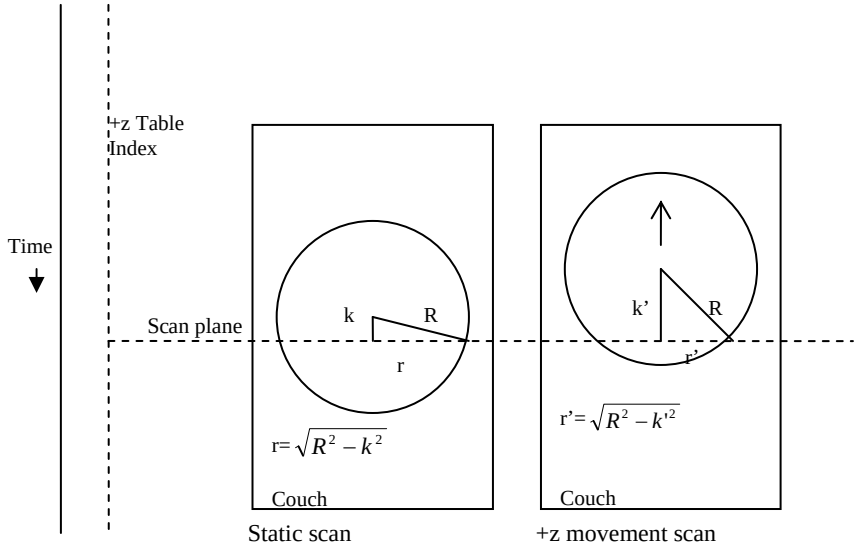


Figure 3.1 Schematic representation of scanning simulation: a sphere of radius R is scanned at a distance k from the sphere centre determined from the table index. An image is produced of radius r (Chen et al 2004).

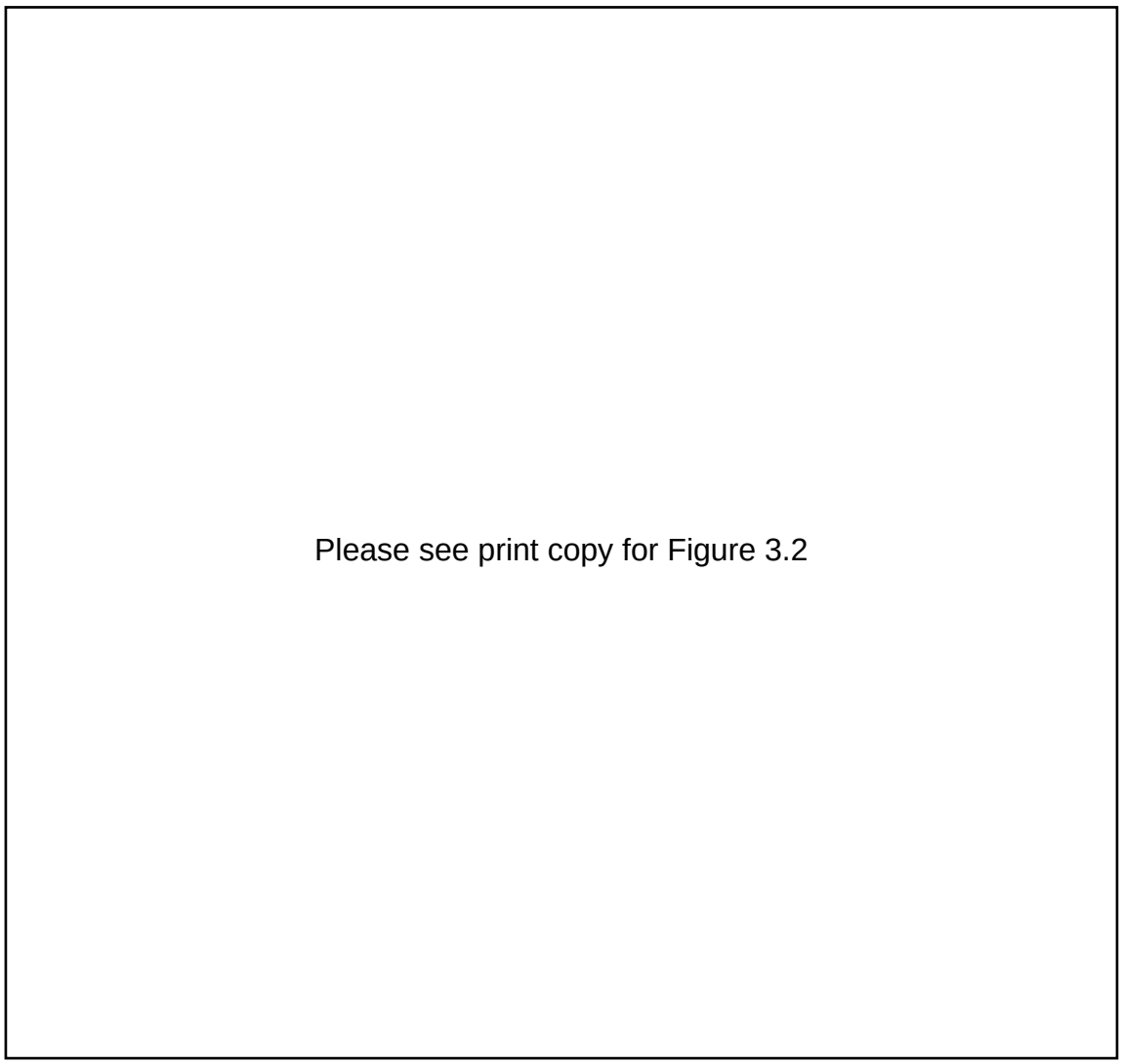


Figure 3.2: Reconstruction illustrated (A) Sinogram for the static sphere (B) Projections through a specific point of the static sphere. (C) Filtered backprojection image (FBP) for static sphere. (D) Sinogram for sphere moving orthogonal to the imaging plane (E) Simple backprojection image for sphere moving orthogonal to imaging plane. (F) FBP image for orthogonal movement. (G) Sinogram of sphere moving in the imaging plane (H) Projections through a specific point blurred due to motion in image plane. (I) FBP for motion in image plane with total volume occupied marked by white line (J) Sinogram for a combination of orthogonal and in plane motion (K) BP image for motion in both planes (L) FBP image for motion in both orthogonal and image planes (Gagne et al 2004).

sinogram format where each horizontal line represents the projection data from a distinct projection angle. Due to the spherical shape, each projection line in this case will be identical (see Figure 3.2(A)). The locus of all line integrals passing through a specific point within the object's cross section in the image space traces out a cosine curve in sinogram space due to the rotational nature of the CT data acquisition. Reconstruction from backprojections is a linear process that results in a blurred image

of the object. Filtering the data prior to reconstruction with a modified ramp filter, filtered backprojection, results in an image that maintains the object's attenuation and geometric properties. This can be seen in figure 3.2(C). The resulting image has a diameter, r which can be calculated from the radius of the object and the table index. The cross section of the sphere exhibits a uniform unit density while the surrounding area displays a uniform density of 0.

If the unit density sphere now moves orthogonally to the imaging plane during acquisition, as shown in Figure 3.1, to a higher z co-ordinate, k', a different intersection of imaging plane and sphere will result. The value, k', could be expressed as:

$$k' = k + A_0 \sin(\omega t + \phi), \quad (3.1)$$

where k is the table index for the static condition, $A_0$ is the amplitude of sphere motion, $\phi$ is phase angle, t is time, indexed to table position and $\omega = 2\pi f$ (Chen et al 2004).

If acquiring an image were instantaneous, then this would result simply in the smaller cross section of r' being represented at the table index which should correspond to r if the sphere were stationary. This would mean that although slices were in the wrong position, and a sphere would not be reconstructed, axial slices would still exhibit radial symmetry and thus appear as perfect circles. Using the principles of 4D CT if this were the case, no artifacts would be expected if the phases were chosen and reconstructed correctly. Gantry rotation time in helical CT however means image acquisition is not instantaneous thus the object's cross section present in the imaging plane will vary during image acquisition and the width and intensity of the sinogram's projection will change accordingly. Profiles through the mean position of the object in the imaging plane will no longer retain the radial symmetry associated with the static object (Gagne 2004). Artifacts will be produced due to the partial projection effect; each beam angle making up an entire projection will produce a line of slightly different width as it intersects with a smaller or larger part of the sphere depending on the cross section present at a specific instant as it moves through the imaging plane. This can be seen in Figure 3.2(D). Figures 3.2(E) and 3.2(F) are images produced by Gagne et al using a MATLAB simulation of a moving object applying a backprojection and filtered backprojection algorithm respectively. The artifacts can be readily observed through a comparison of Figures 3.2(C) and 3.2(F). The background of the latter image no longer

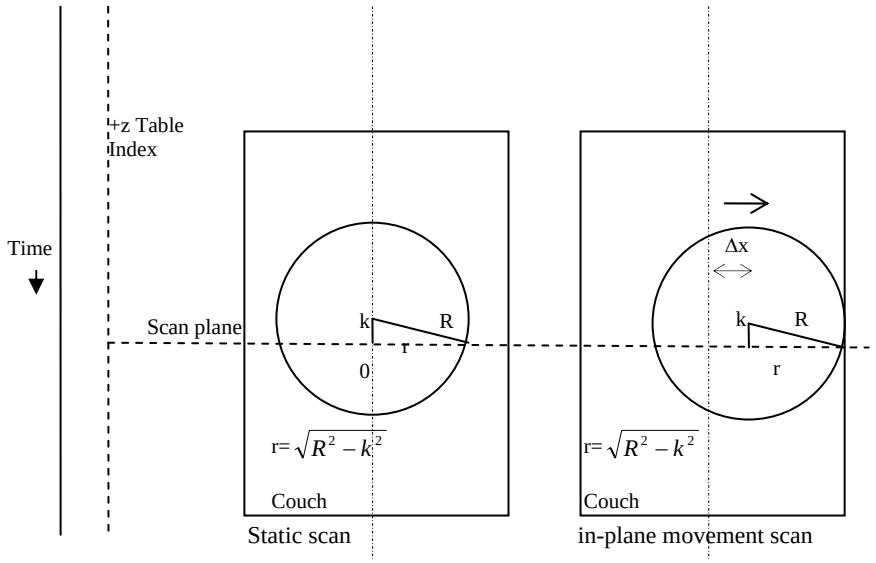


Figure 3.3 Schematic representation of scanning simulation: A sphere is scanned with in-plane motion.

exhibits a density of 0, and the sphere is not homogeneous as it was in 3.2(C). Orthogonal movement to the imaging plane also produces a helical artifact in the sphere due to the variation in cross section over one gantry rotation.

While width and intensity variations in the sinogram are produced by orthogonal motion, positional shifts are created by in-plane motion. Consider the sphere in Figure 3.3 which moves linearly along the horizontal axis of the imaging plane from 0 to x.

Each projection in sinogram space will maintain its original profile but will be shifted in position (see figure 3.2(G) and 3.2(H)). A sine curve will no longer be produced as a result of the locus of all line integrals passing through a point in the objects cross section. The shape will be dependent on the form and extent of motion captured during image acquisition (Gagne et al 2004). In plane motion will also lead to a redistribution of the blurred image density and a redistribution of the filter resulting in a partial sharpening of the motion artifact pattern (refer to figure 3.2 (I)). This produces variations in density in the cross sectional area encompassed by the object's movement.

Lung tumour movement is not confined to simply orthogonal or in-plane motion and consists of a combination of the two. Figures 3.2(J), 3.2(K) and 3.2(L) demonstrate combined in-plane and orthogonal motion for a unit density sphere. The change in

width of the sinogram is due to the orthogonal movement and the positional shifts are due to in-plane movement. The resulting filtered image, figure 3.2(L), lacks the symmetry observed with individual components of motion, and the space surrounding the object exhibits density heterogeneity which is not present in the original static image.

4D CT aims to rectify the problem of artifacts caused by movement through sorting respiratory data into bins corresponding to respiratory phases and reconstructing based on phase (refer to Figure 3.4). This abates the problem of large positioning errors such as those in figure 3.1.1 but doesn't compensate for slice acquisition time, and movement intra-phase. Acquired CT images are also sorted using a nearest-neighbour approach (Ehrhardt et al 2007) which introduces reconstruction artifacts if there are not data segments available for the same respiratory state for each couch position. Variation in breathing amplitude between respiratory cycles is another cause of artifacts in 4D CT as trajectory and periodicity irregularities of respiratory induced organ motion can produce uncertainties in phase correlation between images acquired at a distinct time. 100% of gated scans contain motion artifacts (Keall 2007).

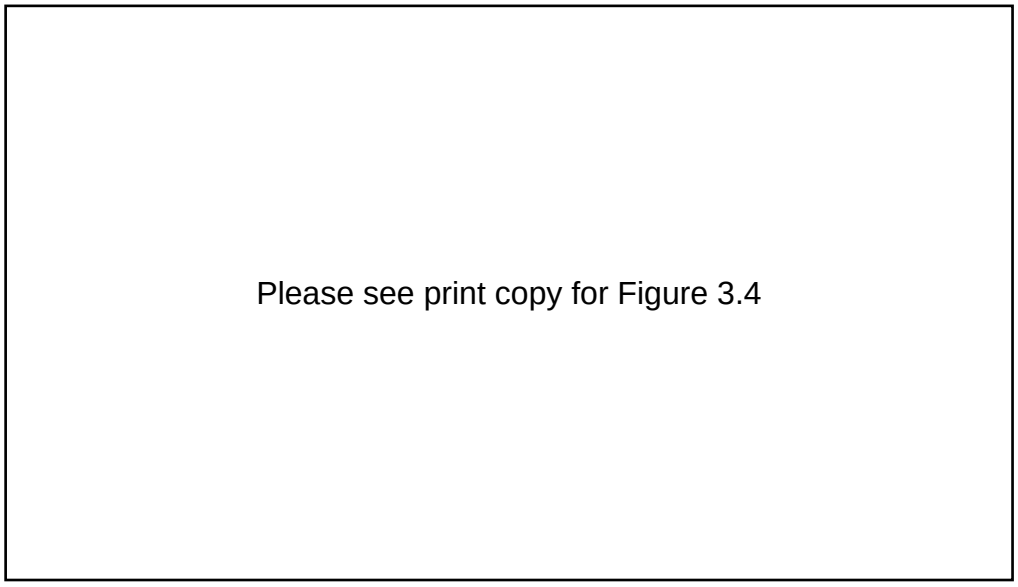


Figure 3.4. 4D CT phase sorting. The breathing cycle is divided into bins into which images are sorted depending on the phase of the breathing cycle they are acquired (Vedam et al 2003).

## 3.2 Aim

The aim of the following experiment is to observe artifacts in gated 4D CT images and discover if a relationship exists between artifact severity and duration of breathing cycle, amplitude of movement, size or density of object. To compare artifacts obtained in non-gated images to those obtained in gated studies and determine optimum scan parameters, if any.

## 3.3 Materials

### 3.3.1 Siemens Sensation Open CT scanner

The Siemens Somatom Sensation Open is a third-generation 20 slice CT scanner. It has a maximum gantry rotation time of 0.5 s and a gantry aperture of 82 cm (Keat 2005). The Sensation Open contains a Straton™ X-ray tube and has a 52.1 degree fan angle. When coupled with the Anzai AZ-733V respiratory gating system the CT scanner can operate in helical or sequential mode.

During helical (or spiral) CT the patient is simultaneously transported at a constant speed through the rotating x-ray beam (refer to figure 3.5). X-rays are emitted at several angles and the attenuation profile measured. Each profile measured is not just at a separate angle but also at a different longitudinal position (Hui 1999). The duty cycle in helical CT mode is 100%. Once the scan is acquired, the Anzai respiratory gating system allows all phases of data to be retrospectively reconstructed and the patient is not affected by the number of respiratory phases to be reconstructed. The pitch is fixed at 0.1 for respiratory gating, and cannot be changed. The selected phase position defines the midpoint of a finite width of image data to be used for that cycle (Wink 2005). The temporal resolution of the scan defines the amount of data used. 180 degree parallel projections are used for reconstruction thus the temporal resolution is defined by one half the gantry rotation speed. For the Siemens Sensation Open this corresponds to 20-25 mm steps in the z direction. In the case of the Siemens Sensation Open, the reconstruction is performed with projections integrated over a 250ms window. If the

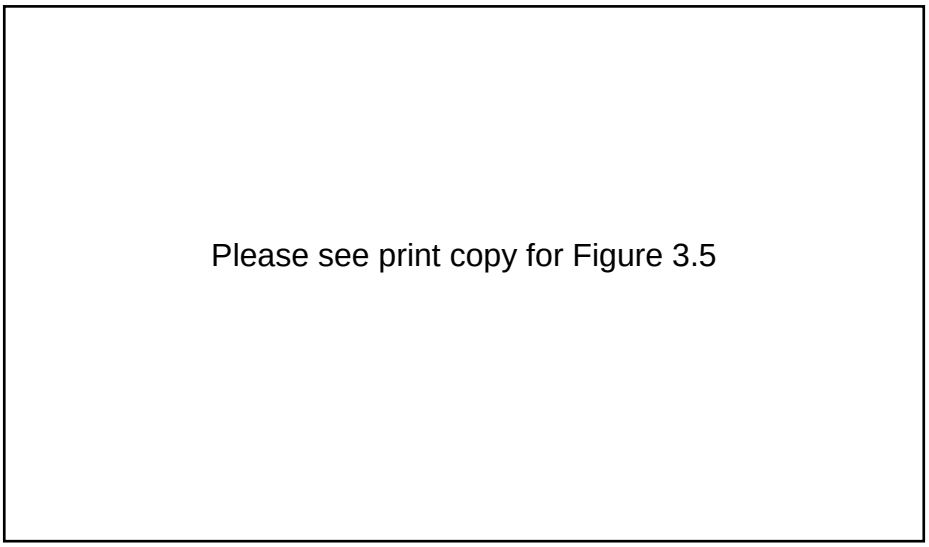


Figure 3.5: Schematic demonstrating principles of helical CT (Kalender 2006).

selected phase positions are defined by less time than the temporal resolution of the scan then the overlapped image data will be used for both image sets (Wink 2005). The final 3D image set contains several sections which were recorded over one half rotation of the scanner at the equivalent time point of the respiration curve (Dinkel 2007).

In sequential mode, images are obtained slice by slice with no table movement during data acquisition. Prospective respiratory gating uses sequential scans triggered by respiration during predefined phase of inhalation or exhalation (Bredenholler et al 2006). Triggering is based on the predicted respiration amplitude of the next peak (100% inspiration). Prospective triggering has the benefit of smaller patient dose than spiral scanning as scan data is only acquired in a selected portion of the breathing cycle. Multiphase reconstruction is not available in this mode, and it does not provide continuous volume coverage with overlapping slices. Siemens recommended that sequential gating not be used with patients with arrhythmic breathing, variable period waveforms, or affinity to coughing or sighing as misregistration of anatomical details may occur (Bredenholler et al 2006). The default gate width for sequential gating is a 100ms window.

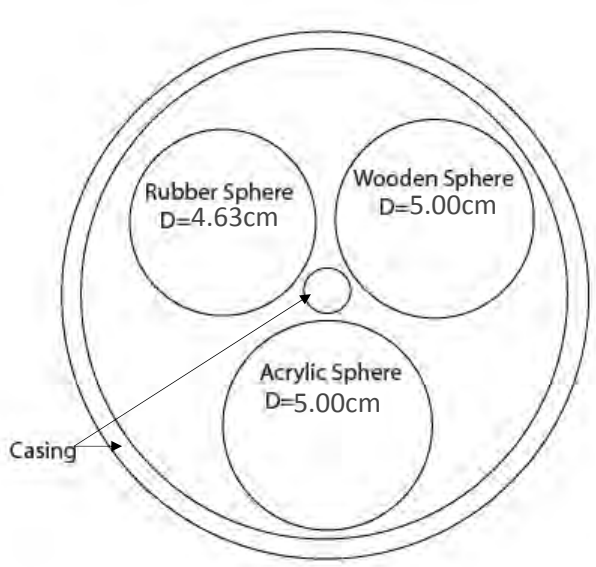


Figure 3.6: Schematic of Anzai phantom showing three spheres of various density and diameter, D.

### 3.3.2 Anzai respiratory phantom

The Anzai respiratory phantom was used to simulate an average breathing cycle. The respiratory phantom contains within it three spheres of different densities (rubber, acrylic and wood) and sizes (refer to figure 3.6). The external diameter of the phantom was measured to be 12.0 cm $\pm$ 0.1 cm; the length of the phantom was measured to be 6.7 cm $\pm$ 0.1 cm. The amplitude of respiratory motion is 1 cm (2 cm peak to peak) and the period of the respiratory cycle is 4 seconds (Anzai Medical Systems 2003). The respiratory phantom has two modes of movement; Normal (sine wave) and Resp. (quasi-respiratory curve) (refer to figure 3.7).

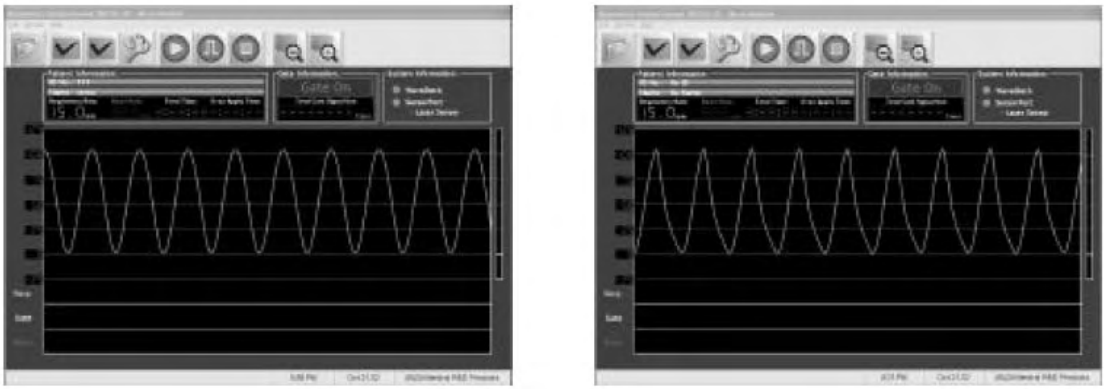

Figure 3.7: Two modes of movement offered by the Anzai Respiratory Gating Phantom; Normal (left) or Resp. (right).

### 3.4 Anzai respiratory phantom measurements: method

The Anzai respiratory gating phantom was aligned parallel to the CT couch such that movement was orthogonal to the scan plane. The phantom was positioned so the centre of the moving cylinder corresponded to centre of the CT gantry axis of rotation. The load cell, which is placed in the belt during patient gated treatment, was positioned in the phantom as shown in figure 3.8. The Anzai phantom was set to Resp. mode, at 15 cycles per minute. The load cell is connected to the sensor port, which amplifies and transmits the analog signal. The wave deck receives the respiratory signal from the sensor port and converts it to a digital signal to be sent to the host computer of the CT system (Bredenholler et al 2006). The Anzai wave deck was attached to the Siemens Sensation Open CT scanner and the respiration curve, scan and reconstruction parameters from the phantom observed at the CT user interface via *Syngo* software (Siemens Medical Solutions, Erlangan, Germany). The rpm chosen was >12 rpm to correspond to the respiratory cycle of the phantom (4 s). A gated scan was performed in helical mode, pitch 0.1, gantry rotation time 0.5 s, 1.5 mm slice, 120 kV, 400 effective mAs. The *Syngo* gating software displays the breathing signal in real-time.

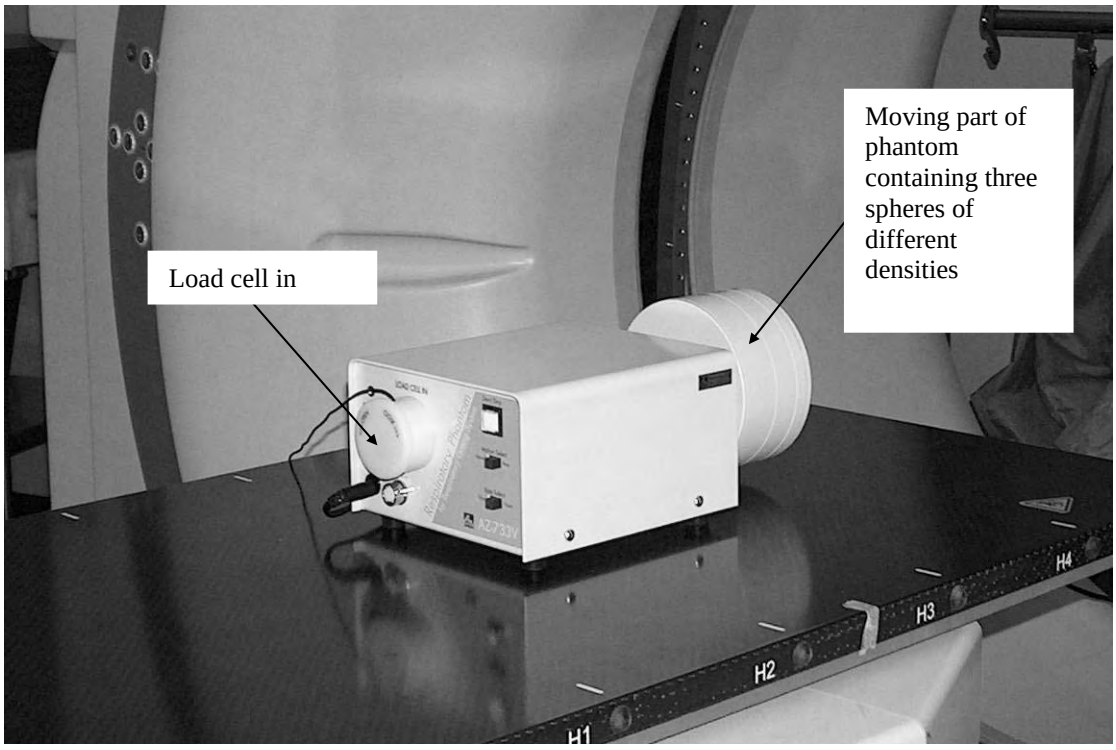


Figure 3.8 Anzai AZ-733V respiratory phantom aligned parallel to CT couch movement.

Once the waveform is collected, the software allows the user to review and correct the phase information of the respiratory signal if the automatic phase calculation software does not function properly due to irregularities in the breathing cycle. Peak and trough positions are indicated on the curve by small dots (sync. points) as shown in figure 3.9 Inspiration and expiration sync points can be inserted, deleted or disabled (Bredenholler 2006).

Phase locations and peak and trough positions were checked before retrospective reconstruction was performed. This step is crucial if real patient data were reconstructed however for a respiratory phantom with a constant period, misalignments are unlikely. Three phases were reconstructed retrospectively: 0% inspiration, 50% inspiration and 100% inspiration. The phases chosen to reconstruct correspond to the steepest portion of the phantom breathing curve (50% inspiration) and the maxima and minima of the curve which are commonly used as part of the duty cycle for patient treatment. The experiment was repeated with the Anzai gating system set to sequential mode. Scans were performed at 0% inspiration, 50% inspiration and 100% inspiration. Scan parameters were unchanged. The reconstruction window was set at 100ms.

An arm was constructed for the phantom so that lateral movement in the image plane was possible (refer to figure 3.10) and the experiment was repeated. Again the centre of the extended moving cylinder was positioned at the CT gantry isocentre. The phantom was set to move at 15rpm. A gated scan was performed in helical mode, pitch 0.1, gantry rotation time 0.5 s, 1.5 mm slice, 120 kV, 400 effective mAs.

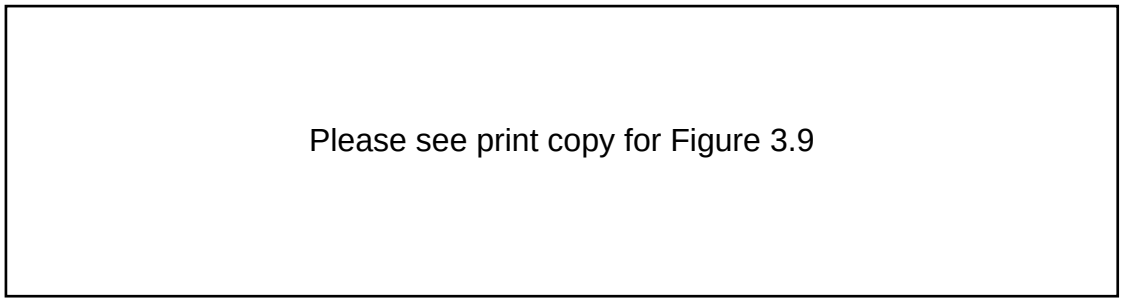


Figure 3.9 Illustration of the user interface for the Siemens Sensation displaying the respiratory signal, phase selected and movable reconstruction points (Dinkel 2007).

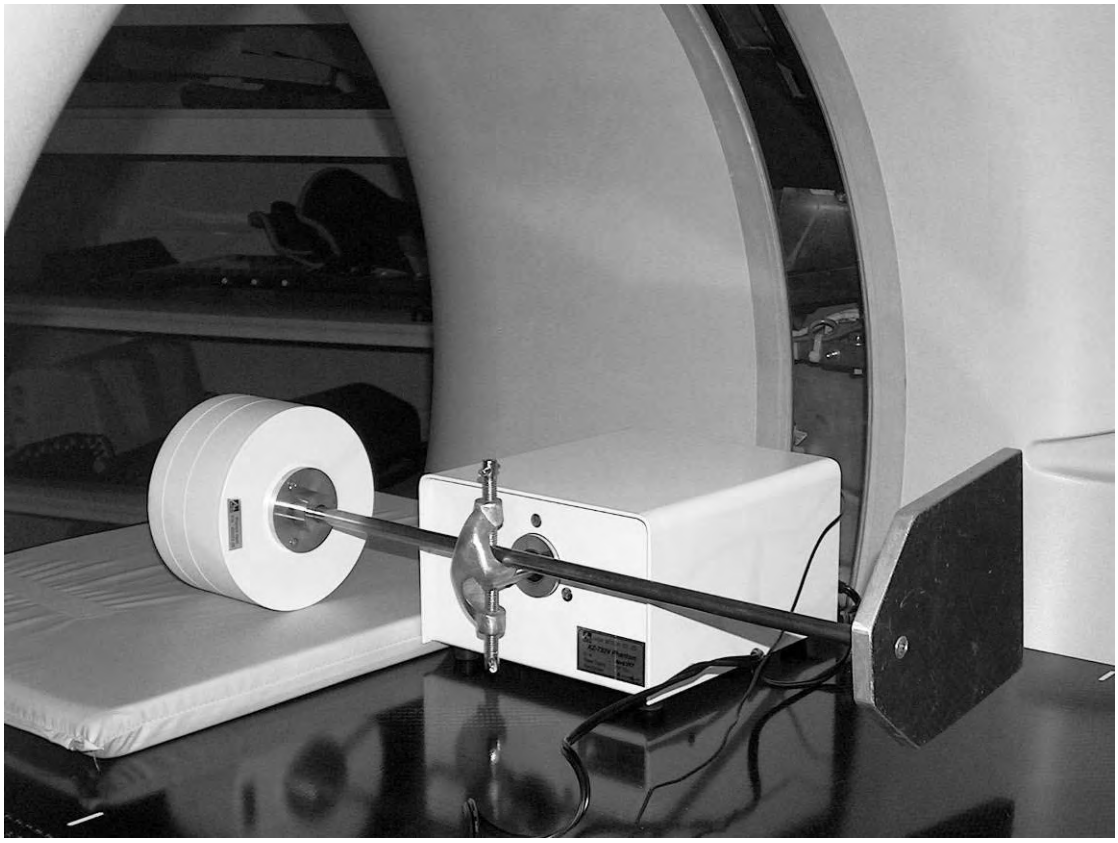

Figure 3.10: Experimental set-up for gated measurements with phantom movement in scan plane.

Reconstructions were performed at 0% inspiration, 50% inspiration and 100% inspiration. An un-gated scan was performed for reference at each set-up (pitch 0.55, 120kV, 1.5 mm slice thickness) with the phantom static relative to the couch.

4D CT scans were DICOM exported to Pinnacle$^3$ (Philips Radiation Oncology Systems, Milpitas, CA) and images analysed. Individual slices were compared visually and the deformation axial cross sections measured. Volumetric accuracy of the three reconstructed spheres was also compared. Volumes were constructed by contouring individual slices in Pinnacle$^3$ using an auto contour threshold of 150-3000 (refer to figure 3.11); window 1601, level -301.

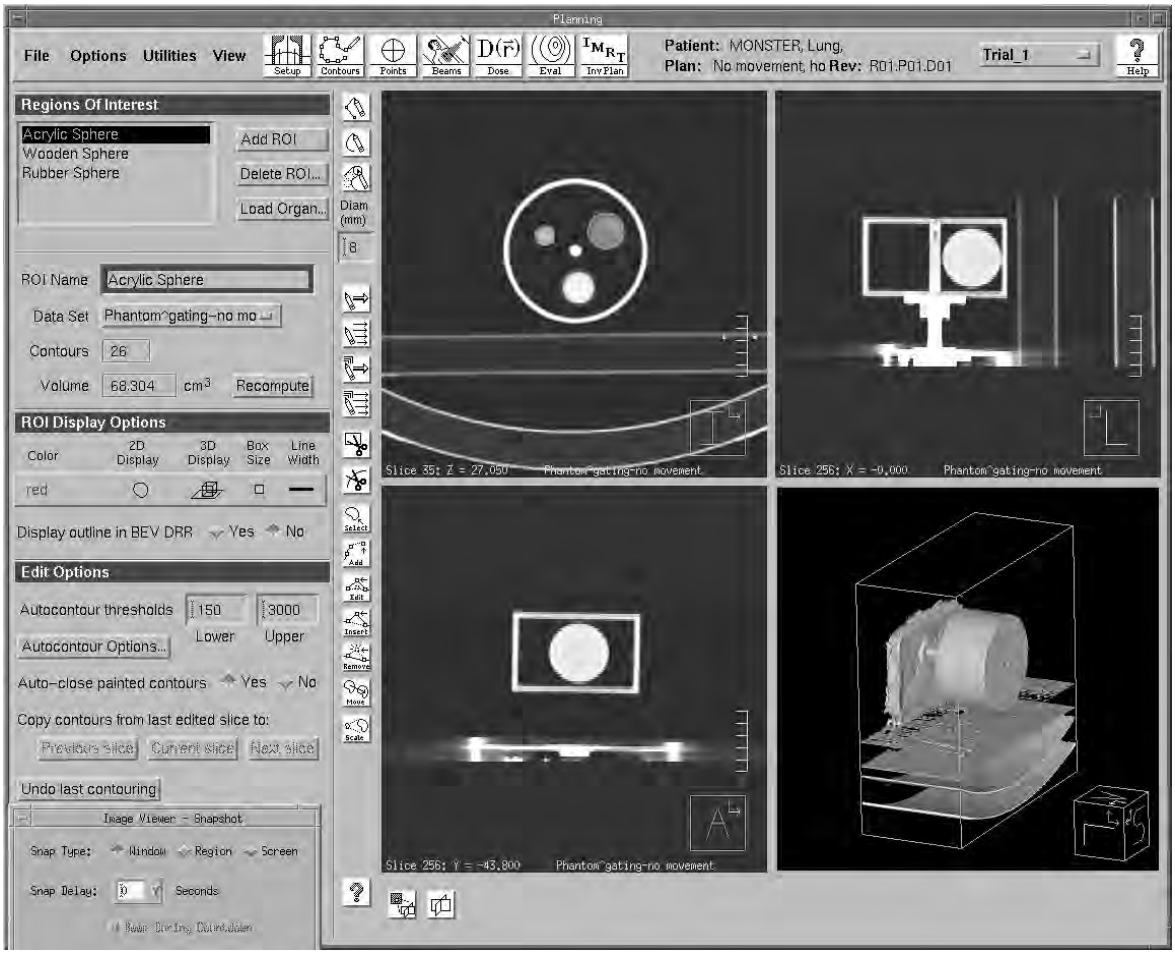


Figure 3.11 Pinnacle[3] user interface showing static motion phantom and autocontour thresholds.

The CT number of each sphere was also found by drawing a 1 $cm^2$ region of interest over the middle of the sphere in Pinnacle[3] on the central axial slice containing the sphere. This was completed for the scan of the static phantom, the gated scan reconstructed at 50% inspiration of the phantom moving in the image plane, and also moving orthogonally to the image plane. Results were tabulated along with the corresponding electron density to water (using the ICCC CT to ED data and converting from physical density to electron density to water) and error in the gated scans noted.

### 3.5 Anzai respiratory phantom measurements: results

Artifacts were observed both in gated helical scans: with the Anzai AZ-733V phantom moving in the scan plane and orthogonally to the scan plane. Figure 3.12 shows 50%

inspiration reconstruction of the acrylic ball moving orthogonally to the scan plane (amplitude 1 cm, period 4 s). Images shown have a window level of 1200 centred at -600. 1 mm slices are reconstructed. The corresponding z value for each image is displayed beneath it. The poles of the spheres appear distorted with spiral-like artifacts. This was discussed by Rietzel et al (2005). As the tube rotates, motion in and out of the imaging plane occurs. The cross section of the phantom in the beam varies. The reconstruction algorithm redistributes densities based on line projections from all angles, thus there is an angular dependency of reconstructed densities resulting in spiral artifacts. At the poles of the sphere there is greater change in axial cross-section radius of the sphere over one rotation resulting in the change in density being more pronounced.

Figure 3.13 demonstrates the artifacts produced by movement in the scan plane. The acrylic ball is again reconstructed at 50% inspiration, (movement amplitude 1 cm, and period 4 s). Images have a window level of 1200 centred at -600. Images are reconstructed every 1 mm, and the z value corresponding to each image is displayed below it. At the poles of the spheres, the axial cross sections no longer exhibit radial symmetry. The cross sections of the sphere appears as an oval (e.g. Figure 3.5.2, z=-502.5). This was expected due to in-plane motion within one full gantry rotation as illustrated previously in figure 3.1.3. Each projection in sinogram space will maintain its original profile but will be shifted in position and a sine curve will no longer be produced as a result of the locus of all line integrals passing through a point in the objects cross section. The oval shape is the result of deformation of the object and will be dependent on the extent of motion during image acquisition.

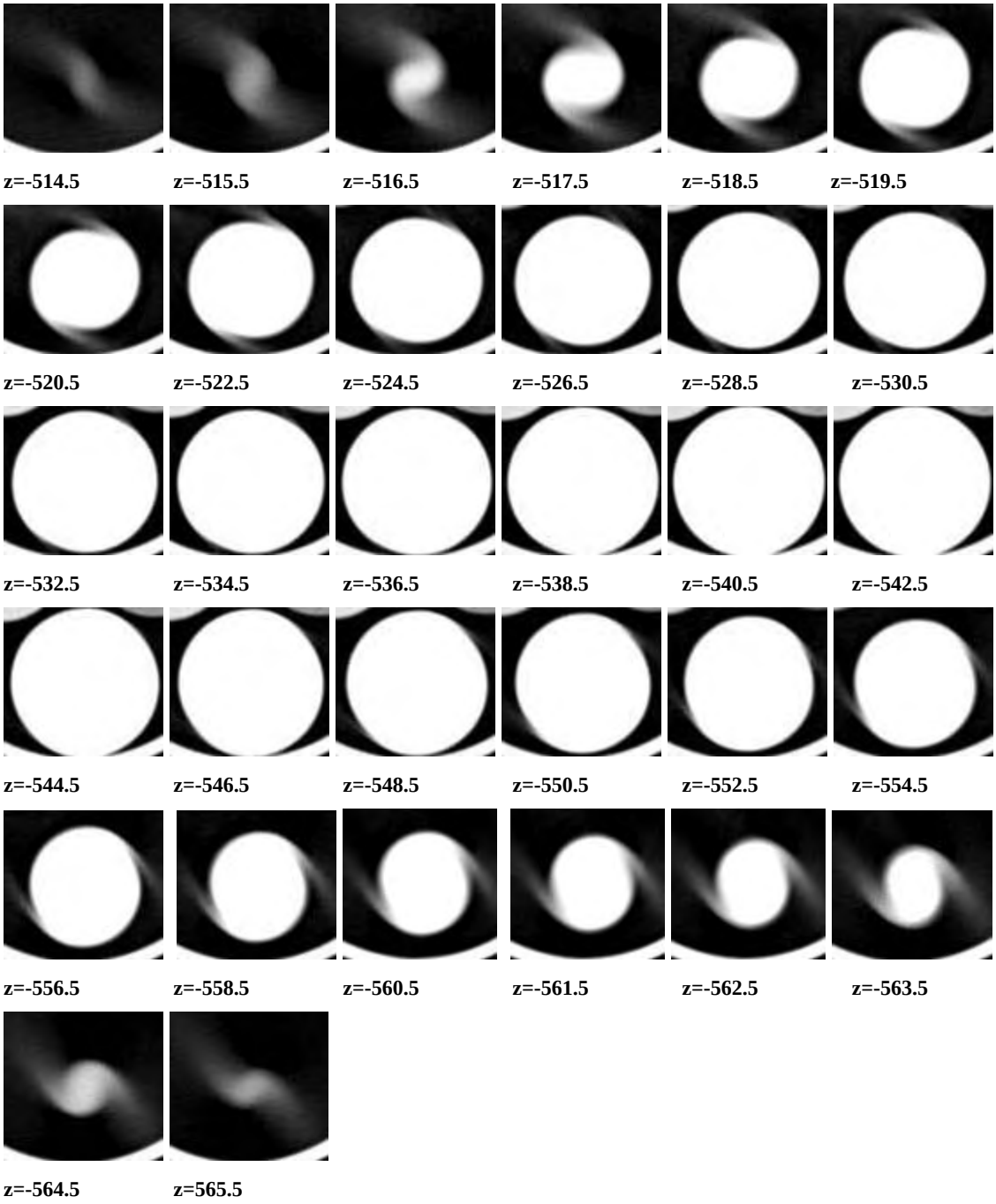


Figure 3.12: Axial slices of the acrylic sphere (diameter 5 cm) 4D CT scanned while periodically moving parallel to couch movement. Image reconstruction averages over a full gantry rotation (0.5 s) Window level 1200 centred at -600. 15rpm, 120kV, 300mAs 1.5 mm slice, 1 mm reconstruction increment.

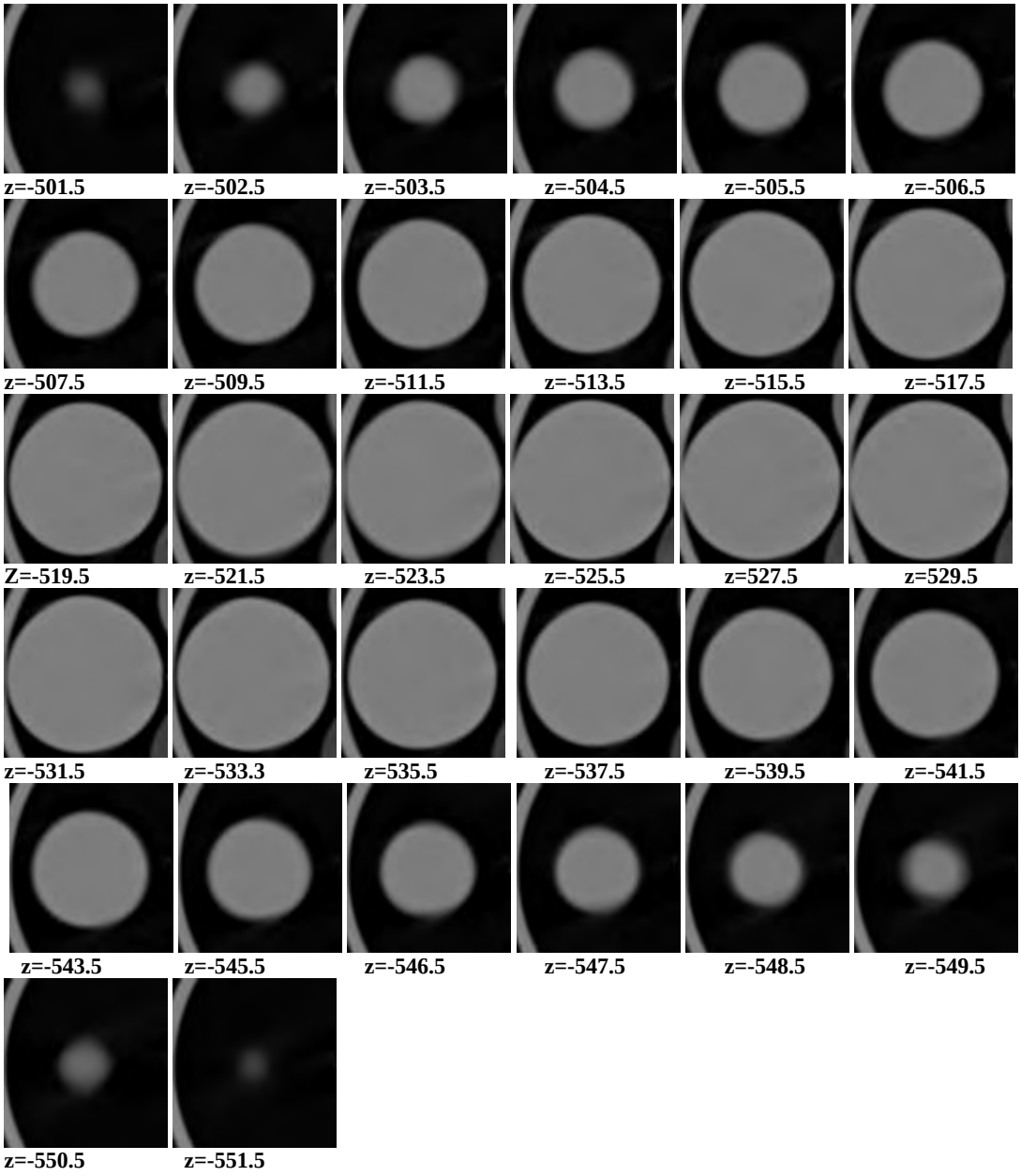


Figure 3.13: Axial slices of the acrylic sphere (diameter 5 cm) 4D CT scanned while periodically moving transverse to scan plane. Image reconstruction averages over a full gantry rotation (0.5 s) Window level 1200 centred at -600. 15rpm, 120kV, 300mAs 1.5 mm slice, 1 mm reconstruction increment. 50% inspiration.

The volumes of the three spheres, as calculated in Pinnacle[3] are shown in table 3.1. The % deviation of each volume from the known volume is shown in brackets. For the un-gated, unmoving sphere this is the standard deviation of three separate static measurements as a percentage of the known volume. Large volumetric deviations were observed in the scans of the moving phantom with no gating applied. The percentage difference in the volume of the spheres calculated by Pinnacle[3] for the un-gated moving scan and the static scan was found to be between 26.6% (wooden sphere) and 33.9% (rubber sphere).

**Table 3.1: Volume determined by Pinnacle[3] for spheres in Anzai AZ-733V respiratory gating phantom. Volumetric deviation (%) from static sphere is shown in brackets.**

| Experimental Setup | Volume of acrylic sphere ($cm^3$) | Volume of wooden sphere ($cm^3$) | Volume of rubber sphere ($cm^3$) |
|---|---|---|---|
| No movement, Ungated | 67.92 (1.5%) | 66.57 (0.6%) | 54.89 (1.6%) |
| Moving orthogonally to image plane, Ungated. | 101.31 (32.9%) | 90.71 (26.6%) | 83.06 (33.9%) |
| Moving orthogonally to image plane, Gated. Reconstructed at 0% inspiration | 67.48 (-0.7%) | 64.83 (-2.7%) | 55.55 (1.2%) |
| Moving orthogonally to image plane, Gated. Reconstructed at 50% inspiration. | 74.89 (9.2%) | 69.85 (4.7%) | 59.19 (7.3%) |
| Moving orthogonally to image plane, Gated. Reconstructed at 100% inspiration. | 68.35 (0.6%) | 66.80 (0.3%) | 55.40 (0.9%) |
| Moving in image plane, Gated. Reconstructed at 0% inspiration | 70.41 (3.5%) | 68.31 (2.6%) | 57.18 (4.0%) |
| Moving in image plane, Gated. Reconstructed at 50% inspiration | 67.32 (-1.0%) | 65.65 (-1.4%) | 55.16 (0.5%) |
| Moving in image plane, Gated. Reconstructed at 100% inspiration | 67.57 (-0.6%) | 65.47 (-1.7%) | 55.81 (1.6%) |
| Moving orthogonal to image plane, Sequential gating mode, 100ms, Reconstructed at 100% inspiration | 73.56 (7.6%) | 69.02 (3.6%) | 58.25 (5.7%) |
| Moving orthogonal to image plane, Sequential gating mode, 100ms, Reconstructed at 50% inspiration | 68.47 (0.7%) | 67.37 (1.2%) | 56.13 (2.2%) |
| Moving orthogonal to image plane, Sequential gating mode, 100ms, Reconstructed at 50% exhalation | 68.90 (1.5%) | 67.14(0.9%) | 56.01 (2.0%) |
| Moving orthogonal to image plane, Sequential gating mode, 100ms, Reconstructed at 100% exhalation | 71.18 (4.5%) | 68.45 (2.8%) | 57.41 (4.4%) |

Gantry rotation time: 0.5 s, Slice width 1.5 mm, Pinnacle[3] autocontour threshold 150-3000.

The volumes calculated from the gated scans of the phantom moving with a period of 4 s were found, in all instances, to be within 10% of the static volume. The scan found to have the largest difference between the volume calculated from the static scan and that calculated from the gated scan was when the phantom was moving orthogonally to the image plane, reconstructed at 50% inspiration. The percentage difference between the volume calculated from the static scan in Pinnacle$^3$ and the gated helical scan of the moving phantom reconstructed at 50% inspiration was found to be 9.2%, 4.7% and 7.3% for the acrylic, wooden and rubber spheres respectively.

The CT numbers found for each sphere and their corresponding relative electron density to water value are shown in table 3.2. It can be seen that there is no deviation in the relative electron density to water value for the acrylic sphere when comparing the static scan, the gated scans of the sphere moving orthogonally to the image plane reconstructed at 50% inspiration, and the gated scan of the sphere moving in the image plane reconstructed at 50% inspiration. The percentage difference in electron density relative to water for the wooden sphere measured on the gated scan reconstructed at 50% inspiration of the phantom moving in the scan plane was found to be -5.0%, and orthogonally to the scan plane was found to be 0%. For the rubber sphere, the percentage difference in relative electron density to water between the gated and static scan was found to be -2.2% for the phantom moving in the scan plane and -1.1% for the scan moving orthogonally to the scan plane. The ACPSEM tolerance (Millar et al 1997) is 2% deviation in CT number to relative electron density conversion.

**Table 3.2: CT numbers calculated for spheres in Anzai AZ-733V respiratory phantom**

| Sphere | Stationary phantom | | Phantom moving in scan plane, 50% inspiration reconstruction | | Phantom moving orthogonally to scan plane, 50% inspiration reconstruction | |
|---|---|---|---|---|---|---|
| | CT Number (+1000) | Electron density relative to $H_20$ | CT Number (+1000) | Electron density relative to $H_20$ | CT Number (+1000) | Electron density relative to $H_20$ |
| Acrylic | 1140 | 1.08 | 1110 | 1.08 | 1119 | 1.08 |
| Wooden | 585 | 0.60 | 554 | 0.57 | 586 | 0.60 |
| Rubber | 875 | 0.89 | 854 | 0.87 | 861 | 0.88 |

Gantry rotation time: 0.5 s, 120kV, 400 effective mAs, Slice width 1.5 mm, Pinnacle$^3$ 1 cm$^2$ ROI.

All electron densities measured on gated helical scans with movement orthogonal to the scan plane were within 2% of the known electron density. The large deviation in electron density for the wooden sphere moving in the image plane can be partially attributed to the fact that wood is an inhomogeneous medium. This experiment was then repeated with a CT to electron density phantom.

### 3.6 Deviation in CT numbers due to motion: Method

The part of the AZ-733V phantom containing the three spheres was removed and the acrylic trolley attached (as shown in figure 3.14). The CT to electron density phantom (CIRS model 062) containing eight different tissue references was placed on an acrylic trolley such that movement would be orthogonal to the imaging plane. The phantom is designed to enable precise correlation of CT data in Hounsfield Units to electron density.

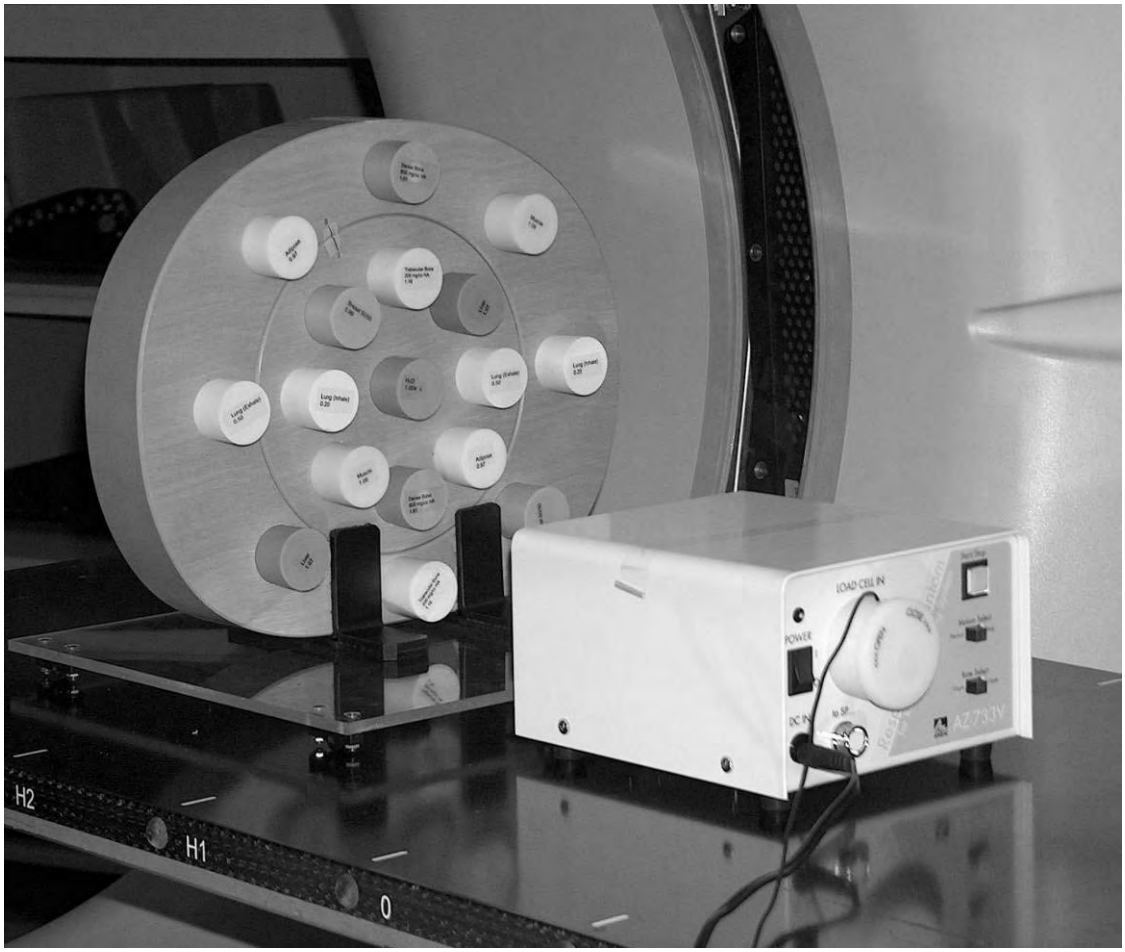


Figure 3.14: CT electron density phantom attached to moving platform (Anzai AZ 733V).

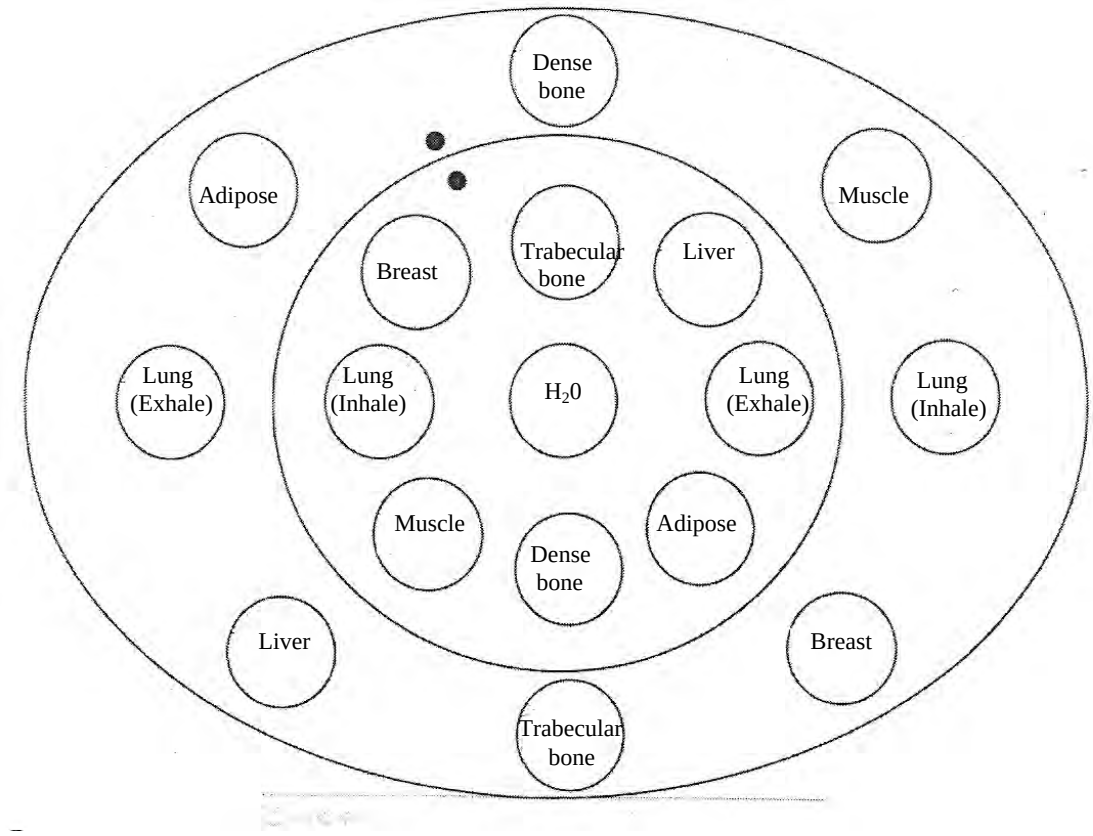


Figure 3.15: Heterogeneity phantom (CIRS 062) set-up for CT number constancy test at ICCC.

The tissue equivalent materials are made by mixing exactly known elemental components within an epoxy resin mix. The elemental compositions are outlined by White et al. (1977). The calculation method between row and CT number was worked out by McCullough (1977) (Metcalfe et al 2007). The CT to ED phantom was placed in the centre of the CT gantry aperture as it would for routine quality assurance**.** The scan parameters on the Siemens Sensation Open CT were set as follows:

1.5 mm slice

120kV

300 effective mAs, where effective mAs=true mAs/pitch

Initially a scan was taken with the phantom unmoving, pitch 0.55. A helical, gated scan was then performed of the phantom moving orthogonally to the scan plane with a period of 4 seconds, amplitude 1 cm. The scan parameters were unchanged: 120kV, 300 effective mAs, and 1.5 mm slice thickness. The pitch for gated images is set to 0.1. Scans were retrospectively reconstructed at 50% exhalation and 20% inspiration. These

values were chosen as they correspond to half of the signal amplitude on inspiration and exhalation. Images were DICOM exported to the treatment planning system (Pinnacle$^3$) and the average CT value found for all tissue substitutes by finding the central slice for each plug along the z axis, and drawing a 1 cm$^2$ region of interest. The electron density to water value was found by using the ICCC CT to ED data and converting physical density to electron density to water. The results were then tabulated and compared to values provided by the manufacturer (CIRS). The experiment was repeated with phantom movement in the scan plan. These results are not shown. Artifacts produced by the electronics when the phantom was placed laterally made CT numbers obtained invalid and the phantom proved too heavy to be moved by the constructed arm. This is future work which needs to be completed.

### 3.7 Deviation in CT numbers due to motion: Results

The electron density for a variety of tissue substitute, bone substitute and lung substitute materials were found. These values were compared to their true values as specified by the manufacturer and the results are tabulated in table 3.3.

**Table 3.3: Measured electron density to water values for a variety of tissue equivalent electron density materials. Percentage difference from relative electron density to water quoted by manufacturer (CIRS) is shown in brackets.**

| Tissue | Relative electron density to water of test object quoted by manufacturer (CIRS) | Relative electron density measured. phantom static | Relative electron density measured. Phantom moving, gated , 20%In reconstruction | Relative electron density measured. Phantom moving, gated, 50%Ex reconstruction |
|---|---|---|---|---|
| ***Inner circle*** | | | | |
| Lung (Inhale) | 0.190 | 0.189 (-0.5%) | 0.210 (10.7%) | 0.230 (23.6%) |
| Lung (Exhale) | 0.489 | 0.492 (0.6%) | 0.499 (2.0%) | 0.508 (4.0%) |
| Adipose | 0.949 | 0.953 (0.4%) | 0.951 (0.2%) | 0.941 (-0.9%) |
| Breast | 0.976 | 0.980 (0.4%) | 0.974 (-0.2%) | 0.981 (-0.4%) |
| Muscle | 1.043 | 1.049 (0.6%) | 1.036 (-0.7%) | 1.022 (-2.8%) |
| Liver | 1.052 | 1.054 (0.2%) | 1.042 (-1.0%) | 1.043 (-0.0%) |
| Trabecular Bone | 1.117 | 1.122 (0.5%) | 1.106 (-1.0%) | 1.107 (-0.9%) |
| Dense Bone | 1.512 | 1.527 (1.0%) | 1.504 (-0.5%) | 1.500 (-0.8%) |
| ***Outer circle*** | | | | |
| Lung (Inhale) | 0.190 | 0.187 (-1.6%) | 0.216 (13.5%) | 0.233 (22.4%) |
| Lung (Exhale) | 0.489 | 0.490 (0.1%) | 0.498 (1.8%) | 0.509 (4.1%) |
| Adipose | 0.949 | 0.949 (0.0%) | 0.930 (-2.0%) | 0.939 (-1.1%) |
| Breast | 0.976 | 0.975 (-0.1%) | 0.976 (0.0%) | 0.972 (-0.4%) |
| Muscle | 1.043 | 1.042 (-0.1%) | 1.031 (-1.2%) | 1.031 (-1.2%) |
| Liver | 1.052 | 1.052 (0.0%) | 1.054 (0.2%) | 1.048 (-0.4%) |
| Trabecular Bone | 1.117 | 1.117 (0.0%) | 1.113 (-0.4%) | 1.108 (-0.8%) |
| Dense Bone | 1.512 | 1.523 (0.7%) | 1.503 (-0.6%) | 1.471 (-2.7%) |

Slice width 1.5 mm, 120kVp, 300 effective mAs. CT numbers determined by 1 cm$^2$ ROI on Pinnacle$^3$.

Agreement was found to be within 1.6% for the static phantom. This complies with the ACPSEM tolerance (Millar et al 1997) of 2% deviation in CT number to electron density conversion. The electron density to water values obtained for adipose, breast, liver, and trabecular bone on the moving, gated phantom were all within the tolerance limit of 2% (ACPSEM). Large deviations of 10.7%-23.6% from the known electron density to water value were observed for lung (inhale) in the reconstructed gated images. Electron density to water values found for the lung (exhale) insert in the gated reconstructed images were 1.8%-4.1% different from the electron density to water value specified by the manufacturer. The electron density to water value for dense bone calculated from the gated object reconstructed at 50% exhalation was found to be 2.7% less than the known value. The electron density value to water recorded for muscle in the gated scan reconstructed at 50% exhalation also exceeded the prescribed tolerance of 2%. The value measured was 2.8% less than the value specified by the manufacturer for the insert.

### 3.8 Construction of a moving respiratory phantom: method and materials

At the time of measurements (May 2007), there were no commercially available phantoms that provided options of changing amplitude and frequency of movement. In order to observe variations in artifact severity with frequency and amplitude a moving respiratory phantom was constructed by the author (figure 3.15). The phantom consisted of a motor attached to a variable power supply. The part of the Anzai phantom containing the spheres of different densities was placed on a trolley attached to the motor via a wooden rod. The trolley is constrained by lead blocks such that the 1-dimensional sinusoidal motion is orthogonal to the scan plane (respiration mainly leads to movement of lung tumours in the superior-inferior direction (Seppenwoolde 2002)). A metal bar attached to the motor rotates with uniform speed and has a series of holes drilled for the rod attachment. The amplitude of movement can be varied depending on the position the rod is attached on the rotating bar (refer to figure 3.16(a)). The period of the rotation of the metal bar is equivalent to the period of simulated respiration, and can be varied. Movement of the trolley is in the form of a simple sine wave. Data on human breathing (George quoted Nioutsikou 2005) suggests that $\cos^4$ dependence would be accurate to

(a)

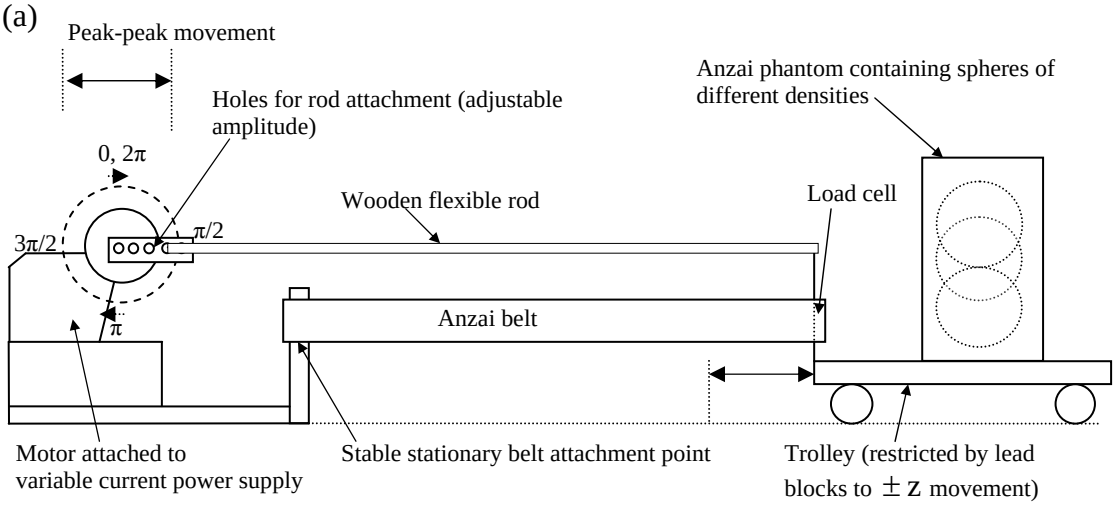


(b)

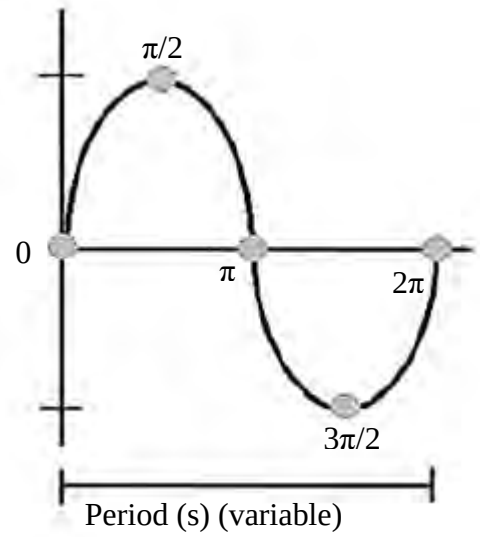


(c)

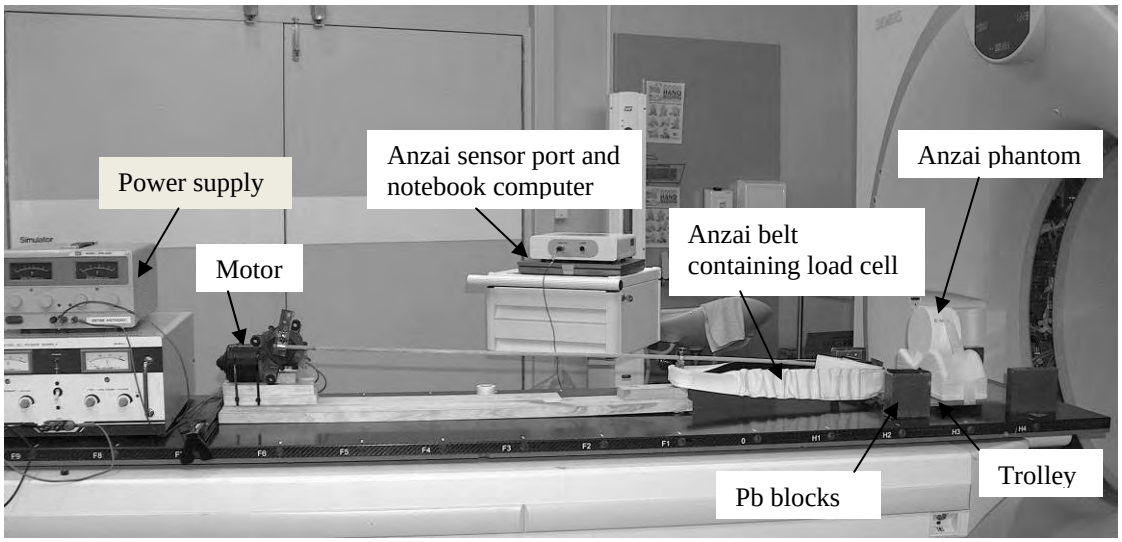


Figure 3.16 (a) Schematic of respiratory motion phantom showing adjustable amplitude waveform (b) Sine waveform produce by constructed respiratory phantom (c) Experimental set-up for respiratory motion phantom measurements on Siemens Sensation Open CT scanner.

replicate a human respiratory cycle however the experiment was not adversely affected by this. The signal is measured by Anzai AZ-733V respiratory gating system. The Anzai belt is attached between the moving trolley and a stable attachment point. As the trolley moves in the +z direction pressure is exerted on the load cell in the belt and the amplitude of the signal increases emulating inhalation. As the trolley moves in the –z direction pressure on the belt is decreased, imitating exhalation. The signal is fed into the sensor port. It was ensured that the sensor port displayed a green light indicating the signal is within range.

Helical scans were performed using the Siemens Sensation Open 20-slice CT scanner. Scan parameters remained constant for all measurements: 400 effective mAs, 120kV, 0.5 s gantry rotation time, pitch 0.1. Slice thickness was set to 1.5 mm, and all reconstructions were performed at 50% inspiration. This phase was chosen as it is mid-ventilation; the object has the greatest speed here thus residual imaging artifacts would be most evident. Measurements were made at four different amplitudes (1.4 cm, 2.4 cm, 3.1 cm, 3.65 cm) for five different periods (6, 10, 15, 20 and 30 cycles per minute). CT scans were retrospectively reconstructed and DICOM exported to Pinnacle$^3$. For all 20 scans, the acrylic, wooden and rubber spheres were contoured on each reconstructed axial slice by using Pinnacle's autocontour threshold between 150-3000 and manually checked and adjusted if necessary (structures joining). The window level was set to Pinnacle$^3$'s lung setting (Window 1601, level -300). The volume of the spheres were then calculated by Pinnacle$^3$ and compared to the average volume of the spheres obtained from three static scans.

### 3.9 Construction of a moving respiratory phantom: results

The volumetric deviations (%) between the moving gated spheres and the static sphere measured by Pinnacle$^3$ are shown in tables 3.3-3.5. Results are described below.

*1.4 cm amplitude movement*

An underestimation of the volume of 22.8%-26.4% was shown for the three spheres when the phantom was moving with smallest amplitude (1.4 cm) and the longest respiratory cycle (6 respirations per minute). When the respiratory cycle was increased to 10 respirations per minute deviations from the known volume as measured in

Pinnacle$^3$ were found to be small (-0.8%-1.7%). At 15 cycles per minute (4 s period), volumes of the gated moving sphere at 50% deviated from their static counterparts 6.6%, 10.8% and 12.5% for the wooden, rubber and acrylic spheres respectively.

**Table 3.3: Volume of rubber sphere (cm$^3$) measured in Pinnacle$^3$. Percentage difference between the gated volume of the moving rubber sphere and the static volume measured using Pinnacle$^3$ is shown in brackets.**

| | 1.4 cm amplitude | 2.4 cm amplitude | 3.1 cm amplitude | 3.65 cm amplitude |
|---|---|---|---|---|
| 6rpm | 42.4 (-22.7 %) | 57.7 (4.9 %) | 65.8 (26.1 %) | 64.4 (13.3 %) |
| 10rpm | 55.8 (0.8 %) | 61.1 (7.5 %) | 67.6 (20.5%) | 64.0 (12.4%) |
| 15rpm | 61.7 (10.8 %) | 62.6 (13.3%) | 68.2 (21.6%) | 74.2 (33.9%) |
| 20rpm | 58.3 (1.5%) | 74.3 (26.8%) | 79.3 (23.8%) | 75.8 (32.0%) |
| 30rpm | 68.0 (35.3%) | 74.5 (22.5%) | 80.8 (49.8%) | 83.2 (40.4%) |

Gantry rotation time: 0.5 s, Slice width 1.5 mm, Pinnacle$^3$ autocontour threshold 150-3000.

**Table 3.4: Volume of wooden sphere (cm$^3$) measured in Pinnacle$^3$. Percentage difference between the gated volume of the moving wooden sphere and the static volume measured using Pinnacle$^3$ is shown in brackets.**

| | 1.4 cm amplitude | 2.4 cm amplitude | 3.1 cm amplitude | 3.65 cm amplitude |
|---|---|---|---|---|
| 6rpm | 49.0 (-26.4%) | 70.8 (6.4 %) | 57.9 (-12.9 %) | 70.5 (5.9%) |
| 10rpm | 66.0 (-0.8%) | 70.6 (6.9 %) | 74.2 (11.4%) | 73.3 (10.1%) |
| 15rpm | 71.0 (6.6 %) | 70.6 (6.1%) | 74.7 (12.2%) | 81.3 (22.2%) |
| 20rpm | 68.9 (3.5%) | 81.3 (22.2%) | 79.5 (19.4%) | 82.6 (24.0%) |
| 30rpm | 71.7 (7.7%) | 81.0 (21.7%) | 87.8 (31.9%) | 91.8 (38.0%) |

Gantry rotation time: 0.5 s, Slice width 1.5 mm, Pinnacle$^3$ autocontour threshold 150-3000.

**Table 3.5: Volume of acrylic sphere (cm$^3$) measured in Pinnacle$^3$. Percentage difference between the gated volume of the moving acrylic sphere and the static volume measured using Pinnacle$^3$ is shown in brackets.**

| | 1.4 cm amplitude | 2.4 cm amplitude | 3.1 cm amplitude | 3.65 cm amplitude |
|---|---|---|---|---|
| 6rpm | 52.9 (-22.8%) | 71.7 (5.2 %) | 86.1 (19.9 %) | 77.4 (17.4%) |
| 10rpm | 68.9 (1.7%) | 73.0 (11.3 %) | 82.3 (23.2%) | 76.8 (16.6%) |
| 15rpm | 75.7 (12.5 %) | 77.4 (14.0%) | 83.1 (24.3%) | 91.5 (35.3%) |
| 20rpm | 70.5 (12.6%) | 86.6 (35.3%) | 84.5 (24.4%) | 90.1 (38.1%) |
| 30rpm | 92.4 (24.0%) | 83.7 (35.6%) | 102.3 (47.1%) | 95.9 (51.6%) |

Gantry rotation time: 0.5 s, Slice width 1.5 mm, Pinnacle$^3$ autocontour threshold 150-3000.

When the period of motion was reduced to 3 s, the deviation from the static volume were found to be 1.5% for the acrylic sphere, 3.5% for the wooden sphere and 12.6% for the rubber sphere. When the phantom movement was set to 30 respirations per minute, large overestimations in the volume of the moving sphere were observed in the gated helical scans reconstructed at 50% inspiration. The rubber sphere was found to be 35.3% larger than the volume of the static sphere as measured in Pinnacle$^3$.The wooden sphere was found to be 7.6% larger and the acrylic sphere 24.0% larger than the volume of the static sphere.

*2.4 cm amplitude movement*

The volumetric deviation of the gated spheres moving with a period of 10 s was found to be 4.9%-6.4%. When the respiratory period of the phantom was increased to 10 respirations per minute (rpm), the volumetric deviations were found to be 7.5%, 6.9% and 11.3% for the rubber sphere, wooden sphere and acrylic spheres respectively. At 15 cycles per minute the percentage difference in volume of the gated moving rubber sphere from the acrylic sphere measured when static was found to be 13.3%. The percentage difference in volume of the moving gated wooden sphere from that calculated from the static scan was found to be 6.1%, and for the gated moving rubber sphere was 14.0%. When the constructed phantom was scanned with respiratory periods of 3 s and 2 s, the volume of the spheres was greatly overestimated. When the respiratory period of the phantom was 3 s, the volume of the spheres calculated from the gated scans and the static scans differed by 26.8%, 22.2% and 35.2% for the rubber, wooden and acrylic spheres respectively. When the respiratory period of the constructed phantom was set to 2 s (30rpm), the percentage difference between the static and gated scan was found to be 22.5% for the rubber sphere, 21.7% for the wooden sphere and 35.6% for the acrylic sphere.

*3.1 cm amplitude*

The percentage difference between the gated volume of the sphere moving with a respiratory cycle of 6rpm and the static volume of the sphere measured by Pinnacle$^3$ was found to be 26.1%, -12.9% and 19.9% for the rubber, wooden and acrylic spheres respectively. When the phantom was moving with a period of 6 seconds, all volumes measured from gated images were larger than the volume measured from the static phantom; The volume of the rubber sphere measured from the data reconstructed at

50% inspiration was found to be 20.5% larger than that of the volume calculated from the static scan, the difference in volume of the wooden sphere was found to be 11.4% and the acrylic sphere 23.2%. When the period of movement of the respiratory phantom was set to 4 s, results also showed an overestimation of the volumes measured. The deviation of the gated volume from the static volume was found to be 21.6%, 12.2% and 24.3% for the rubber, wooden and acrylic spheres respectively. The percentage difference between the volumes measured from the gated scan when the phantom was moving with a period of 3 s and the static scan was found to be 23.8%, 19.4% and 44.4% for the rubber, wooden and acrylic spheres respectively. When the respiratory period of the phantom was reduced to 2 s, a large overestimation of the volume of the gated spheres resulted; the rubber sphere deviated from the static volume by 49.8%, the wooden sphere by 31.9% and the acrylic by 47.1%.

*3.65 cm amplitude*

The phantom was set to have an amplitude of movement of 3.65 cm, and a period of 10 s. The percentage difference between the static volume measured in Pinnacle$^3$ and the volume measured from the gated dataset reconstructed at 50% inspiration was found to be 13.3% for the rubber sphere, 5.9% for the wooden sphere and 17.4% for the acrylic sphere. When the period was decreased to 6 s, the percentage difference in volume from the static scan was found to be 12.4%, 10.0% and 16.6% for the rubber, wooden and acrylic spheres respectively. Large volumetric deviations were observed when the period was decreased to 4 s, 3 s and 2 s. When the period of the respiratory phantom was set to 4 s, the percentage difference between the volume of the gated moving sphere and the static volume measured in Pinnacle$^3$ was found to be 33.90% for the rubber sphere; the wooden sphere had a percentage difference of 22.2% and the acrylic sphere 35.5%. Similar results were found when the period of motion of the phantom was set to 3 s. The deviation in volume between that measured on the gated scan and that measured on the static scan was found to be 32.0%, 24.0% and 38.1% for the rubber, wooden and acrylic spheres respectively. Deviation between the volume measured on the gated scan and that on the static scan was greatest when the amplitude of the phantom's movement was set to 3.65 cm and the period of motion was 2 s. This is an extreme case combining deep breathing with a very fast period, however fast breathing is generally associated with shallow respiratory motion. The percentage difference between the volume measured on the gated scan and that of the static scan was found to

be 40.4% for the rubber sphere, 38.0% for the wooden sphere and 51.6% for the acrylic sphere.

Volumetric deviations do not significantly characterise the artifacts seen in gated images. Screen captures from Pinnacle[3] shown in figures 3.17-3.19 demonstrate qualitatively the extent of the artifacts. The images shown are for an amplitude of 2.4 cm and are representative of results achieved for other amplitudes. 2.4 cm amplitude corresponds to the limit of tumour motion that would be experienced clinically (Lung tumours move up to 5 cm (Keall 2007)).

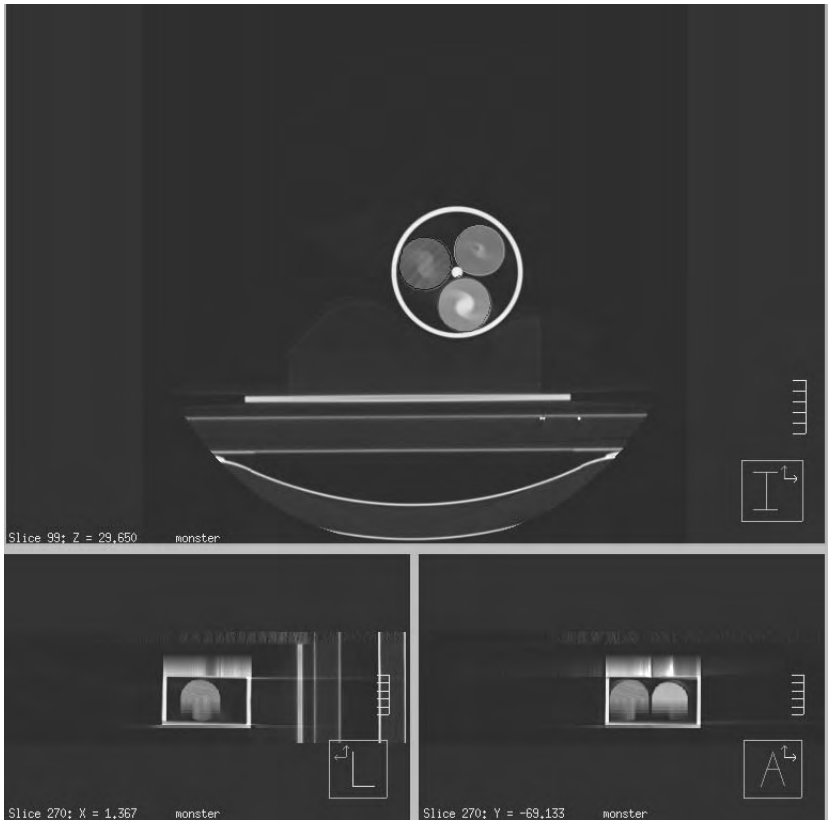


Figure 3.17: Pinnacle[3] user interface illustrating artifacts observed for 50% inspiration reconstruction, 2.4 cm amplitude movement, 6 respirations per minute (10 s period). Window 1601, level -300.

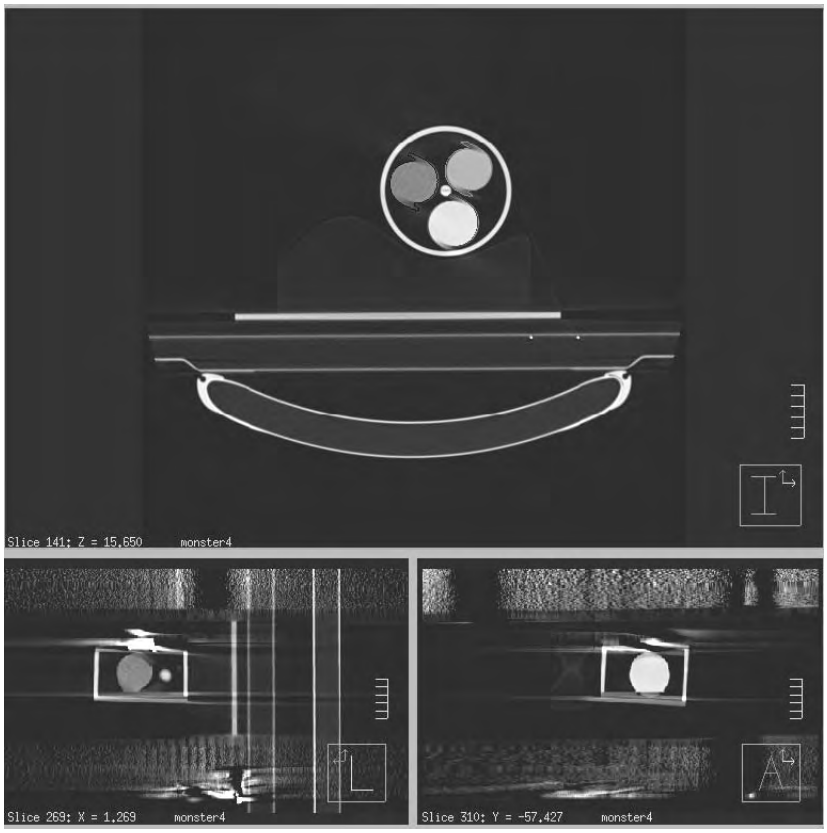


Figure 3.18: Pinnacle[3] user interface illustrating artifacts observed for 50% inspiration reconstruction, 2.4 cm amplitude movement, 10 respirations per minute (6 s period). Window 1601, level- 300.

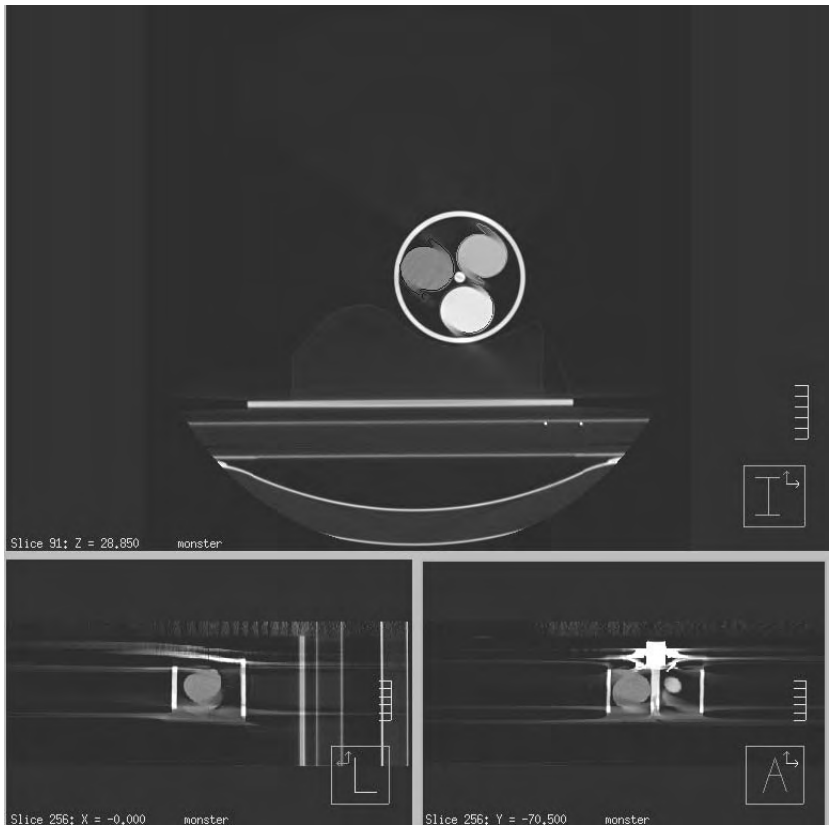


Figure 3.19: Pinnacle[3] user interface illustrating artifacts observed for 50% inspiration reconstruction, 2.4 cm amplitude movement, 30 respirations per minute (2 s period). Window 1601, level -300.

### 3.10 Discussion

Motion artifacts were observed on all gated CT scans. Residual motion artifacts were seen in gated helical scans when the object was moving in the scan plane, and also when the object was moving orthogonally to the scan plane. These artifacts are caused by an object's movement within the imaging plane during tube rotation as explained by Gagne et al (2004) and Rietzel et al (2005). The results obtained for orthogonal movement concur with those from Rietzel (figure 1.0). Large deviations are seen at the poles of the sphere due to the greater change in the axial cross-section radius of the sphere over one rotation at this location.

Volumetric differences in gated studies of the Anzai AZ-733V phantom in all cases were within 10%. The Anzai AZ-733V phantom has movement corresponding to an average breathing cycle (4 s) and an amplitude feasible for tumour movement (1 cm). The largest deviation in volume determined from the reconstructed gated scans was found to be when the phantom was moving orthogonally to the image plane and reconstructed at 50% inspiration. This was expected as partial projection artifacts are proportional to displacement per time and motion is the fastest in phases 25-75%. Rietzel et al (2005) compared 4D CT images of phantoms moving orthogonally to the imaging plane and found that volumetric differences in a spherical object with radius 1.8 cm, amplitude 1 cm, were within 5% if 29 images per slice were reconstructed. The larger deviation in volume found in gated images in this work can be attributed to this being a helical scan whereas Rietzel et al (2005) used a cine scan with a greater number of slices reconstructed per couch position, improving temporal resolution. The determination of the volume of the sphere is also very sensitive to window levelling and this may have contributed to the larger volumes. 50% inspiration (mid-ventilation) was where volumes differed the most from their static counterparts and this is where the object has greatest speed, thus residual motion artifacts would be expected to be the greatest here.

In slice motion was found to produce less motion artifacts. Motion artifacts were still present in sequentially gated images, and would be expected to increase in a clinical situation due to irregularities in patient breathing cycles.

CT numbers for the spheres in the Anzai AZ-733V phantom moving orthogonally to the scan plane reconstructed at 50% inspiration were calculated to be within 1.1% of the values obtained from the static scan. Greater distortions (up to 5%) were observed for the rubber and wooden spheres moving in the image plane. This result concurs with that simulated by Gagne et al (2004) and observed by Smeenk et al (2007) who found that greater distortions from the true density distribution are observed for lateral motion compared to cranial-caudal motion. Measurements made using the CIRS 062 phantom indicated that gated scans of objects moving orthogonally to the image plane will experience deviations in CT number, and therefore calculated electron density. The result obtained here is not conclusive. More measurements of different density objects moving with a variety of periods and amplitudes need to be made. In-plane measurement was not possible with the constructed variable-amplitude phantom due to size. A special apparatus to move this heavier phantom for these measurements (other than the clamp stand) would have been necessary. This would be useful future work for another student.

In measurements performed with the constructed phantom, the percentage difference in the volume of the spheres measured on the gated scans from the static scans was observed to increase as the amplitude of motion increases. The deviation in volume measured from the static scan was also seen to increase as the frequency of respiration (phantom movement) was increased. Again this was expected as partial projection artifacts are proportional to displacement per time (Rietzel 2005); a longer motion period means that the magnitude of motion within each slice is reduced. Similarly, if the motion period is kept constant, a smaller amplitude movement means that the object has less distance to travel in the same amount of time, and motion intra-slice is reduced.

Volumetric differences do not sufficiently characterise the image distortion observed in the images and error in the images cannot be attributed entirely to partial projection effects. Figures 3.17-3.19 illustrate the full extent of the distortion in the gated images. Figure 3.16 shows the Pinnacle$^3$ user interface illustrating artifacts observed for 50% inspiration reconstruction, 2.4 cm amplitude movement, 6 respirations per minute (10 s period). A flattening of the sphere in the z direction can be observed in the 4D images due to an undersampling of data for certain phases. A data sufficiency condition has been explored by a number of authors including Keall (2006) as shown in equation 1.0;

$$\text{Gantry rotation time}\left(\frac{1}{pitch}+\frac{fan\_angle}{360^{o}}\right)\geq \text{Breathing period.} \qquad (1.0)$$

If the appropriate values for the Siemens Sensation Open CT scanner and the scan parameters used in the experiment are substituted into equation 1.0 (pitch 0.1, gantry rotation time 0.5 s, and fan angle of 52.1 degrees) a limit is obtained for the breathing period of 5.072 s. As the period of motion shown in figure 3.17 is 10 s gaps in the 4D CT dataset would be expected. The data sufficiency condition introduced by Pan et al (2004) is similar where

$Pitch \leq \frac{T_g}{T_b + T_g}$ for the full-scan reconstruction where $T_g$ is the gantry rotation time and $T_b$ is the breathing period.

$Pitch \leq \frac{T_g}{T_b + \frac{2}{3}T_g}$ for the half-scan reconstruction. The reasoning behind this was discussed in the literature review and illustrated in figure 1.2. If the gantry rotation time of 0.5 s is substituted and the pitch value of 0.1, the breathing cycle used must be less than or equal to 4.67 s to avoid under-sampling. The longer the breathing cycle, the smaller the pitch factor must be and the longer the acquisition time. The gated images acquired with a breathing cycle of around 5 s (10rpm and 15rpm) were found to have the least difference in volume from the static scans, as expected. The object retains its spherical shape and axial and coronal slices show circular cross sections (figure 3.18) for amplitude 1.4 cm and 2.4 cm. This situation corresponds to that which would be observed in the clinic with the average breathing period between 3 and 5 seconds and the maximum extent of tumour motion being 5 cm (Keall 2006). Figure 3.19 demonstrates the effect of oversampling due to a short respiratory period (2 s). The deviation in volume here was found to be equivalent to that observed for non-gated moving images. The object no longer resembles a sphere. Wolthaus (2006) suggested a lower pitch or more choices of gantry rotation speed would be desirable in overcoming the artifacts (current gantry rotation speeds are 0.5 or 1 s).

Irregular breathing would further affect volumetric accuracy of gated structures. Mutaf et al (2007) found that phase assignment errors could lead to volumetric inaccuracies of up to 40% in the delineation of target volumes and independent checks of 4D CT sorting procedure should be performed for each case. The data obtained in this

experiment was from a phantom and thus had a reproducible respiratory frequency. Reconstruction points were also checked manually on the CT user interface for all phantom data collected to ensure accurate designation of peak and troughs in the 'breathing cycle'. Patients breathing cycles may vary for both inter and intra-fraction and in a clinical setting stepladder artifacts, as described by Dinkel et al (2007), would be expected due to misregistration of respiratory motion and frequency irregularities. Rietzel et al (2005) suggest that artifacts due to irregular breathing are greater than speed induced artifacts such as those seen at 50% inspiration. In a clinical situation, a further deviation from the known volume and shape of the object would be expected.

In a controlled situation where a moving object has a 4 s-6 s period, an amplitude of movement less than 2.5 cm and a reproducible breathing cycle, 4D CT produces tolerable artifacts. Reconstructed images retain their initial shape, and volumetric inaccuracies are far less than those observed in non-gated images of the same moving object. Results obtained in this work agree with those found by Rietzel et al (2005) and predicted by Gagne et al (2004). The large deviation seen in the volume and shape of the reconstructed objects when moving with periods 3 s or less, and 10 s indicates that subjects with these breathing cycles may not benefit from 4D CT using the Siemens Sensation Open CT scanner. Clinicians should be aware that significant artifacts will still be present in 4D CT images taken of subjects with these respiratory periods. The results obtained are CT scanner and scan parameter dependent. Monitoring of the patient's breathing cycle for a period prior to the 4D CT scan is recommended. This is also supported by the results found in chapter two which indicate that breathing periods increase and regulate with time spent lying on the couch.

# CHAPTER IV

# CONCLUSION AND FUTURE WORK

It is recommended, based on the results from this thesis that if the Anzai AZ-733V system is to be used with the Siemens Sensation Open CT scanner for 4D CT and the Real-time Position Management (RPM) system is to be used for gated treatment, that the external marker be only positioned at the umbilicus. The coefficient of determination ($R^2$) between the Anzai and RPM waveforms was found for six marker positions over a sample of 15 staff volunteers and when positioned at the umbilicus the signals from the two systems responded similarly to abdominal movement due to respiratory motion; the mean coefficient of determination between systems was found to be 0.925.

This work indicates that respiratory signals obtained from external surrogates are dependant on location and monitoring method. When both the Anzai AZ-733V respiratory gating system and the RPM system markers were positioned midway between xiphoid process and umbilicus, the mean coefficient of determination between the waveforms obtained by the two systems was found to be 0.788 and when the RPM and Anzai systems were positioned at the xiphoid process the mean coefficient of determination was reduced further to 0.611. This can be attributed to monitoring method and the discrepancies of sensors due to sensitivity with regards to variations of cross-sectional perimeter and anterior-posterior movement of the chest wall.

When the external surrogates were positioned at separate locations on the chest wall results were found to vary. The mean coefficient of determination value between systems were found to be 0.776 when the Anzai load cell was positioned at the umbilicus and the RPM retro-reflective marker was positioned at the xiphoid process, 0.752 when the Anzai marker was positioned at the xiphoid process, and the RPM marker positioned at the umbilicus and 0.878 when the Anzai marker was positioned at the umbilicus and the RPM marker positioned midway between xiphoid process and umbilicus. Results highlighted the importance of external surrogate position to the signal obtained, regardless of the type of sensor used, and indicated that it is imperative

that the external marker position on the chest wall remained fixed between planning and treatment. This should be included in respiratory gating protocols.

The subjects studied were all healthy volunteers and it would be expected correlation between the two systems would be reduced further for patients with breathing difficulties. Ethics approval has been granted for future work including a patient-based study measuring breathing waveforms at the Illawarra Cancer Care Centre (refer to figure A169). The survey of these patients is continuing in the clinic, however currently there is no processed data available for publication in this thesis. The relationship between tumour motion and the signal gained by the external surrogate was not considered in this work, and provides the basis for future work. The phase shift between internal tumour motion and external surrogate motion may not only be dependent on viscoelastic properties of the lung and the position of the tumour, but also directly influenced by the placement of the external marker on the chest wall.

Artifacts were observed in all 4D CT images. The Anzai AZ-733V respiratory gating system was coupled with the Siemens Sensation Open CT scanner and 4D CT images were acquired of the commercially-available Anzai respiratory phantom. When the phantom was moving with controlled amplitude of 1 cm and a period of 4 s, the volume of the sphere reconstructed from the gated images were found to be within 10% of the volume calculated of the static sphere. Reconstructed images retain their initial shape, and volumetric inaccuracies are far less than those observed in non-gated images of the same moving object.

A moving respiratory phantom was developed and artifacts in 4D CT using the Siemens Sensation Open CT scanner observed over four amplitudes five frequencies of movement. At high frequencies (periods of less than 3 s), and large amplitudes (greater than 3.1 cm) large deviations from the static volume of the spheres were observed ranging from 19.4%-51.6%. Objects were moving fastest here, and partial projection artifacts are apparent in all reconstructed gated images at these amplitudes and frequencies due to movement of the object in the scan plane during gantry rotation. Distortion in these images was also attributed to oversampling of data. At very low frequencies (periods of 10 s or less) images appeared highly distorted along the z-axis and volumetric distortions were found to range from -26.4%-26.1%. Data sufficiency

conditions were not fulfilled at such low frequencies as images do not cover the entire breathing cycle. When realistic amplitudes for tumour movement were considered (1.4 cm and 2.4 cm) for average patient breathing periods (4 s and 6 s) the deviation of the reconstructed gated spheres from the static sphere was found to range from -0.8 to 14%. A reconstruction phase of 50% inspiration was used for this experiment and results would be expected to improve if 0% inspiration or 0% exhalation reconstruction phases were applied. This is a more controlled situation than for patient breathing and in a clinical situation misalignment and breathing irregularities would also contribute to artifacts in 4D CT.

Recommendations are made that a patient's breathing cycle should be measured for a period of time prior to 4D CT. Once the breathing cycle has regulated, the reproducibility and period of respiration can be assessed. Clinicians should be aware that significant artifacts will still be present in 4D CT images using the Siemens Sensation Open CT scanner and inaccurate delineation of target volumes may result for subjects with breathing cycles less than 3 s or greater than 10 s. 4D CT provides the possibility of precise localisation of a moving target however the validity of results should always be considered. Further investigations are needed into the effect of irregular breathing pattern on the magnitude of volumetric inaccuracies and artifacts in gated studies.

## BIBLIOGRAPHY


Allen, A., Siracuse, K., Balter, J. et al (2004) Evaluation of the influence of breathing on the movement and modelling of lung tumours" *International Journal of Radiation Oncology ·Biology· Physics, v*58, pp 1251-1257

Anzai Medical Systems (2003) "User's Manual: Respiratory Phantom Ver. 1.0" Anzai Medical, Tokyo

*Anzai Medical Systems*, [Homepage of Anzai Medical systems], [Online] Available: http://www.anzai-med.co.jp/eigo/az733v.htm. [Accessed 2006, Aug 1]

Balter, J., Haken, T., R and Lawrence, T. (1996) "Uncertainties in CT-based radiation therapy treatment planning associated with patient breathing" *International Journal of Radiation Oncology ·Biology· Physics* v36, pp 167-174

Beddar, A., Kainz, K., Briere, T. et al (2007) "Correlation between internal fiducial tumour motion and external marker motion for liver tumours imaged with 4D-CT" *International Journal of Radiation Oncology Biology Physics*, v67 (2) 630-638

Berbeco, R., Nishioka,S., Chen, G. et al (2005) " Residual motion of lung tumours in gated radiotherapy with external respiratory surrogates" *Physics in Medicine & Biology.v*50, pp 3655-3667

Bobko, P. (2005) "Correlation and Regression" Sage Publications, London

Borgert, J., Krüger, S., Timinger, H. et al (2006) "Respiratory motion compensation with tracked internal and external sensors during CT-guided procedures" *Computer Aided Surgery*, v11 (3), pp 119-125

Bortfield, T., Jokivarsi, K., Goitein, M. et al (2002) "Effects of intra-fraction motion on IMRT dose delivery: Statistical analysis and simulation" *Physics in Medicine & Biology, v*47, pp 2203-20

Bredenholler, C., Feuerlein, U. (Ed.) (2006) “Somatom Emotion 16 Application Guide” Siemens Medical Solutions Inc, Germany

*Cancer in Australia: A Snapshot 2001* [Homepage of Australia Bureau of Statistics], [Online] Available: http://www.abs.gov.au/AUSSTATS/abs@.nsf/ProductsbyReleaseDate/3B21BA4596DCDD6FCA2571D10017185C?OpenDocument [Accessed 2007, Nov 23]

Chen, G., Kung, J. et al “Artifacts in Computed Tomography Scanning of Moving Objects” (2004) *Seminars in Radiation Oncology*, v14 (1) pp19-26

Chi, P., Balter, P., Luo, D. et al (2006) “Relation of external surface to internal tumour motion studied with cine CT” *Medical Physics* v33 (9) pp 3116-3123

Choi, H., Choi, B. et al (2004) “Pitfalls, artifacts, and remedies in multi-detector row CT coronary angiography” *Radiographics* v24, pp 787-800

*Computerised Imaging Reference Systems Inc (CIRS)* [Homepage Computerised Imaging Reference Systems], [Online] Available: http://www.cirsinc.com/062_rad.html [Accessed 2007, July 10]

De Groote, A., Verbandt, Y., Paiva, M. Et al (2000) “Measurement of thoracoabdominal asynchrony: importance of sensor sensitivity to cross section deformations” Journal of Applied Physiology, v88, pp 1295-1302

Dietrich, L., Jetter, S., Tücking, T. et al (2006) “Linac-integrated 4d cone beam CT: first experimental results” *Physics in Medicine & Biology*, v51, pp 2939-2952

Dinkel, J., Welzel, T., Bolte, H. et al (2007) “Four-dimensional multislice helical CT of the lung: Qualitative comparison of retrospectively gated and static images in an ex-vivo system” *Radiotherapy and Oncology* doi:10.1016/j.radonc.2007.09.003

Ehrhardt, J., Werner, R., Saring, D. et al (2007) “An optical flow based method for improved reconstruction of 4DCT data sets acquired during free breathing” *Medical Physics*, **34** 2 ,711-721

Ford, E., Mageras, G., Yorke, E. et al (2003) “Respiration correlated spiral CT: a method for measuring respiratory-induced motion for radiation treatment planning” *Medical Physics*, v30, pp88-97

Gagne, I., Robinson, D. (2004) “The impact of tumour motion upon CT image integrity and target delineation” *Medical Physics*, v31 (12) pp 3378-3392

Gagne, I., Robinson, D. et al (2005) “The use of phase sequence image sets to reconstruct the total volume occupied by a mobile lung tumour.” *Medical Physics* v32 (7) pp 2211-2221

Gierga, D., Brewer, J., Sharp, G. et al (2005) “The correlation between internal and external markers for abdominal tumours: implications for respiratory gating” *International Journal of Radiation Oncology ·Biology· Physics* v61 (5) pp 1551-1558

Hanley, J., Debois, M., Mah, D. et al (1999) “Deep inspiration breath hold technique for lung tumours: The potential value of target immobilisation reduced lung tumours in dose escalation” *International Journal of Radiation Oncology· Biology ·Physics*. v45, pp 603-611

Hoisak, J., Sixel, K., Tirona, R. et al (2006) “Prediction of lung tumour position based on spirometry and on abdominal displacement: Accuracy and reproducibility” *Radiotherapy and Oncology*, v78, pp339-346

Hoisak, J., Sixel, K., Tirona, R. et al, (2004) “Correlation of lung tumour motion with external surrogate indicators of respiration” *International Journal of Radiation Oncology· Biology ·Physics*. v60 pp 1298-1306

Hui, H. (1999) “Multi-slice helical CT: scan and reconstruction” *Medical Physics* v26 (1) pp 5-17

ICRU (International Commission on Radiation Units and Measurements) (1999) “Report 62: Prescribing, recording, and reporting photon beam therapy” ICRU, Bethesda, Maryland.

ICRU (International Commission on Radiation Units and Measurements) (1999) “Report 50: Prescribing, recording, and reporting photon beam therapy” ICRU, Bethesda, Maryland.

Imura, M., Yamazaki, K., Shirato, H. et al (2005) “Insertion and fixation of fiducial markers for setup and tracking of lung tumours in radiotherapy” *International Journal of Radiation Oncology· Biology ·Physics*. v63, pp 1442-1447

Ionascu, D., Jiang, S., Nishioka, S. Et al (2007) “Internal-external correlation investigations of respiratory induced motion of lung tumours” *Medical Physics*, v34 (10) pp 3893-3903

Jiang, S. (2006) “Technical aspects of image-guided respiration-gated radiation therapy” *Medical Dosimetry v*31, pp141-151

Kalender, W. (2006) “X-ray computed tomography” *Physics in Medicine & Biology* v.51 pp R29-R43

Kanoulas, E., Aslam, J., Sharp, G. (2007) “Derivation of the tumour position from external respiratory surrogates with periodical updating of the internal/external correlation” *Physics in Medicine & Biology* v52, pp5443-5456

Keall, P. (2007) “Respiratory Gating” (Lecture) Royal Prince Alfred Hospital, Sydney

Keall, P., Mageras, G., Balter, J. et al (2006) “The management of respiratory motion in radiation oncology report of AAPM Task Group 76” *Medical Physics*, v33, 10, pp3871-3900

Keall, P., Vedam, S, George, R et al (2006) “The clinical implementation of respiratory gated intensity-modulated radiotherapy” *Medical Dosimetry*, v31, 2, pp 152-162

Keall, P. (2004) “4-dimensional computed tomography imaging and treatment planning” *Seminars in Radiation Oncology* v14 pp81-90

Keat, N., Platten, D. et al (2005) “Report 05071: Siemens Sensation Open CT scanner technical evaluation” Centre for evidence-based purchasing, London

Killoran, J., Allen, A., Kann, B. Et al (2008) “Inter fractional variability of breathing phase definition as determined by fiducial location” *Medical Physics* v35, 2, pp 753-763

Kini, V., Vedam, S., and Keall, P. et al (2003) “Patient training in respiratory-gated radiotherapy” *Medical Dosimetry* v28, pp7-11

Kleshneva, T., Muzik, J. and Alber, M. (2006) “An algorithm for automatic determination of the respiratory phases in four-dimensional computed tomography” *Physics in Medicine & Biology*, v51, pp 269-276

Koch, N., Liu, H., Starkschall, G. et al. (2004) “Evaluation of internal lung motion for respiratory-gated radiotherapy using MRI: Part 1-correlation internal lung motion with skin fiducial motion” *International Journal of Radiation Oncology· Biology ·Physics*. v60 pp 1459-72

Li, X. A, Stepaniak, C. and Gore, E. (2006) “Technical and dosimetric aspects of respiratory gating using a pressure-sensor motion monitoring system” *Medical Physics*, v33, pp 145-153

Lu, H., Brett, R., Sharp, G. (2007) “A respiratory-gated treatment system for proton therapy” *Medical Physics*, v34 (8) pp 3273- 3278

Lu, W., Parihk, P., Hubenschmidt, J. et al (2006) “A comparison between amplitude sorting and phase-angle sorting using external respiratory measurement for 4D CT” *Medical Physics*, v33, 8, pp 2964-2974

Lu, W., Ruchala, J., Chen, Q. (2006) “Real-time respiration monitoring using the radiotherapy treatment beam and four-dimensional computed tomography (4DCT)-a conceptual study*”* *Physics in Medicine & Biology*, v21, 4469-4495.

Luo, Q. (1999) “Artefacts in X-ray CT” Research Imaging Centre, University of Texas, USA

Mageras, G., Pevsner, E., Yorke, K., et al (2004) “Measurement of lung tumour motion using respiration-correlated CT”. *International Journal of Radiation Oncology· Biology ·Physics*. v60, pp 933-941

Metcalfe, P., Kron, T., Hoban, P. (2007) “The physics of radiotherapy x-rays and electrons” Medical Physics Publishing, Madison, Wisconsin.

Millar, M., Cramb, J., Das, R. et al (1997) “ACPSEM position paper: Recommendations for the safe use of external beams and sealed brachytherapy sources in radiation oncology” *Journal of the Australasian College of Physical Scientists and Engineers in Medicine*, v20, 3, Sup 1-35

Mutaf, Y., Antolak, J., Brinkmann, H. (2007) “The impact of temporal inaccuracies on 4D CT image quality” *Medical Physics*, v34, pp 1615-1622

*North Carolina State University*, [Homepage Image Analysis Laboratory], [Online] Available: http://www.ece.ncsu.edu/imaging/MedImg/SIMS/GF19.gif [Accessed 2008, Jan 10]

Nelson, C., Starkschall, G., Balter, P. et al (2007) “Assessment of lung tumour motion and set-up uncertainties using implanted fiducials” *International Journal of Radiation Oncology· Biology ·Physics*. v67, 3, pp 915-923

Nelson, C., Starkschall, G., Balter, P. et al (2005) “Respiration-correlated treatment delivery using feedback-guided breath hold: a technical study” *Medical Physics. v*32**,** pp 175–81

Nioutsikou, E., Bedford, J., Webb, S., et al (2006) “Quantifying the effect of respiratory motion on lung tumour dosimetry with the aid of a breathing phantom with deforming lungs” *Physics in Medicine & Biology*, 51, pp 3359-3374.

Nøttrup, T., Korreman, S., Pedersen, A. (2007) “Intra- and interfraction breathing variations during curative radiotherapy of lung caner” *Radiotherapy and Oncology* v84 pp 40-48

Pan, T. (2004) “Comparison of helical and cine acquisitions for 4D-CT imaging with multislice CT” *Medical Physics* v32 (2) pp 627-634

Pan, T. Lee, T., Rietzel, E. et al (2004) “4D-CT imaging of a volume influenced by respiratory motion on multi-slice CT” *Medical Physics* v31, 2, pp 333-340

Ramsey, C., Scaperoth, D. et al (1999) “Clinical efficiency of respiratory gated conformal radiation therapy” *Medical Dosimetry*, v24, 2, pp 115-119

Riedel, M. (2006) “Respiratory motion estimation: Tests and comparison of different sensors” Munich University of Technology, Erlangan, Germany

Rietzel, E., Liu, A., Doppke, H. et al “Design of 4D treatment planning target volumes” *International Journal of Radiation Oncology· Biology· Physics.* v66, 1, pp 287-295

Rietzel, E., Pan, T. and Chen, G (2005) “Four-dimensional computed tomography: image formation and clinical protocol” *Medical Physics*, v32, 4, pp 874-889

Seppenwoolde, Y., Shirato, H., Kitamura, K. et al (2002) “ Precise and Real-time measurement of 3D tumour motion in lung due to breathing and heartbeat, measured during radiotherapy” *International Journal of Radiation Oncology· Biology· Physics.* v53, pp 822-834

Stepaniak, C., Gore, E. and Li, X. (2005)" Determination of appropriate lung volume for dosimetric planning and analysis from 4D CT*" Medical Physics v*32, p1946 (abs)

[Homepage of The Cancer Council Australia], [Online], Available: http://www.cancer.org.au//File/HealthProfessionals/Clinical%20Guidelines/lungguidelinesforGPs.pdf [Accessed 2007, Nov 16]

Timinger, H., Krüger S., Dietmayer, K. et al (2005) "Motion compensation coronary interventional navigation by means of diaphragm tracking and elastic motion models" *Physics in Medicine & Biology*, v50, 3, pp 491-503.

Tsunashima, Y., Sakae, T. et al (2004) "Correlation between the respiratory waveform measured using a respiratory sensor and 3D tumour motion in gated radiotherapy" *International Journal of Radiation Oncology· Biology· Physics.* v60, pp 951-8

Underberg, R., Lagerwaard, F., Cuijpers, J., et al (2004) "Four-dimensional CT scans for treatment planning in stereotactic radiotherapy for stage I lung cancer," *International Journal of Radiation Oncology· Biology· Physics.* v60 pp1283–1290

*Varian Medical Systems*, [Homepage of Varian Medical systems], [Online] Available: http://www.varian.com/ [Accessed 2006, September 22]

Vedam, S., Keall, O., Kini, V. et al (2003) "Acquiring a four-dimensional computed tomography dataset using an external respiratory signal" *Physics in Medicine and Biology* v48, pp45-62

Vedam, S., Keall, P., Kini, V. et al (2001) "Determining parameters for respiration-gated radiotherapy" *Medical Physics*, v28, 10, pp 2139-2146

Vedam, S., Kini, V., Keall, P. et al (2003) "Quantifying the predictability of diaphragm motion during respiration with a non-invasive external marker" *Medical Physics* v30 pp 505-513

Wagner, T., Meeks, S., Bova, F. et al (2007) “Optical tracking technology in stereotactic radiation therapy” *Medical Dosimetry*, v32 (2) pp 111-120

Webb, S. (2005) “Radiotherapy physics: the next ten years of technical development” *Imaging Oncology* v1 pp43-50

White D.R. (1977) “The formulation of tissue substitute materials using basic interaction data” *Physics in Medicine and Biology*, 22: 889–899

Wink, N., McNitt-Gray, M., and Solberg, T. (2005) “Optimisation of multi-slice helical respiration-correlated CT: the effects of table speed and rotation time” *Physics in Medicine & Biology*, v50, pp 5717-5729

Williams, J., Thwaites, D. (2000) “Radiotherapy physics in practice” Oxford University Press, Oxford

Wilting. J., Timmer, J. (1999) “Artefacts in spiral-CT images and their relation to pitch and subject morphology” *European Radiology* v9, pp 316-322

Wolthaus, J., Schneider, C., Sonke, J. (2006) “Mid-ventilation CT scan construction from four-dimensional respiration-corelated CT scans for radiotherapy planning of lung cancer patients” *International Journal of Radiation Oncology· Biology· Physics* v65 (5) pp 1560-1571

Yan, H., Zhu, G., Munther, A., Kim, J. (2006) “The correlation evaluation of a tumour tracking system using multiple external markers” *Medical Physics* v33 (11) pp4073-4084

Yorke, E., Rozenweig, K., Wagman, R. et al (2005) “Interfractional anatomic variation in patients treated with respiration-gated radiotherapy.” *Journal of applied clinical medical physics*, v6, 2, 19-31

Zhang, T., Lu, W., Olivera, G. et al (2007) “Breathing-synchronised delivery: A potential four-dimensional tomotherapy treatment technique” *International Journal of Radiation Oncology· Biology· Physics* v68 (5) pp 1572-1578

# APPENDIX

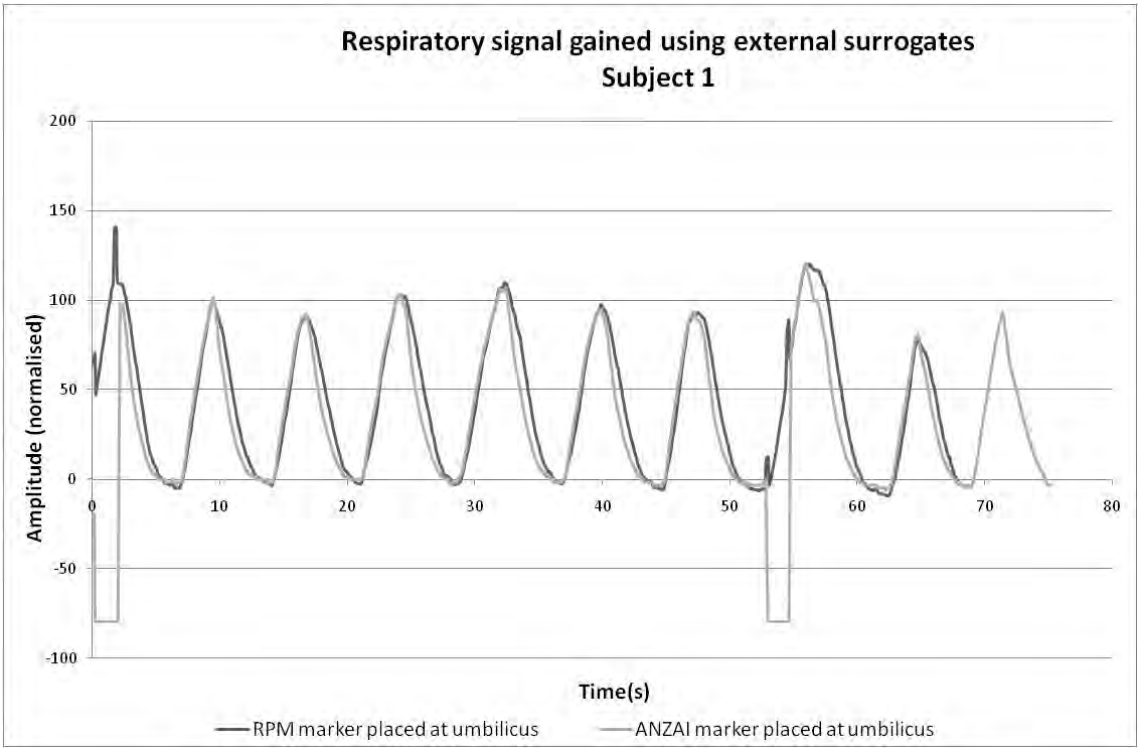


Figure A1: Respiratory signals gained using both RPM marker and Anzai belt positioned at umbilicus for subject 1.

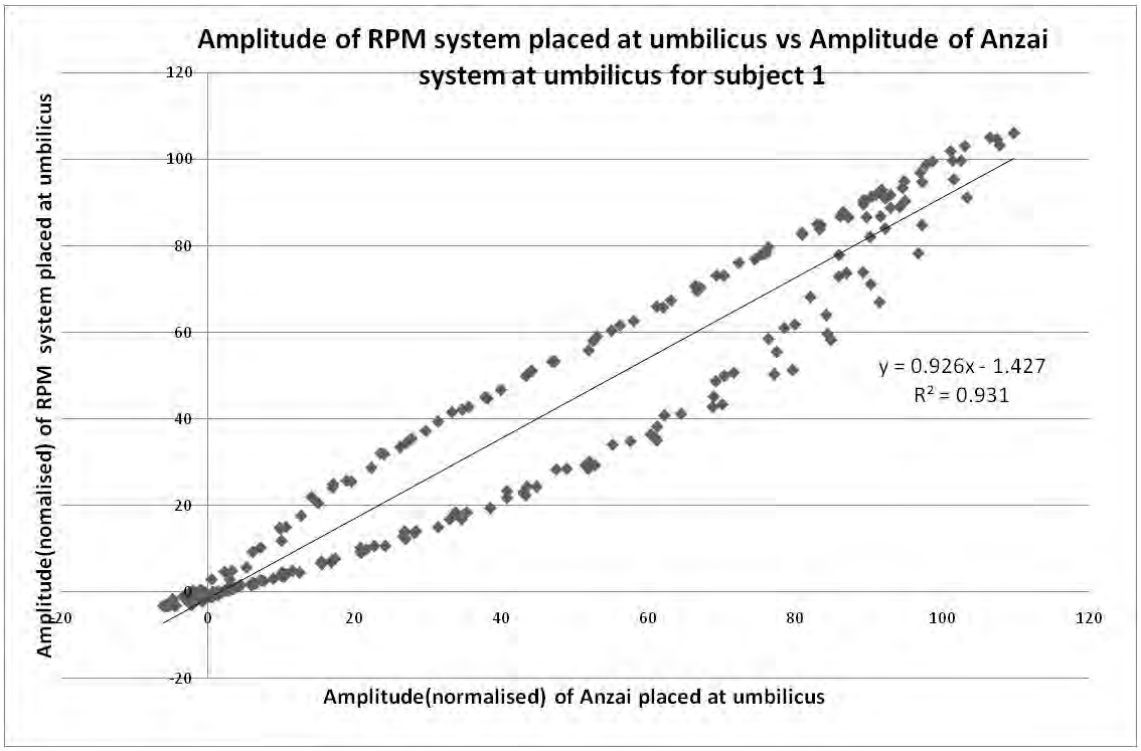


Figure A2: Determination of coefficient of determination for both RPM and Anzai positioned at umbilicus, subject 1.

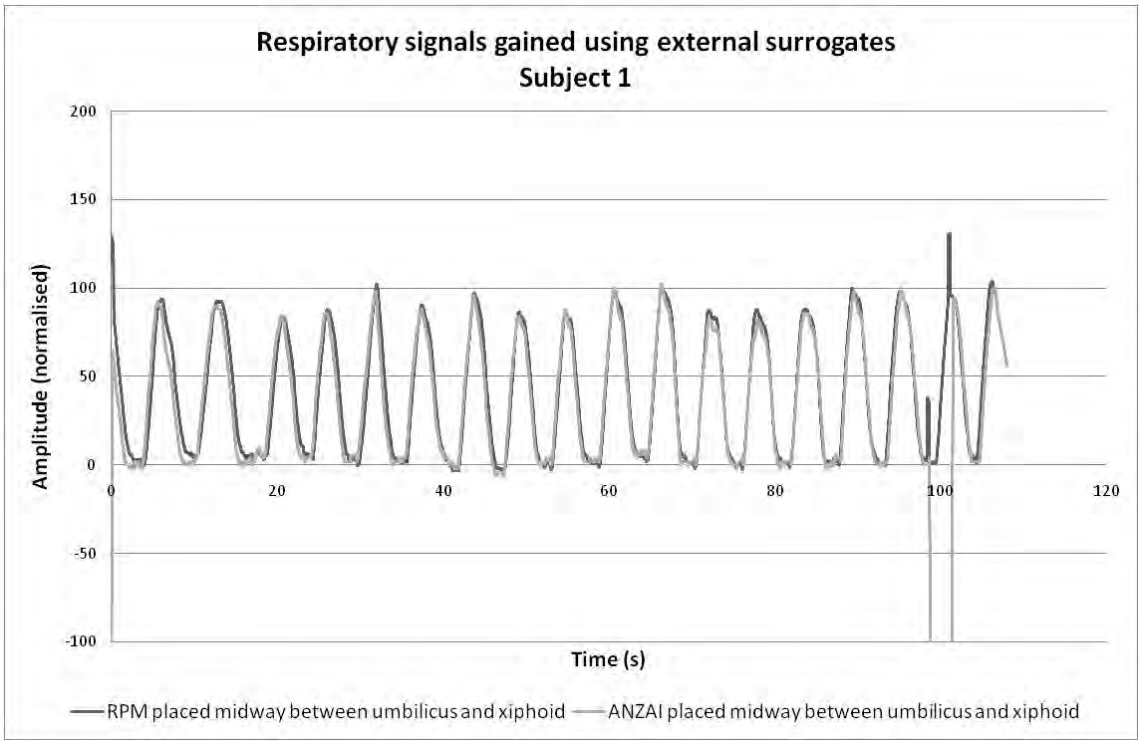


Figure A3: Respiratory signals gained using both RPM marker and Anzai belt positioned midway between umbilicus and xiphoid for subject 1.

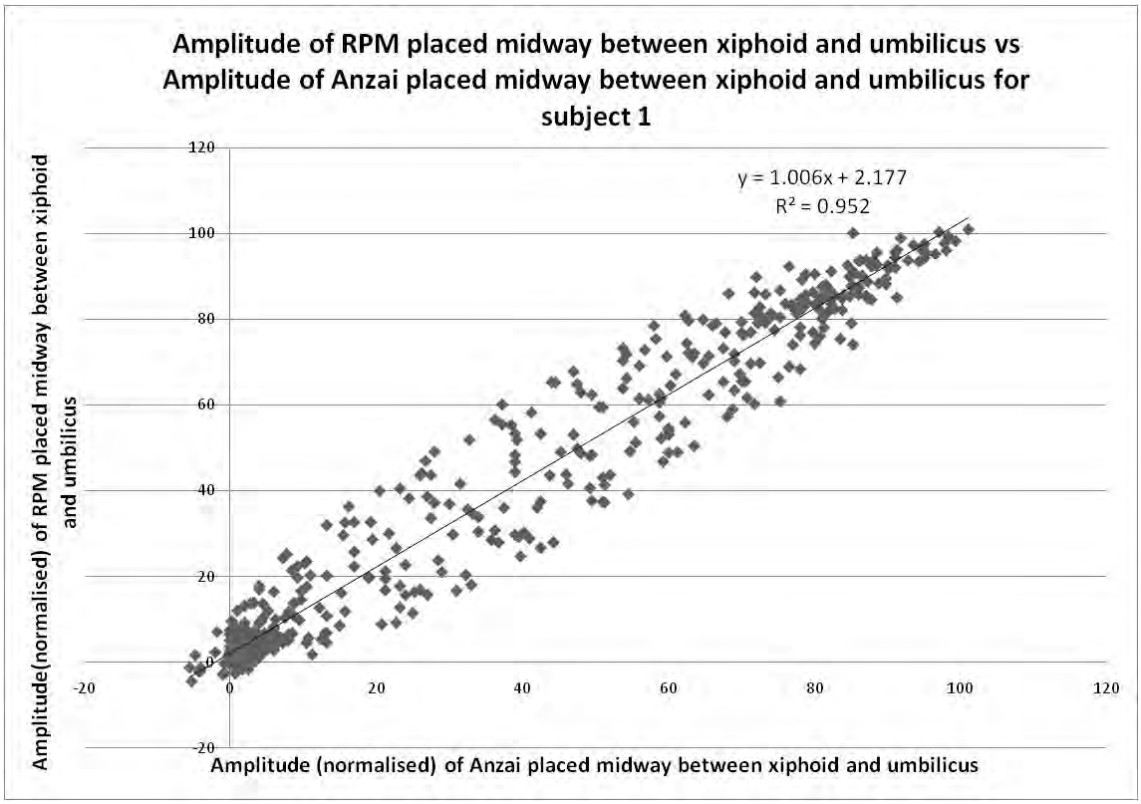


Figure A4: Determination of coefficient of determination for both RPM and Anzai positioned midway between xiphoid and umbilicus, subject 1.

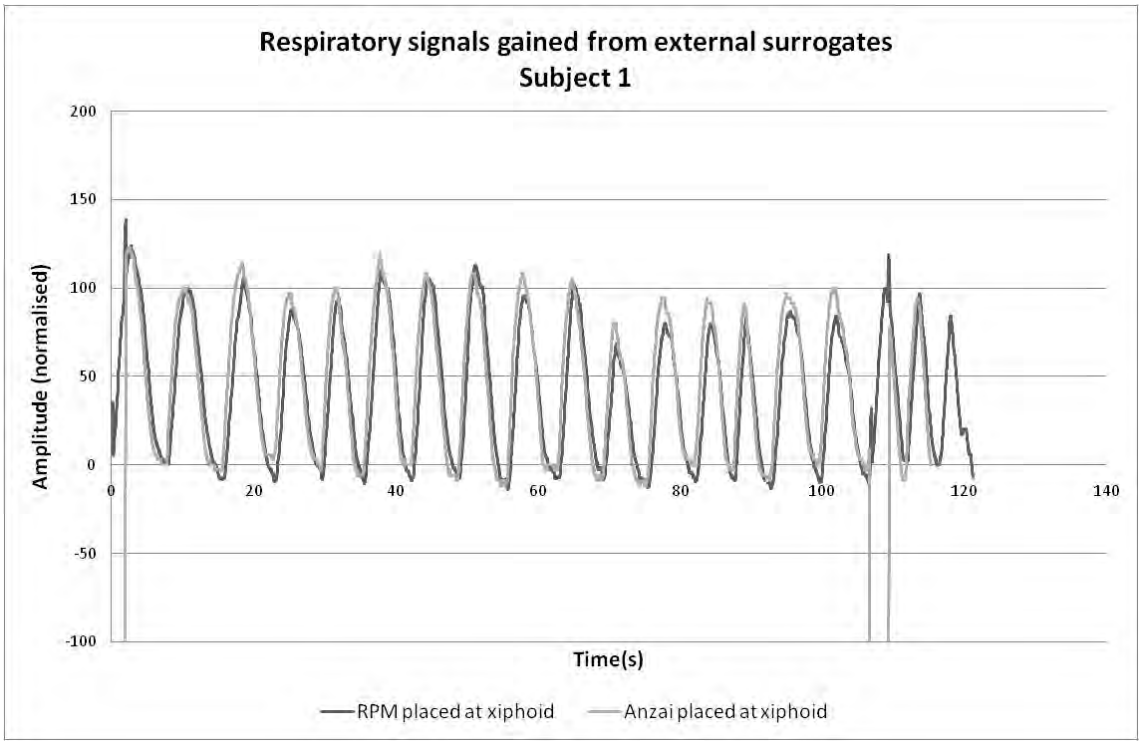


Figure A5: Respiratory signals gained using both RPM marker and Anzai belt positioned at xiphoid for subject 1.

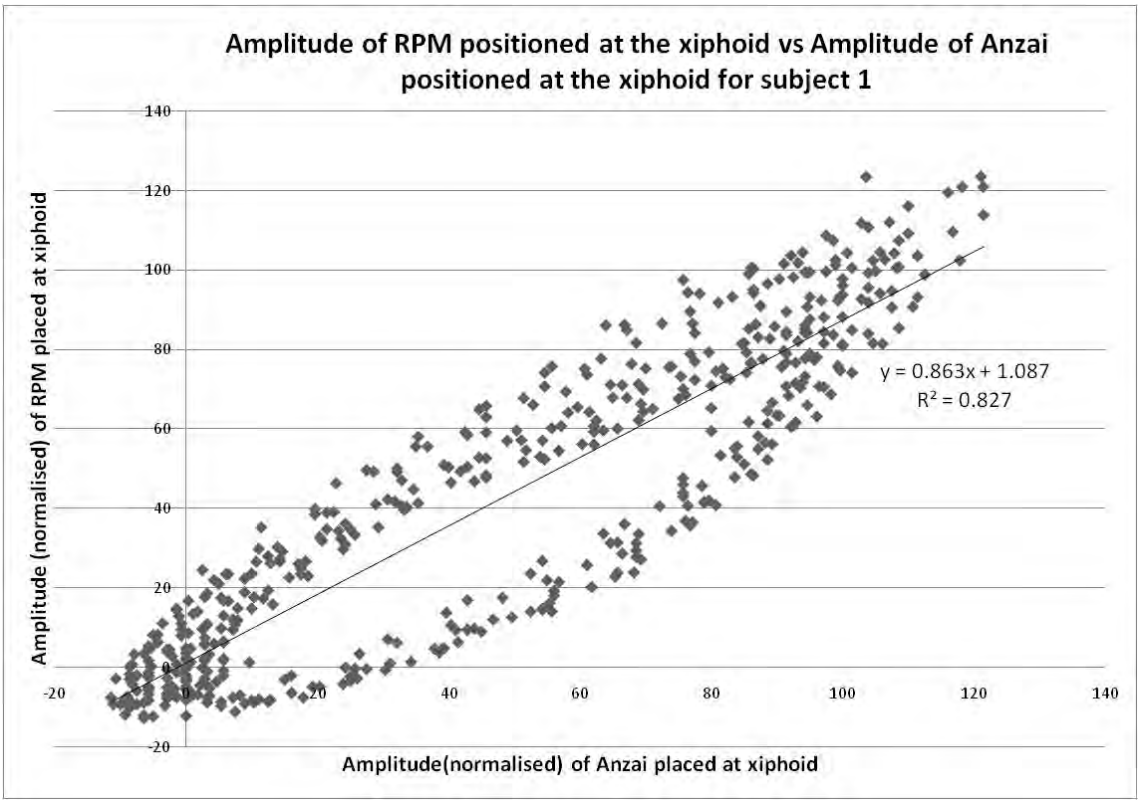


Figure A6: Determination of coefficient of determination for both RPM and Anzai positioned at xiphoid, subject 1.

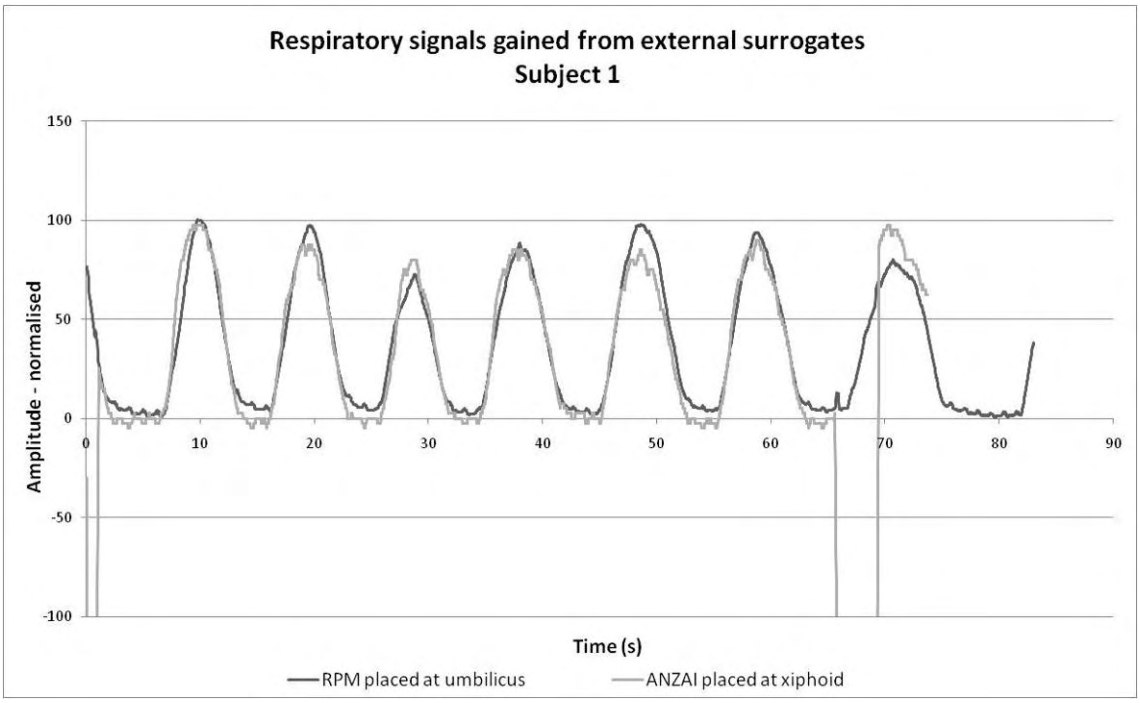


Figure A7: Respiratory signals gained using RPM marker positioned at the umbilicus and Anzai belt positioned at xiphoid for subject 1.

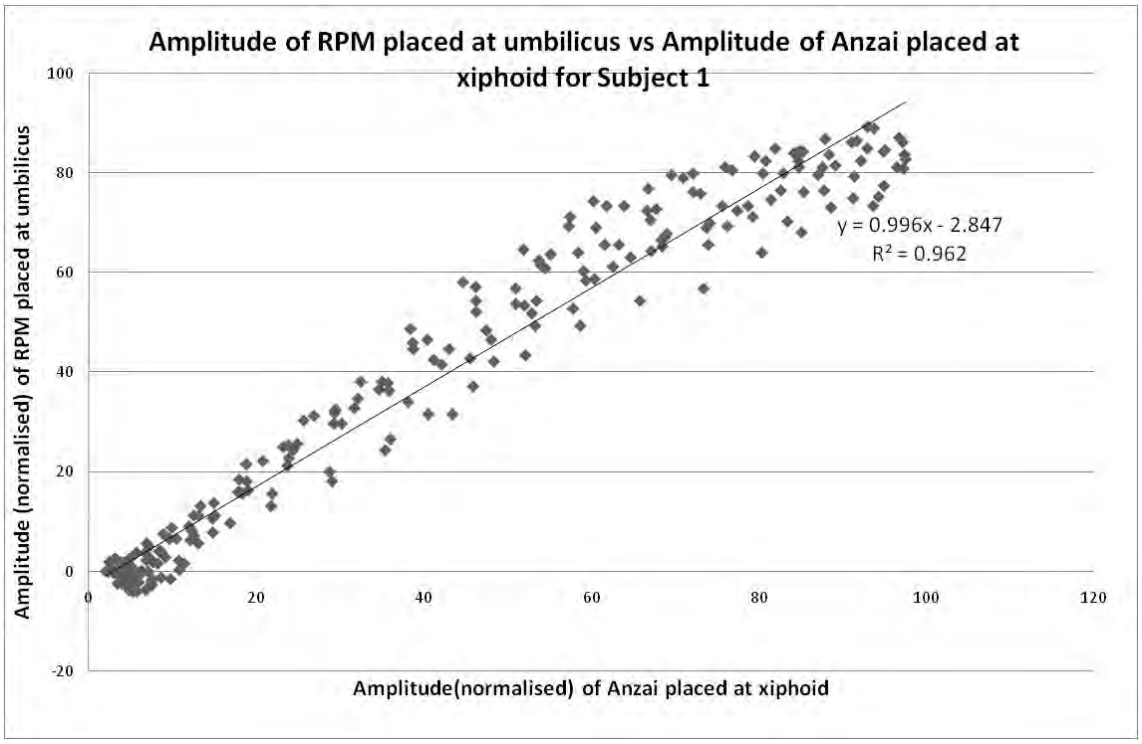


Figure A8: Determination of coefficient of determination for RPM positioned at the umbilicus and Anzai positioned at xiphoid, subject 1.

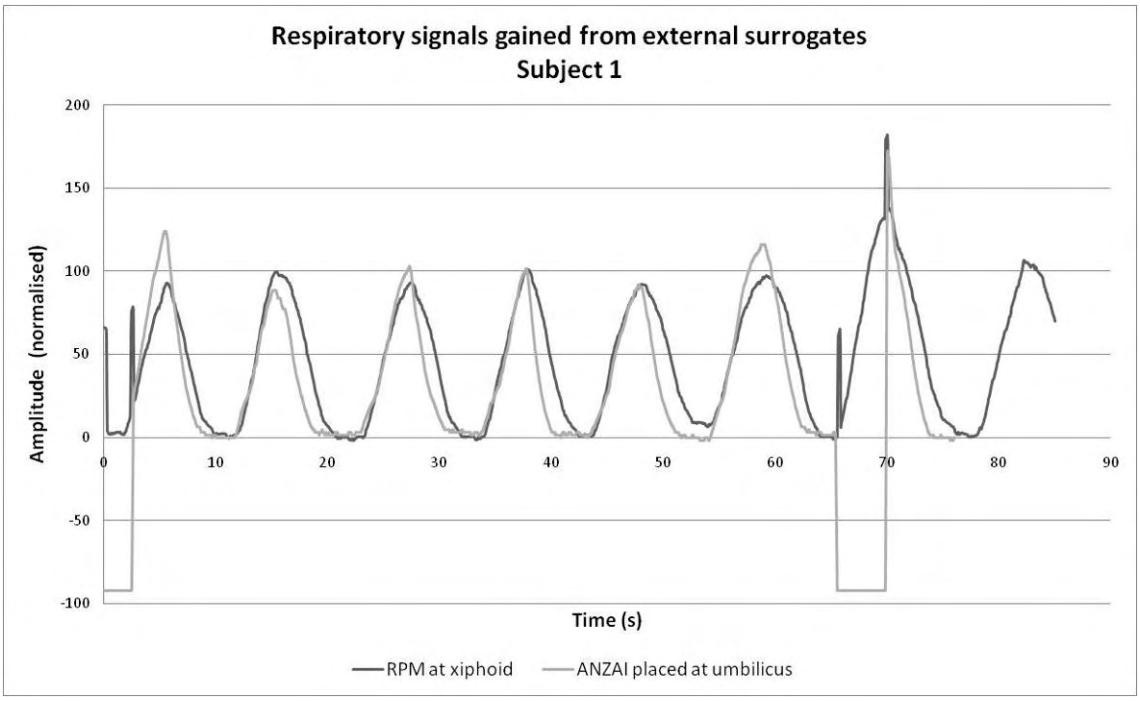


Figure A9: Respiratory signals gained using RPM marker positioned at the xiphoid and Anzai belt positioned at umbilicus for subject 1.

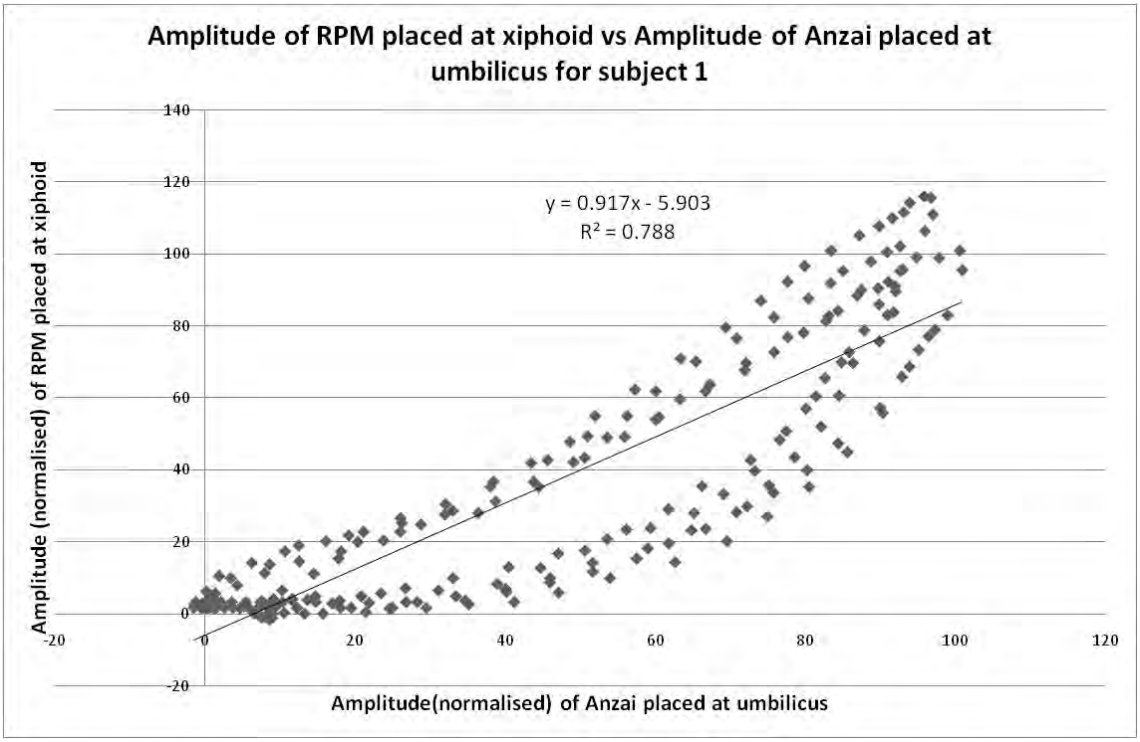


Figure A10: Determination of coefficient of determination for RPM positioned at the xiphoid and Anzai positioned at umbilicus, subject 1.

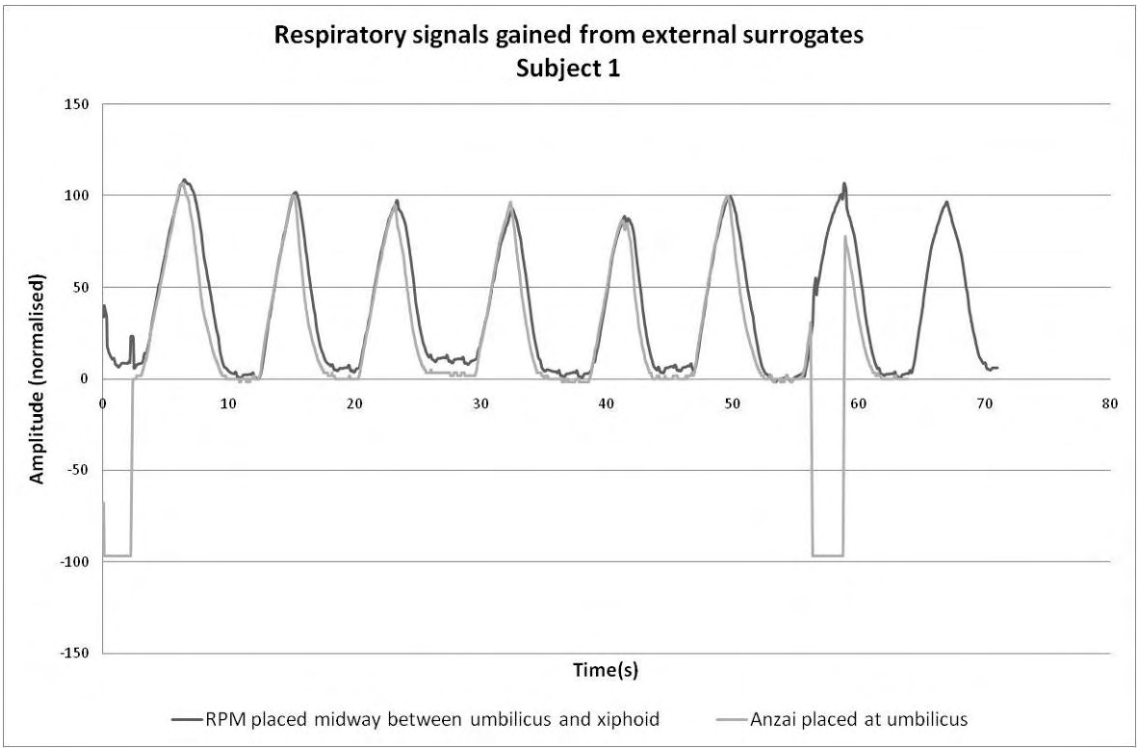


Figure A11: Respiratory signals gained using RPM marker positioned midway between xiphoid and umbilicus and Anzai belt positioned at umbilicus for subject.

1

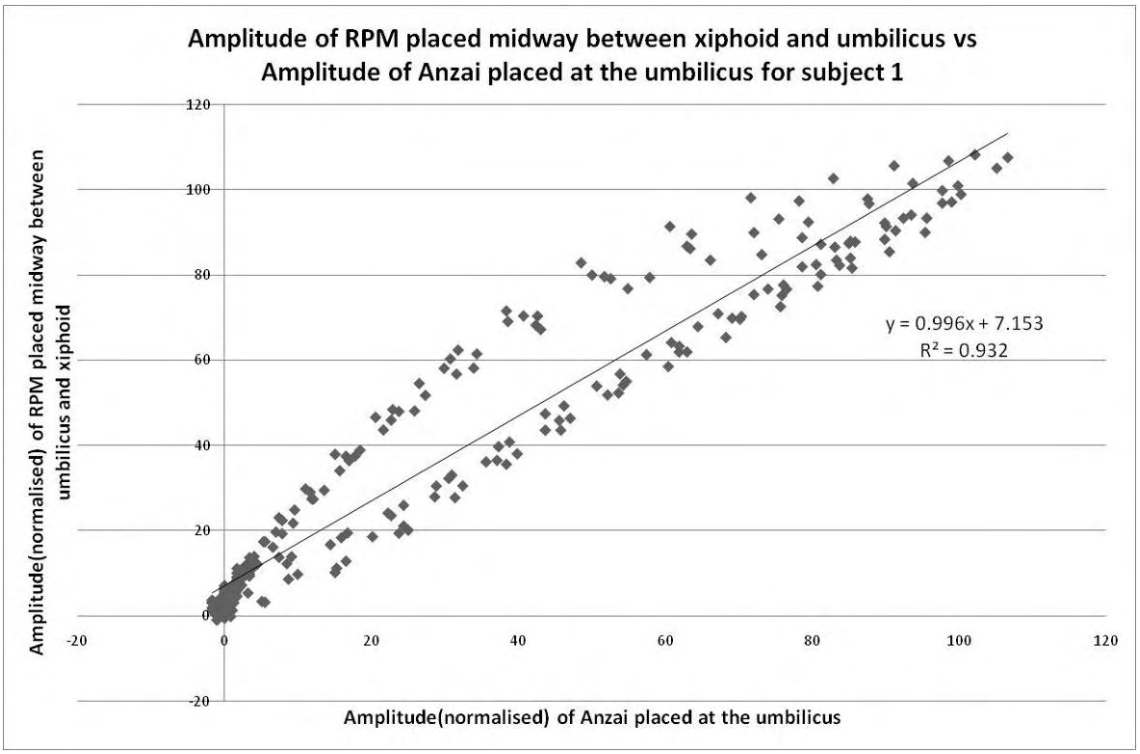


Figure A12: Determination of coefficient of determination for RPM positioned midway between xiphoid and umbilicus and Anzai positioned at umbilicus, subject 1.

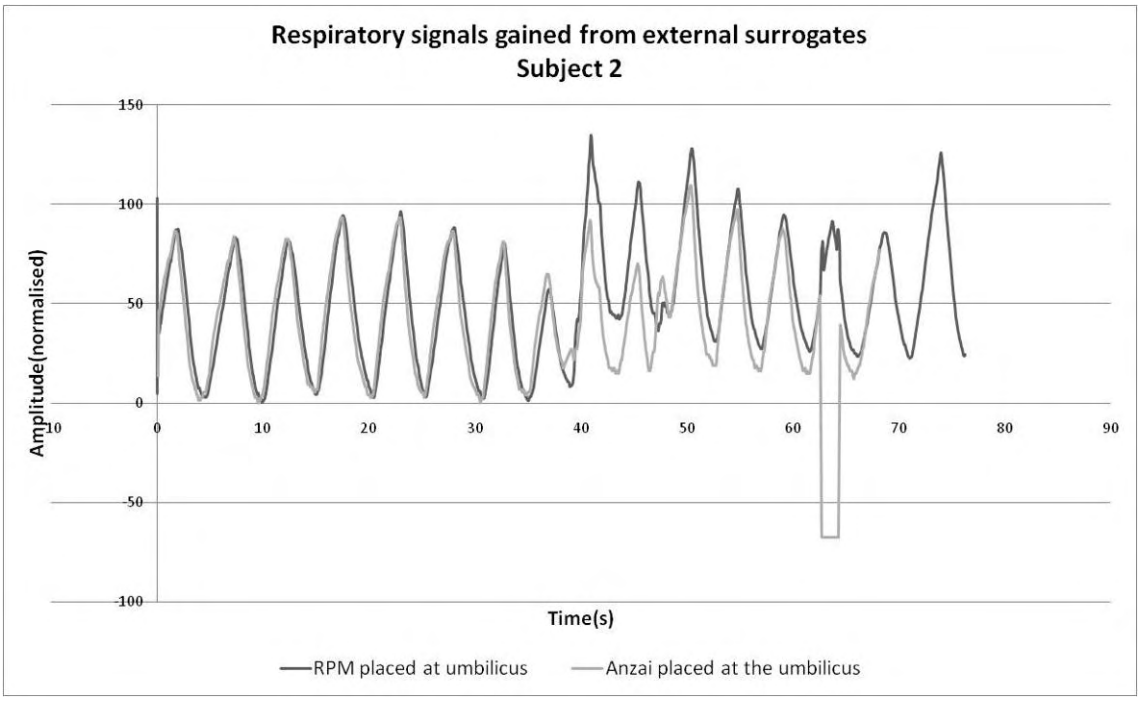


Figure A13: Respiratory signals gained using both markers positioned at the umbilicus for subject 2.

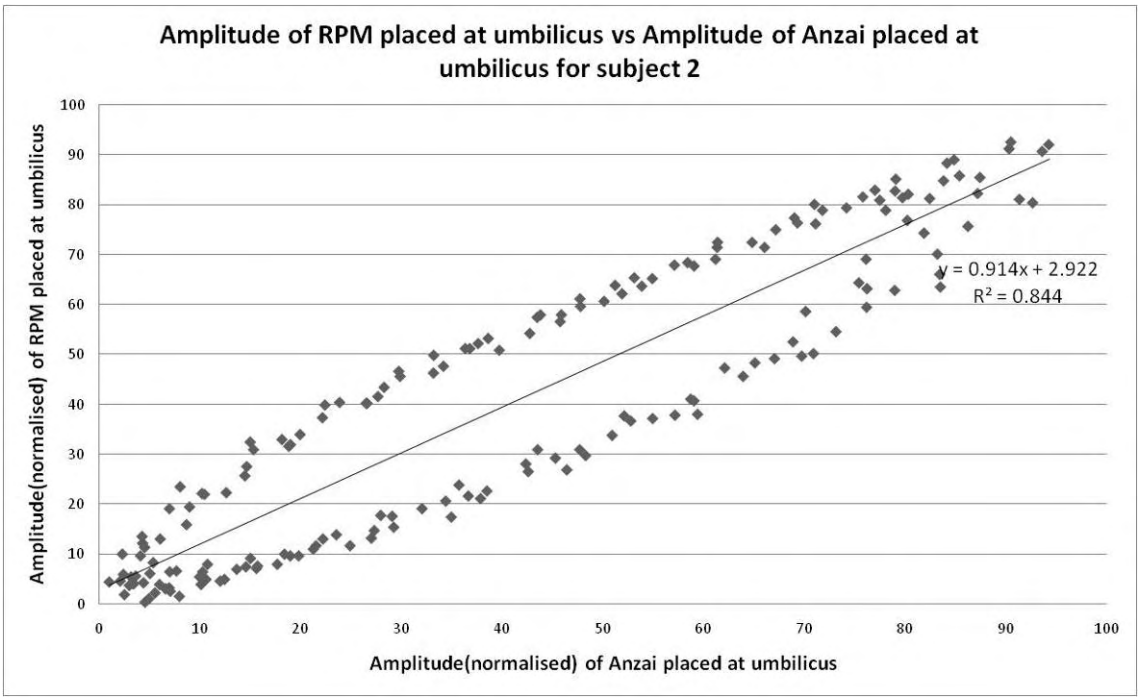


Figure A14: Respiratory signals gained using both RPM marker and Anzai belt positioned at umbilicus for subject.

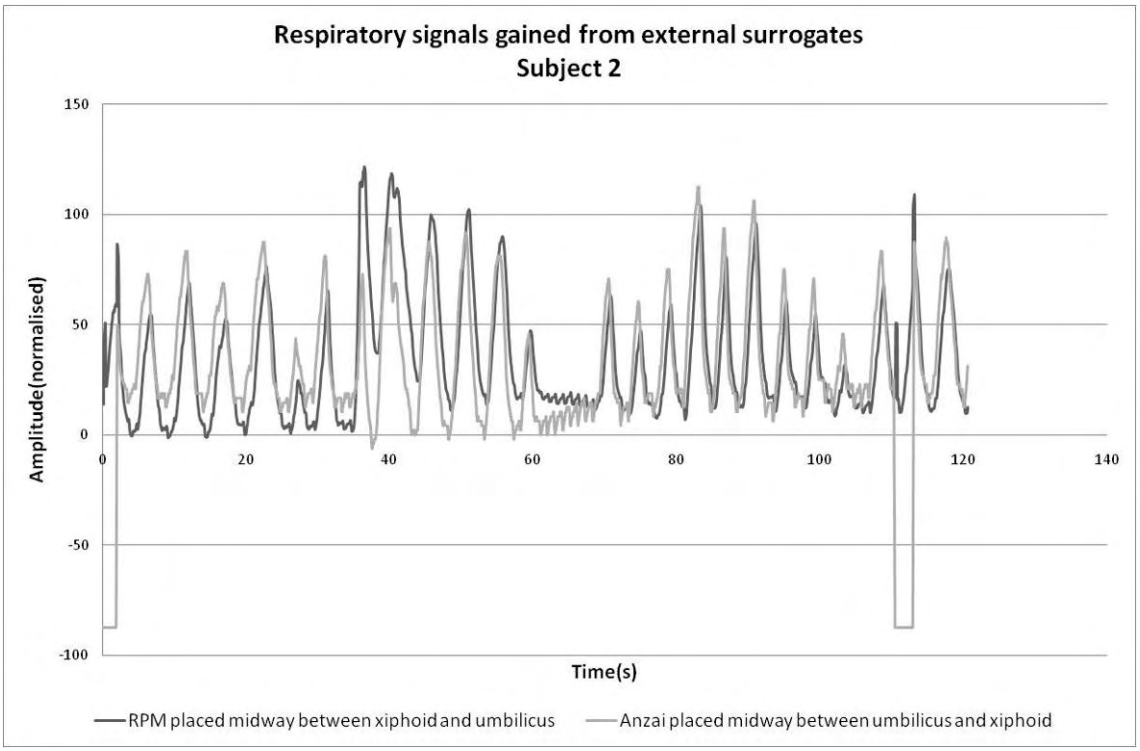


Figure A15: Respiratory signals gained using both RPM marker and Anzai belt positioned midway between umbilicus and xiphoid for subject 2.

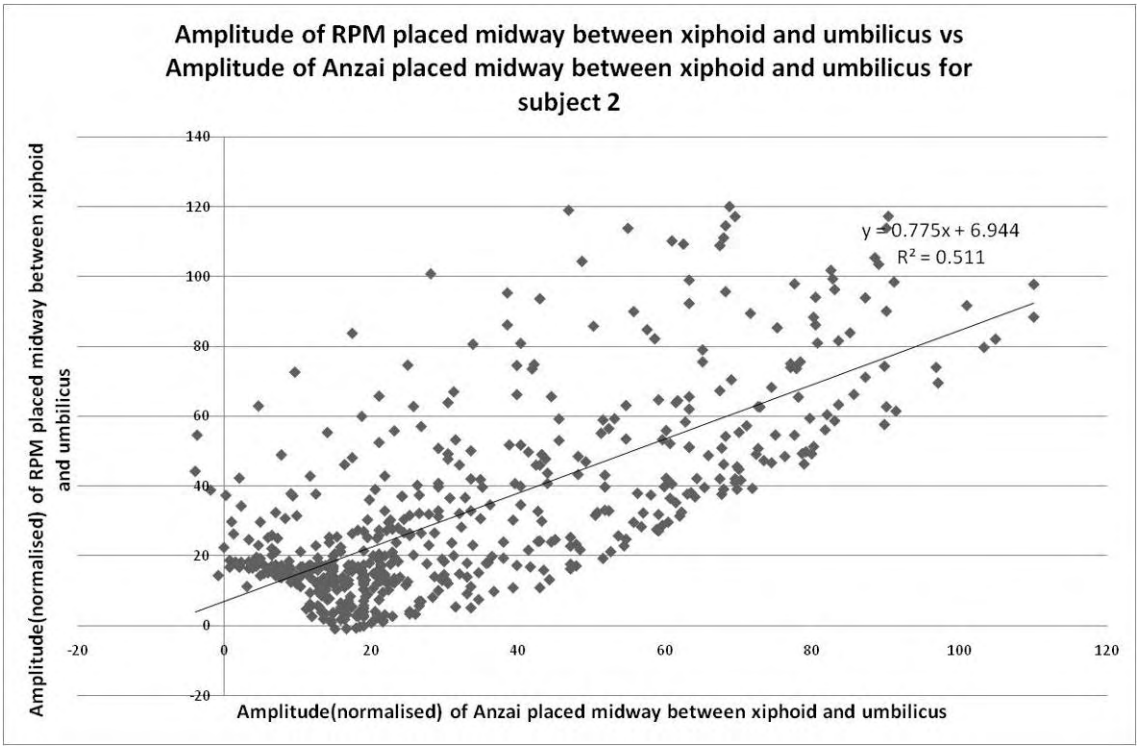


Figure A16: Determination of coefficient of determination for both RPM and Anzai positioned midway between xiphoid and umbilicus, subject 2.

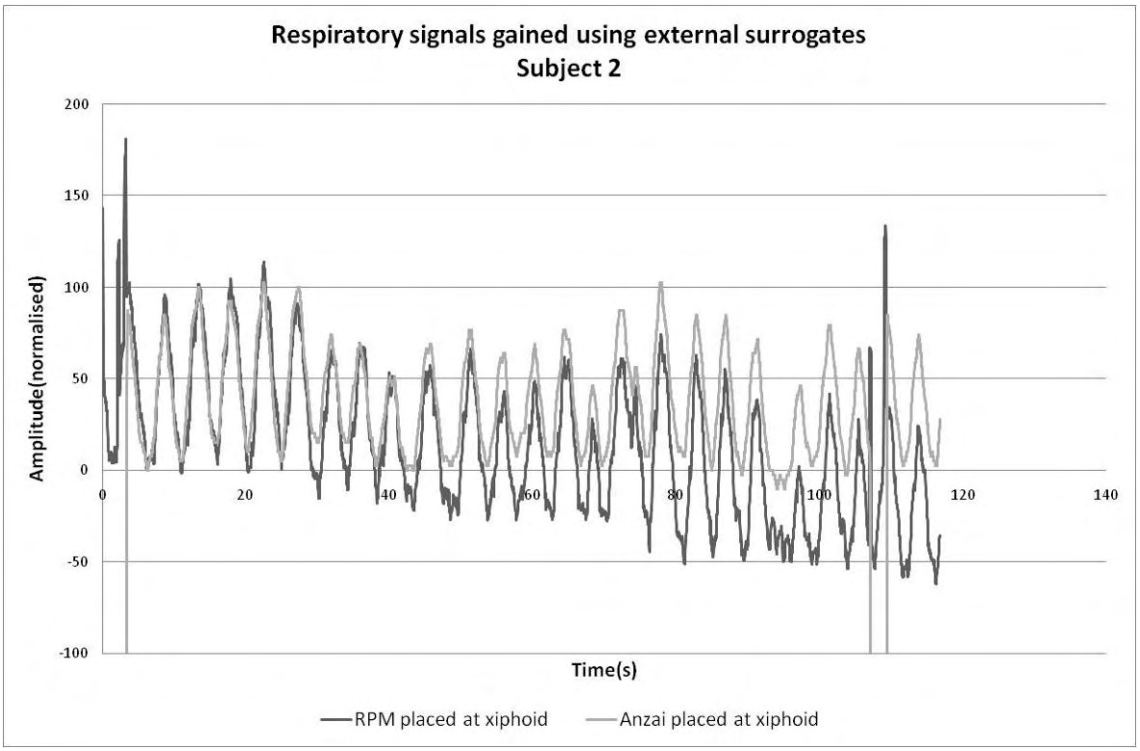


Figure A17: Respiratory signals gained using both RPM marker and Anzai belt positioned at xiphoid for subject 2.

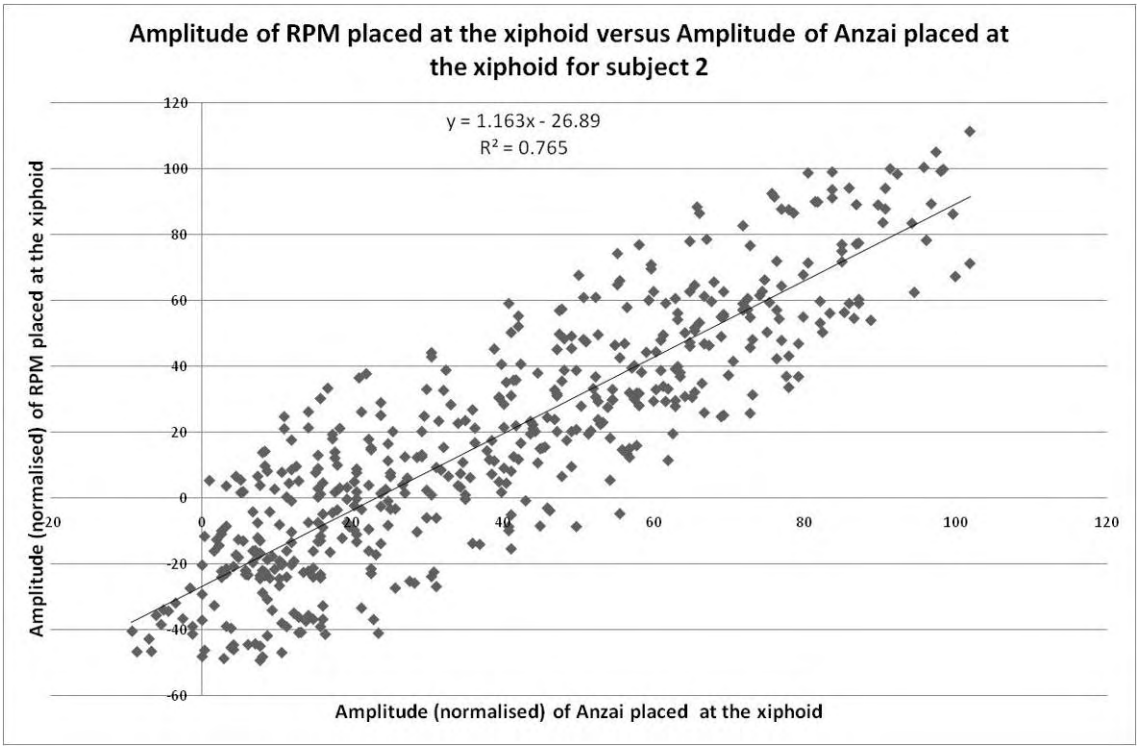


Figure A18: Determination of coefficient of determination for both RPM and Anzai positioned at xiphoid, subject 2.

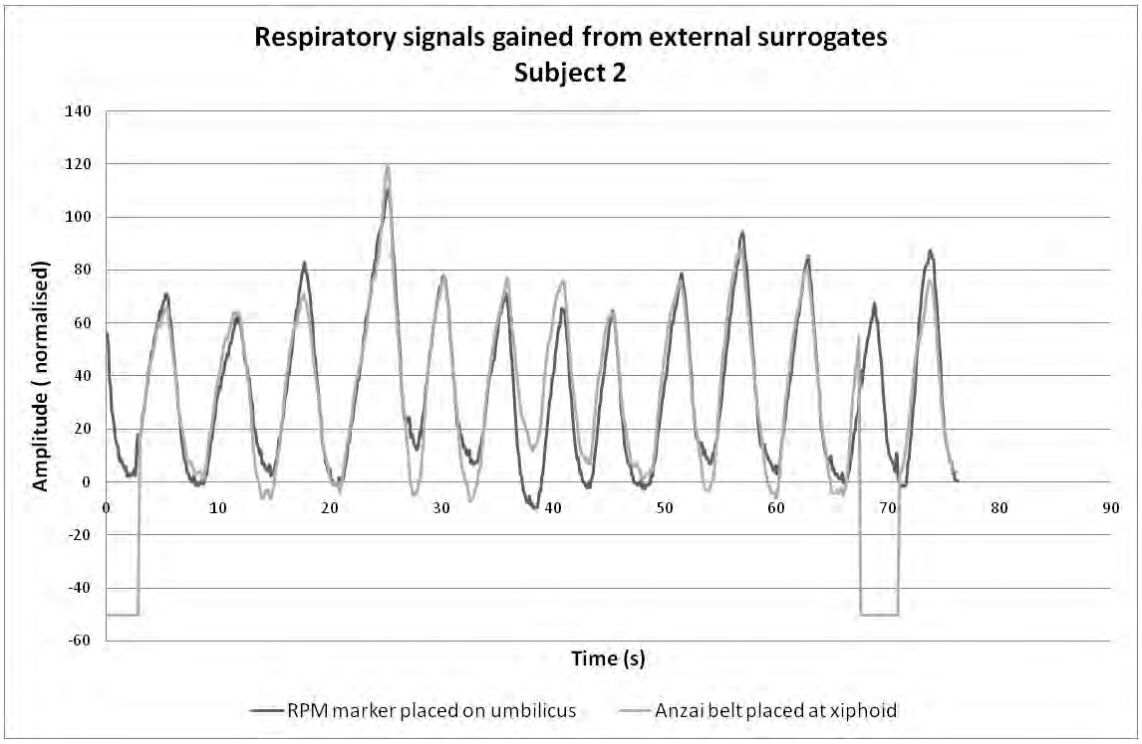


Figure A19: Respiratory signals gained using RPM marker positioned at the umbilicus and Anzai belt positioned at xiphoid for subject 2.

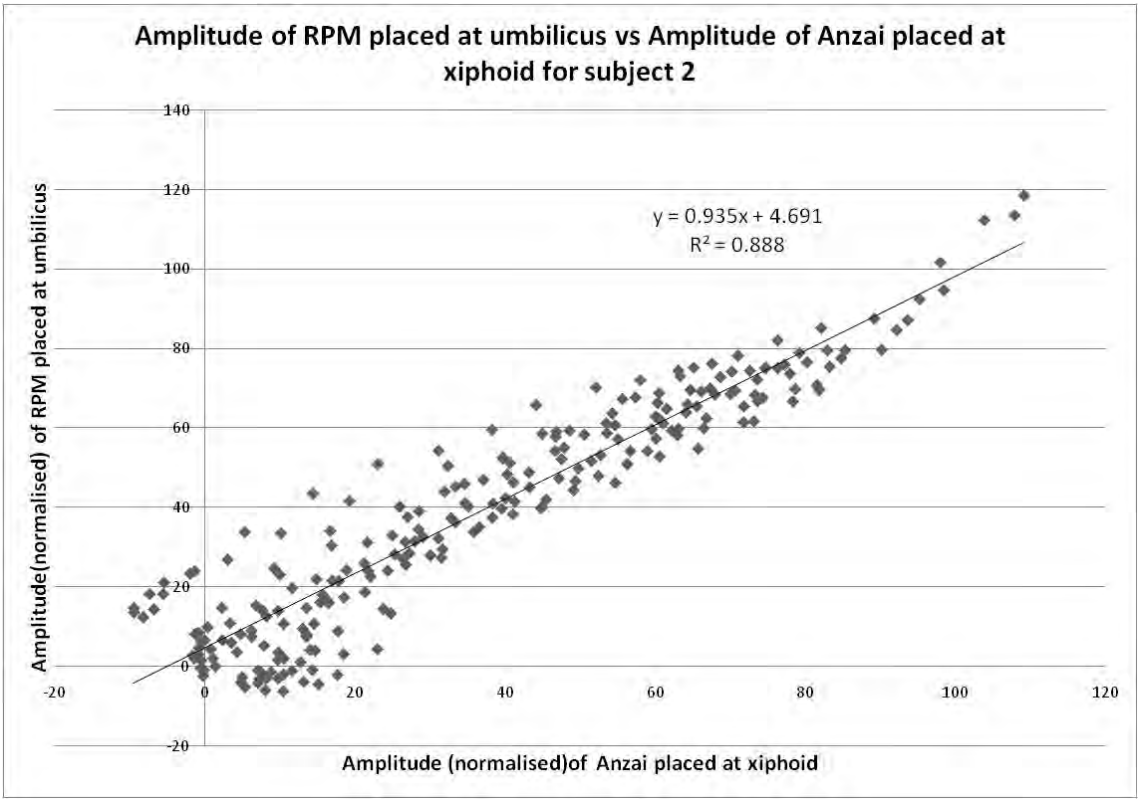


Figure A20: Determination of coefficient of determination for RPM positioned at the umbilicus and Anzai positioned at xiphoid, subject 2.

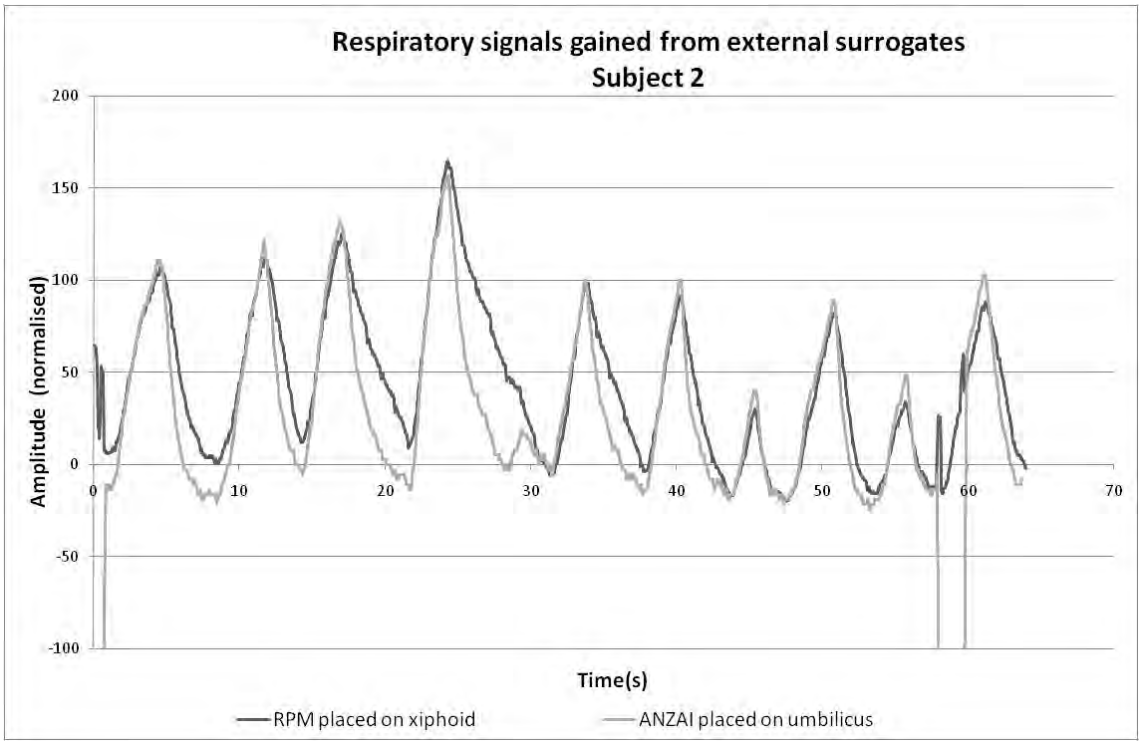


Figure A21: Respiratory signals gained using RPM marker positioned at the xiphoid and Anzai belt positioned at umbilicus for subject 2.

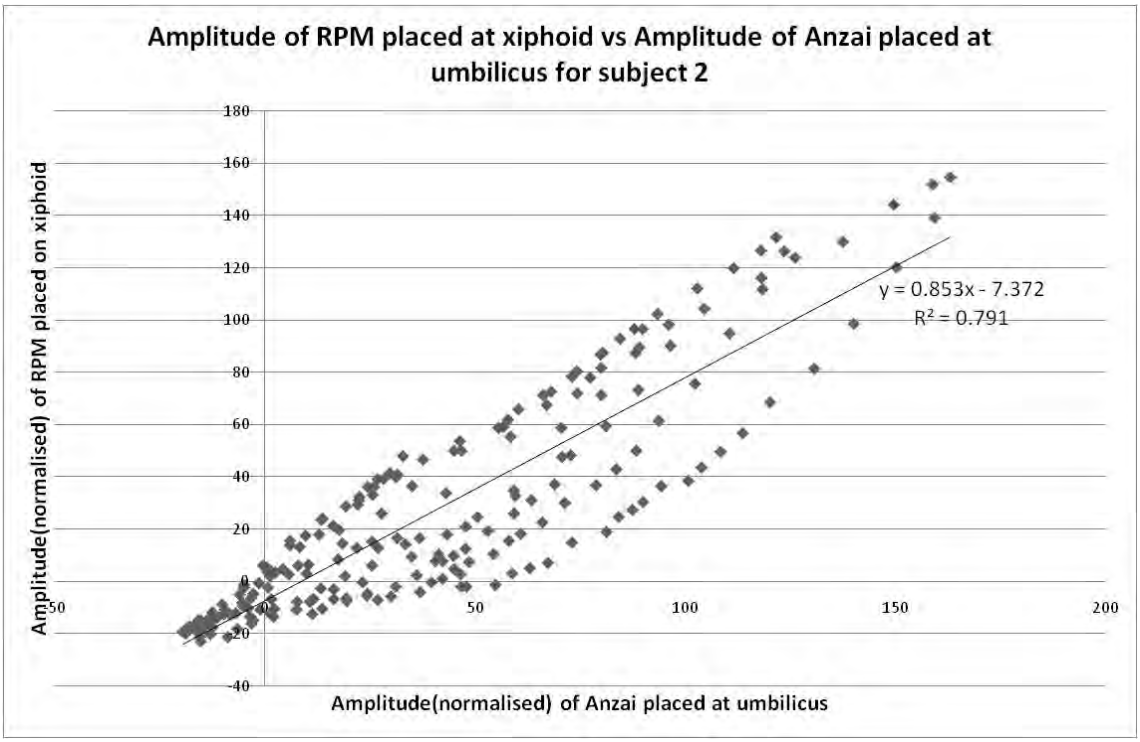


Figure A22: Determination of coefficient of determination for RPM positioned at the xiphoid and Anzai positioned at umbilicus, subject 2.

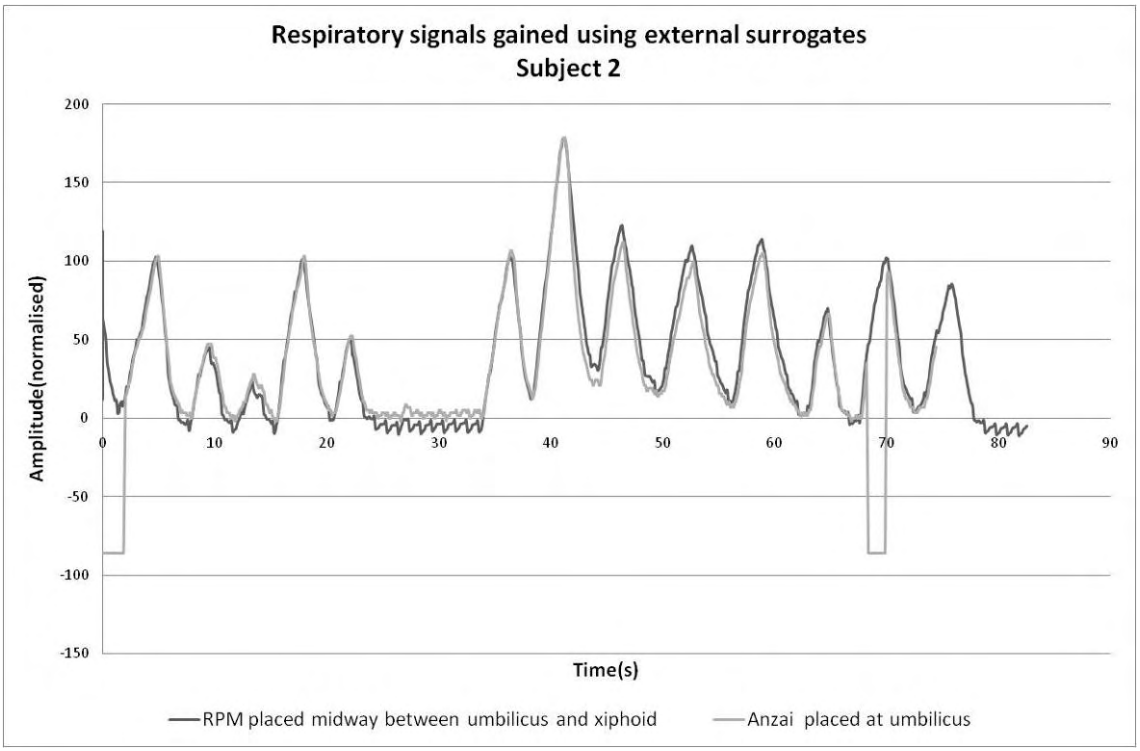


Figure A23: Respiratory signals gained using RPM marker positioned midway between xiphoid and umbilicus and Anzai belt positioned at umbilicus for subject 2.

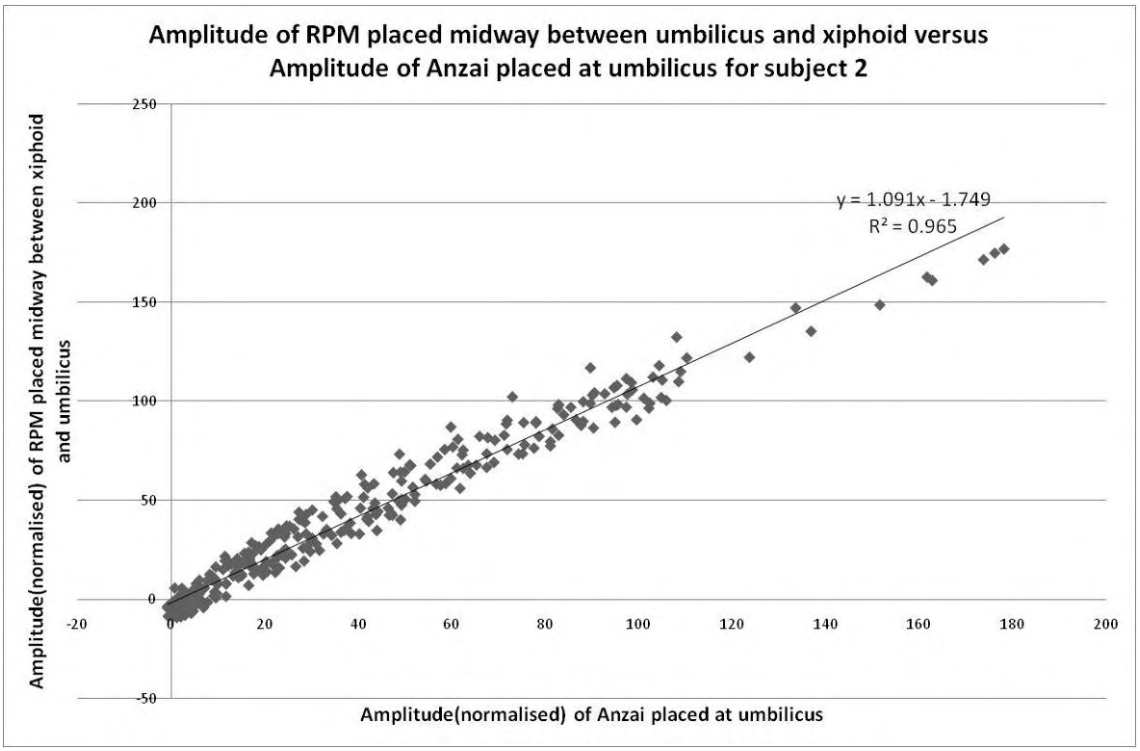


Figure A24: Determination of coefficient of determination for RPM positioned midway between xiphoid and umbilicus and Anzai positioned at umbilicus, subject 2.

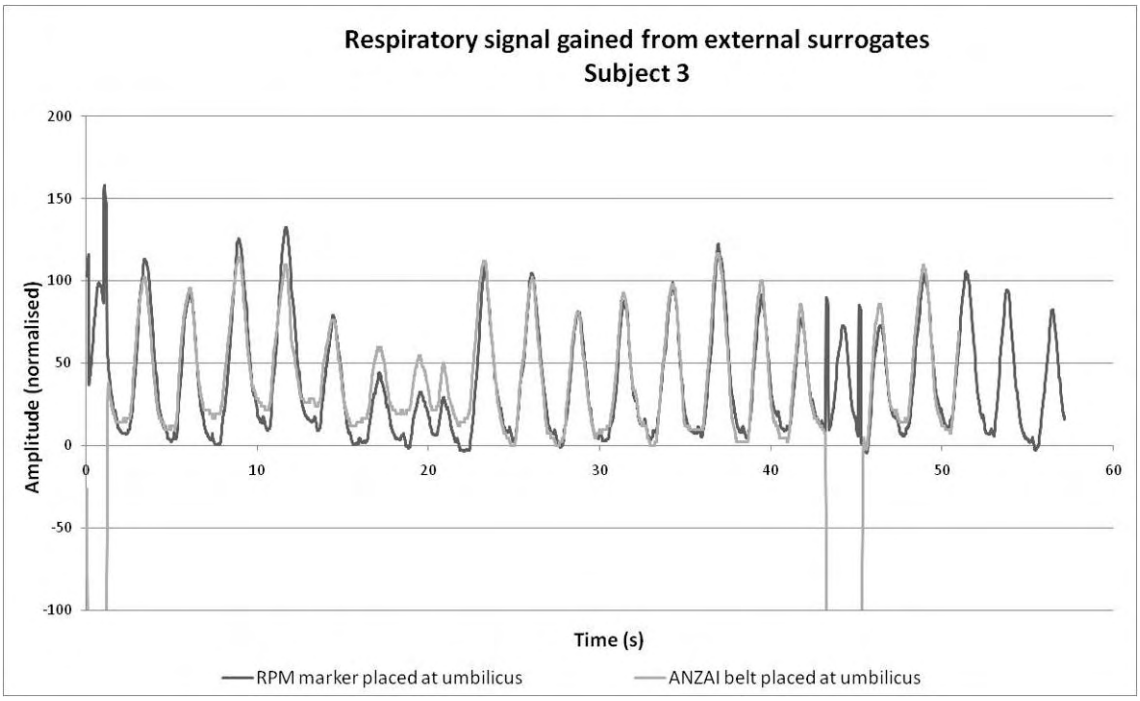


Figure A25: Respiratory signals gained using both RPM marker and Anzai belt positioned at umbilicus for subject 3.

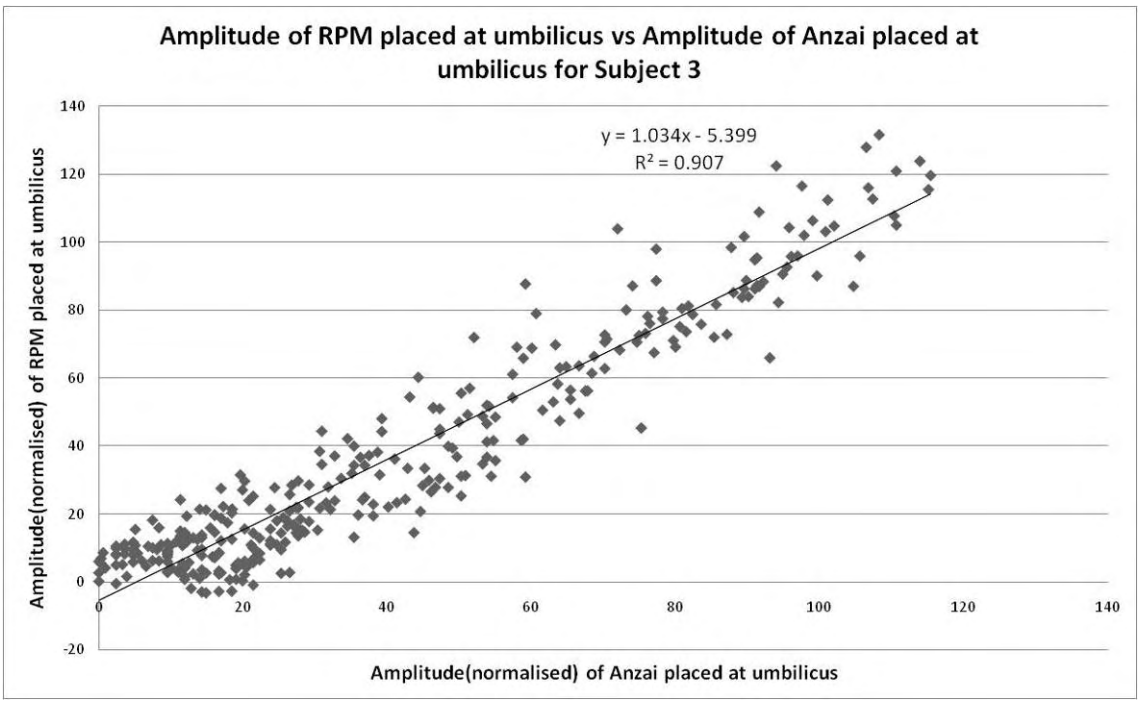


Figure A26: Determination of coefficient of determination for both RPM and Anzai positioned at umbilicus, subject 3.

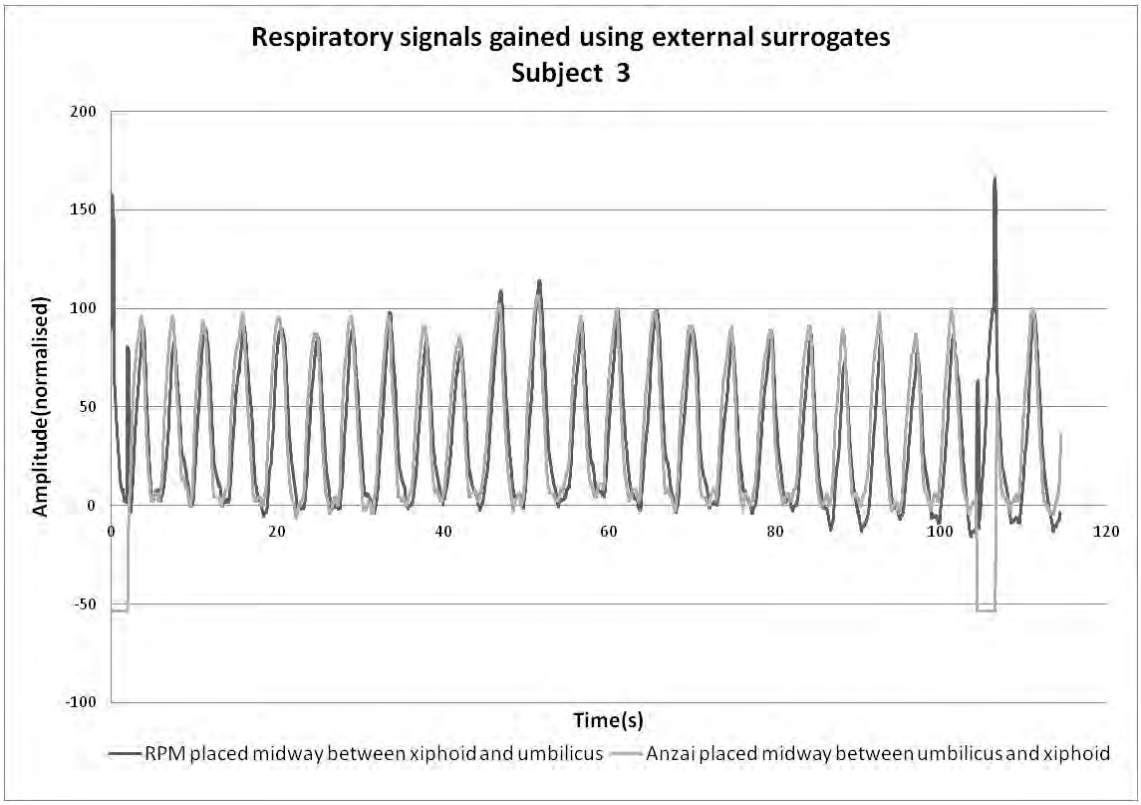


Figure A27: Respiratory signals gained using both RPM marker and Anzai belt positioned midway between umbilicus and xiphoid for subject 3.

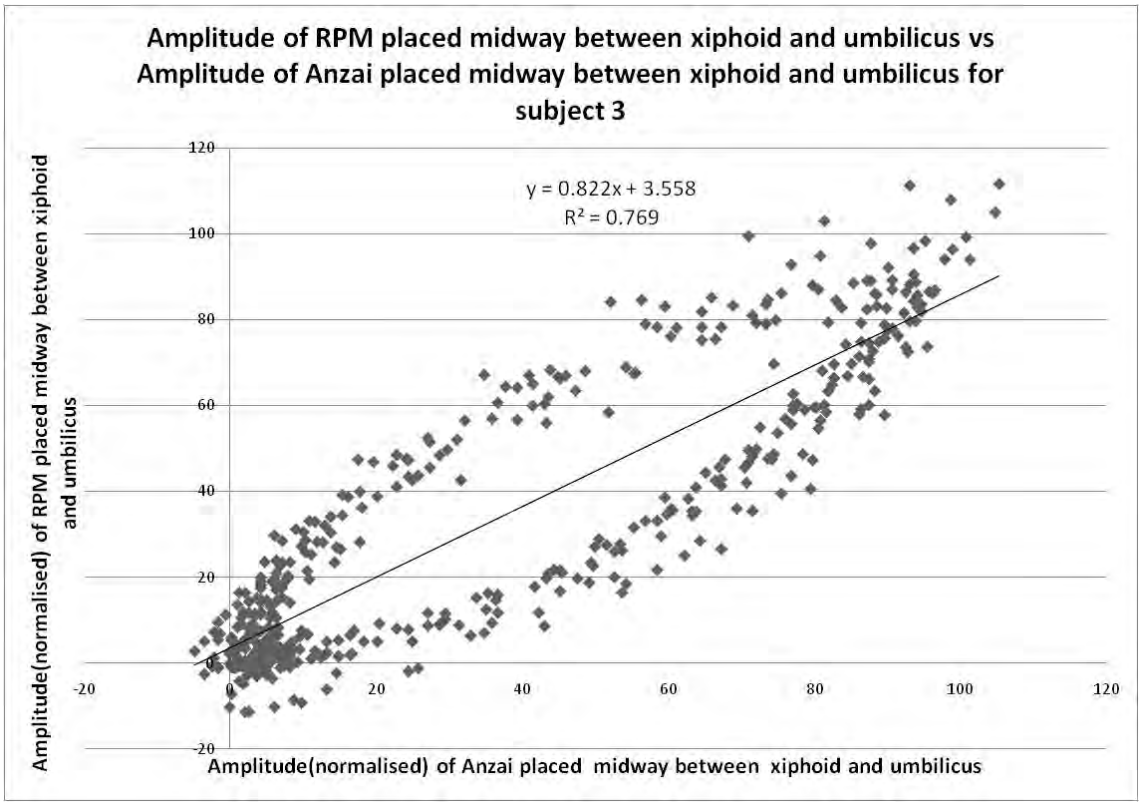


Figure A28: Determination of coefficient of determination for both RPM and Anzai positioned midway between xiphoid and umbilicus, subject 3.

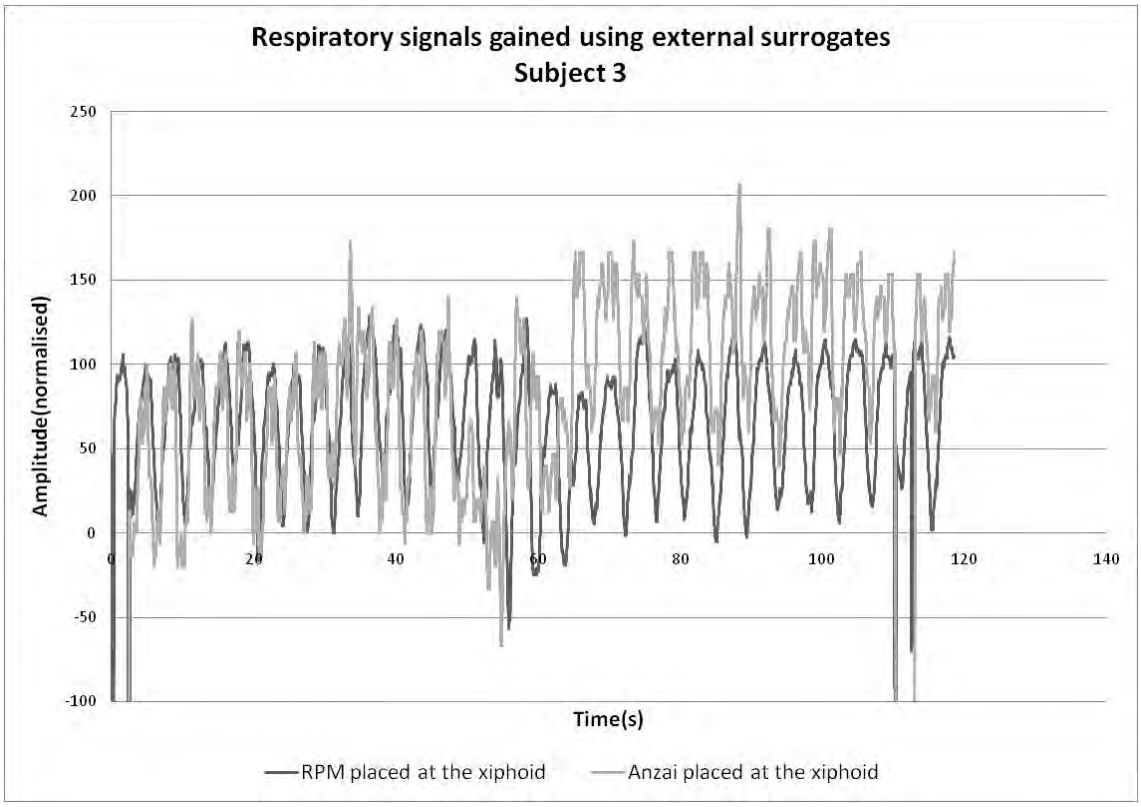


Figure A29: Respiratory signals gained using both RPM marker and Anzai belt positioned at xiphoid for subject 3.

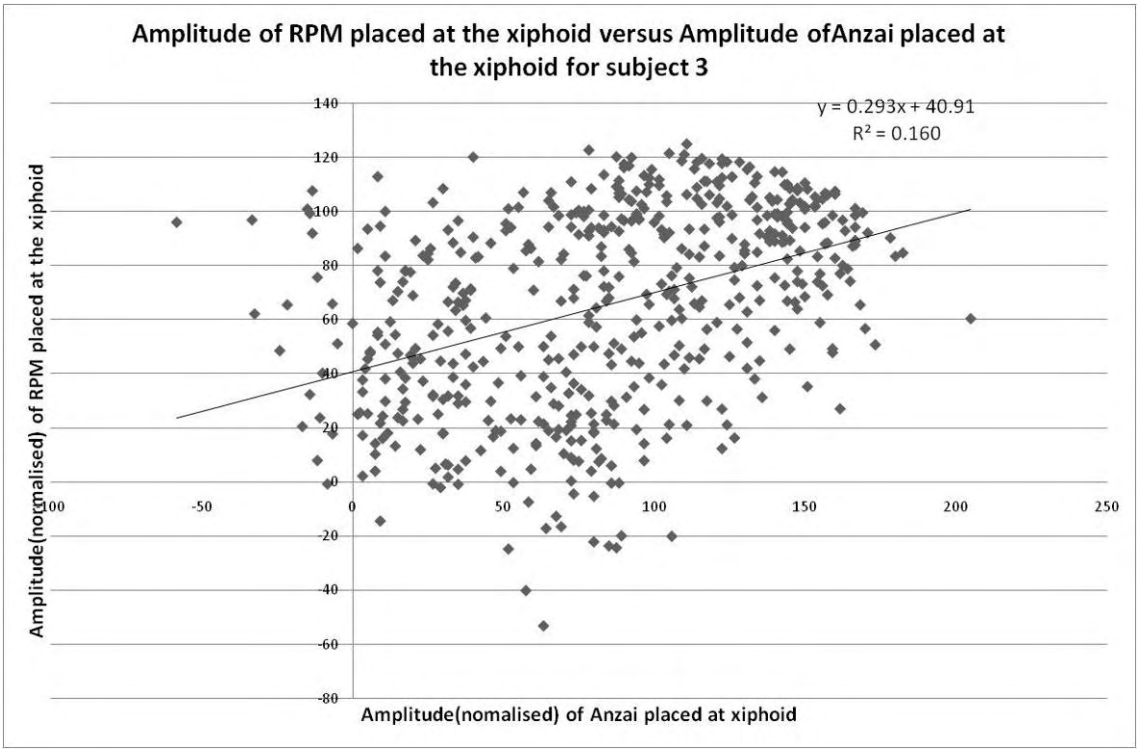


Figure A30: Determination of coefficient of determination for both RPM and Anzai positioned at xiphoid, subject 3.

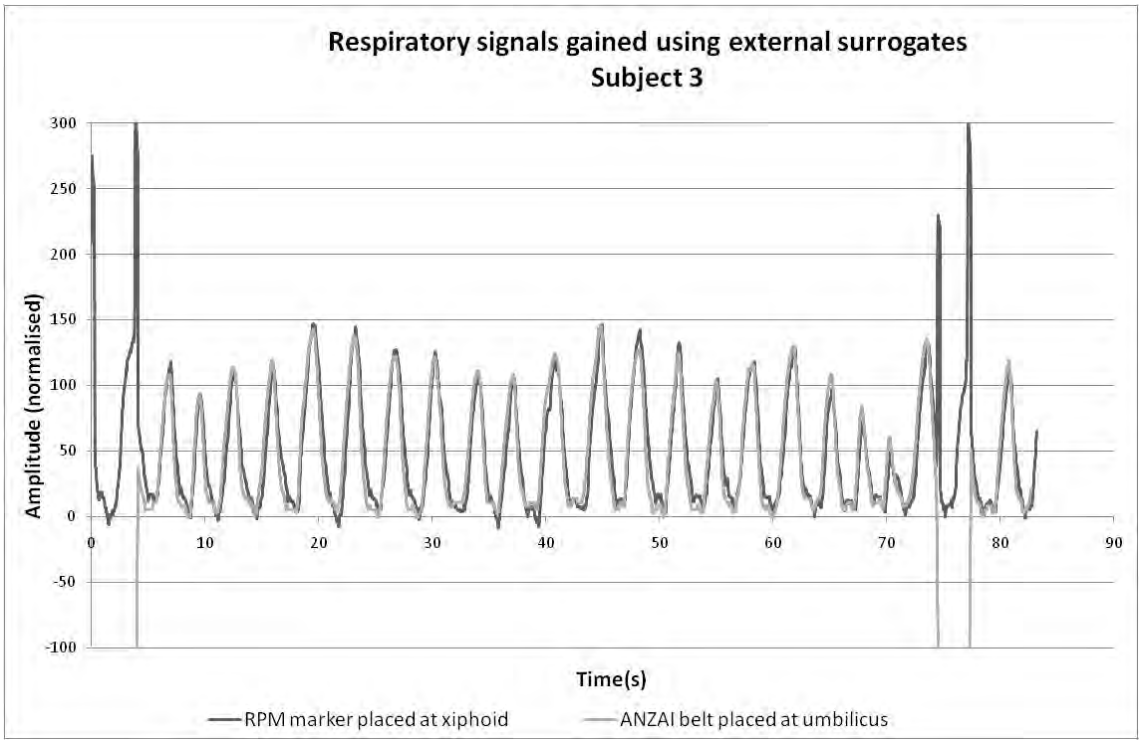


Figure A31: Respiratory signals gained using RPM marker positioned at the xiphoid and Anzai belt positioned at umbilicus for subject 3.

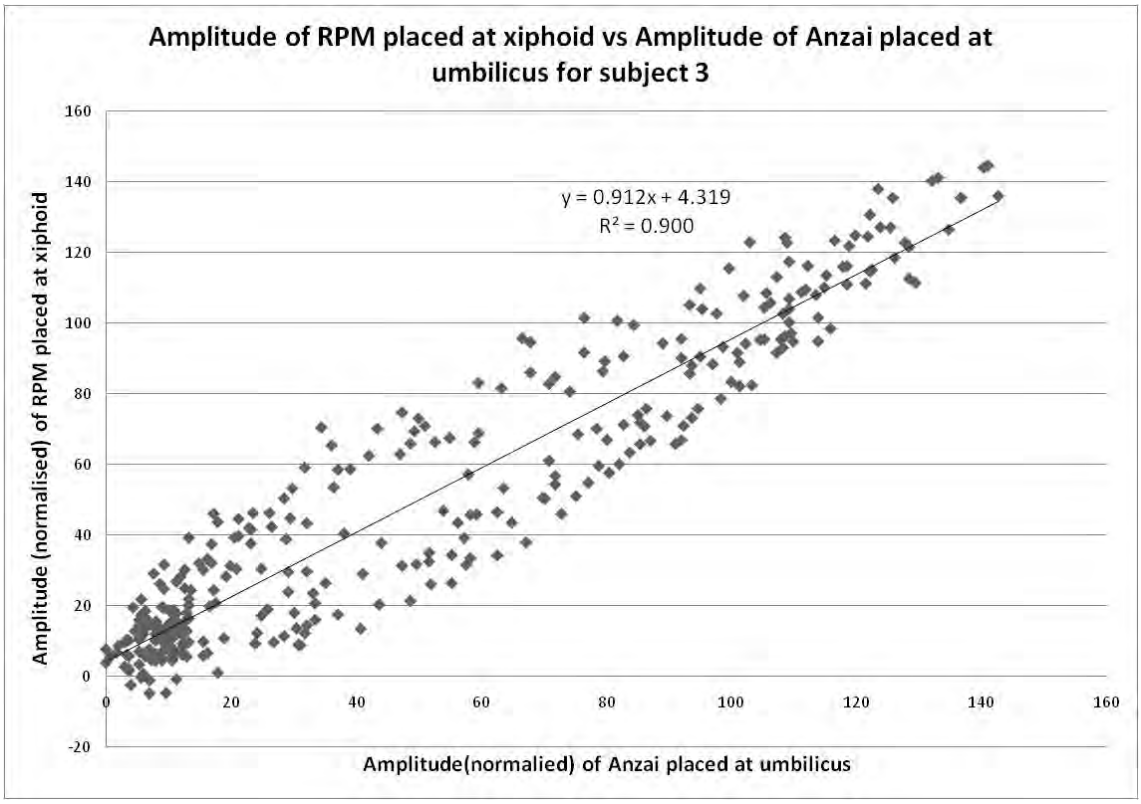


Figure A32: Determination of coefficient of determination for RPM positioned at the xiphoid and Anzai positioned at umbilicus, subject 3.

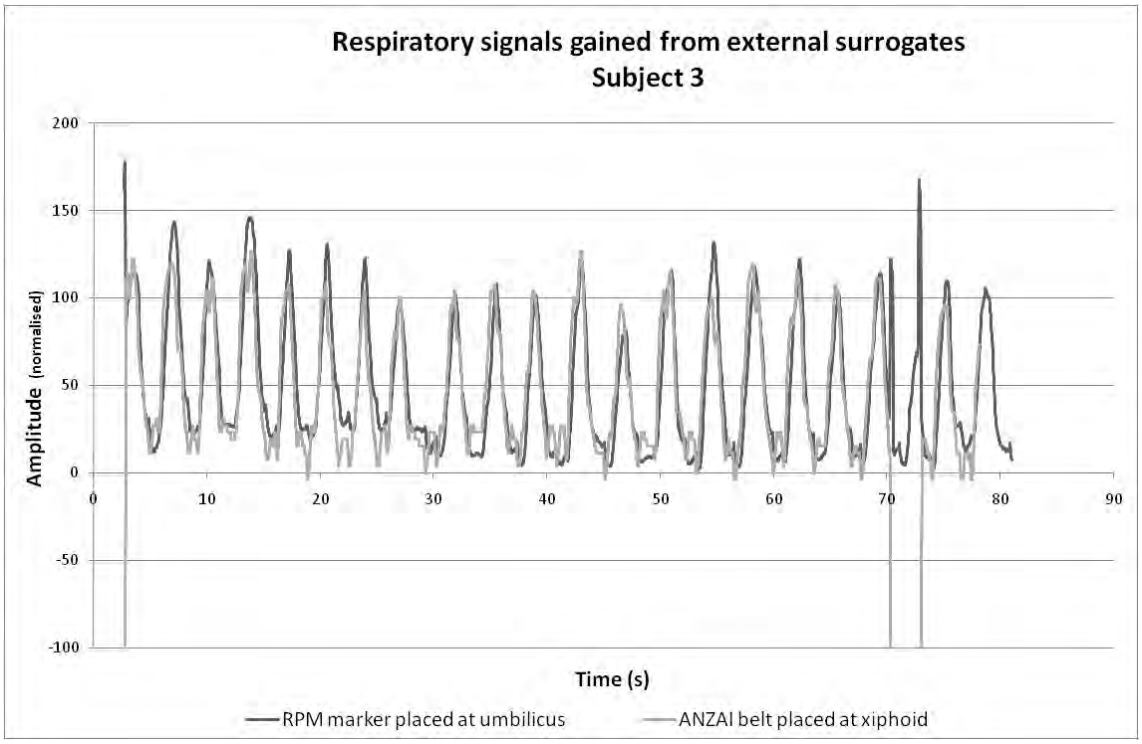


Figure A33: Respiratory signals gained using RPM marker positioned at the umbilicus and Anzai belt positioned at xiphoid for subject 3.

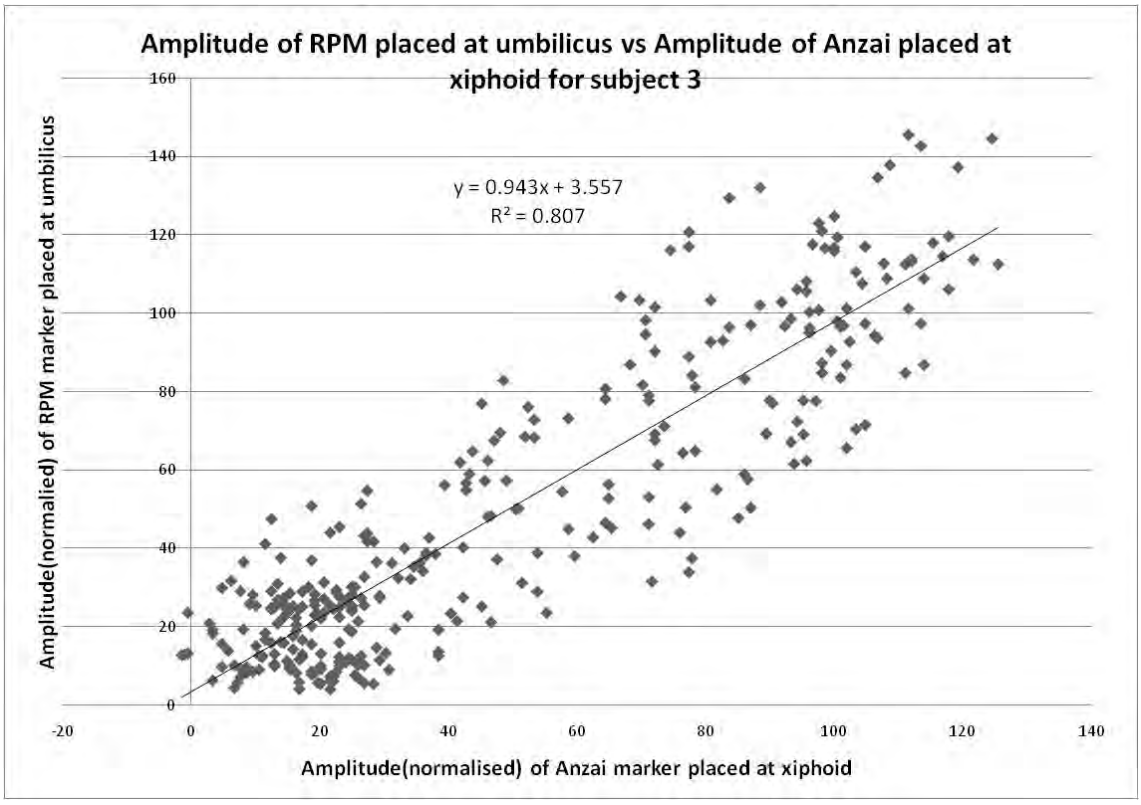


Figure A34: Determination of coefficient of determination for RPM positioned at the umbilicus and Anzai positioned at xiphoid, subject 3.

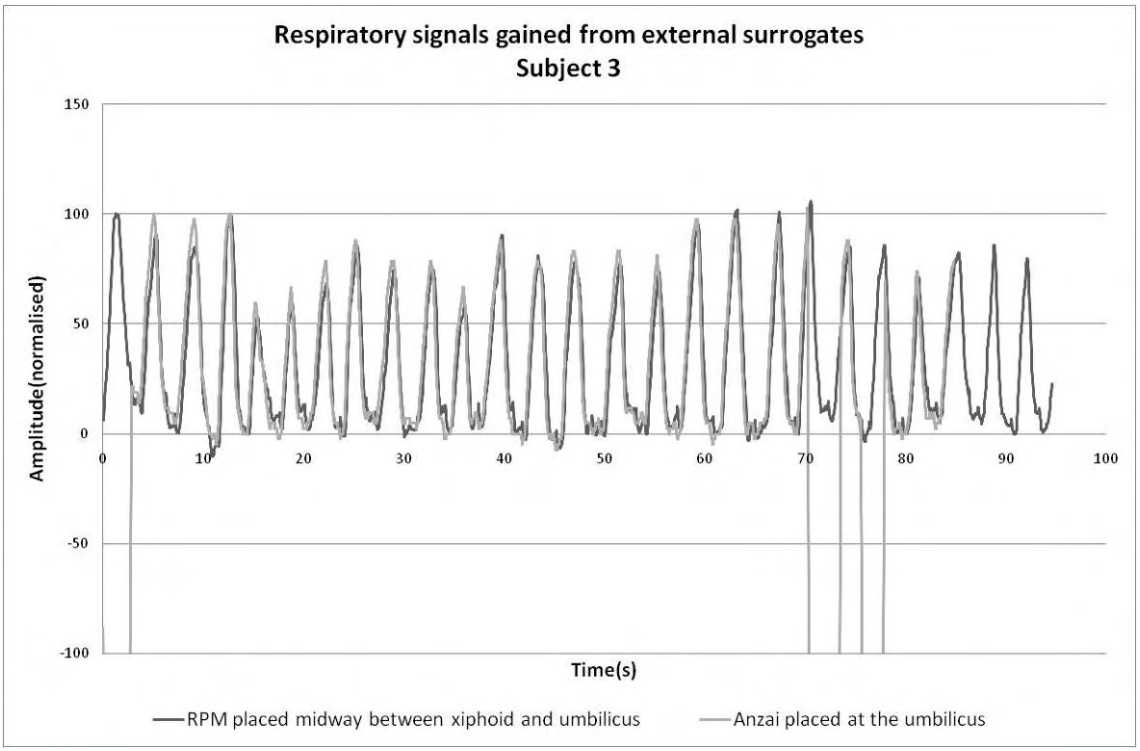


Figure A35: Respiratory signals gained using RPM marker positioned midway between xiphoid and umbilicus and Anzai belt positioned at umbilicus for subject 3.

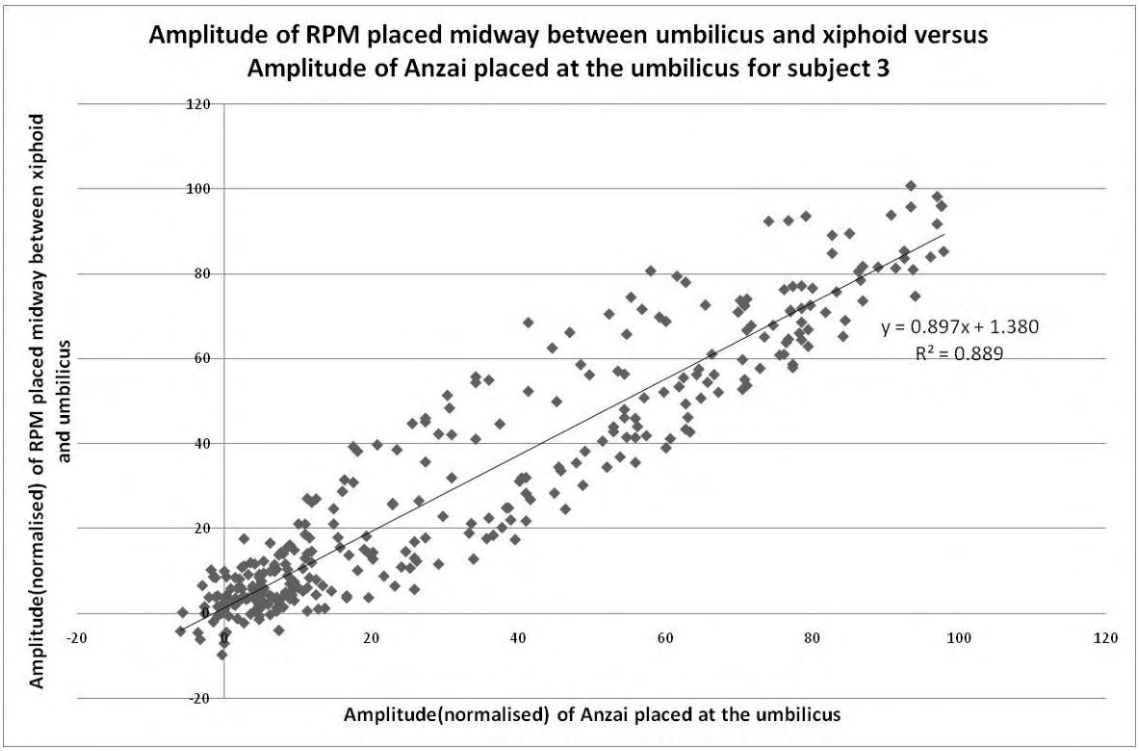


Figure A36: Determination of coefficient of determination for RPM positioned midway between xiphoid and umbilicus and Anzai positioned at umbilicus, subject 3.

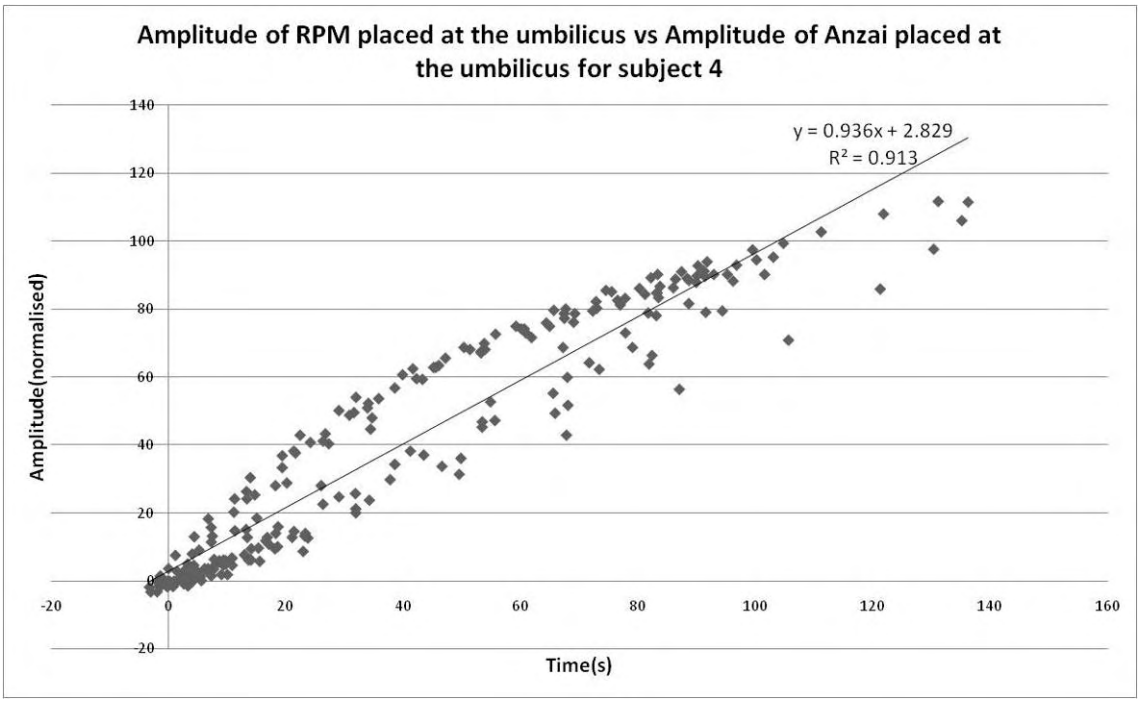


Figure A37: Respiratory signals gained using both RPM marker and Anzai belt positioned at umbilicus for subject 4.

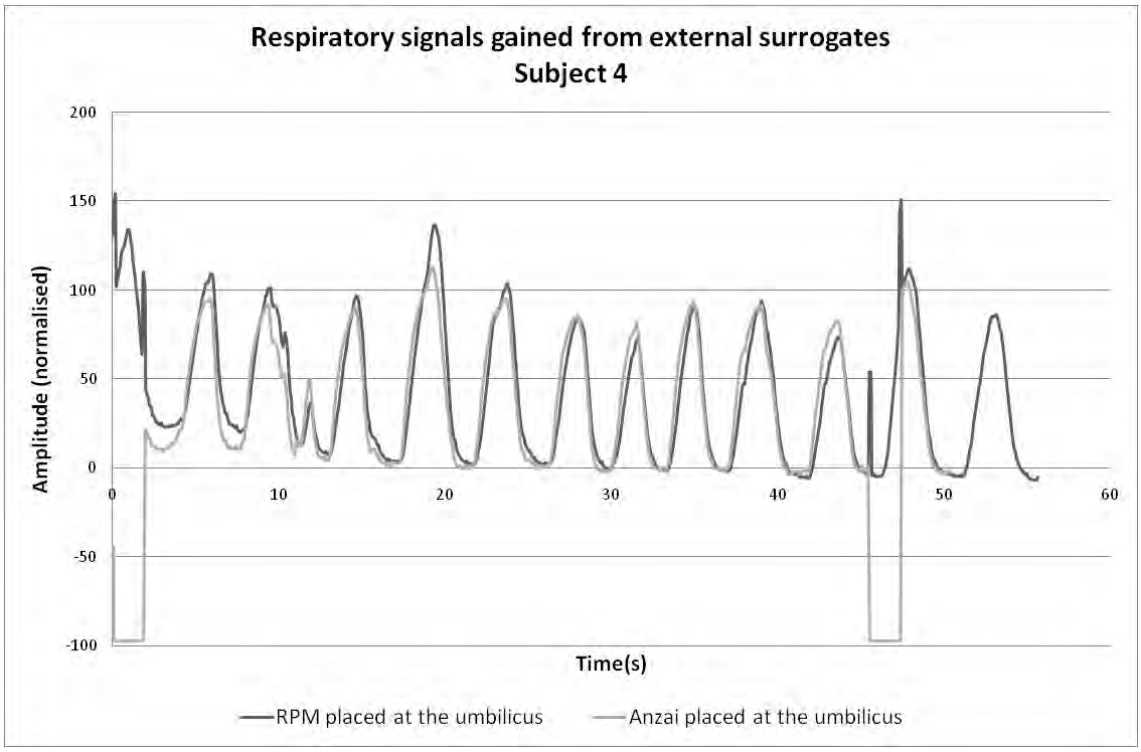


Figure A38: Determination of coefficient of determination for both RPM and Anzai positioned at umbilicus, subject 4.

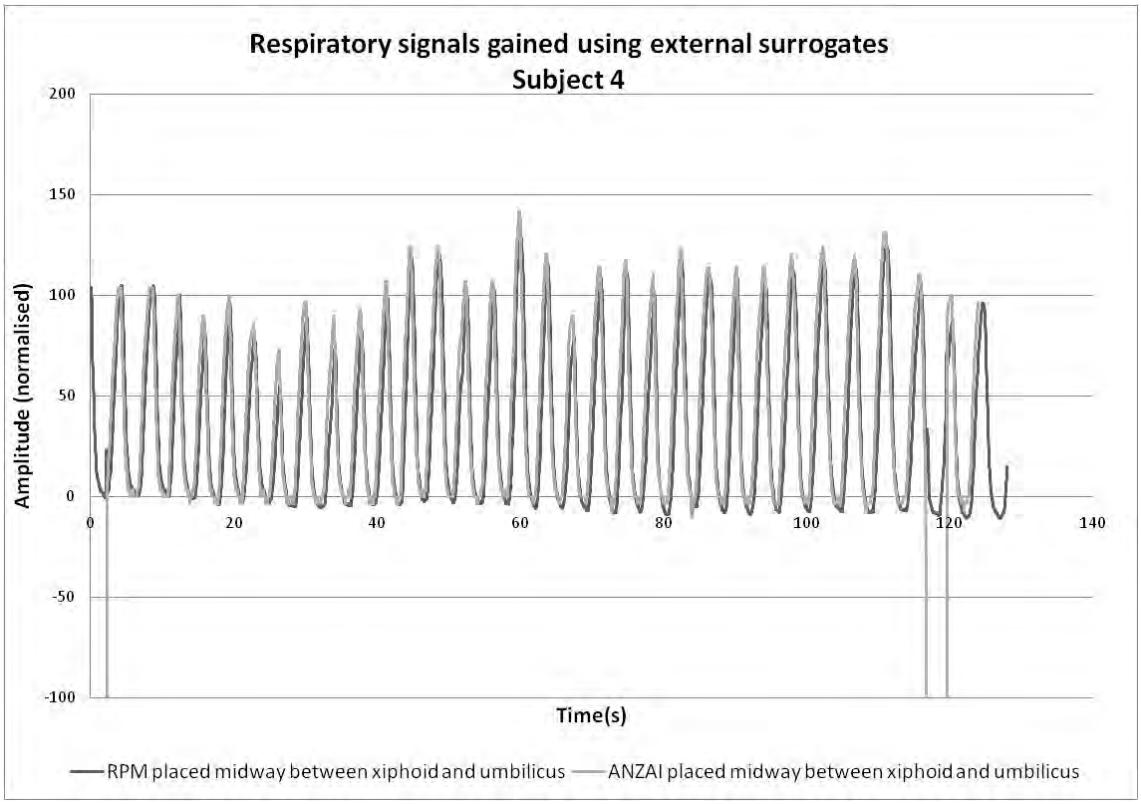


Figure A39: Respiratory signals gained using both RPM marker and Anzai belt positioned midway between umbilicus and xiphoid for subject 4.

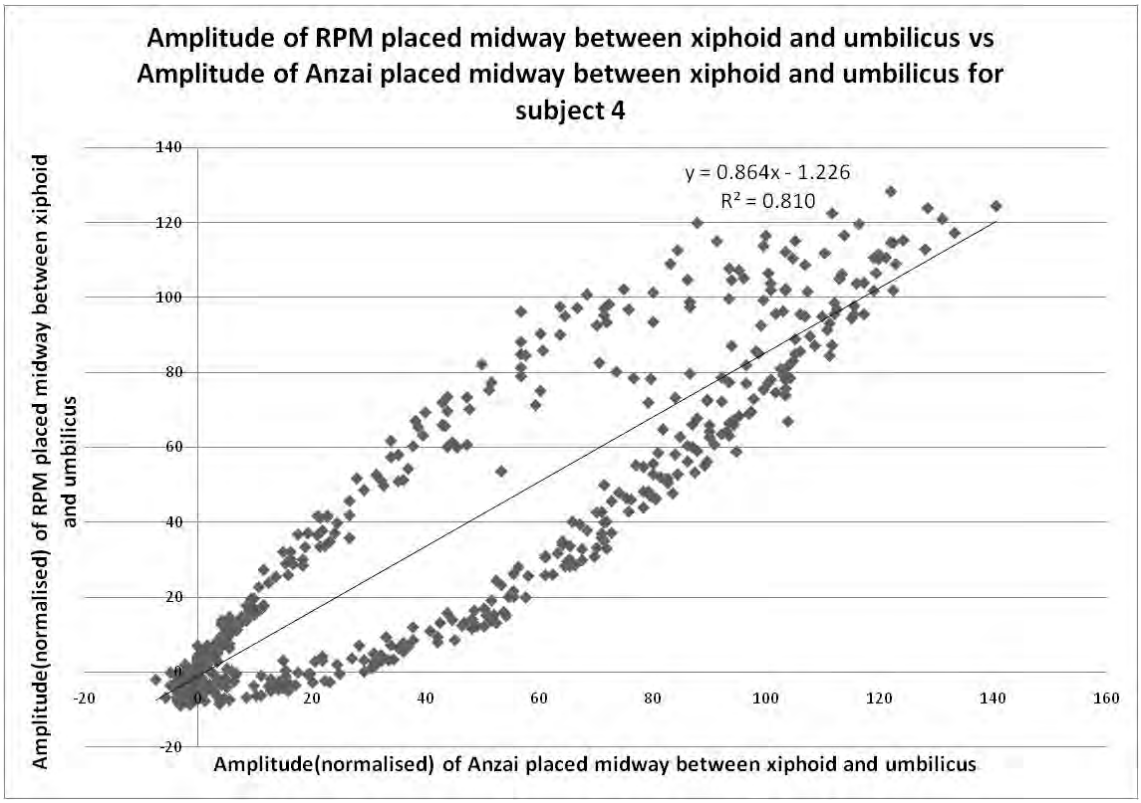


Figure A40: Determination of coefficient of determination for both RPM and Anzai positioned midway between xiphoid and umbilicus, subject 4.

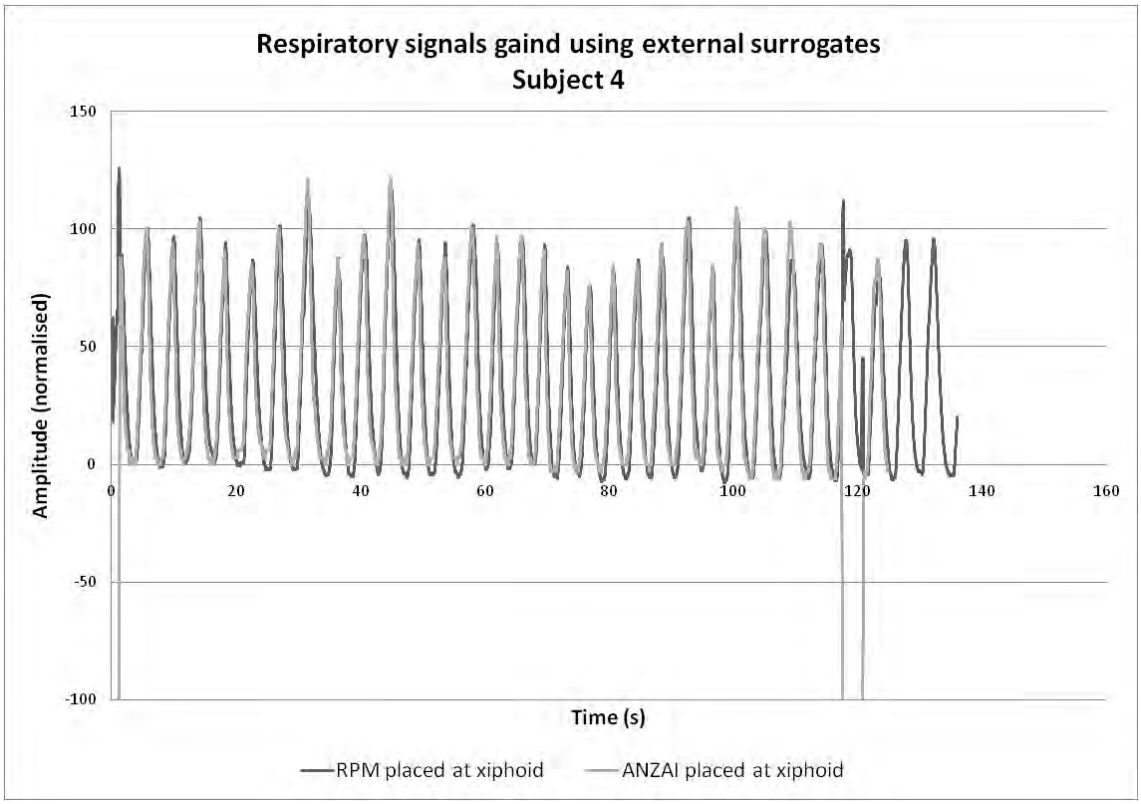


Figure A41: Respiratory signals gained using both RPM marker and Anzai belt positioned at xiphoid for subject 4.

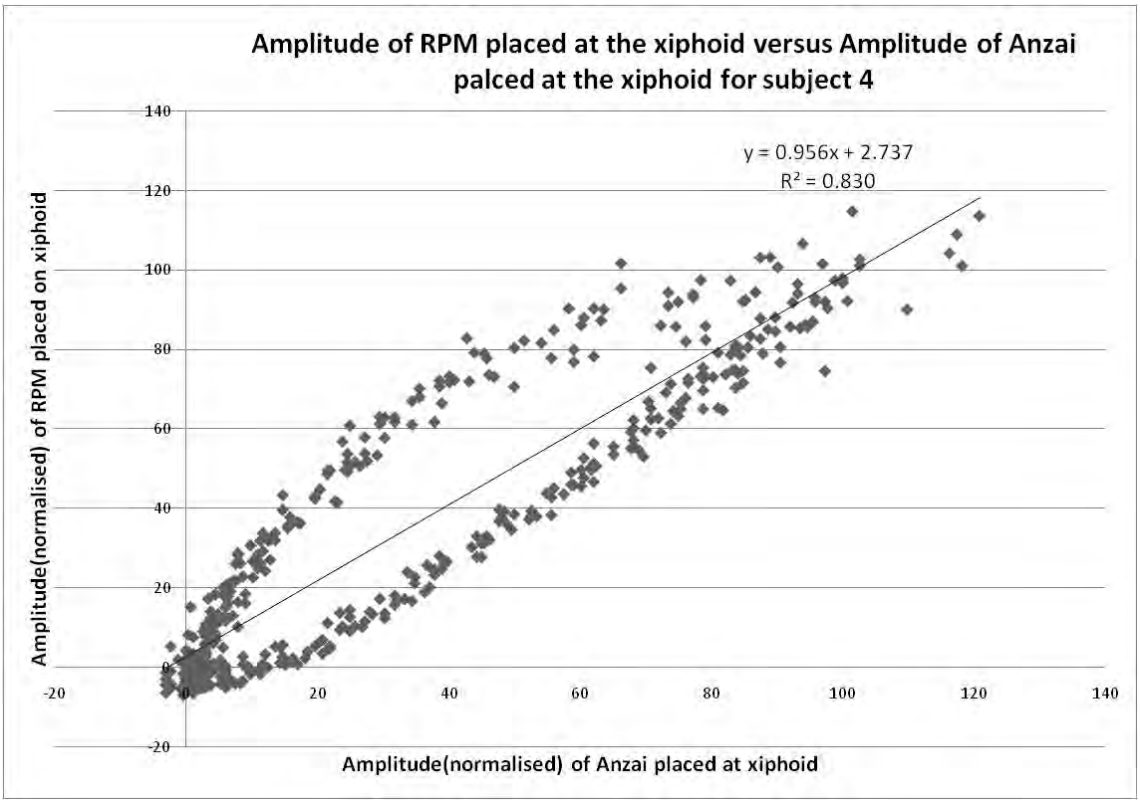


Figure A42: Determination of coefficient of determination for both RPM and Anzai positioned at xiphoid, subject 4.

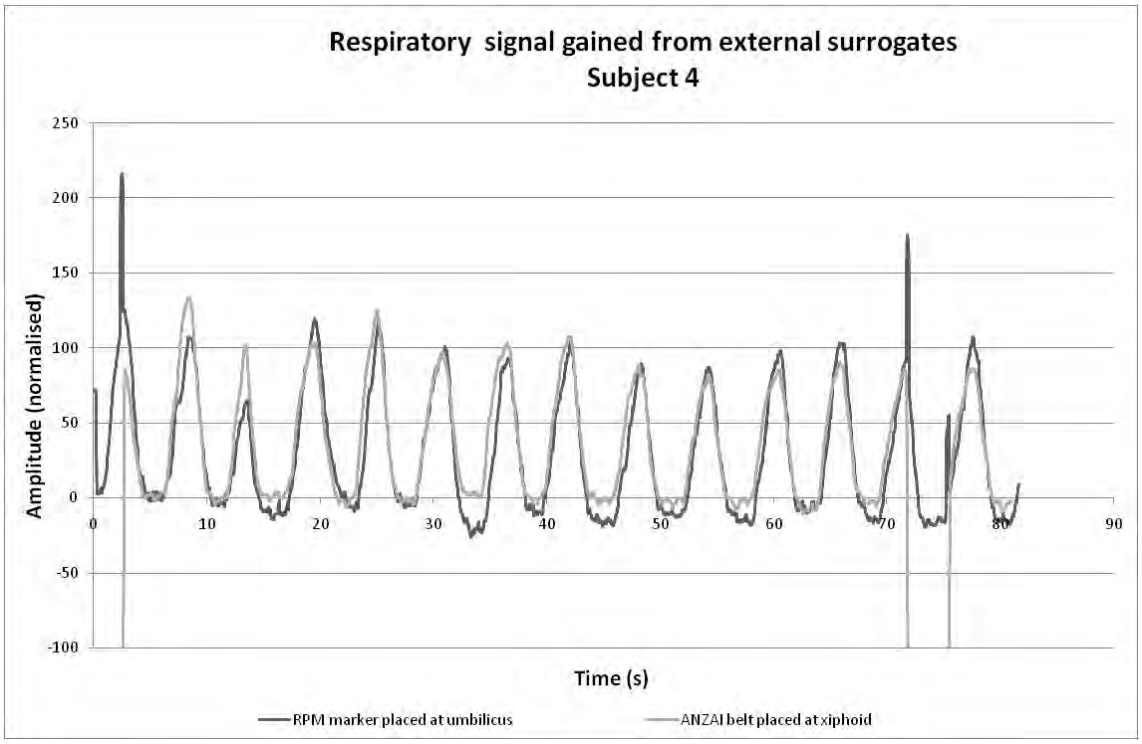


Figure A43: Respiratory signals gained using RPM marker positioned at the umbilicus and Anzai belt positioned at xiphoid for subject 4.

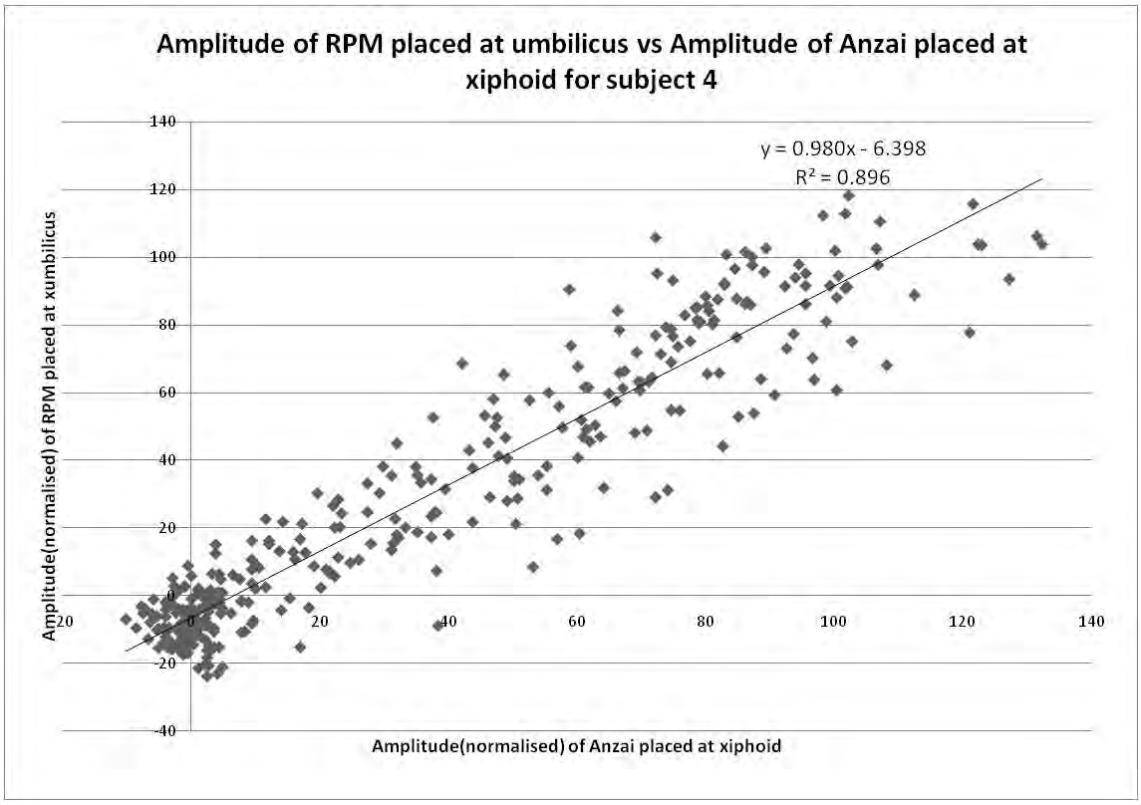


Figure A44: Determination of coefficient of determination for RPM positioned at the umbilicus and Anzai positioned at xiphoid, subject 4.

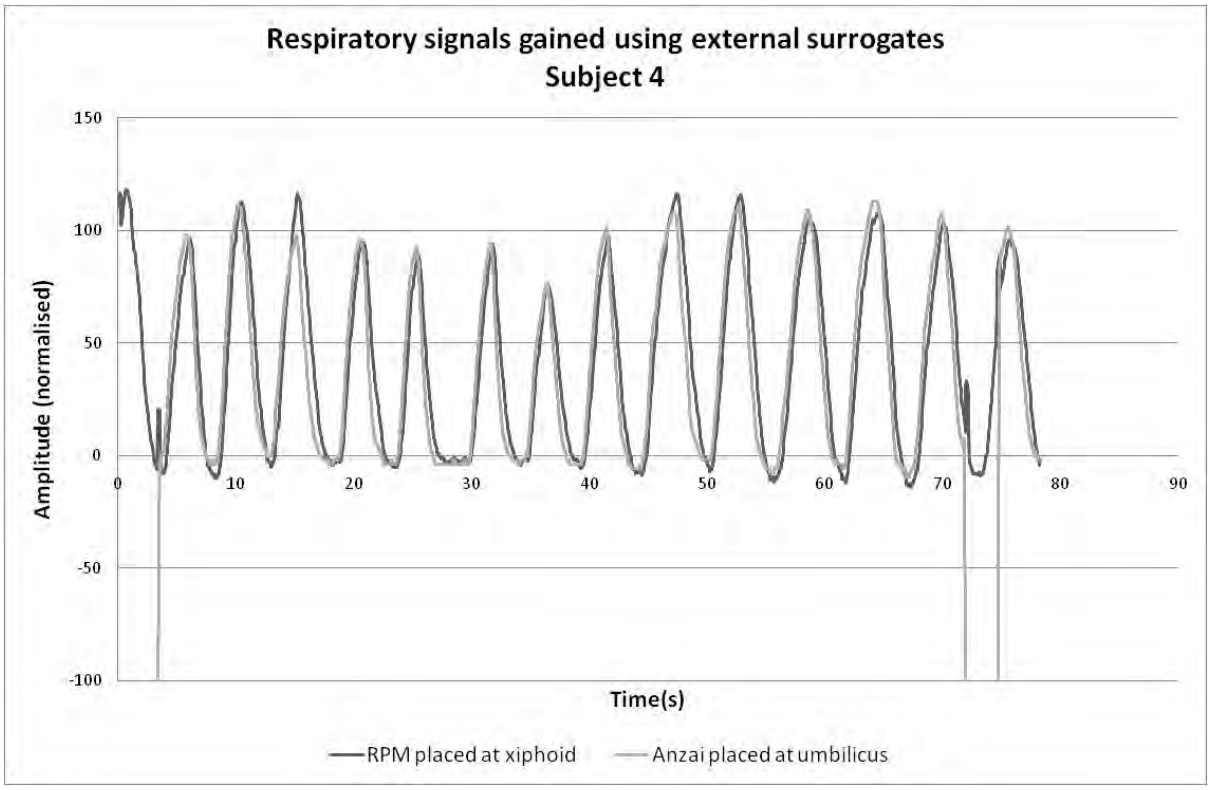


Figure A45: Respiratory signals gained using RPM marker positioned at the xiphoid and Anzai belt positioned at umbilicus for subject 4.

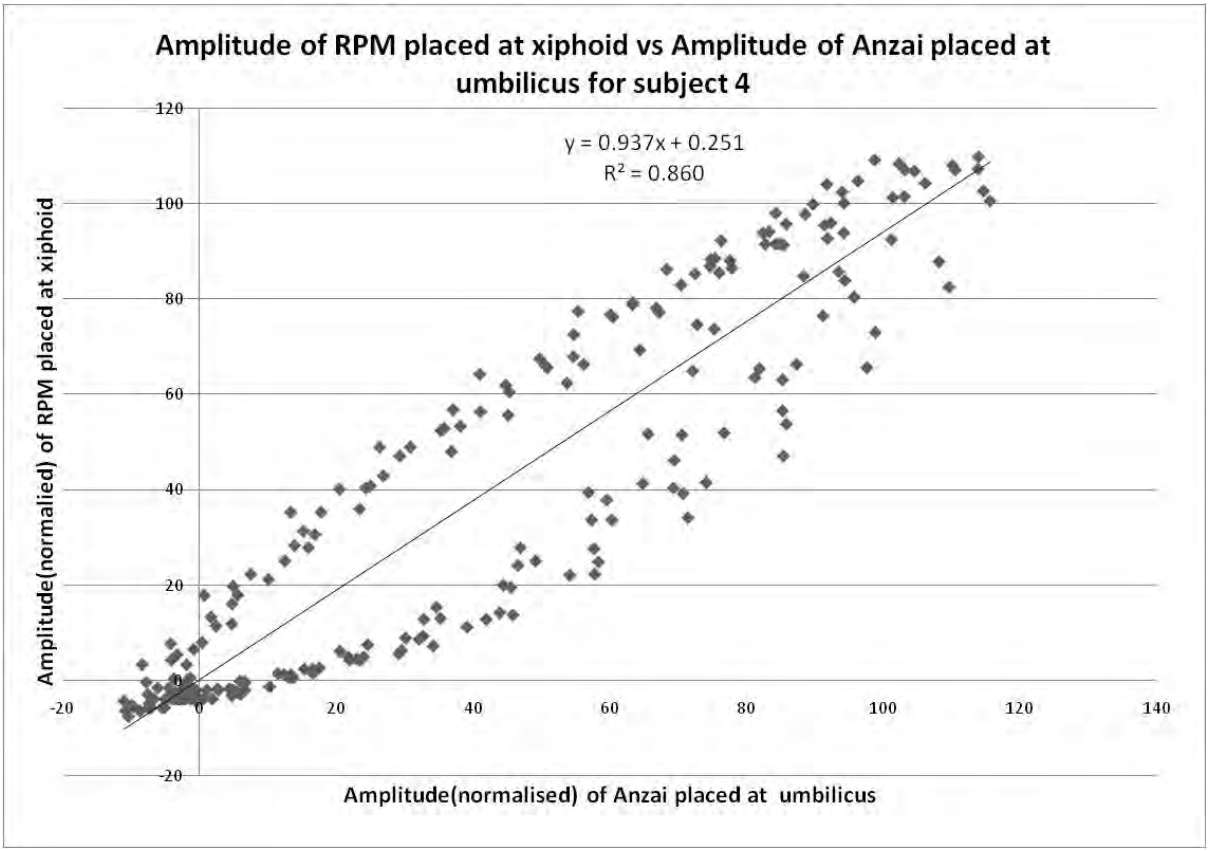


Figure A46: Determination of coefficient of determination for RPM positioned at the xiphoid and Anzai positioned at umbilicus, subject 4.

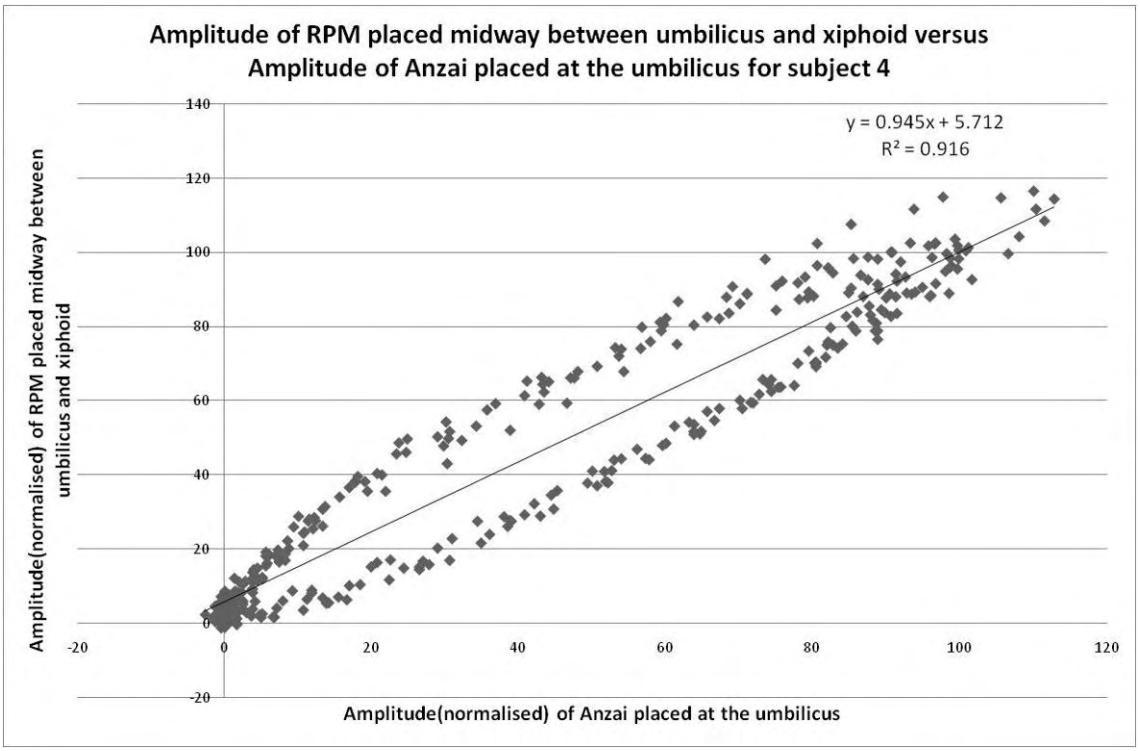


Figure A47: Respiratory signals gained using RPM marker positioned midway between xiphoid and umbilicus and Anzai belt positioned at umbilicus for subject 4.

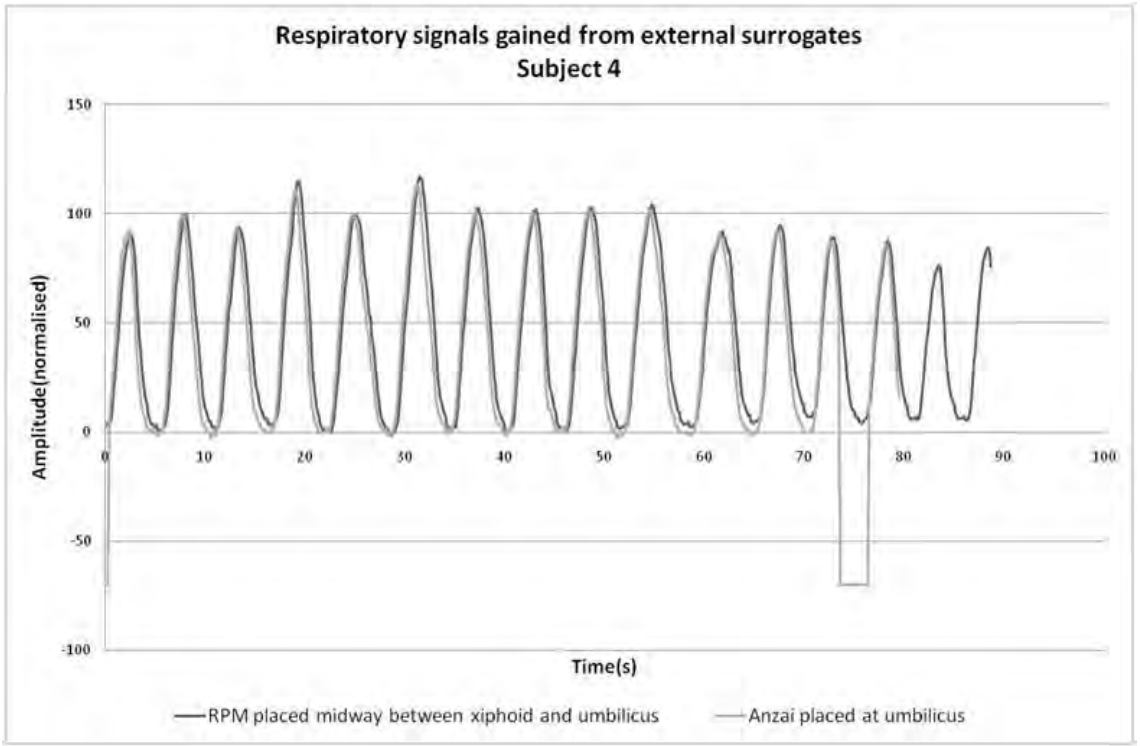


Figure A48: Determination of coefficient of determination for RPM positioned midway between xiphoid and umbilicus and Anzai positioned at umbilicus, subject 4.

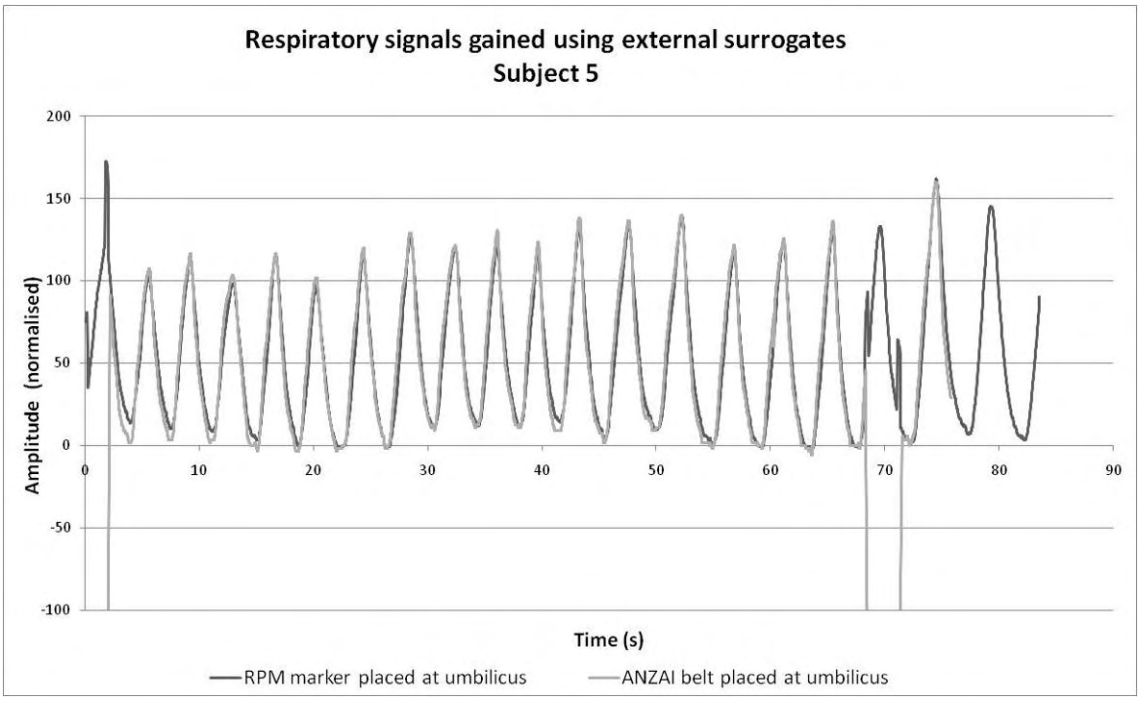


Figure A49: Respiratory signals gained using both RPM marker and Anzai belt positioned at umbilicus for subject 5.

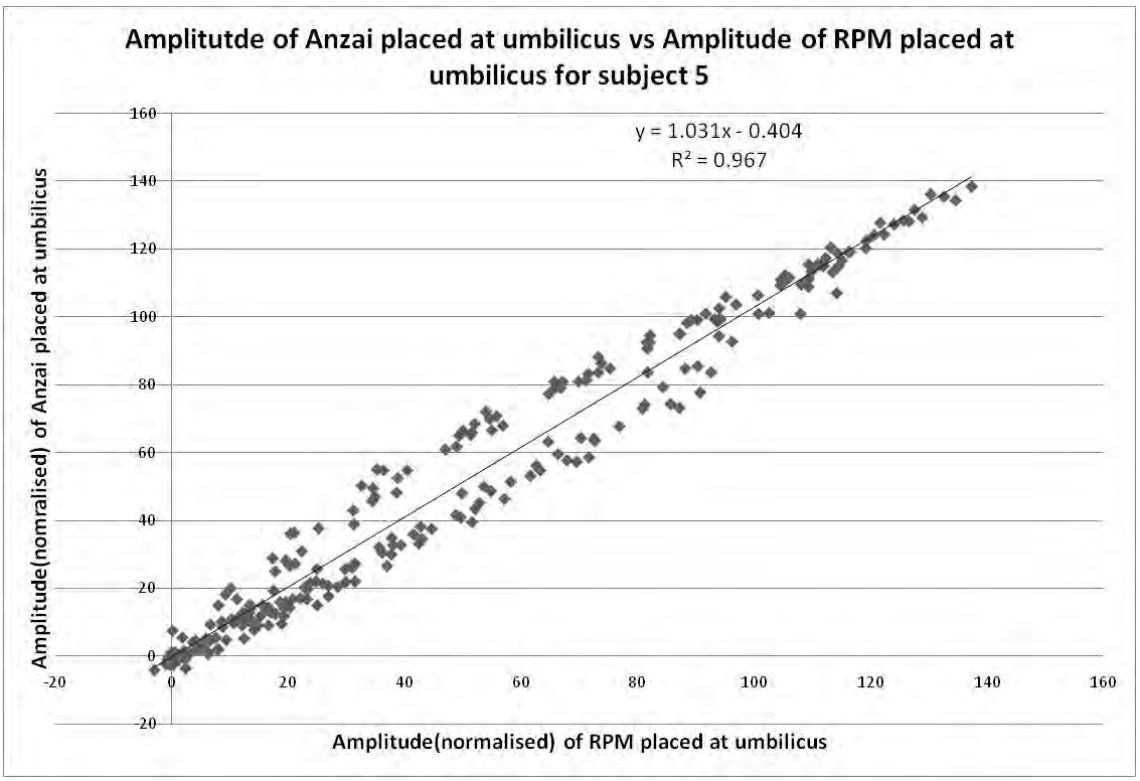


Figure A50: Determination of coefficient of determination for both RPM and Anzai positioned at umbilicus, subject 5.

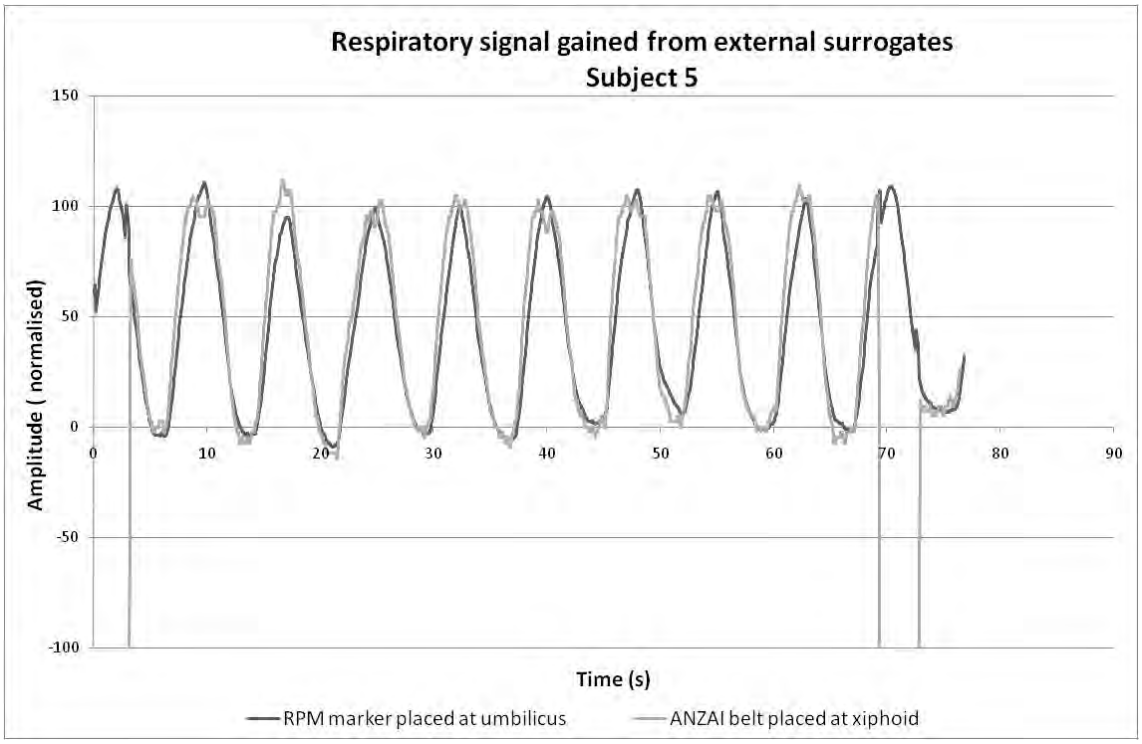


Figure A51: Respiratory signals gained using RPM marker positioned at the umbilicus and Anzai belt positioned at xiphoid for subject 5.

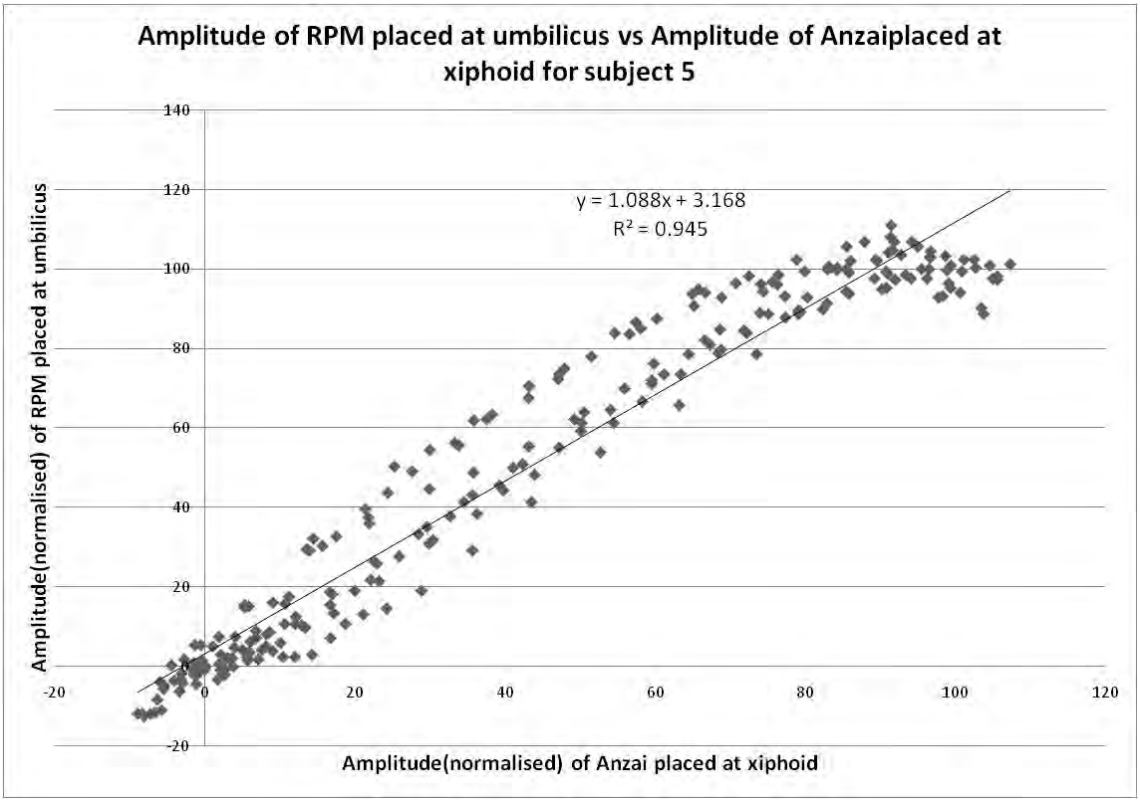


Figure A52: Determination of coefficient of determination for RPM positioned at the umbilicus and Anzai positioned at xiphoid, subject 5.

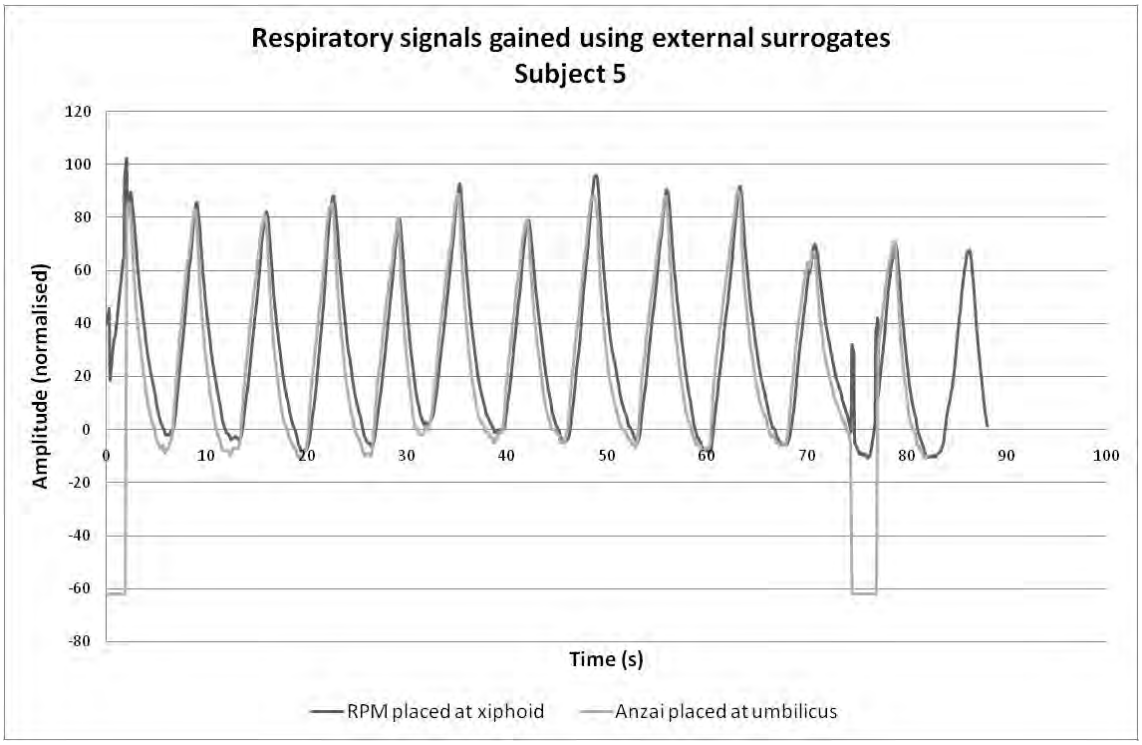


Figure A53: Respiratory signals gained using RPM marker positioned at the xiphoid and Anzai belt positioned at umbilicus for subject 5.

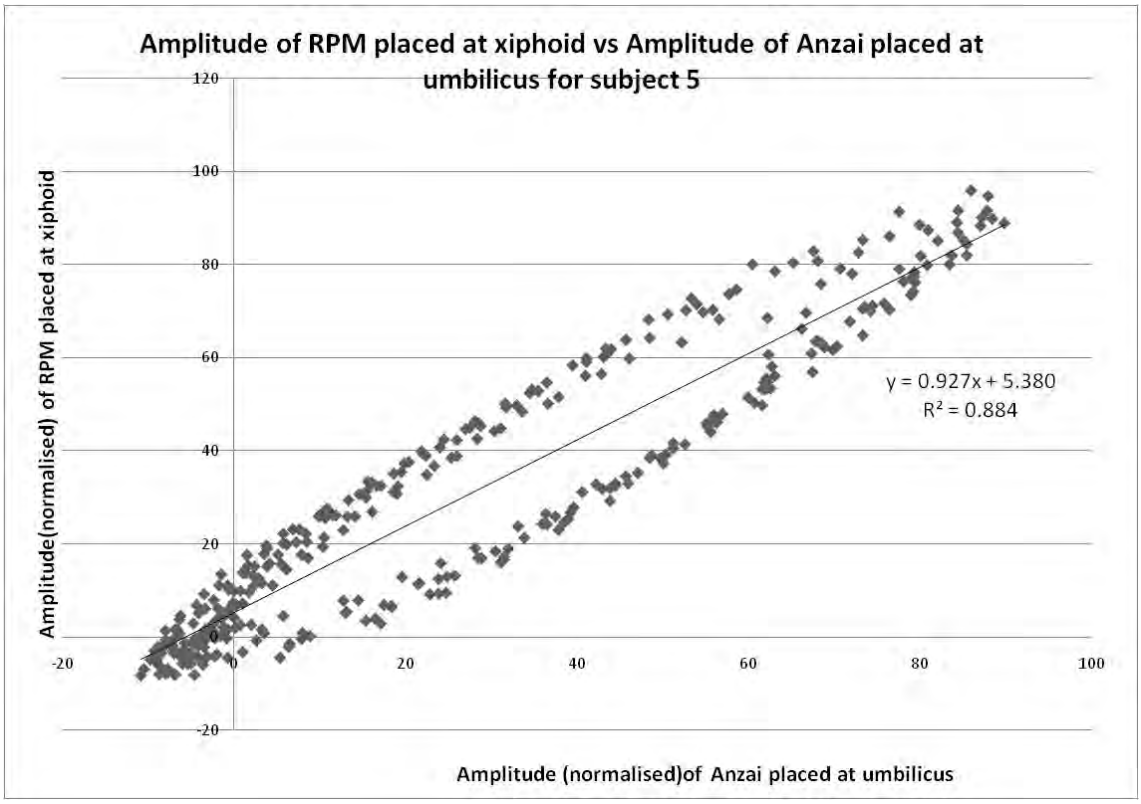


Figure A54: Determination of coefficient of determination for RPM positioned at the xiphoid and Anzai positioned at umbilicus, subject 5.

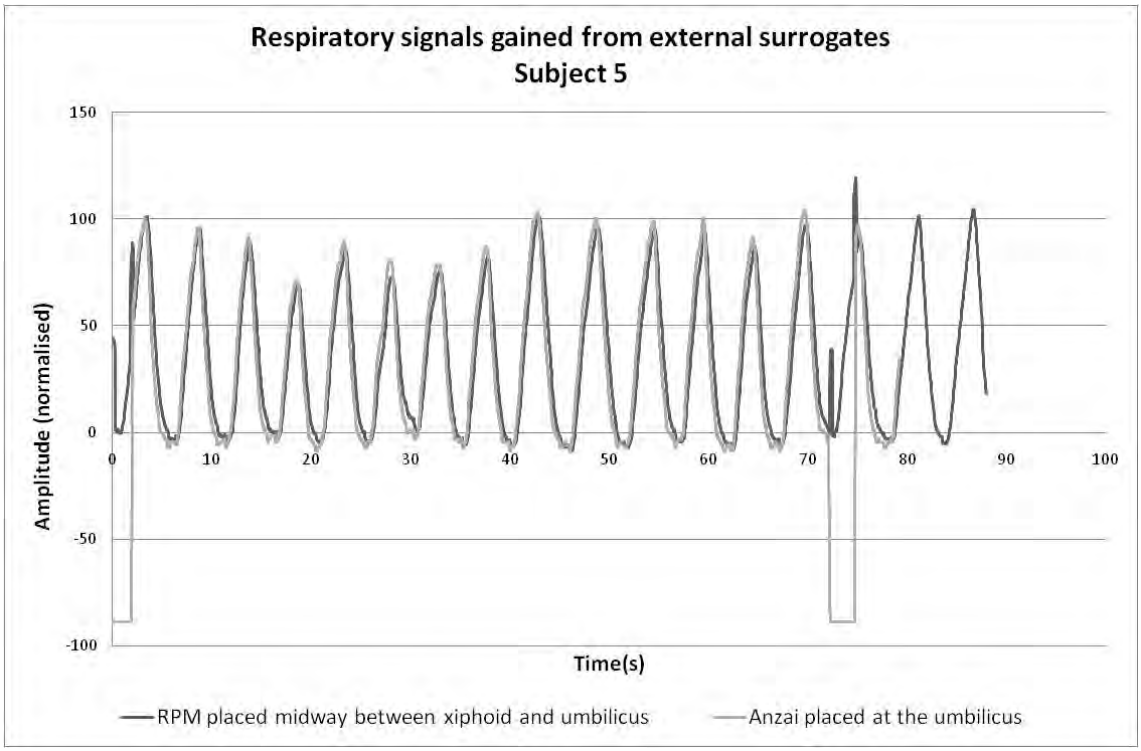


Figure A55: Respiratory signals gained using RPM marker positioned midway between xiphoid and umbilicus and Anzai belt positioned at umbilicus for subject 5.

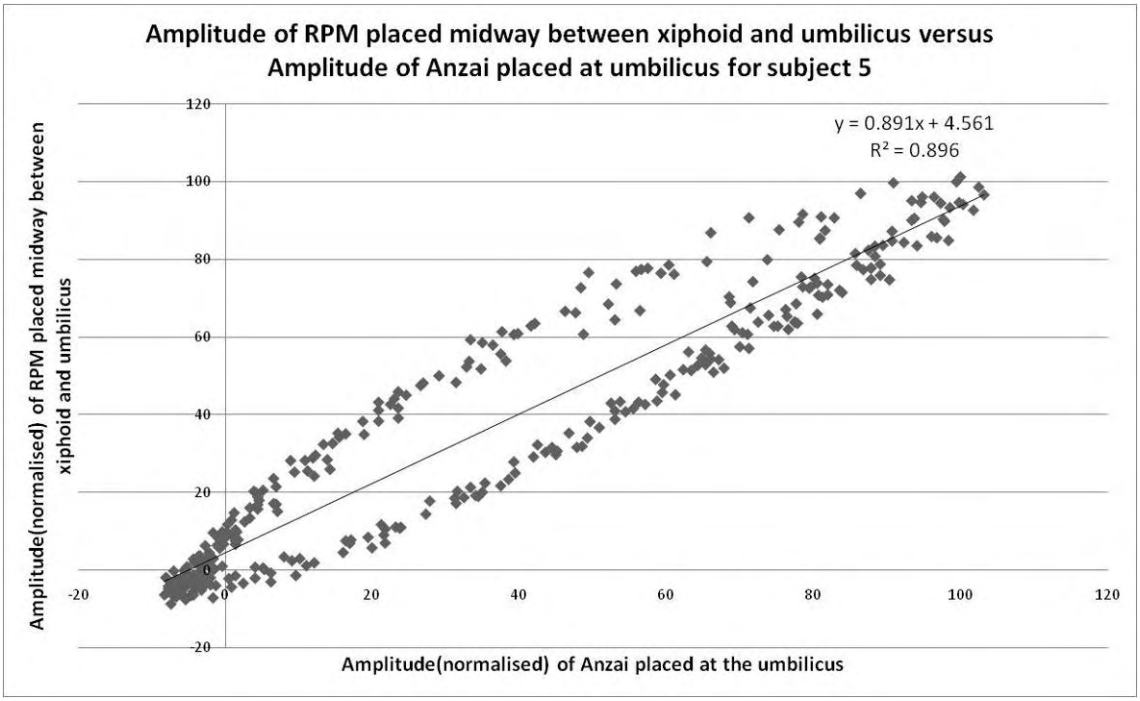


Figure A56: Determination of coefficient of determination for RPM positioned midway between xiphoid and umbilicus and Anzai positioned at umbilicus, subject 5.

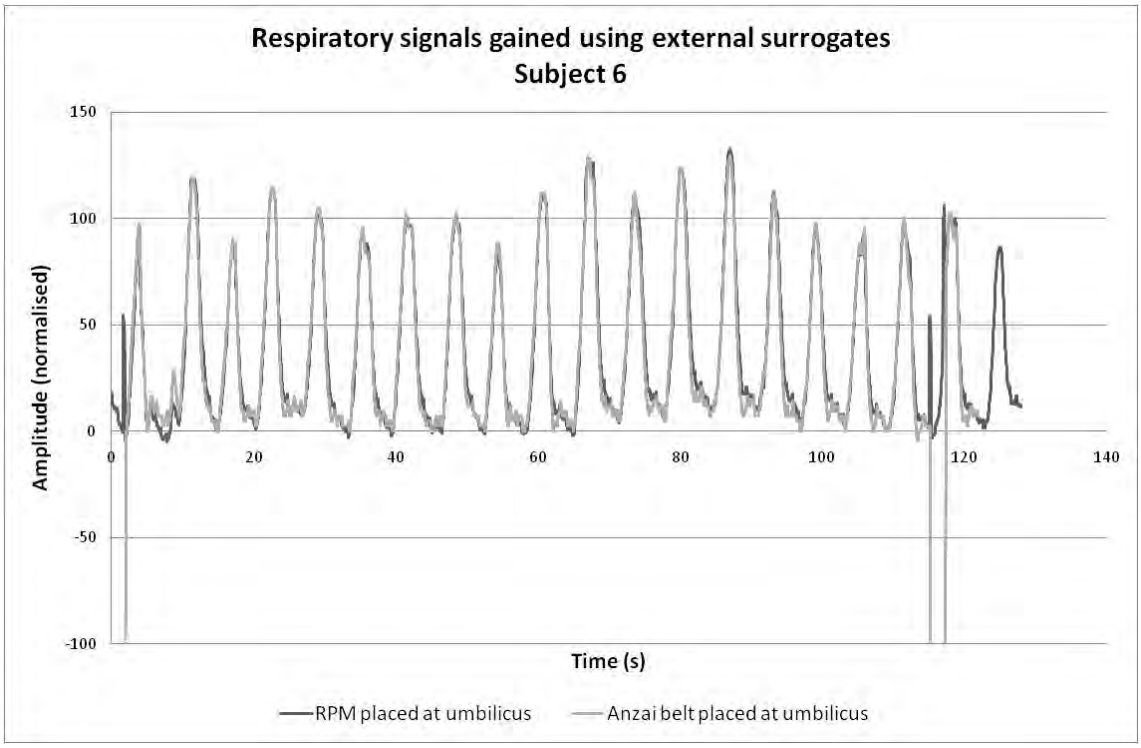


Figure A57: Respiratory signals gained using both RPM marker and Anzai belt positioned at umbilicus for subject 6.

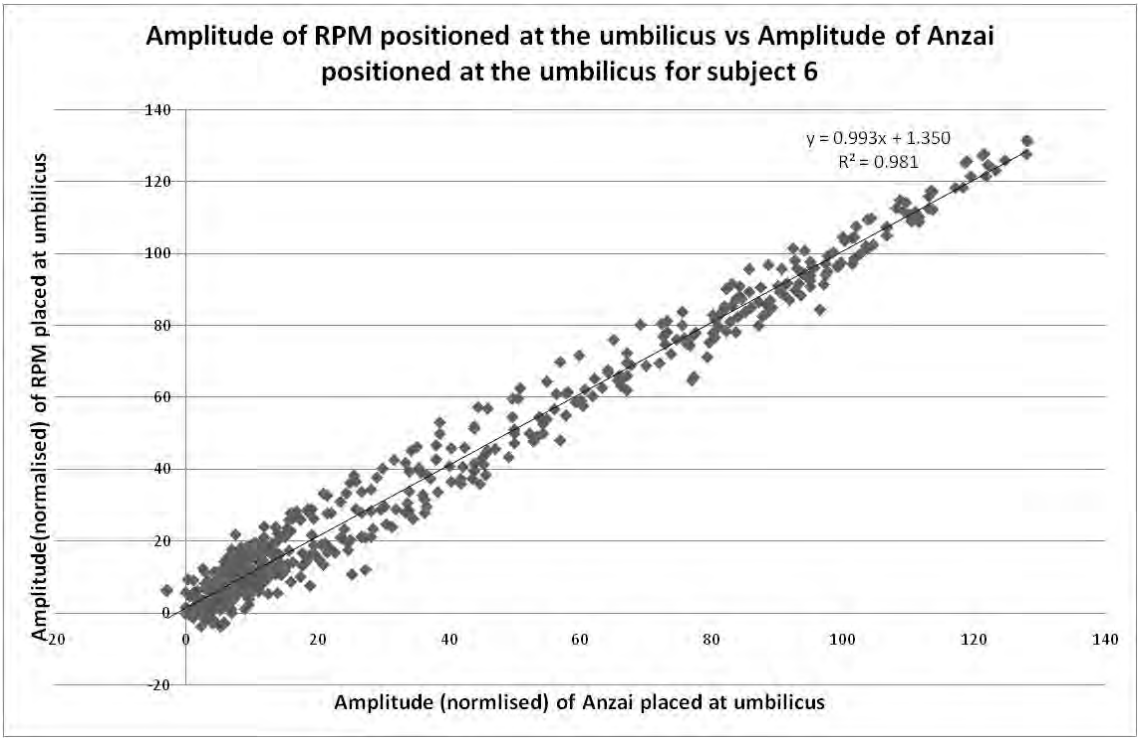


Figure A58: Determination of coefficient of determination for both RPM and Anzai positioned at umbilicus, subject 6.

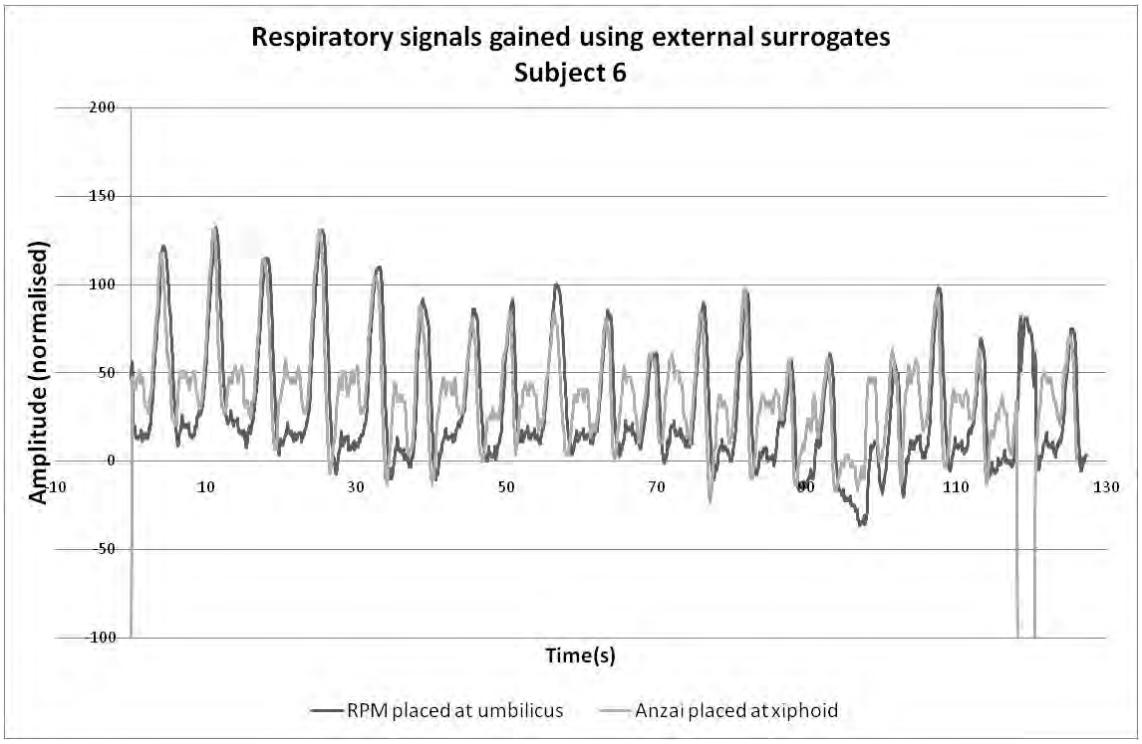


Figure A59: Respiratory signals gained using RPM marker positioned at the umbilicus and Anzai belt positioned at xiphoid for subject 6.

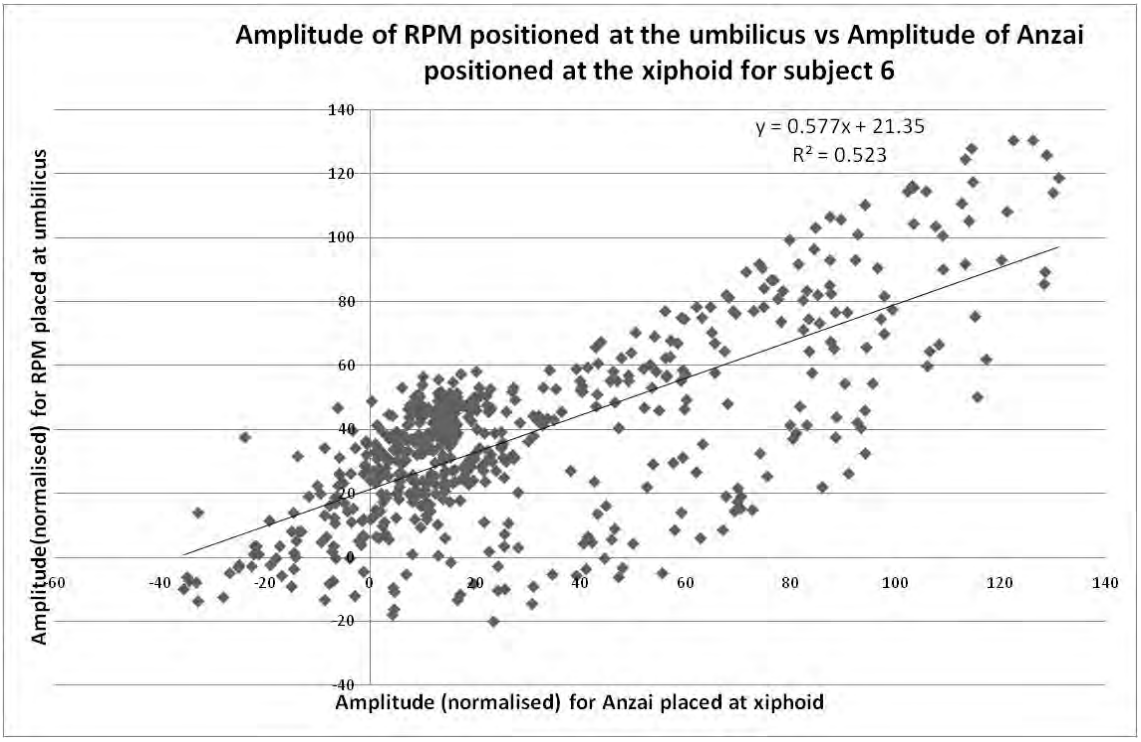


Figure A60: Determination of coefficient of determination for RPM positioned at the umbilicus and Anzai positioned at xiphoid, subject 6.

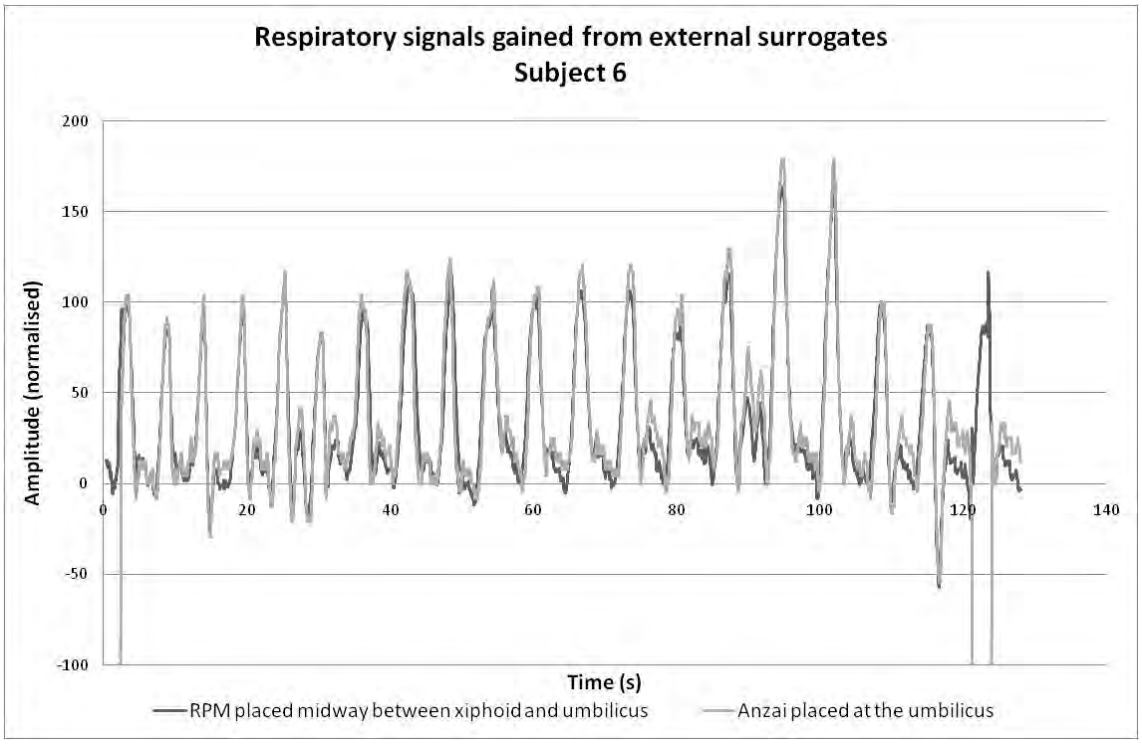


Figure A61: Respiratory signals gained using RPM marker positioned midway between xiphoid and umbilicus and Anzai belt positioned at umbilicus for subject 6.

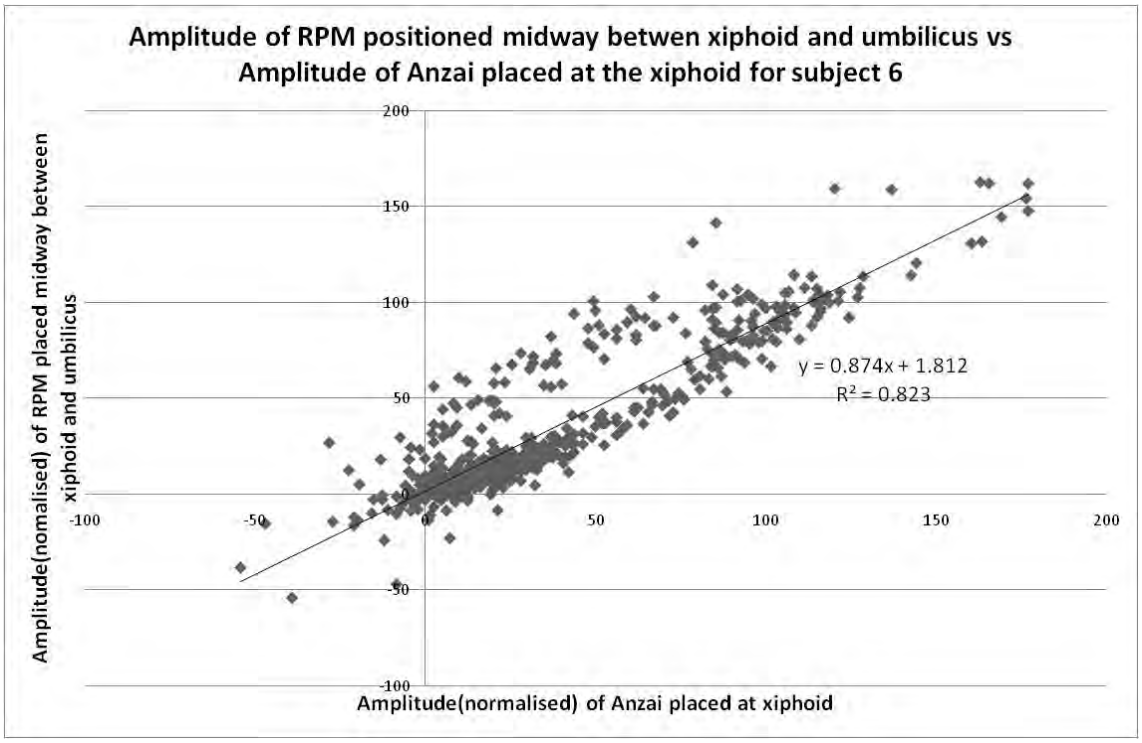


Figure A62: Determination of coefficient of determination for RPM positioned midway between xiphoid and umbilicus and Anzai positioned at umbilicus, subject 6.

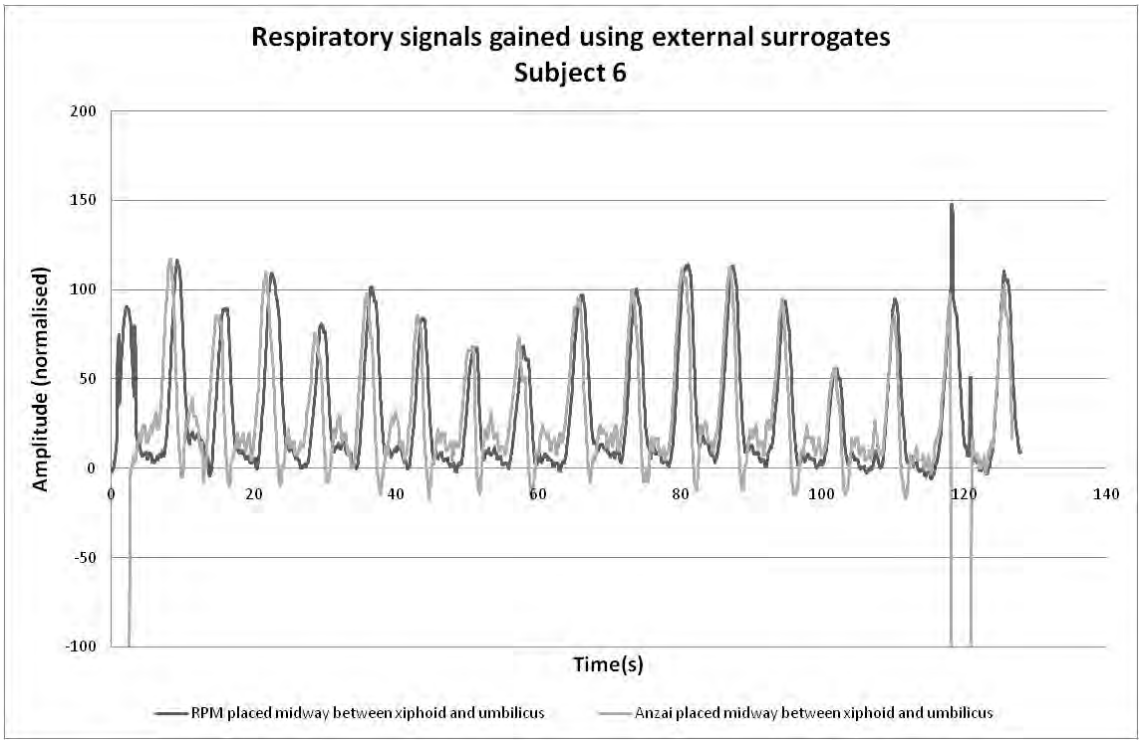


Figure A63: Respiratory signals gained using both RPM marker and Anzai belt positioned midway between umbilicus and xiphoid for subject 6.

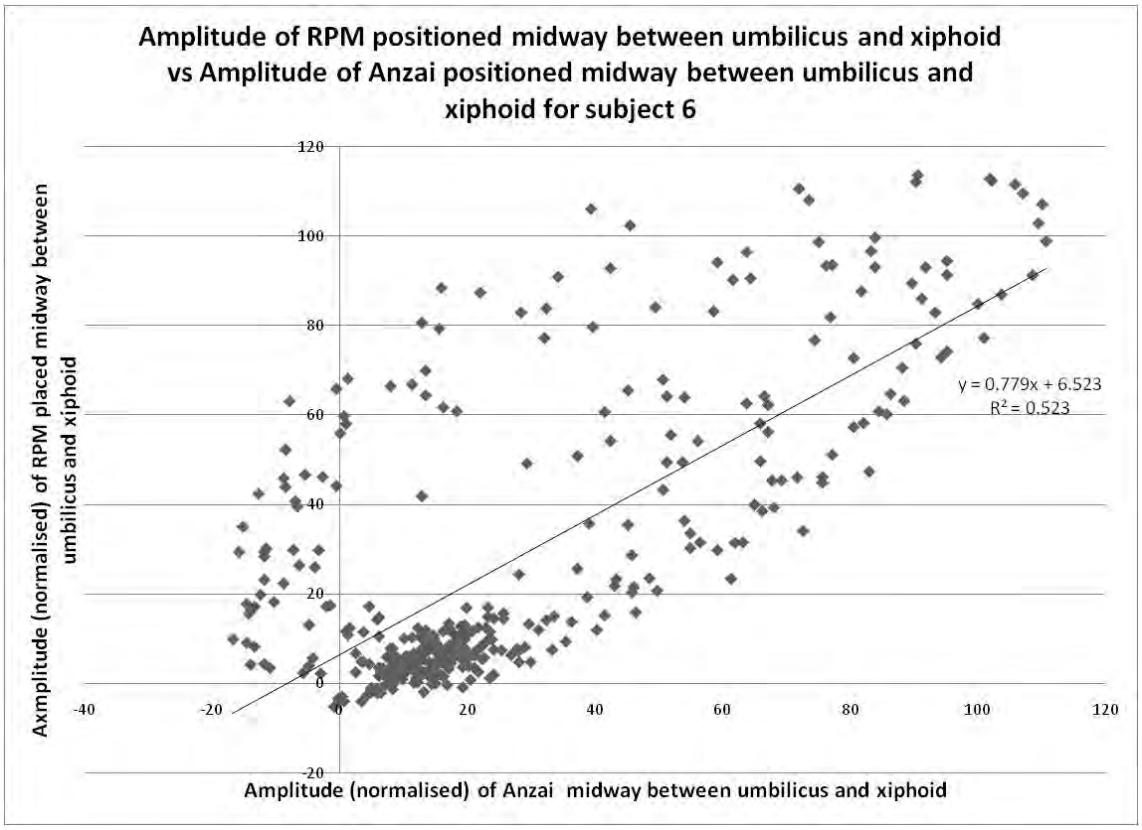


Figure A64: Determination of coefficient of determination for both RPM and Anzai positioned midway between xiphoid and umbilicus, subject 6.

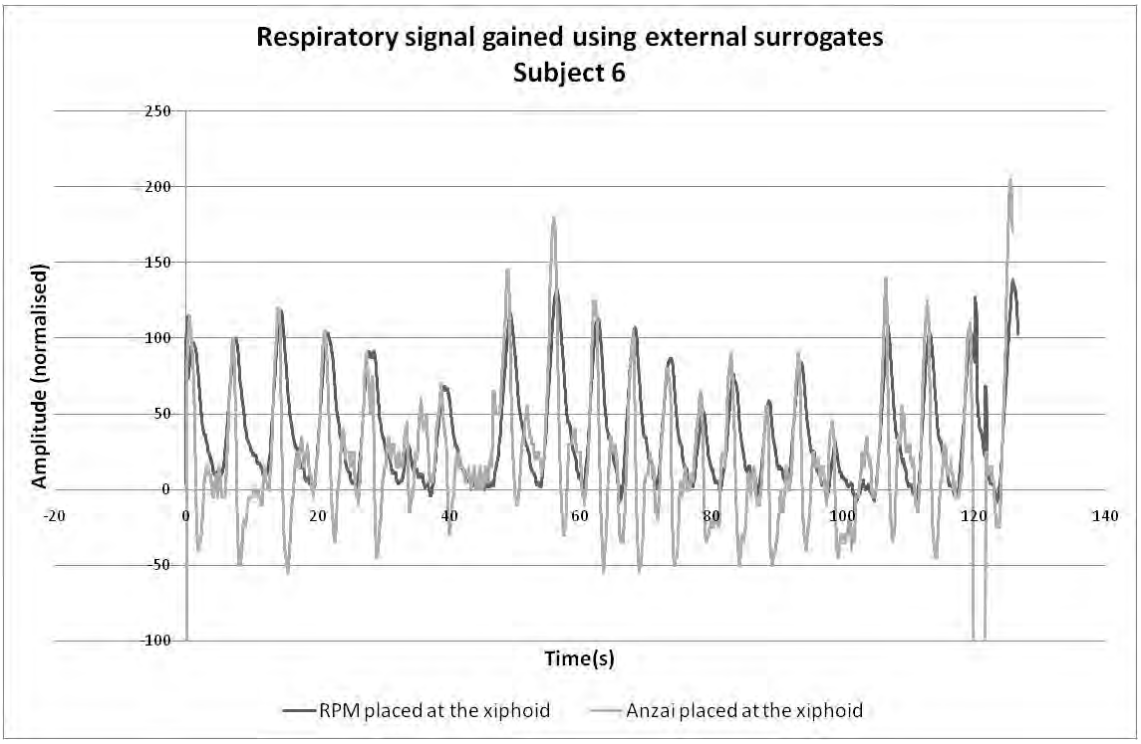


Figure A65: Respiratory signals gained using both RPM marker and Anzai belt positioned at xiphoid for subject 6.

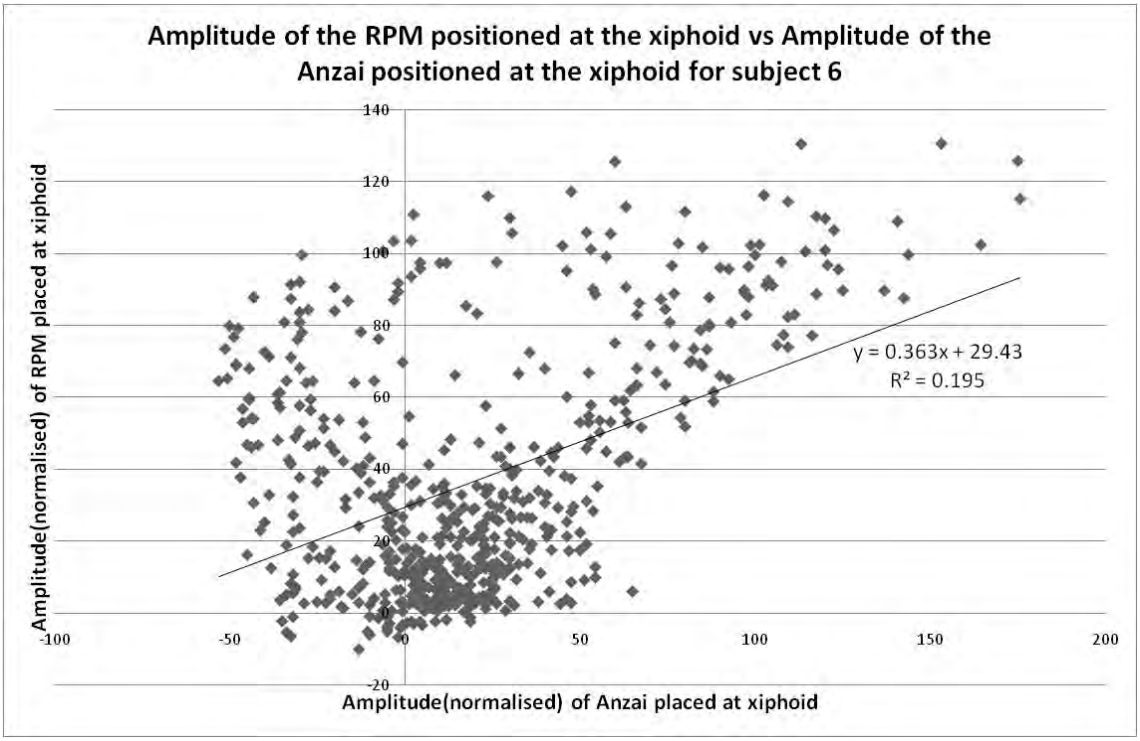


Figure A66: Determination of coefficient of determination for both RPM and Anzai positioned at xiphoid, subject 6.

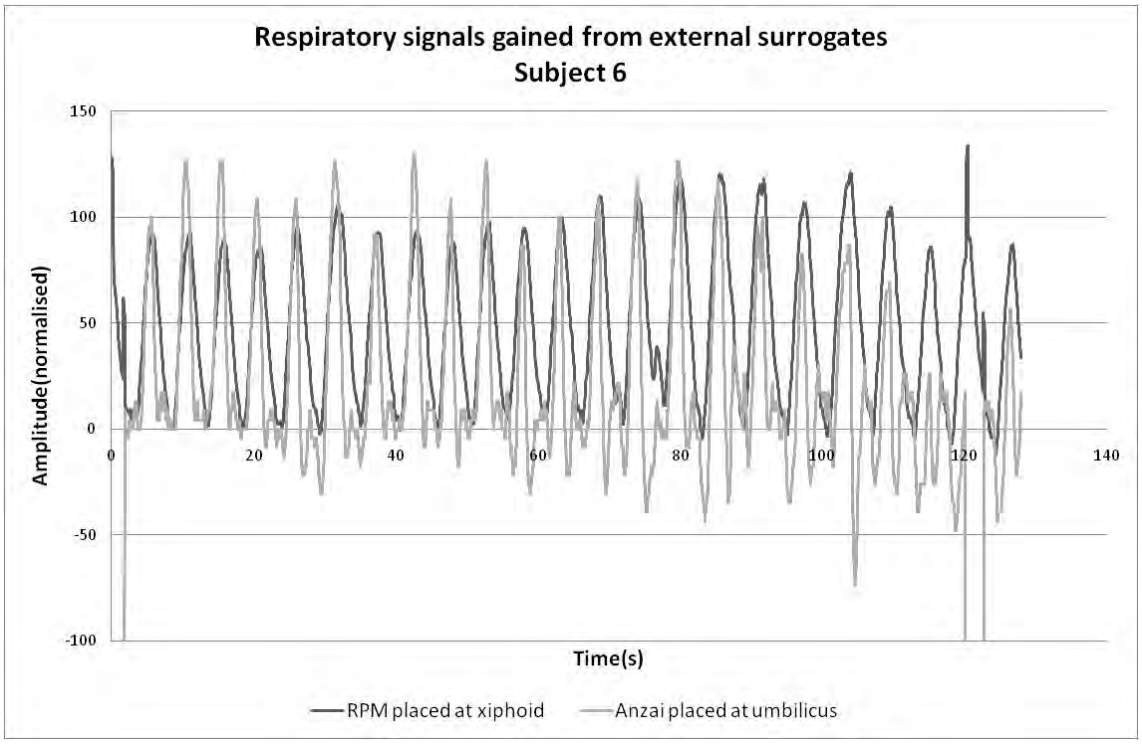


Figure A67: Respiratory signals gained using RPM marker positioned at the xiphoid and Anzai belt positioned at umbilicus for subject 6.

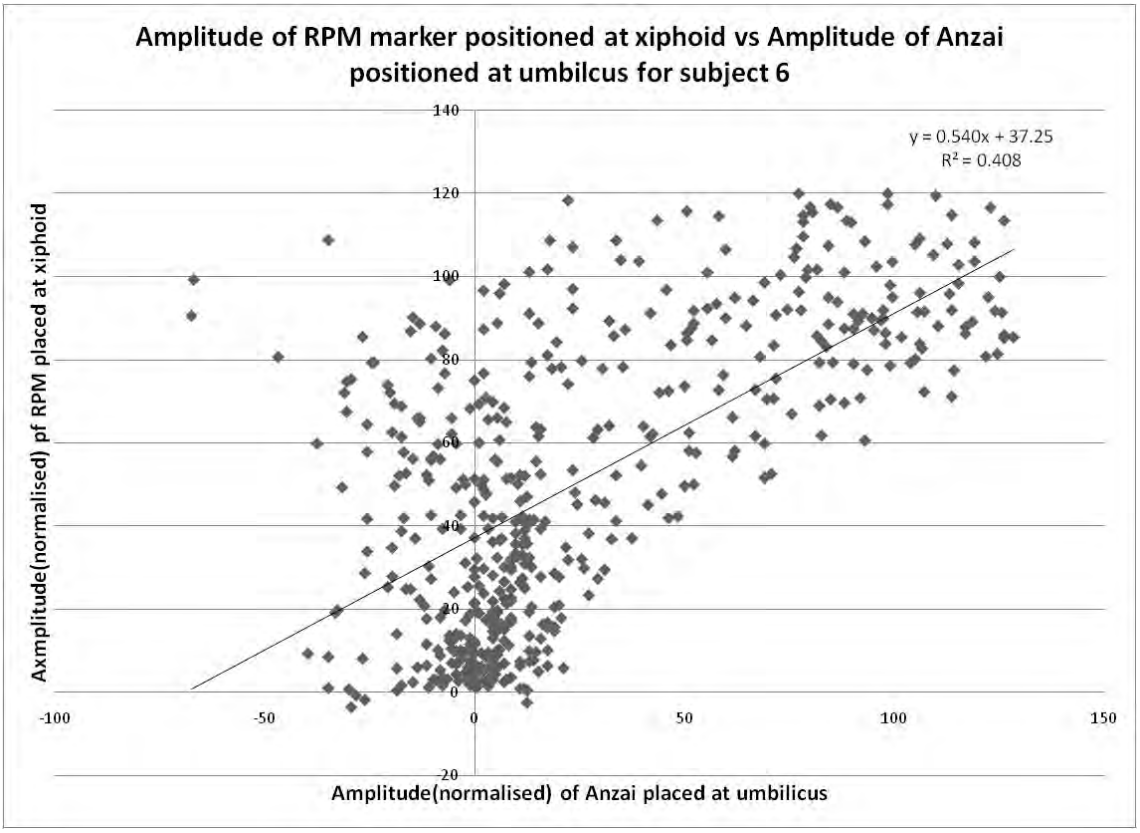


Figure A68: Determination of coefficient of determination for RPM positioned at the xiphoid and Anzai positioned at umbilicus, subject 6.

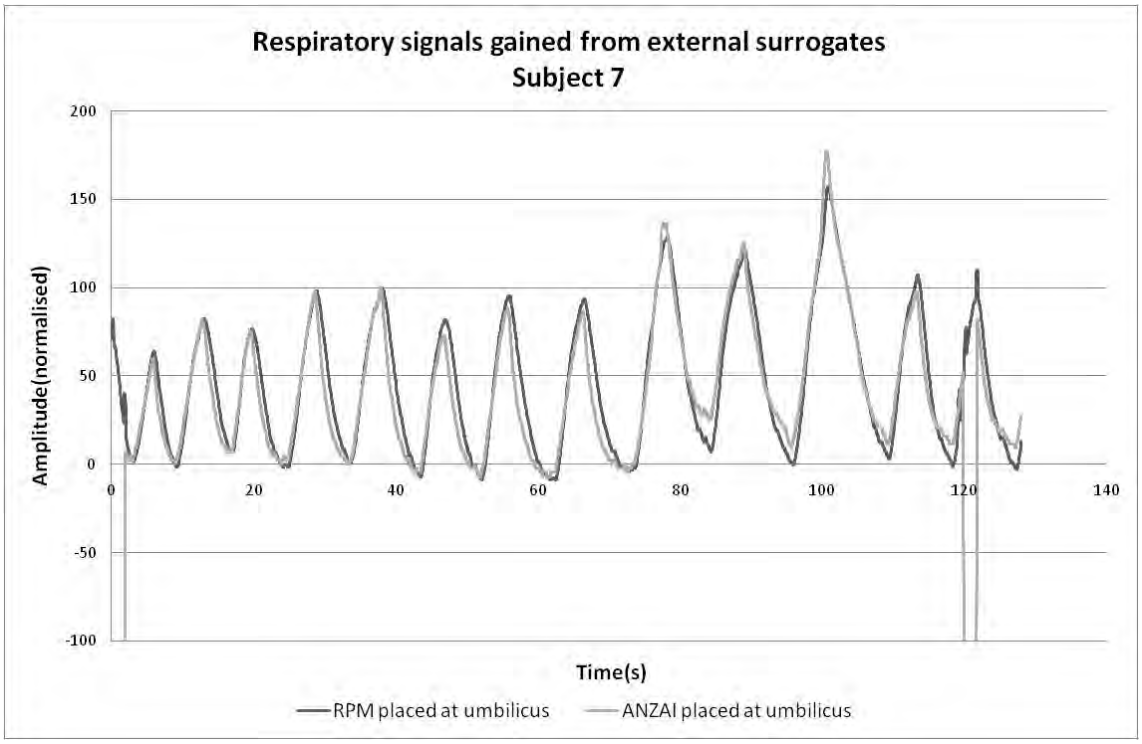


Figure A69: Respiratory signals gained using both RPM marker and Anzai belt positioned at umbilicus for subject 7.

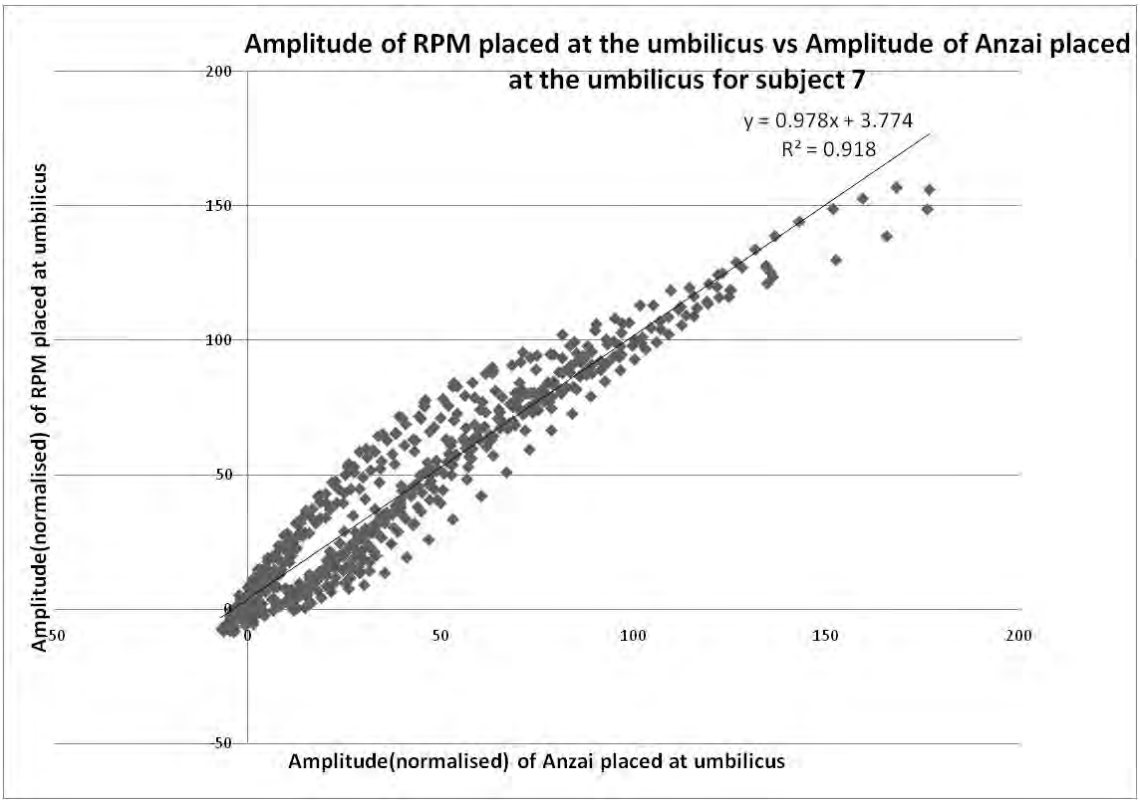


Figure A70: Determination of coefficient of determination for both RPM and Anzai positioned at umbilicus, subject 7.

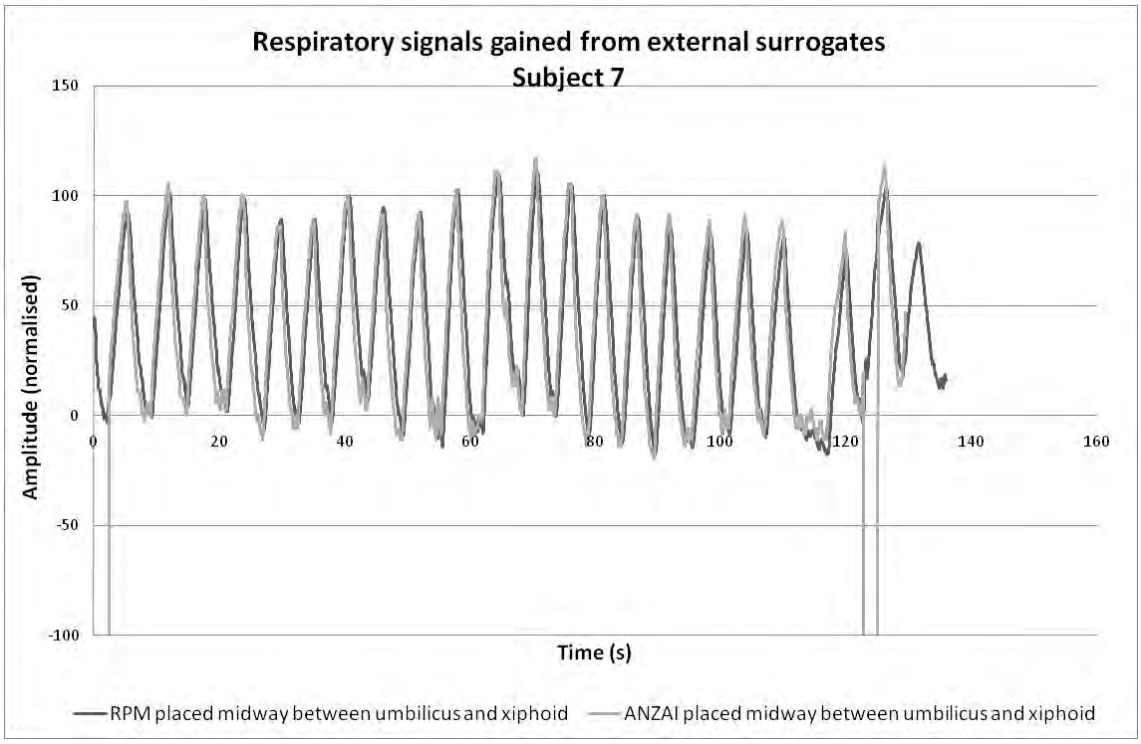


Figure A71: Respiratory signals gained using both RPM marker and Anzai belt positioned midway between umbilicus and xiphoid for subject 7.

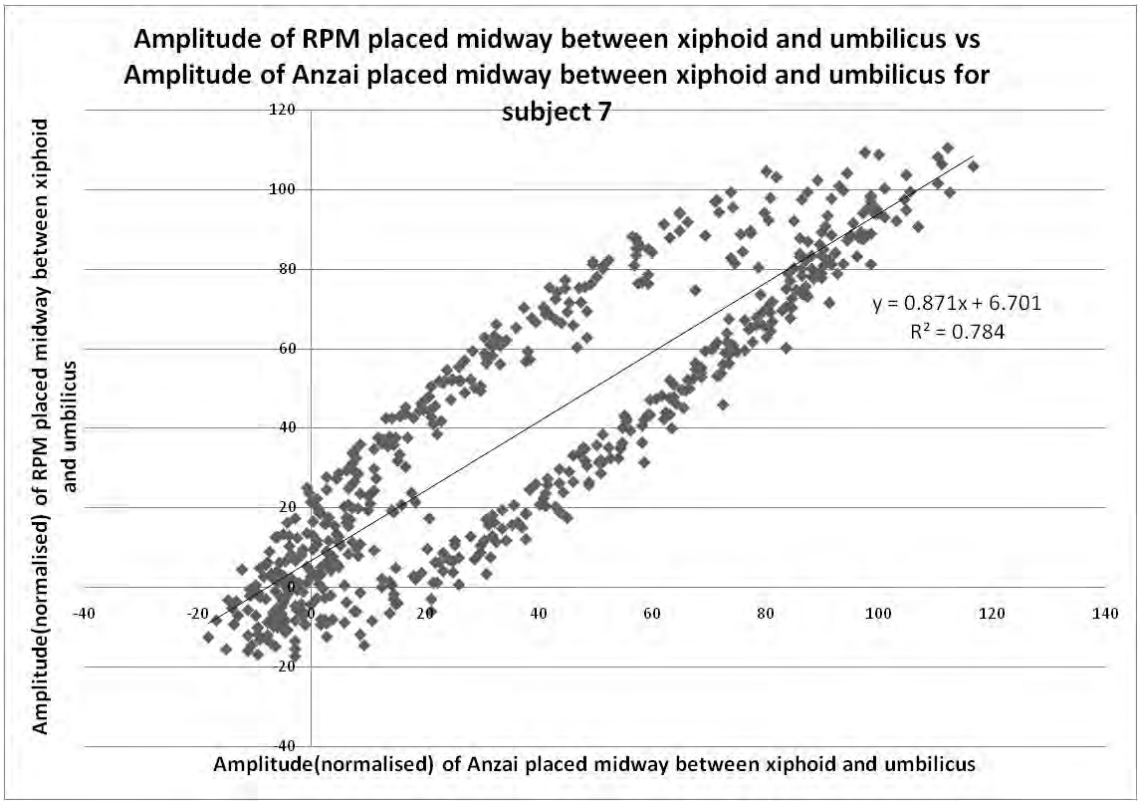


Figure A72: Determination of coefficient of determination for both RPM and Anzai positioned midway between xiphoid and umbilicus, subject 7.

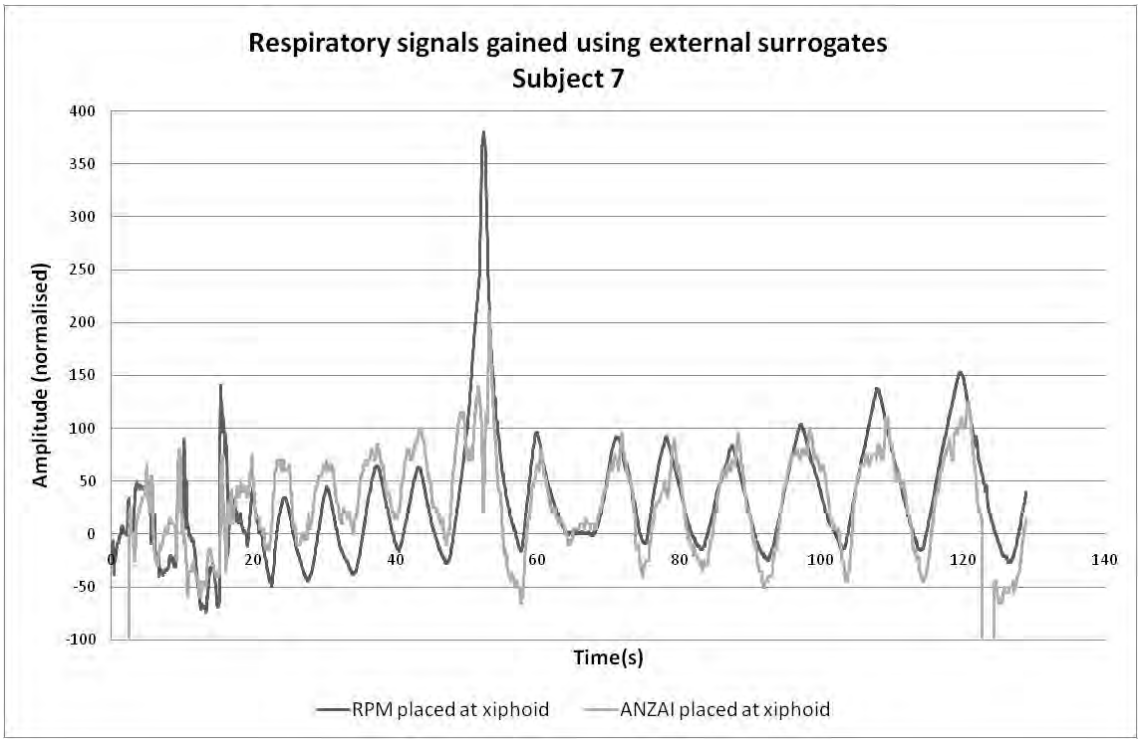


Figure A73: Respiratory signals gained using both RPM marker and Anzai belt positioned at xiphoid for subject 7.

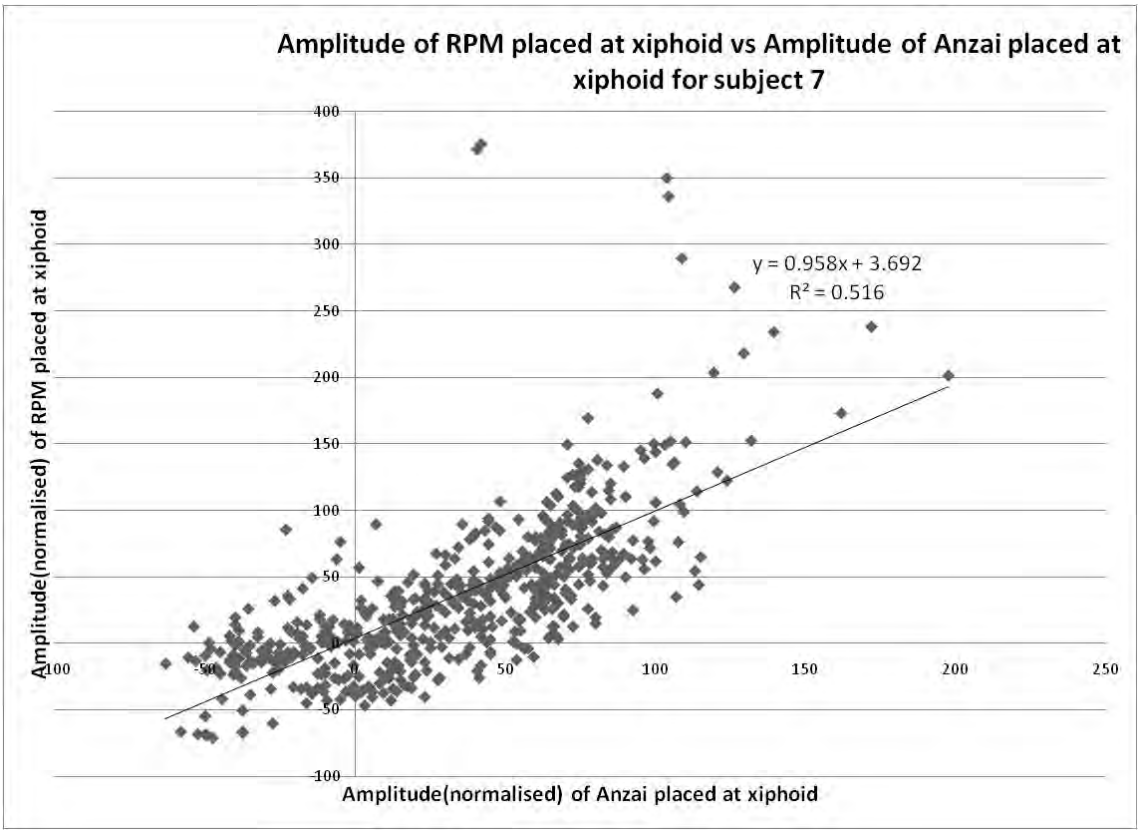


Figure A74: Determination of coefficient of determination for both RPM and Anzai positioned at xiphoid, subject 7.

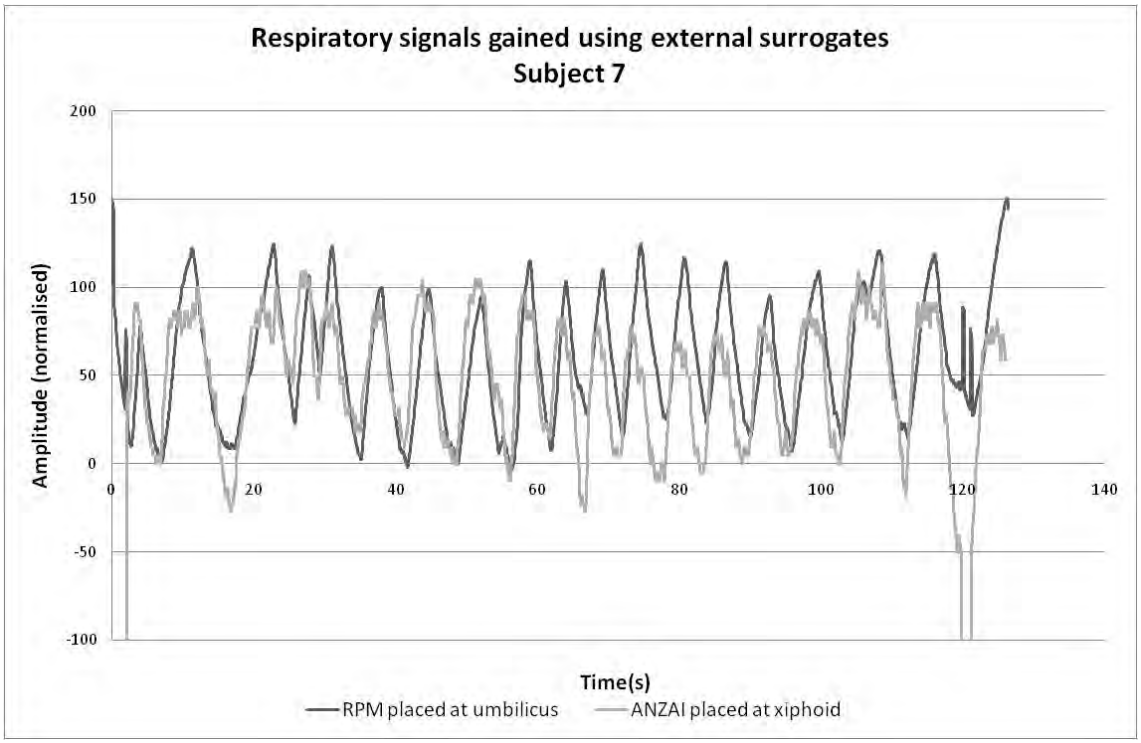


Figure A75: Respiratory signals gained using RPM marker positioned at the umbilicus and Anzai belt positioned at xiphoid for subject 7.

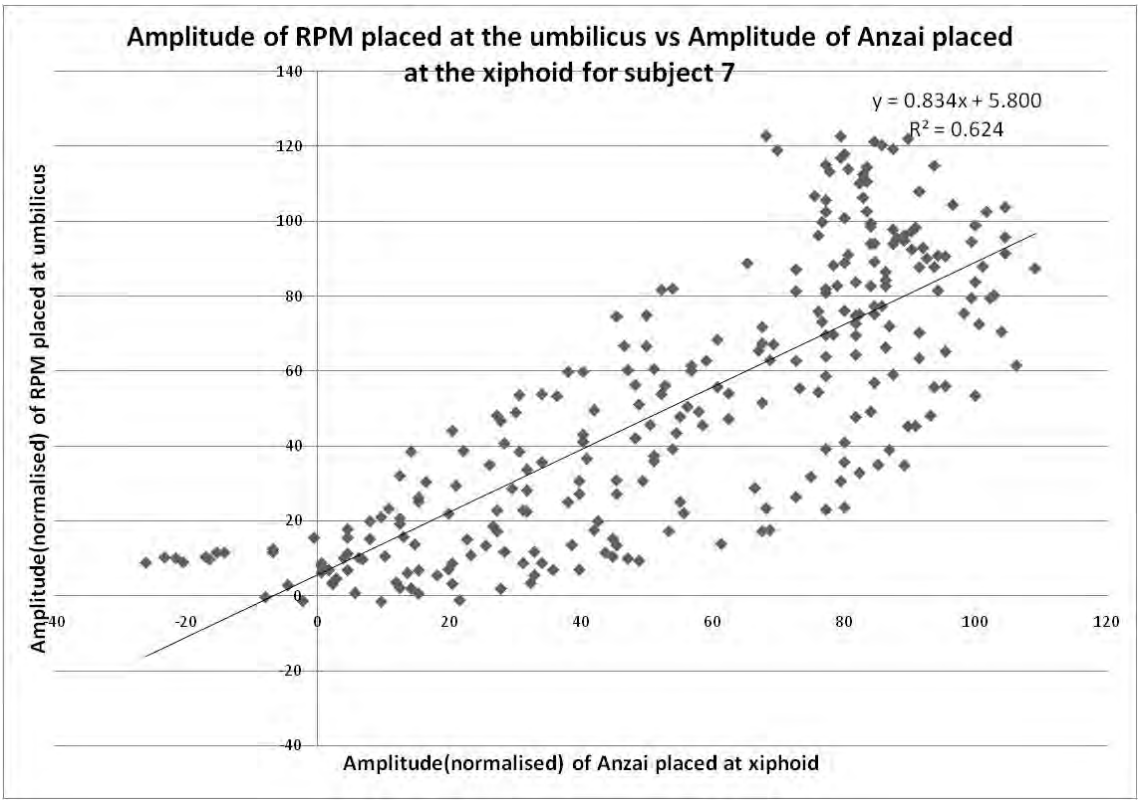


Figure A76: Determination of coefficient of determination for RPM positioned at the umbilicus and Anzai positioned at xiphoid, subject 7.

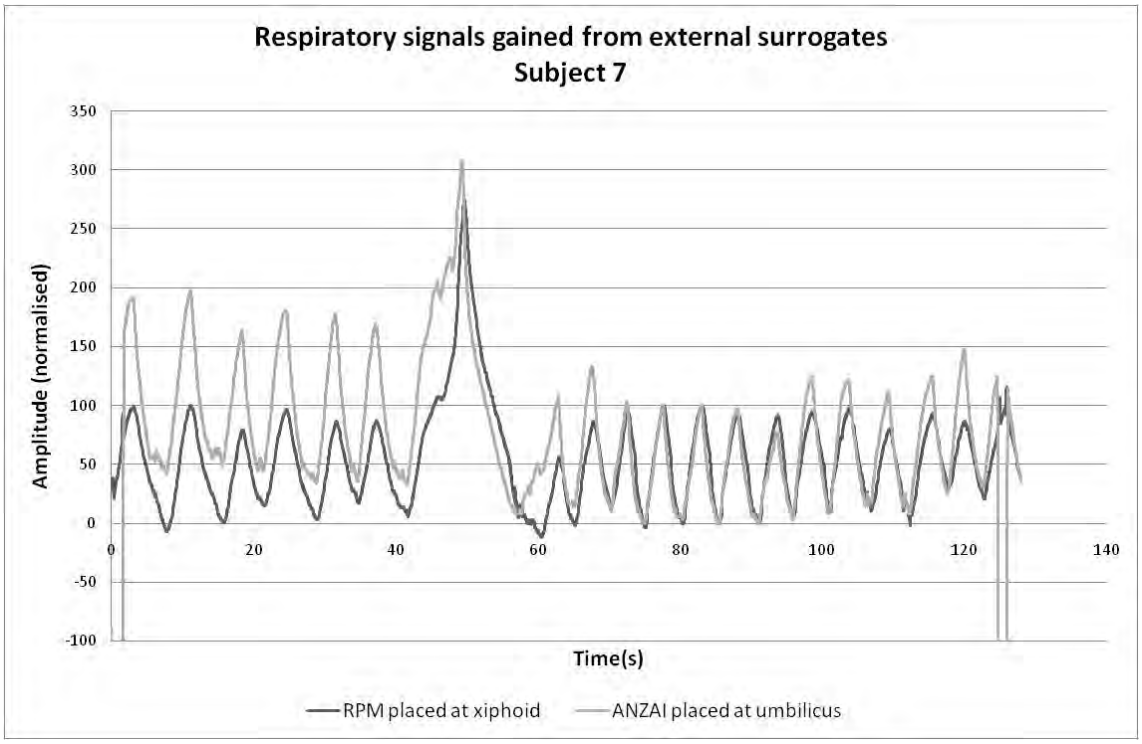


Figure A77: Respiratory signals gained using RPM marker positioned at the xiphoid and Anzai belt positioned at umbilicus for subject 7.

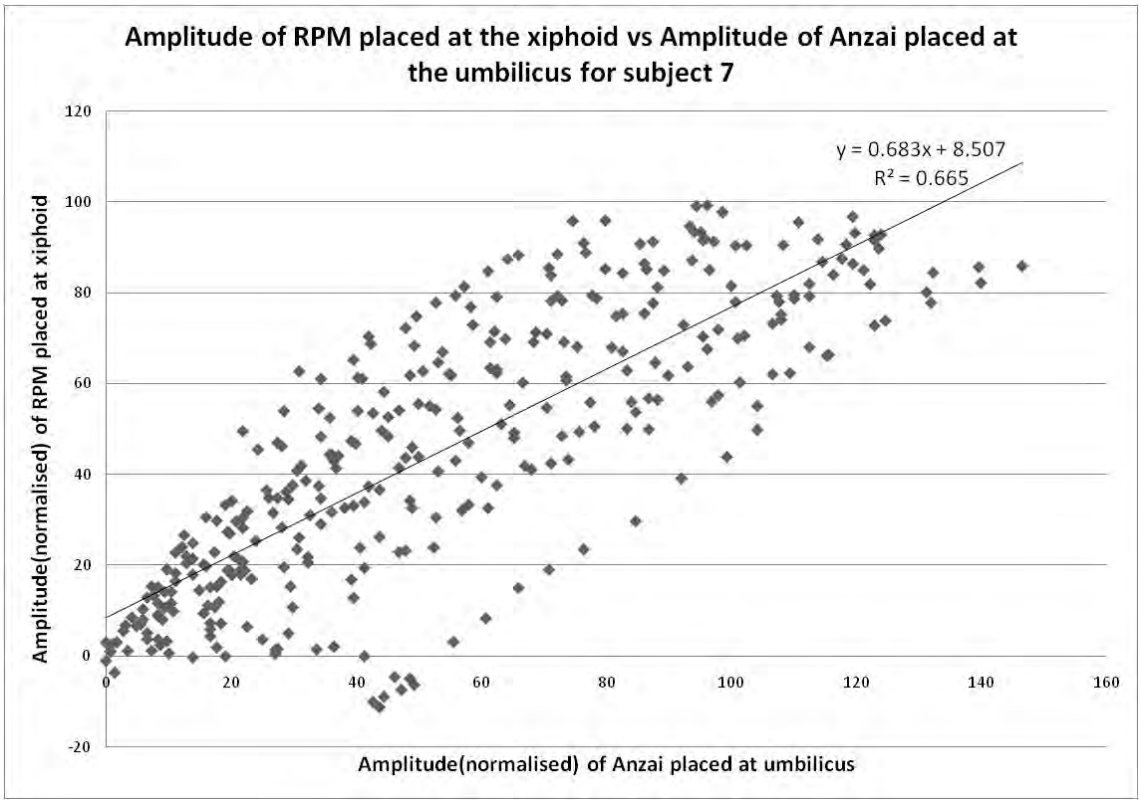


Figure A78: Determination of coefficient of determination for both RPM and Anzai positioned at xiphoid, subject 7.

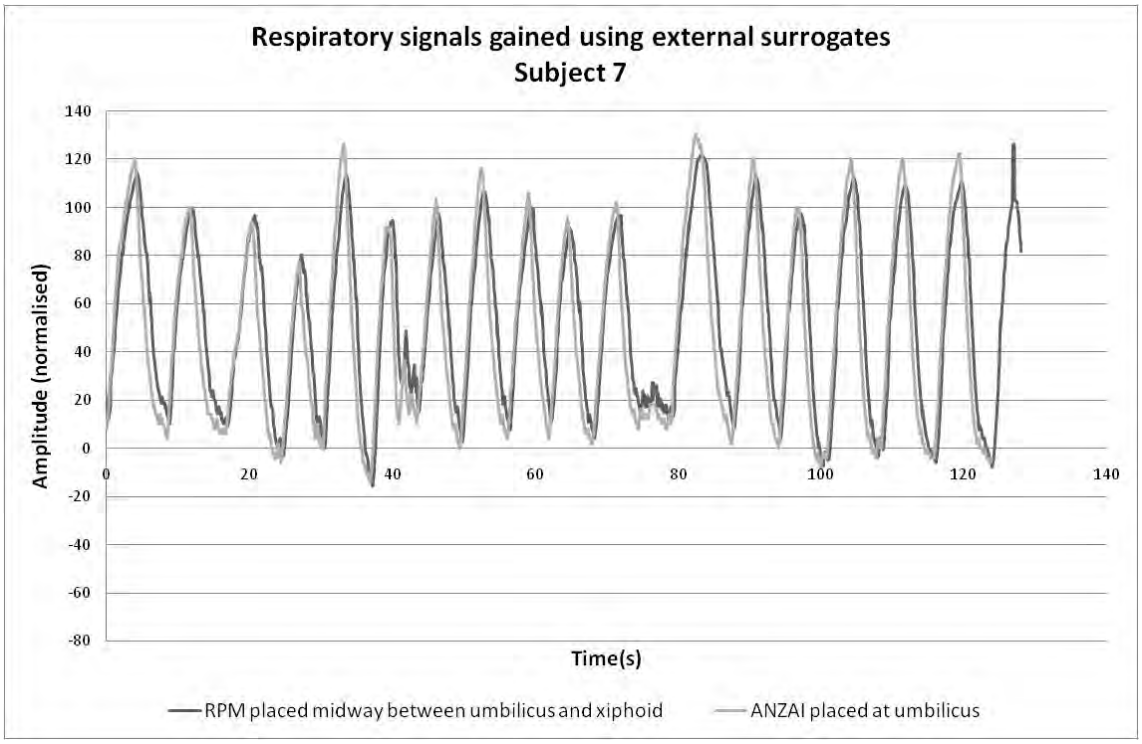


Figure A79: Respiratory signals gained using RPM marker positioned midway between xiphoid and umbilicus and Anzai belt positioned at umbilicus for subject 7.

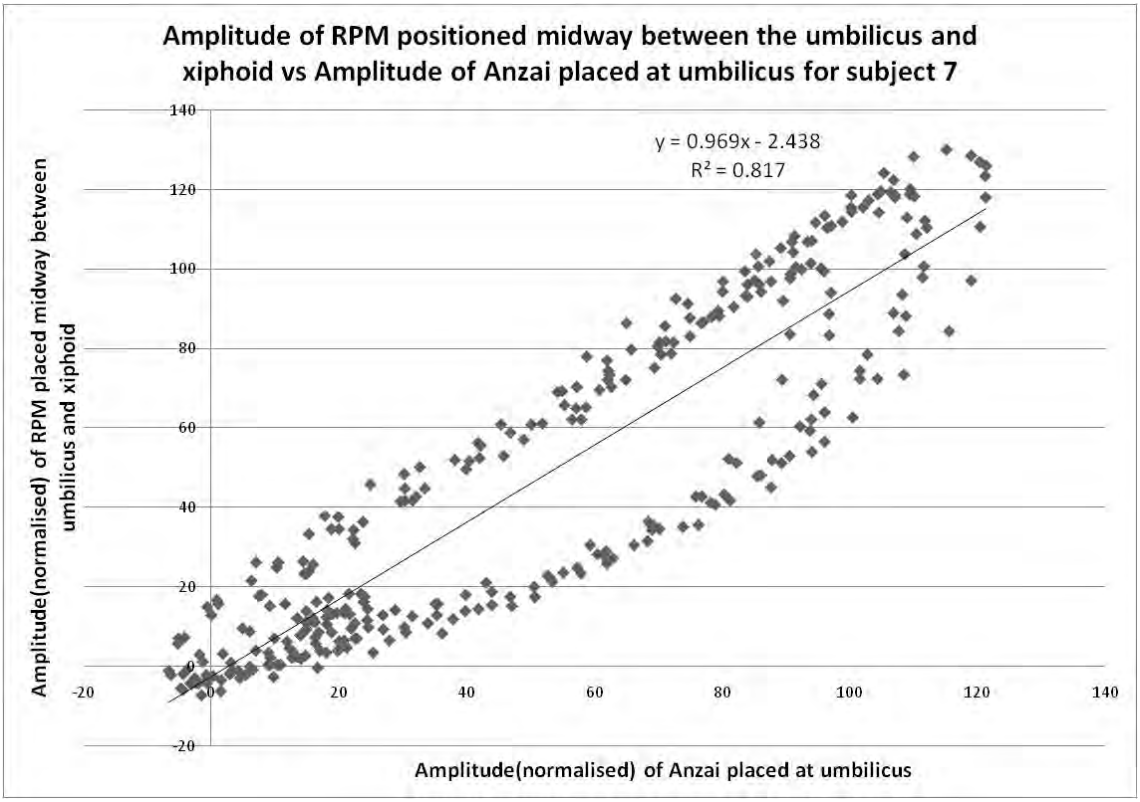


Figure A80: Determination of coefficient of determination for RPM positioned midway between xiphoid and umbilicus and Anzai positioned at umbilicus, subject 7.

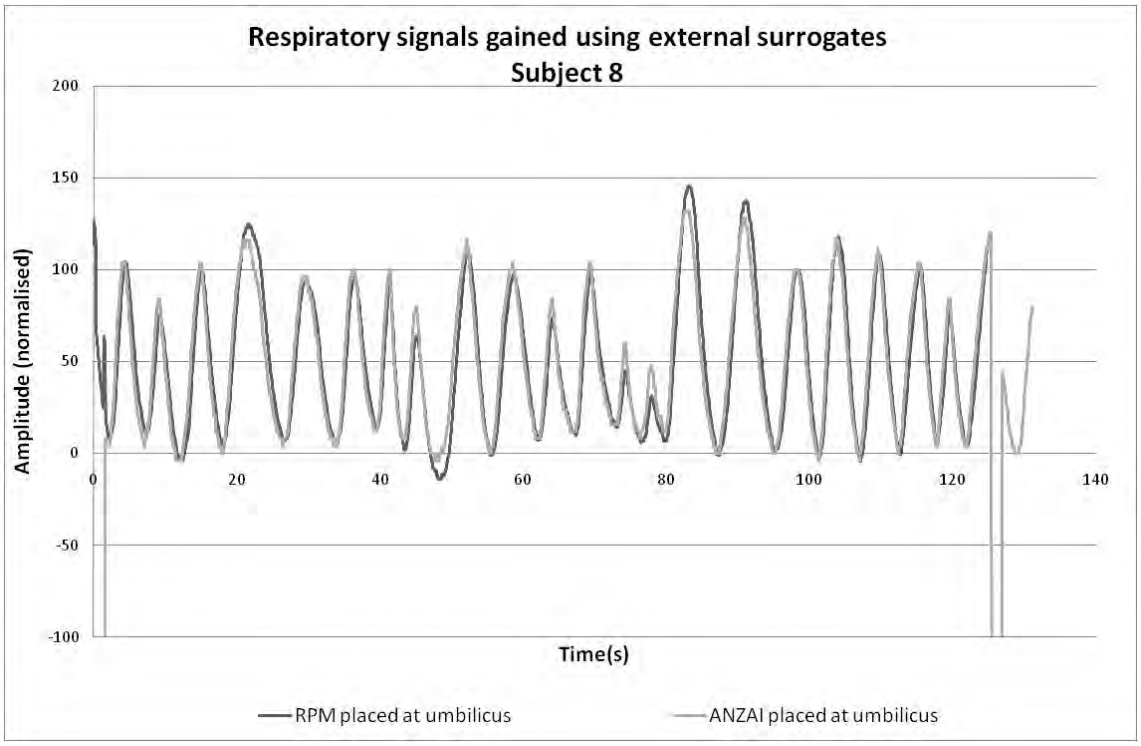


Figure A81: Respiratory signals gained using both RPM marker and Anzai belt positioned at umbilicus for subject 8.

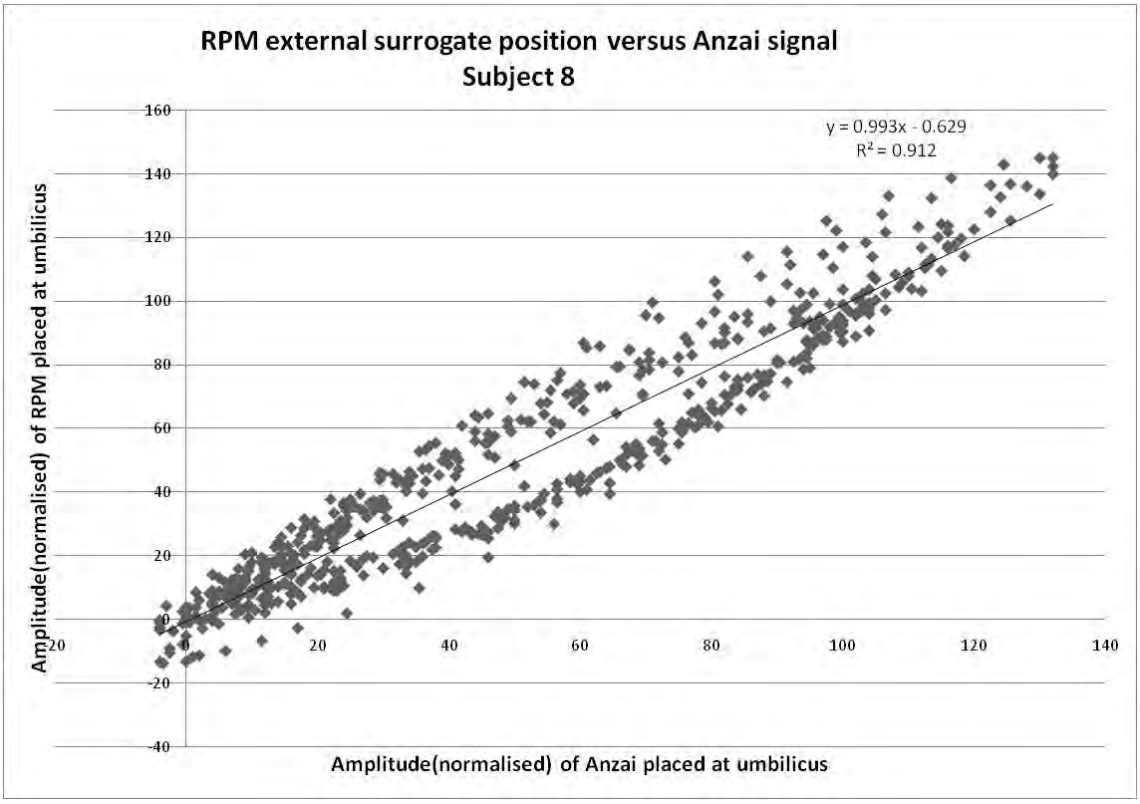


Figure A82: Determination of coefficient of determination for both RPM and Anzai positioned at umbilicus, subject 8.

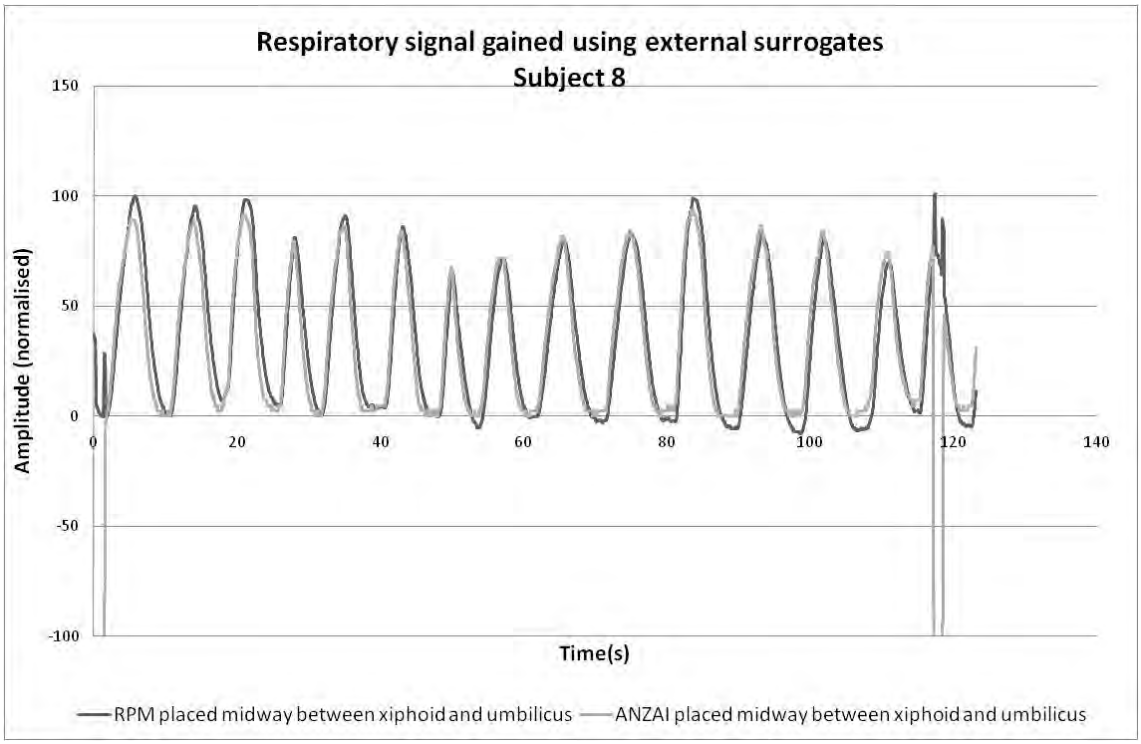


Figure A83: Respiratory signals gained using both RPM marker and Anzai belt positioned midway between umbilicus and xiphoid for subject 8.

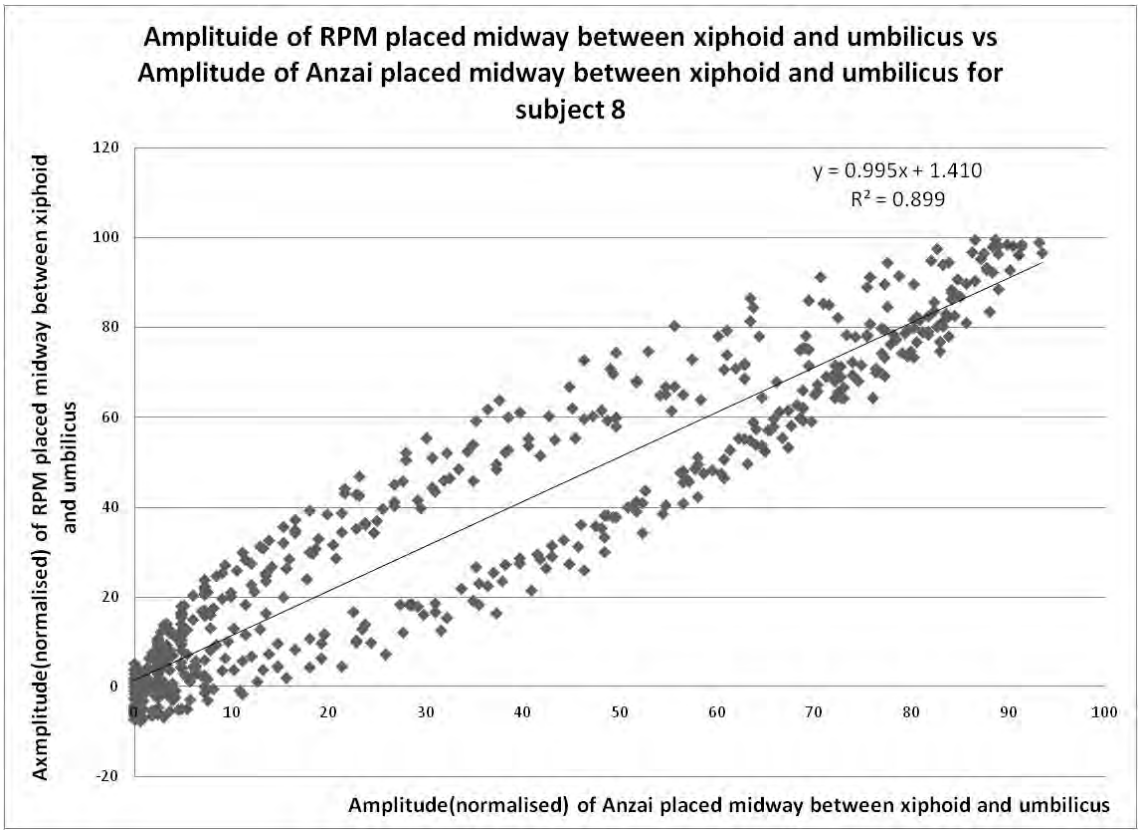


Figure A84: Determination of coefficient of determination for both RPM and Anzai positioned midway between xiphoid and umbilicus, subject 8.

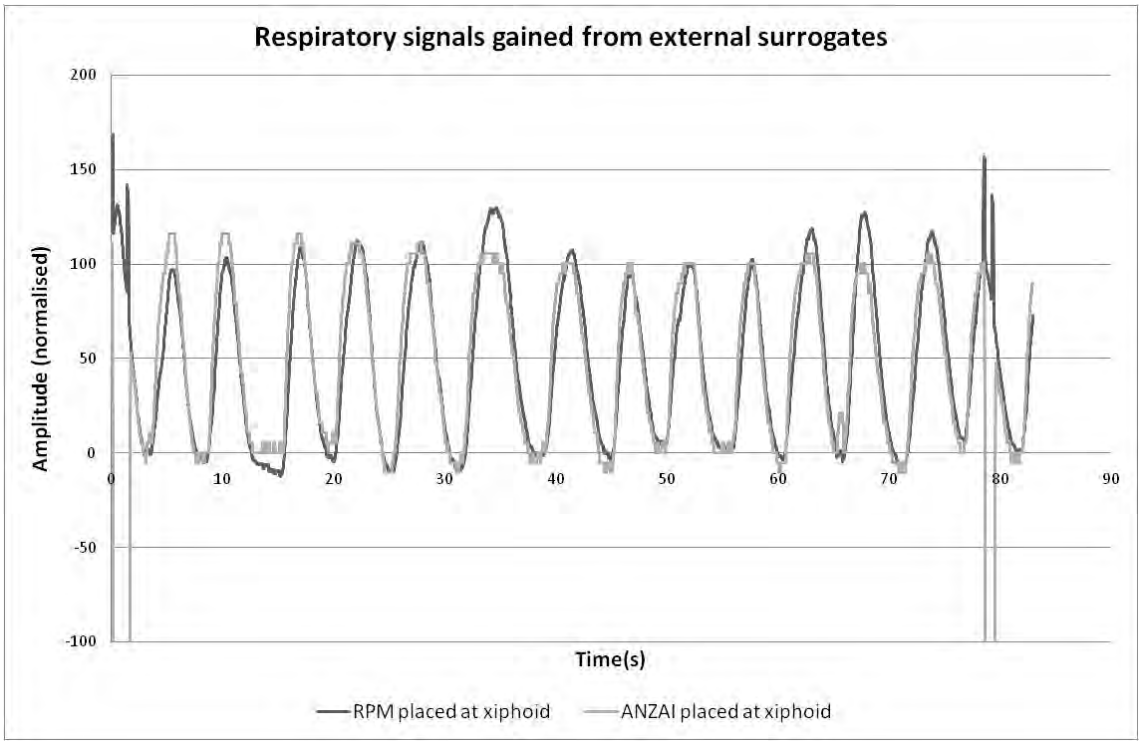


Figure A85: Respiratory signals gained using both RPM marker and Anzai belt positioned at xiphoid for subject 8.

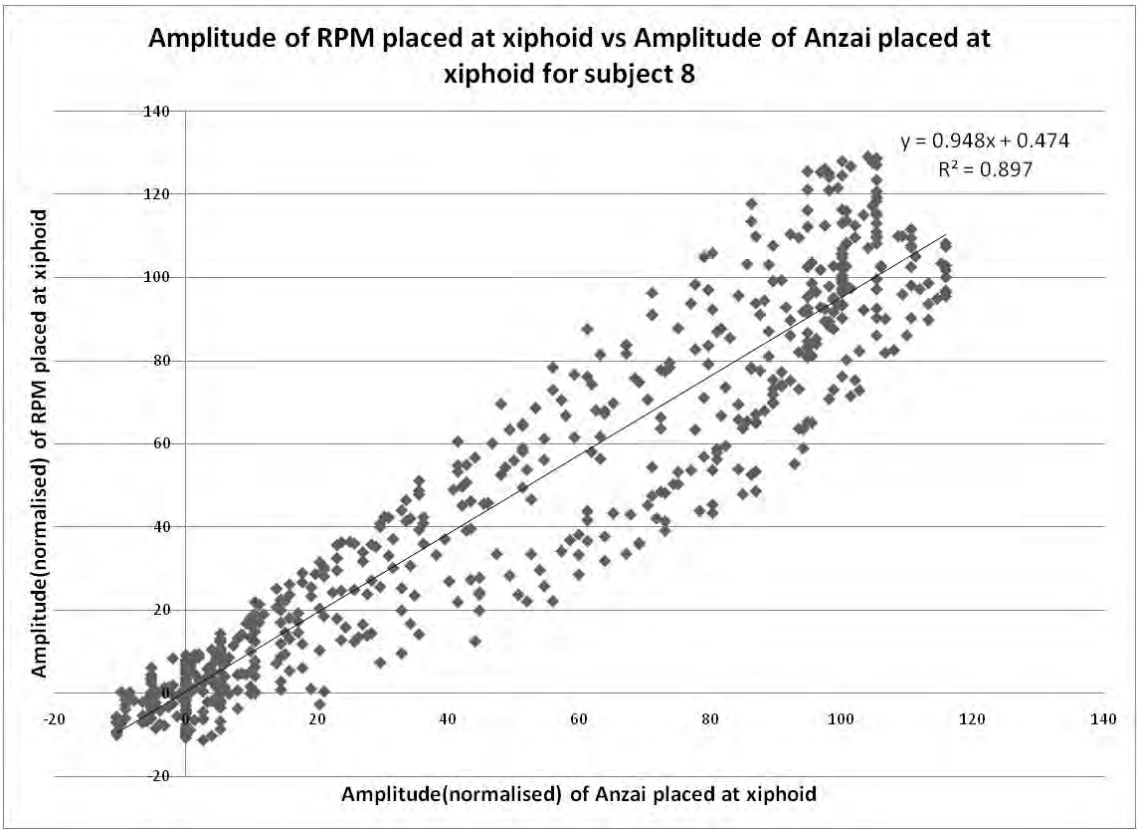


Figure A86: Determination of coefficient of determination for both RPM and Anzai positioned at xiphoid, subject 8.

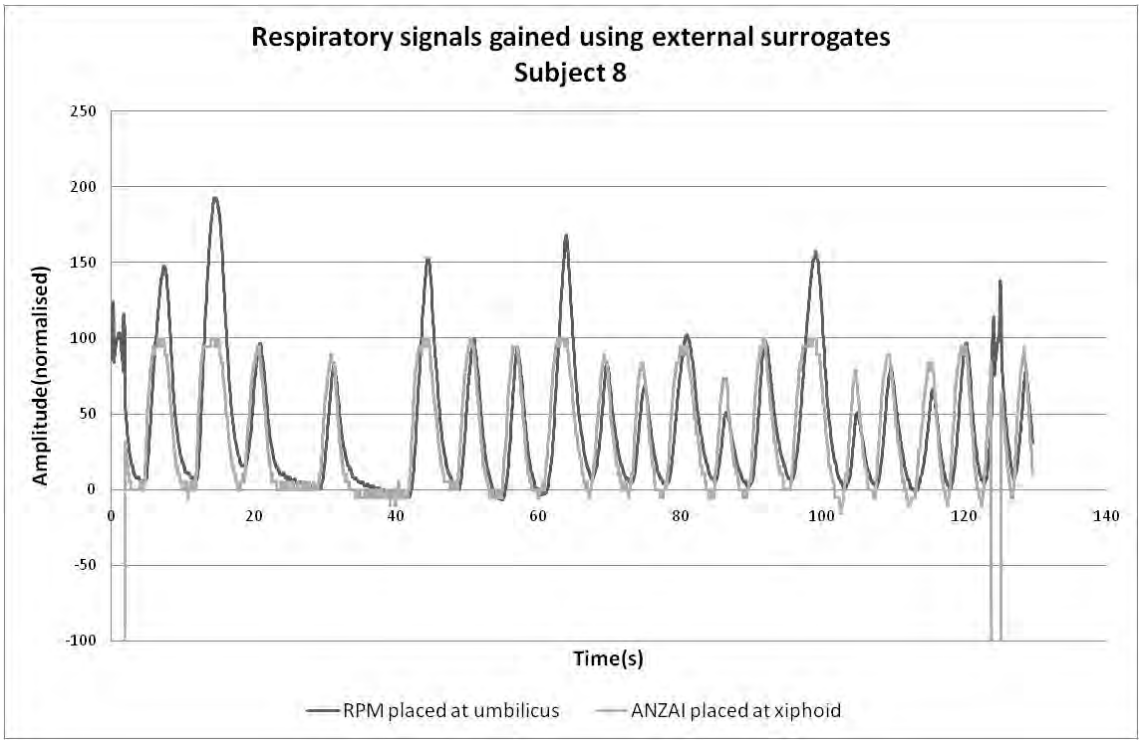


Figure A87: Respiratory signals gained using RPM marker positioned at the umbilicus and Anzai belt positioned at xiphoid for subject 8.

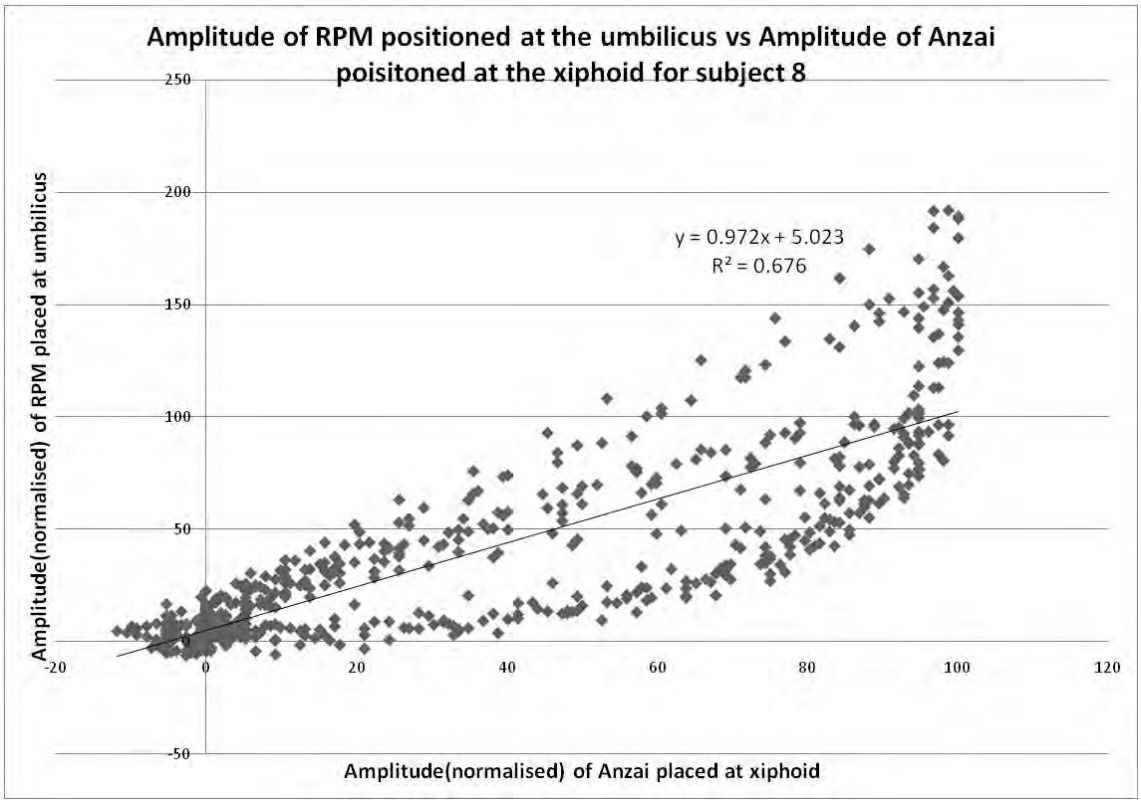


Figure A88: Determination of coefficient of determination for RPM positioned at the umbilicus and Anzai positioned at xiphoid, subject 8.

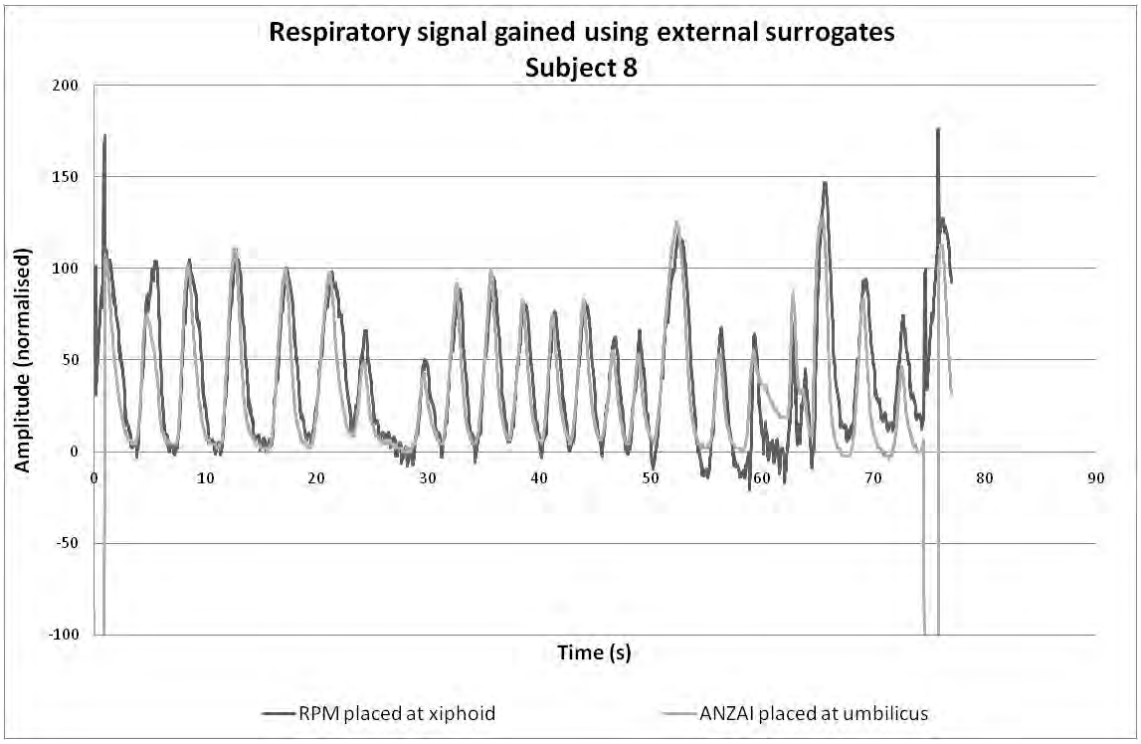


Figure A89: Respiratory signals gained using RPM marker positioned at the xiphoid and Anzai belt positioned at umbilicus for subject 8.

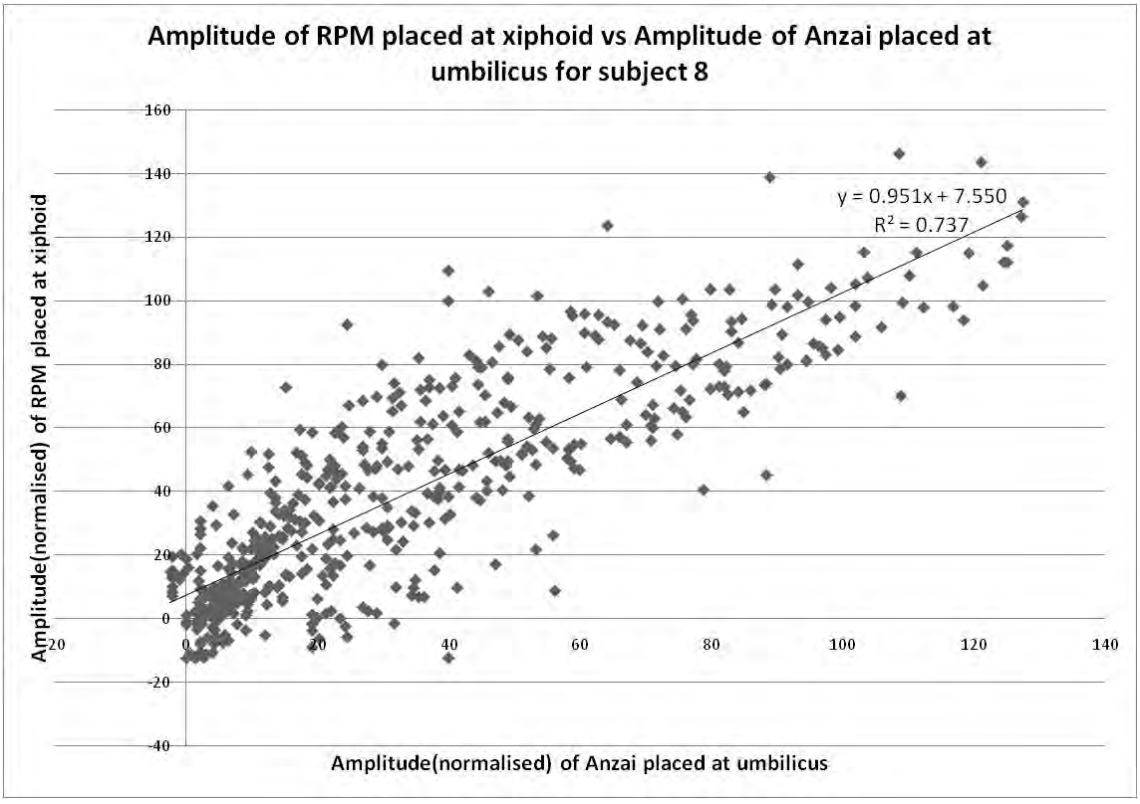


Figure A90: Determination of coefficient of determination for RPM positioned at the xiphoid and Anzai positioned at umbilicus, subject 8.

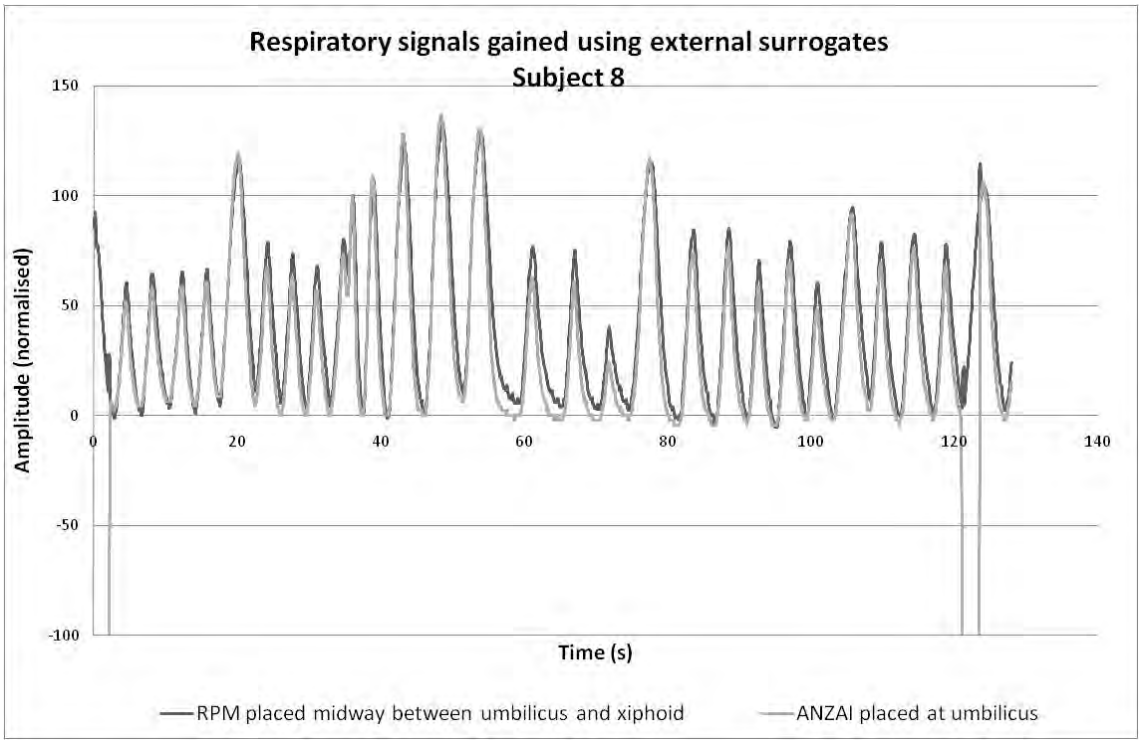


Figure A91: Respiratory signals gained using RPM marker positioned midway between xiphoid and umbilicus and Anzai belt positioned at umbilicus for subject 8.

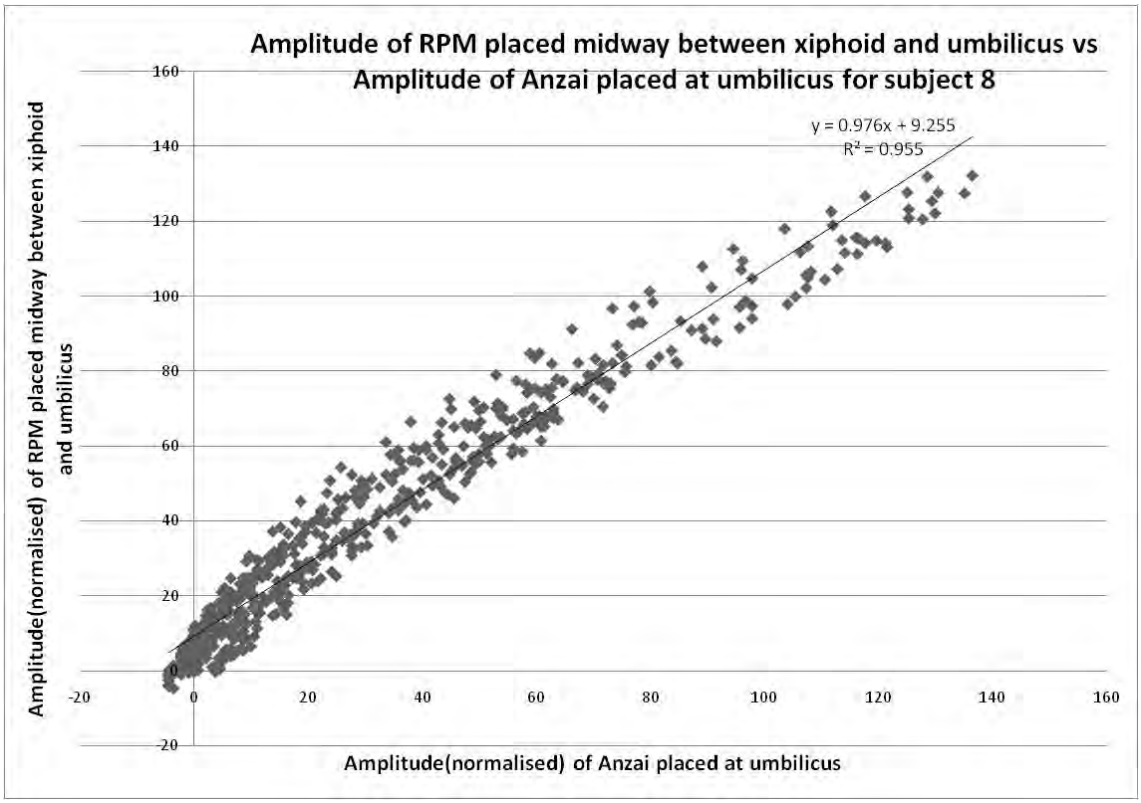


Figure A92: Determination of coefficient of determination for RPM positioned midway between xiphoid and umbilicus and Anzai positioned at umbilicus, subject 8.

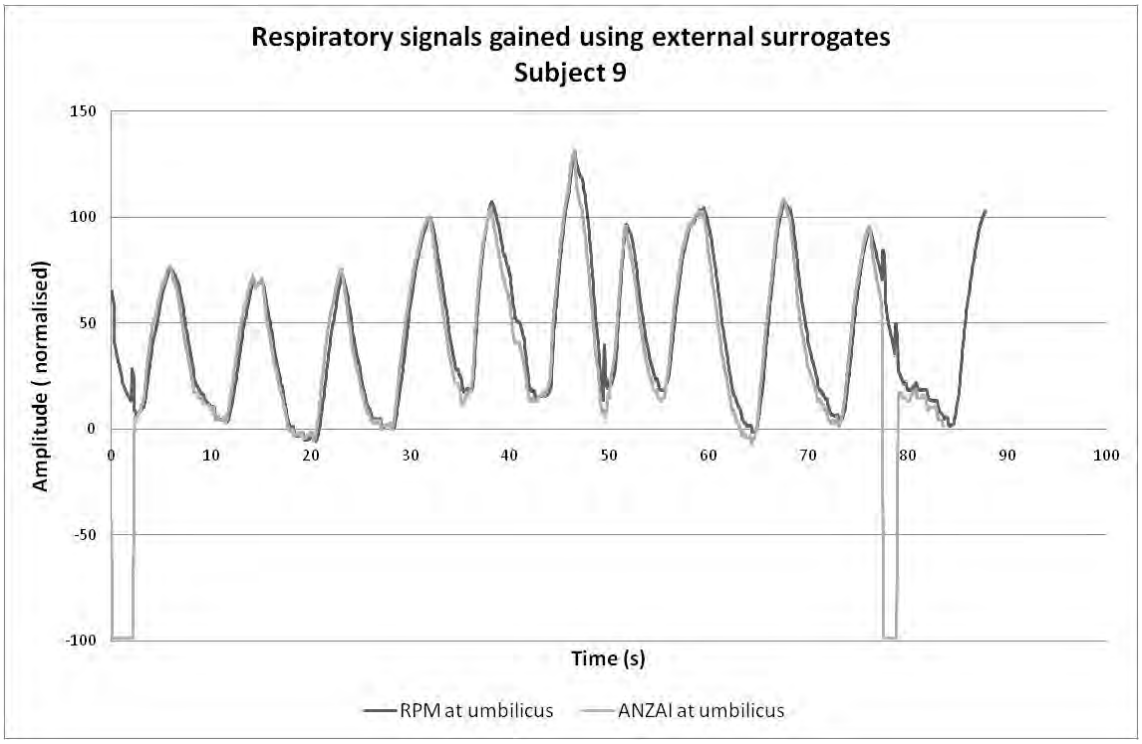


Figure A93: Respiratory signals gained using both RPM marker and Anzai belt positioned at umbilicus for subject 9.

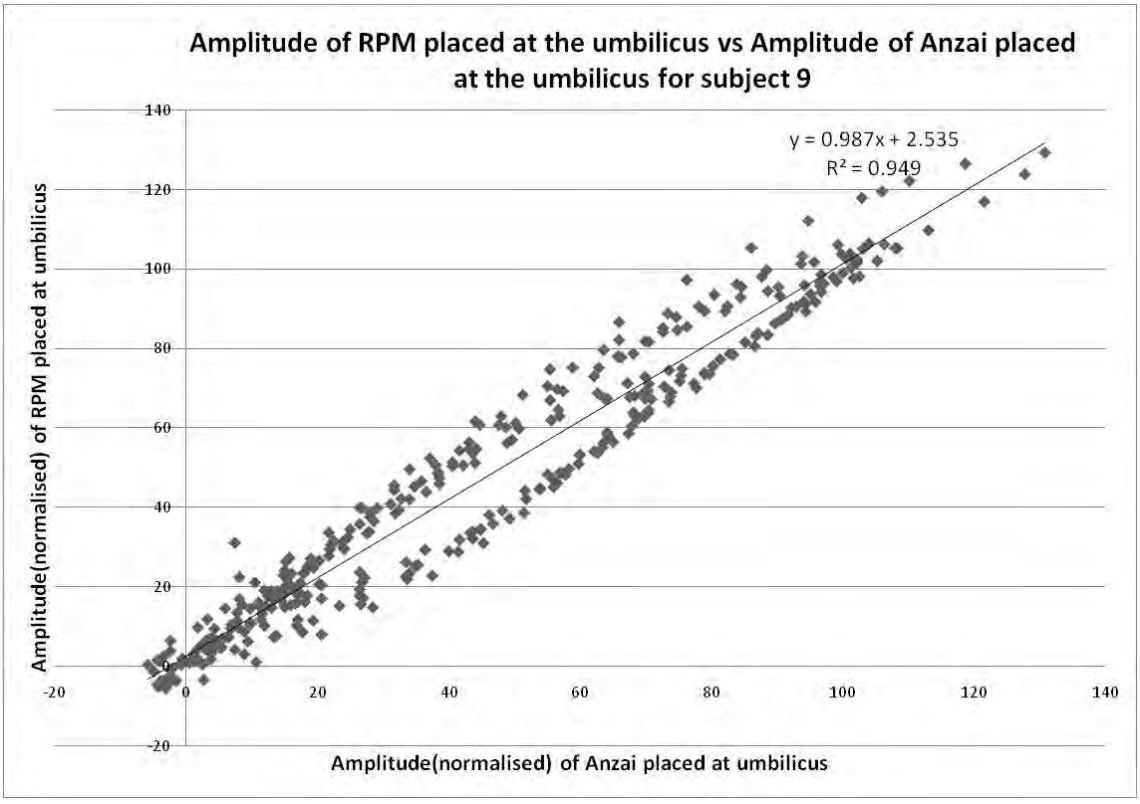


Figure A94: Determination of coefficient of determination for both RPM and Anzai positioned at umbilicus, subject 9.

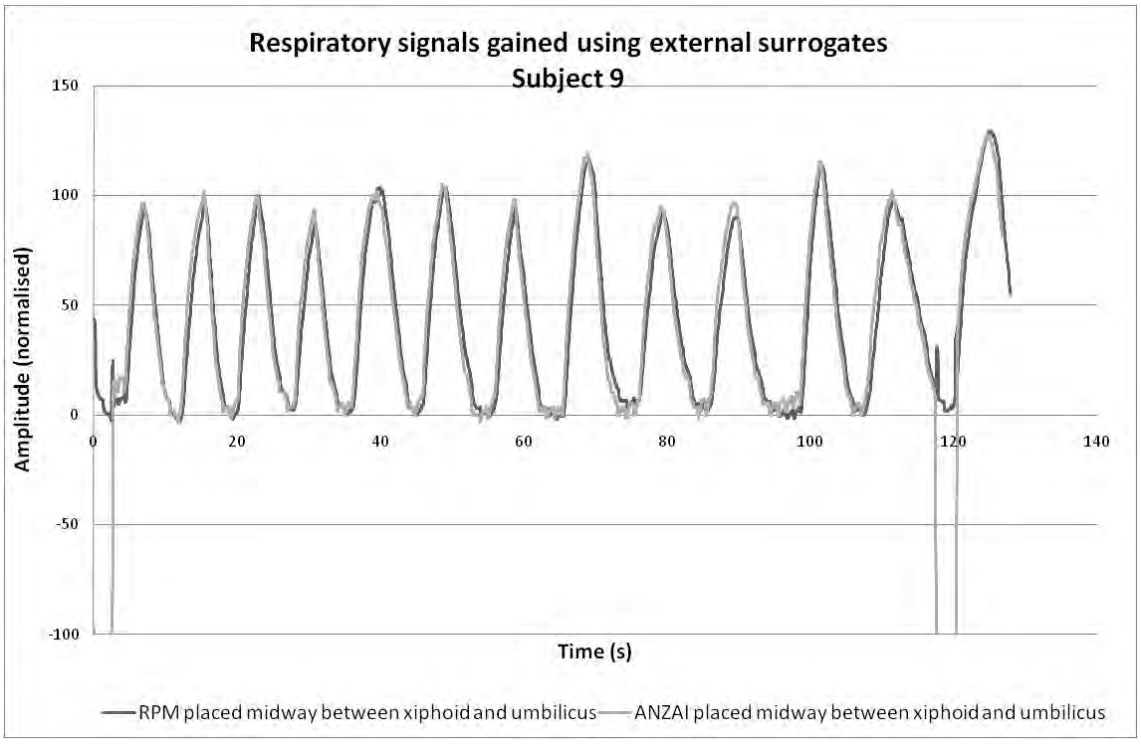


Figure A95: Respiratory signals gained using both RPM marker and Anzai belt positioned midway between umbilicus and xiphoid for subject 9.

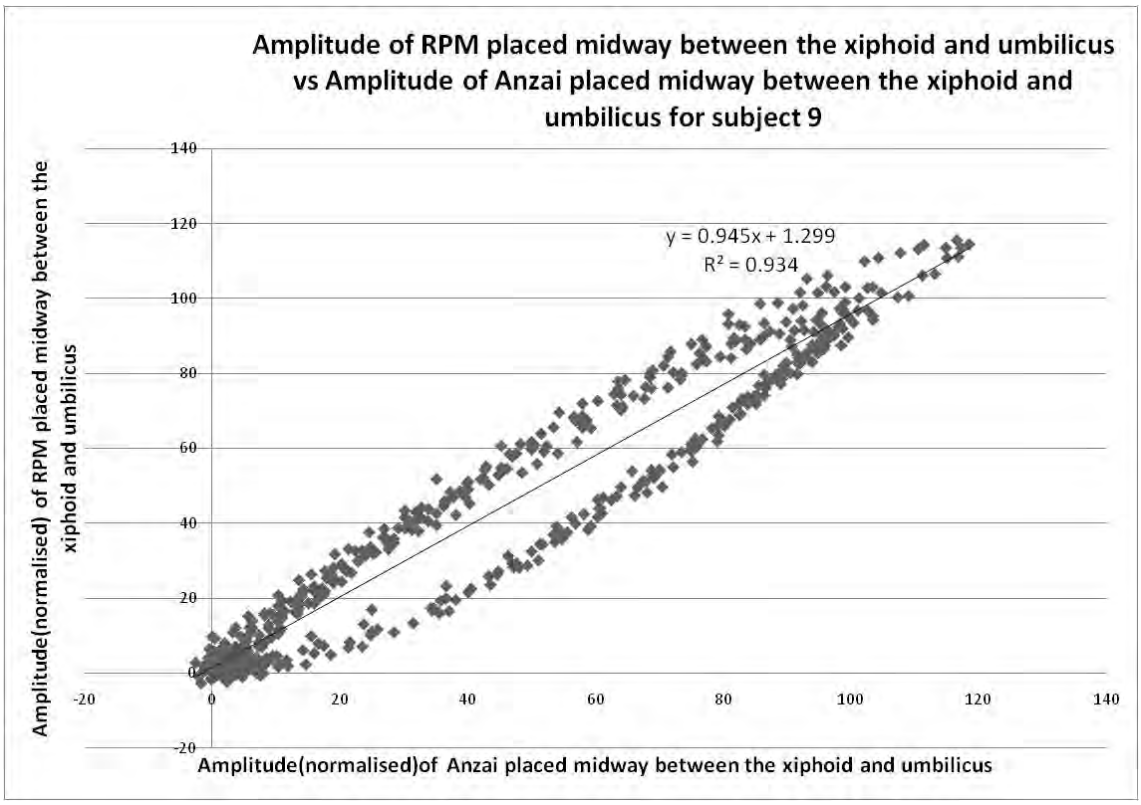


Figure A96: Determination of coefficient of determination for both RPM and Anzai positioned midway between xiphoid and umbilicus, subject 9.

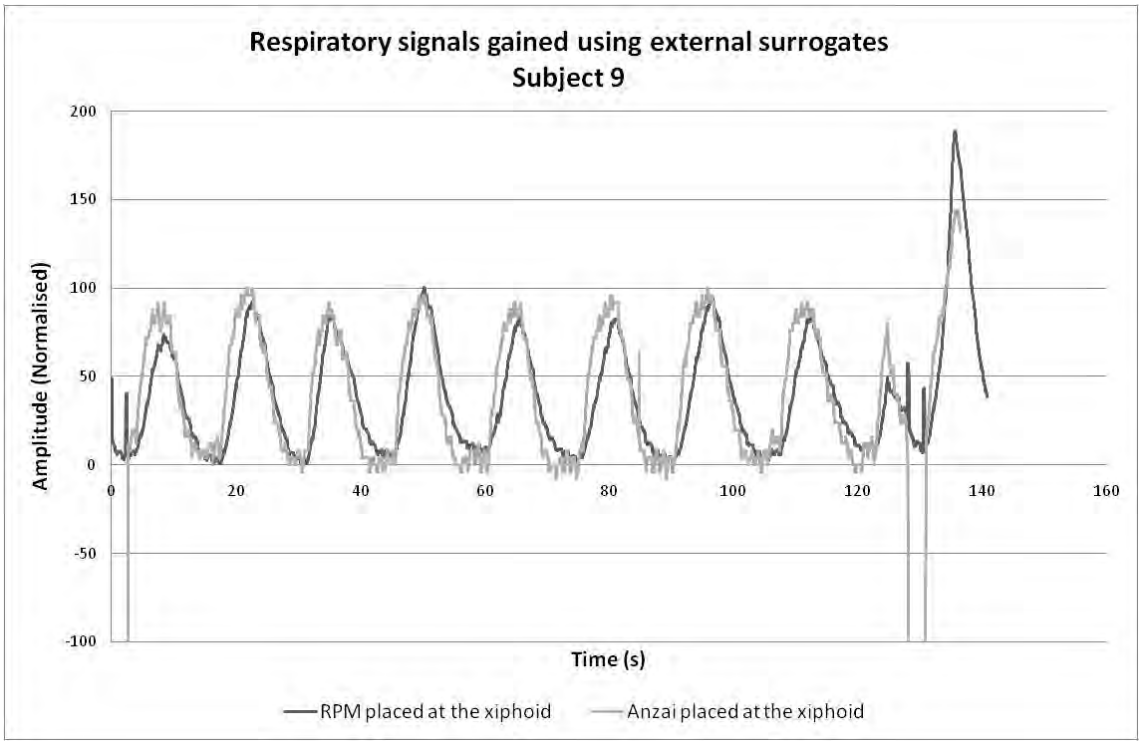


Figure A97: Respiratory signals gained using both RPM marker and Anzai belt positioned at xiphoid for subject 9.

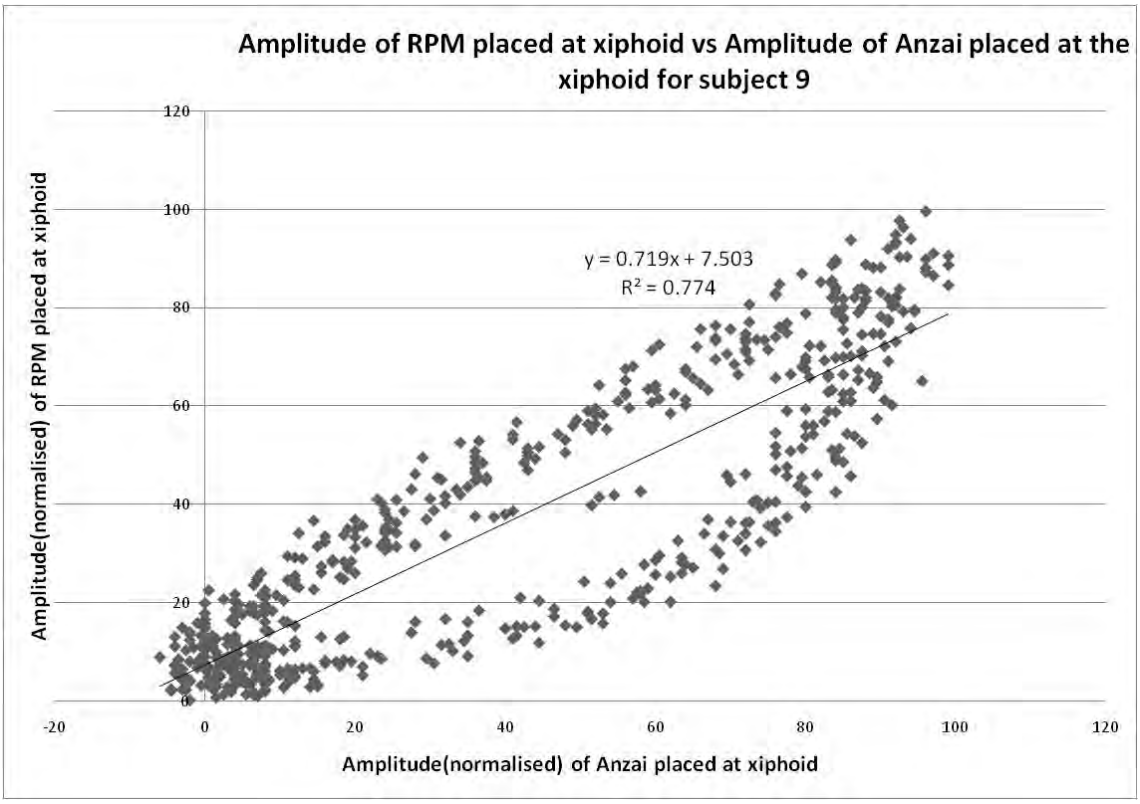


Figure A98: Determination of coefficient of determination for both RPM and Anzai positioned at xiphoid, subject 9.

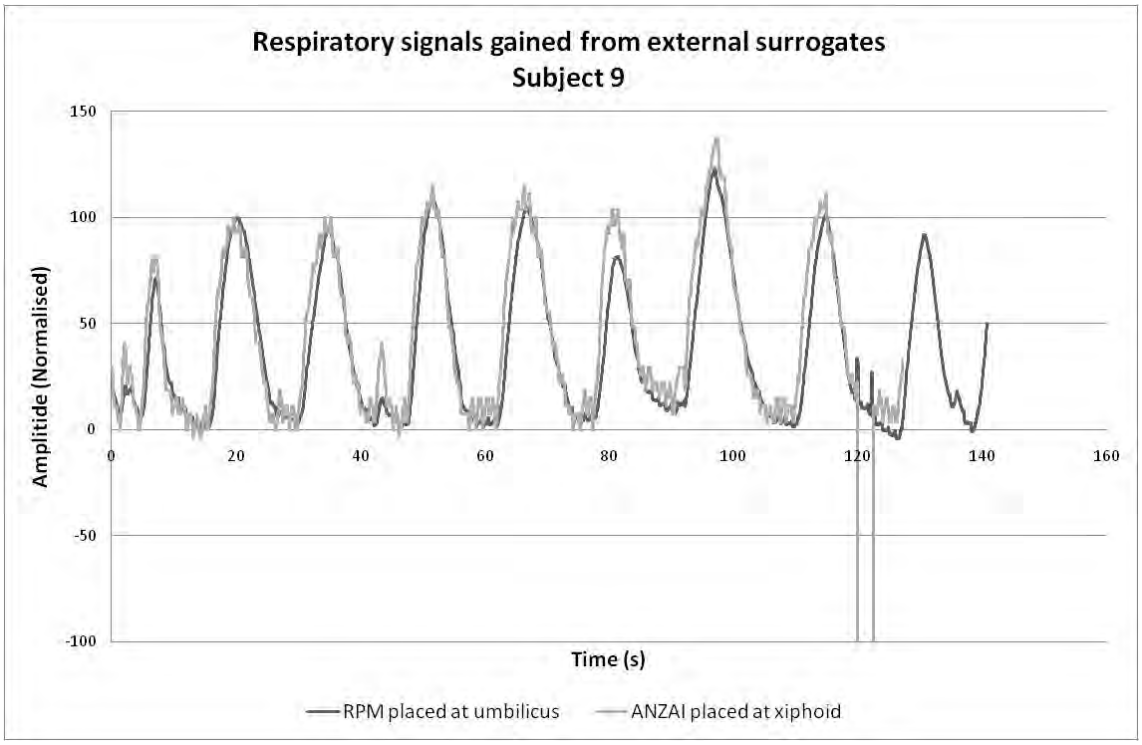


Figure A99: Respiratory signals gained using RPM marker positioned at the umbilicus and Anzai belt positioned at xiphoid for subject 9.

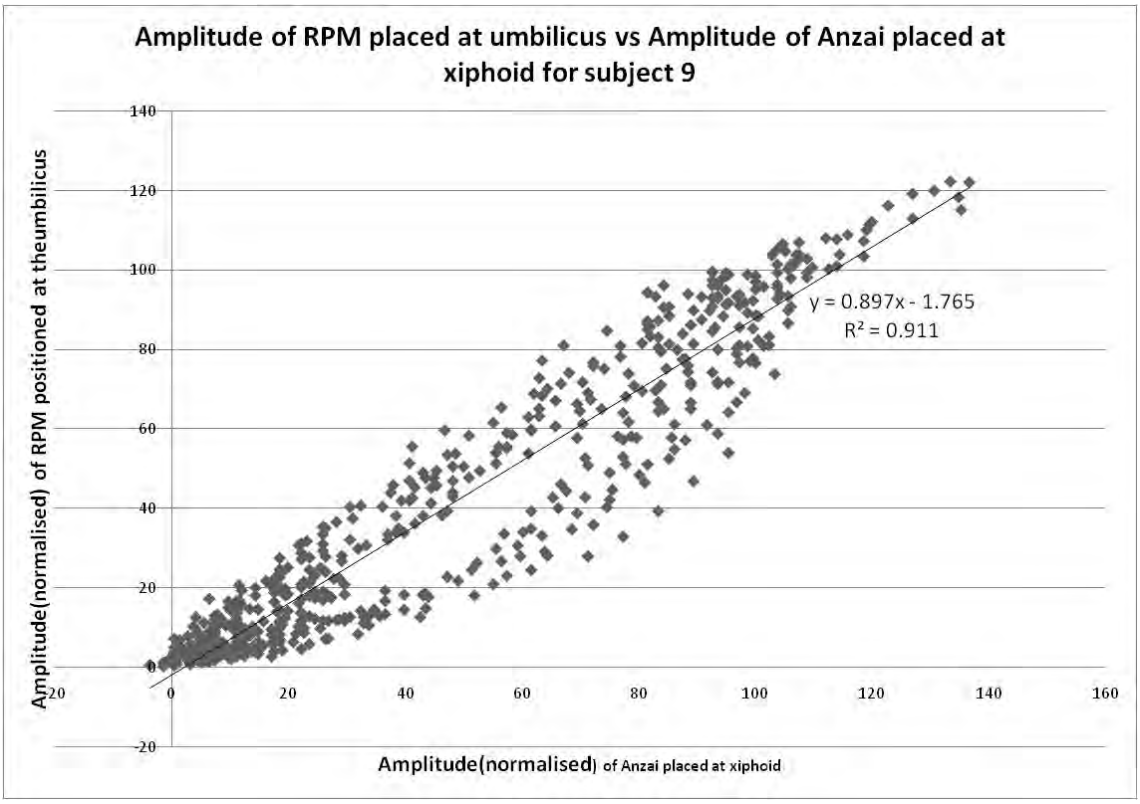


Figure A100: Determination of coefficient of determination for RPM positioned at the umbilicus and Anzai positioned at xiphoid, subject 9.

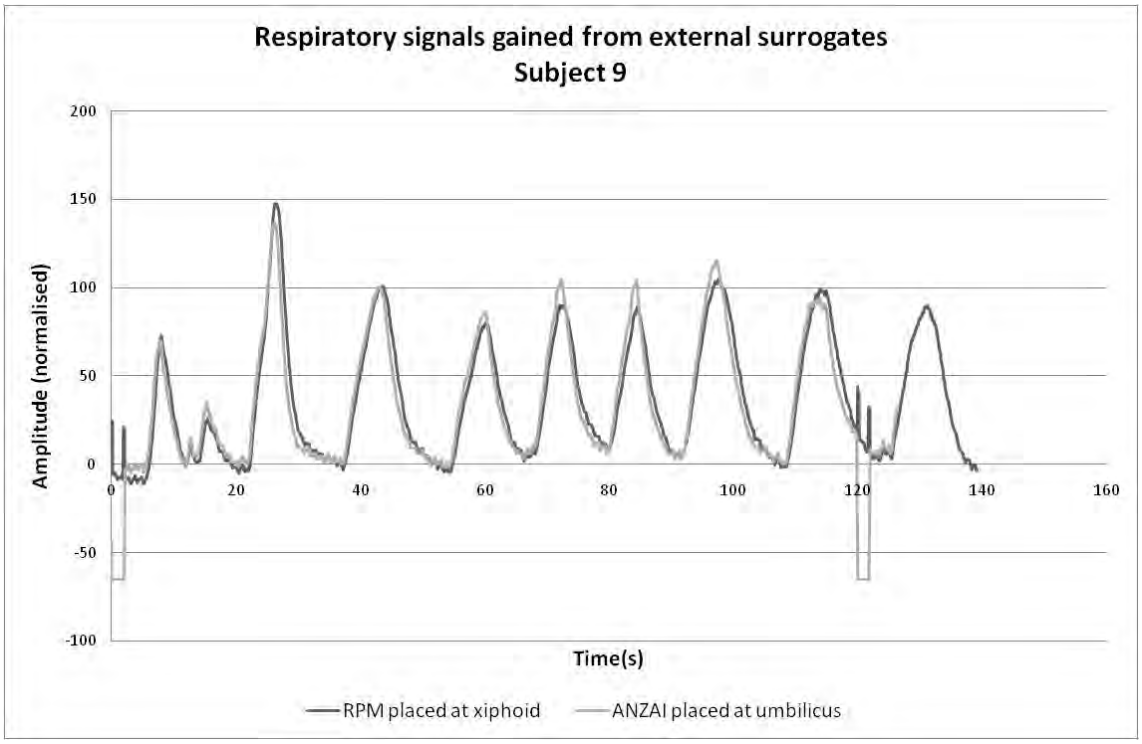


Figure A101: Respiratory signals gained using RPM marker positioned at the xiphoid and Anzai belt positioned at umbilicus for subject 9.

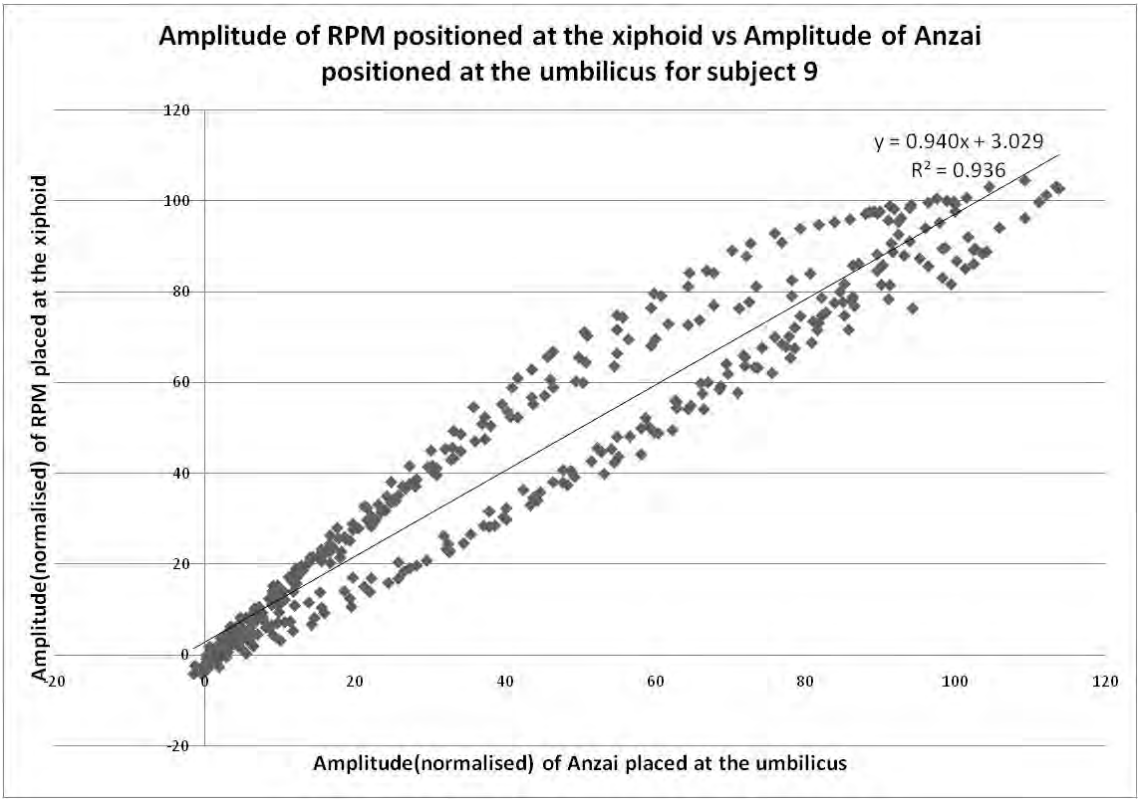


Figure A102: Determination of coefficient of determination for RPM positioned at the xiphoid and Anzai positioned at umbilicus, subject 9.

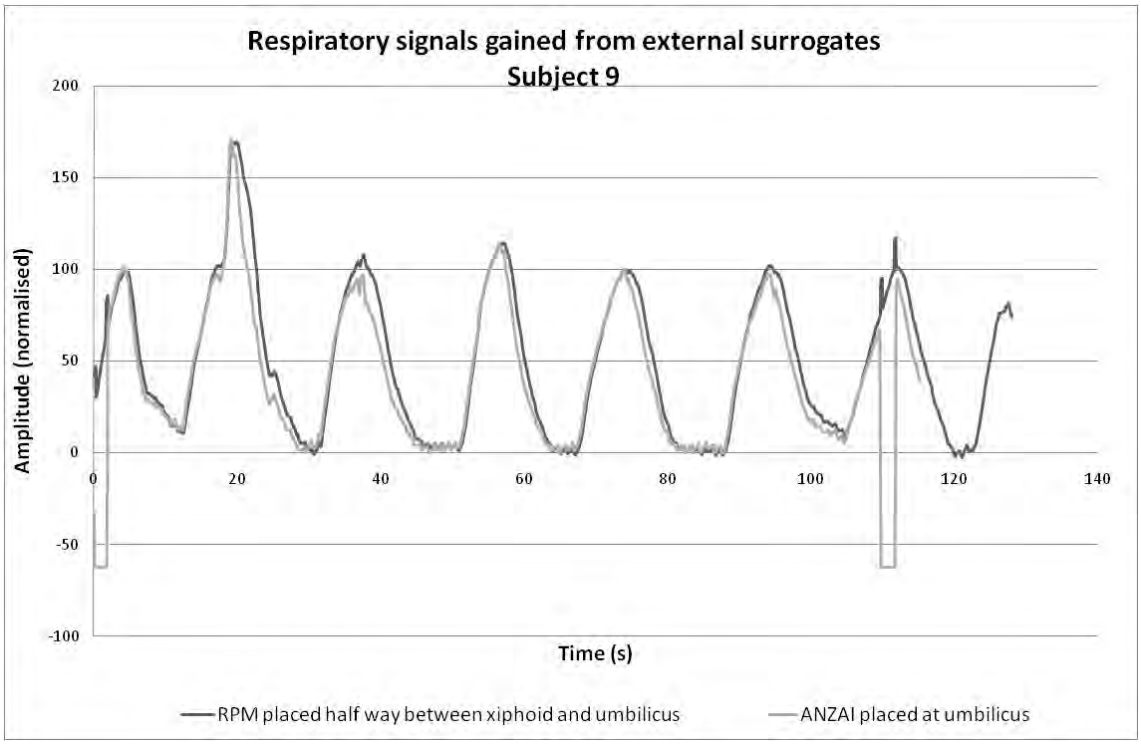


Figure A103: Respiratory signals gained using RPM marker positioned midway between xiphoid and umbilicus and Anzai belt positioned at umbilicus for subject 9.

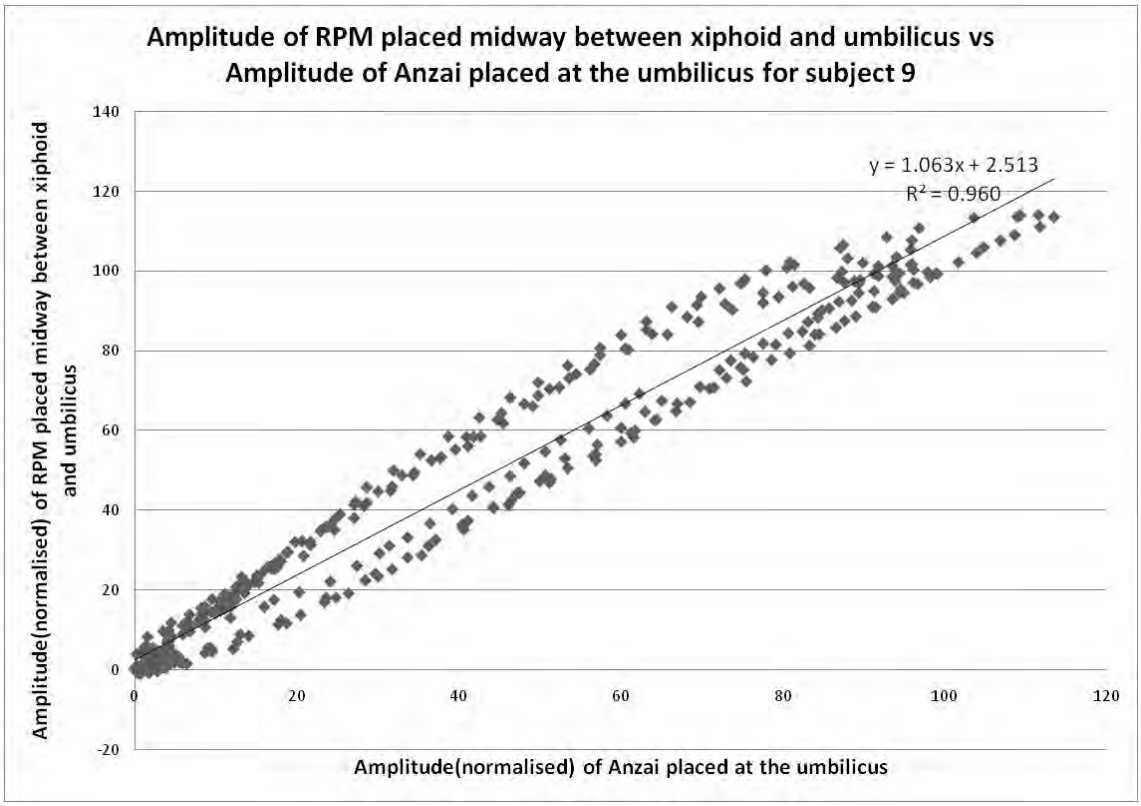


Figure A104: Determination of coefficient of determination for RPM positioned midway between xiphoid and umbilicus and Anzai positioned at umbilicus, subject 9.

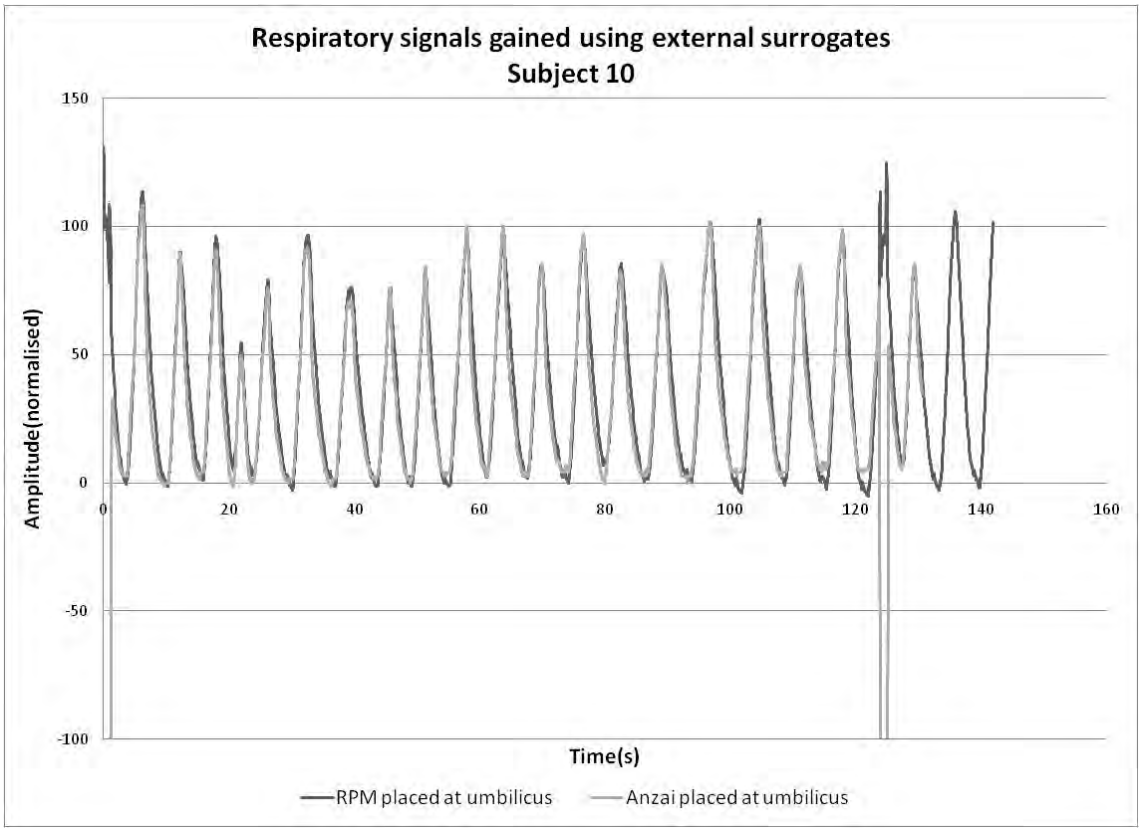


Figure A105: Respiratory signals gained using both RPM marker and Anzai belt positioned at umbilicus for subject 10.

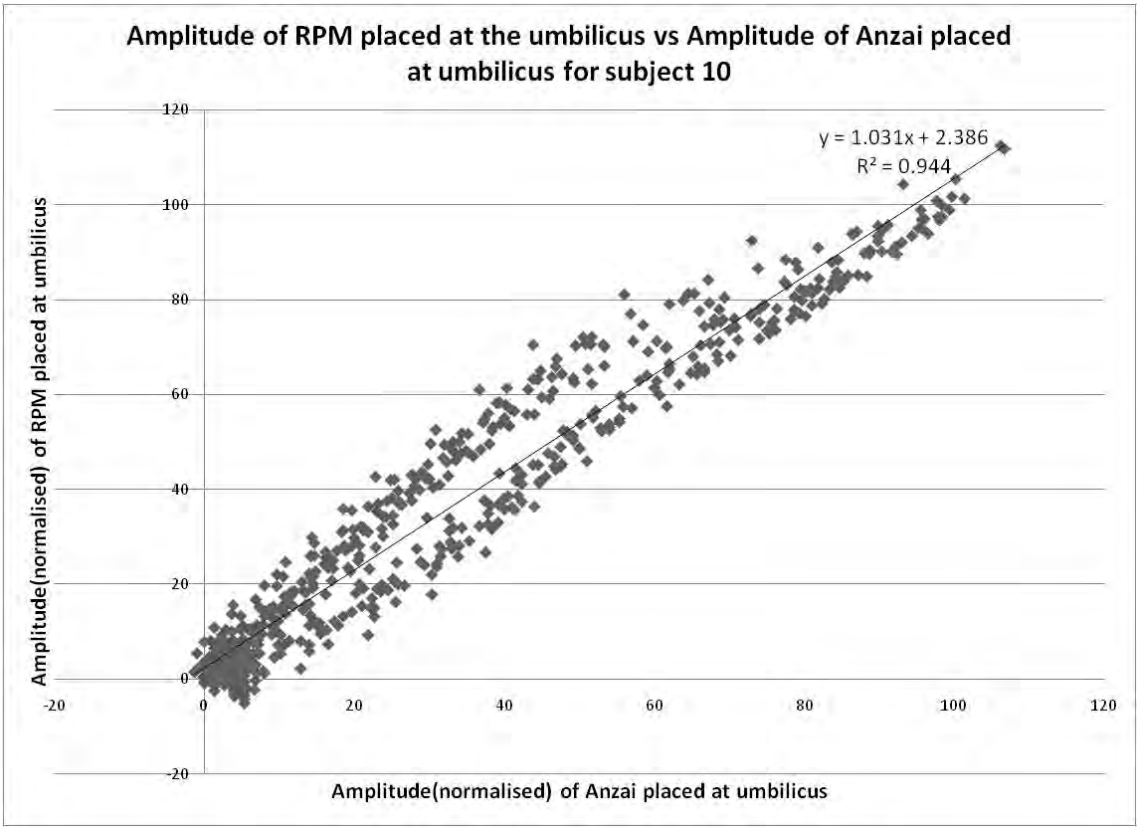


Figure A106: Determination of coefficient of determination for both RPM and Anzai positioned at umbilicus, subject 10.

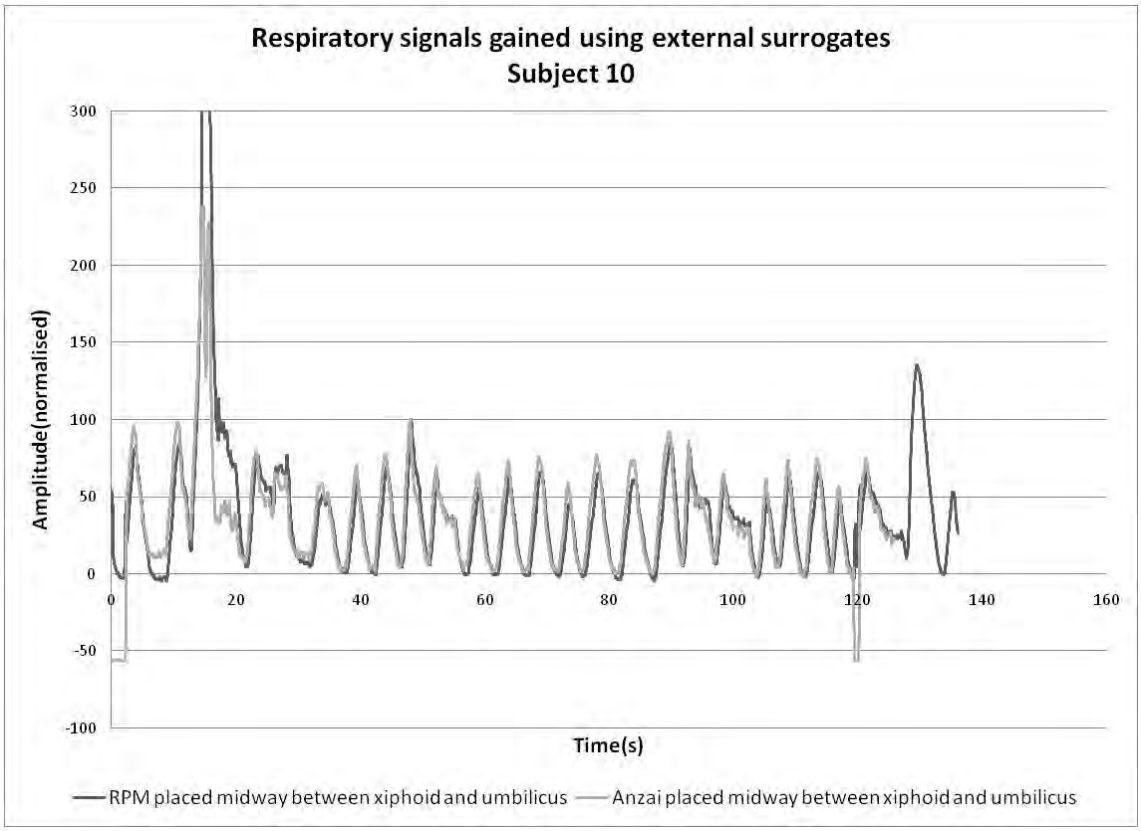


Figure A107: Respiratory signals gained using both RPM marker and Anzai belt positioned midway between umbilicus and xiphoid for subject 10.

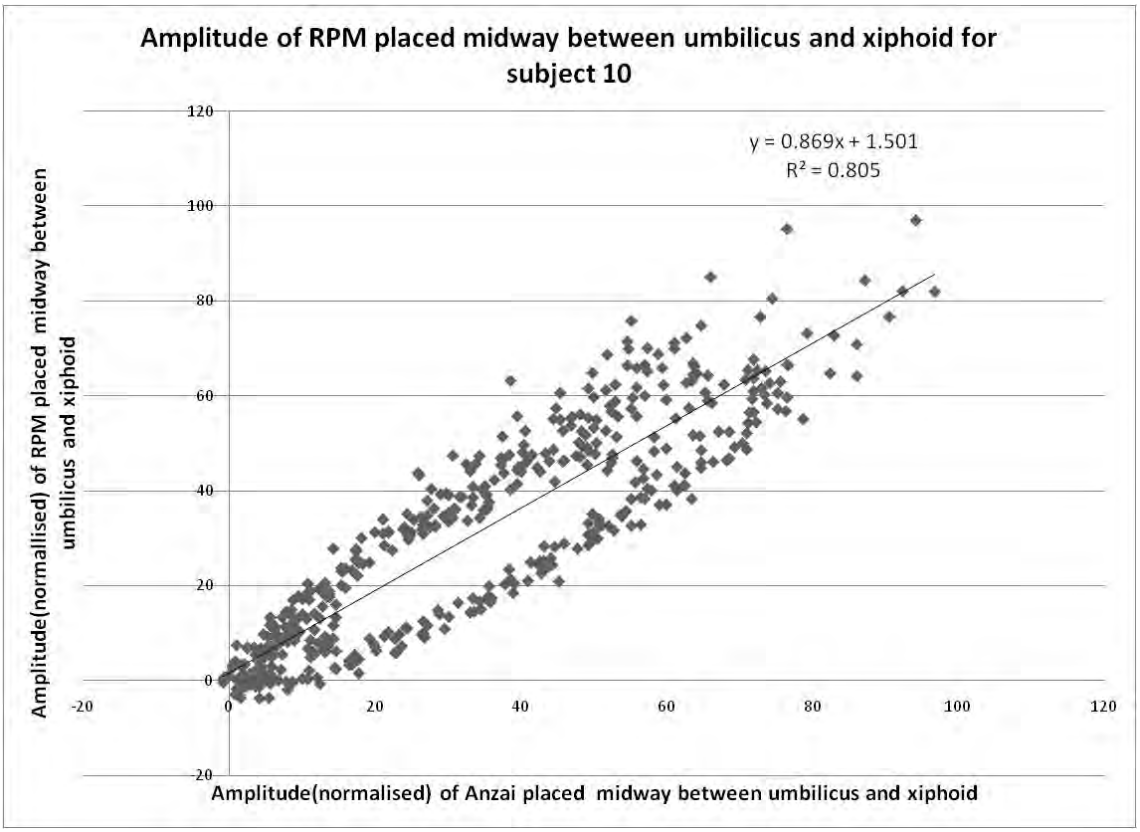


Figure A108: Determination of coefficient of determination for both RPM and Anzai positioned midway between xiphoid and umbilicus, subject 10.

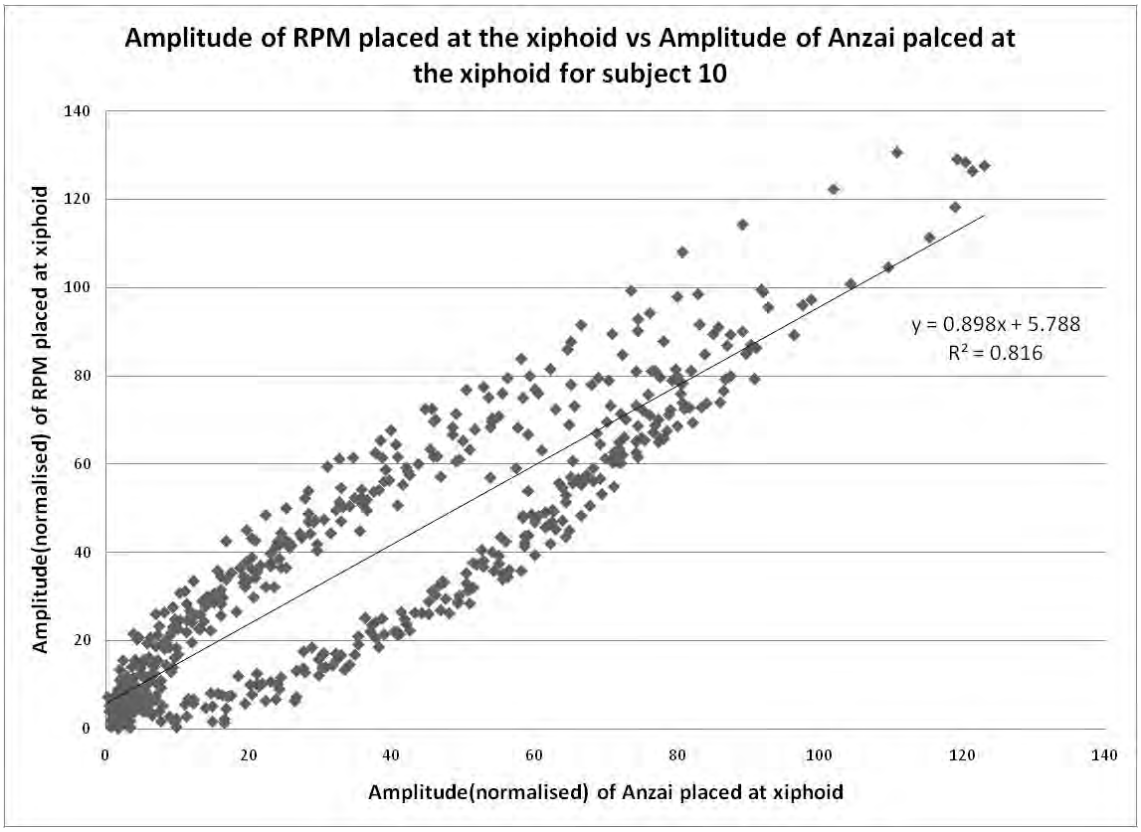


Figure A109: Respiratory signals gained using both RPM marker and Anzai belt positioned at xiphoid for subject 10.

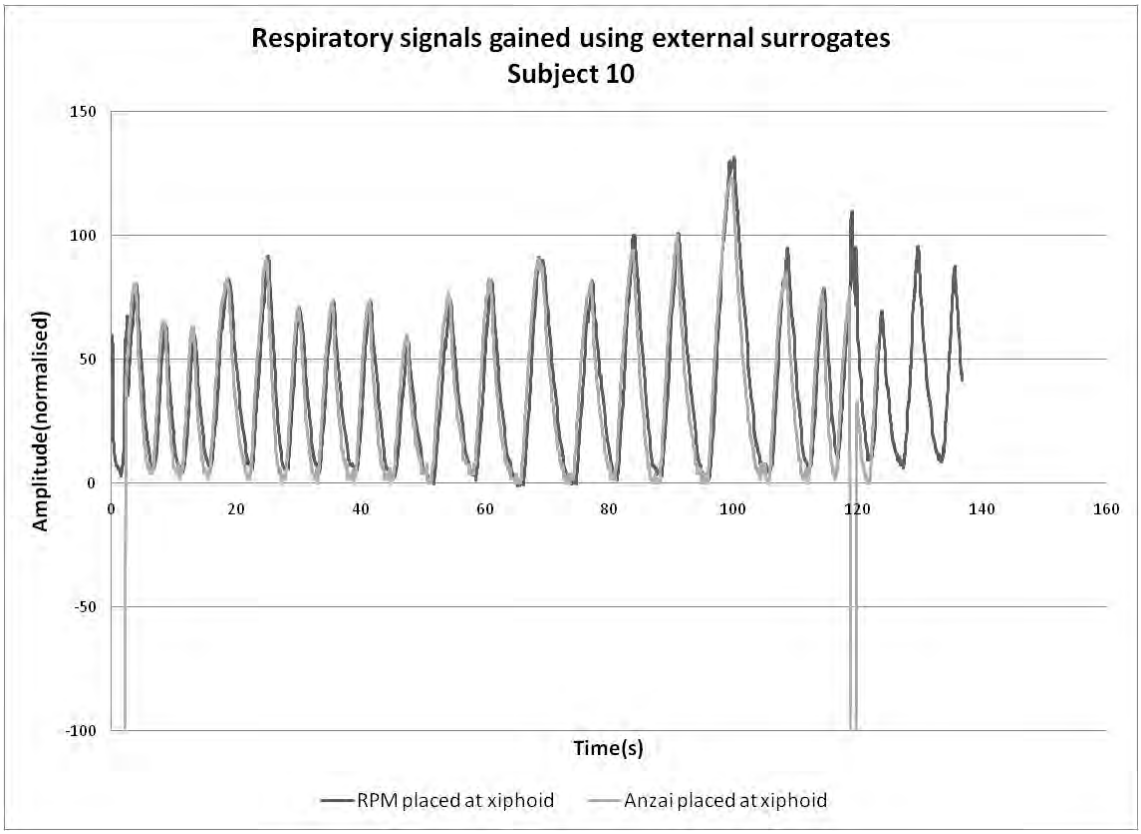


Figure A110: Determination of coefficient of determination for RPM positioned at the xiphoid and Anzai positioned at umbilicus, subject 10.

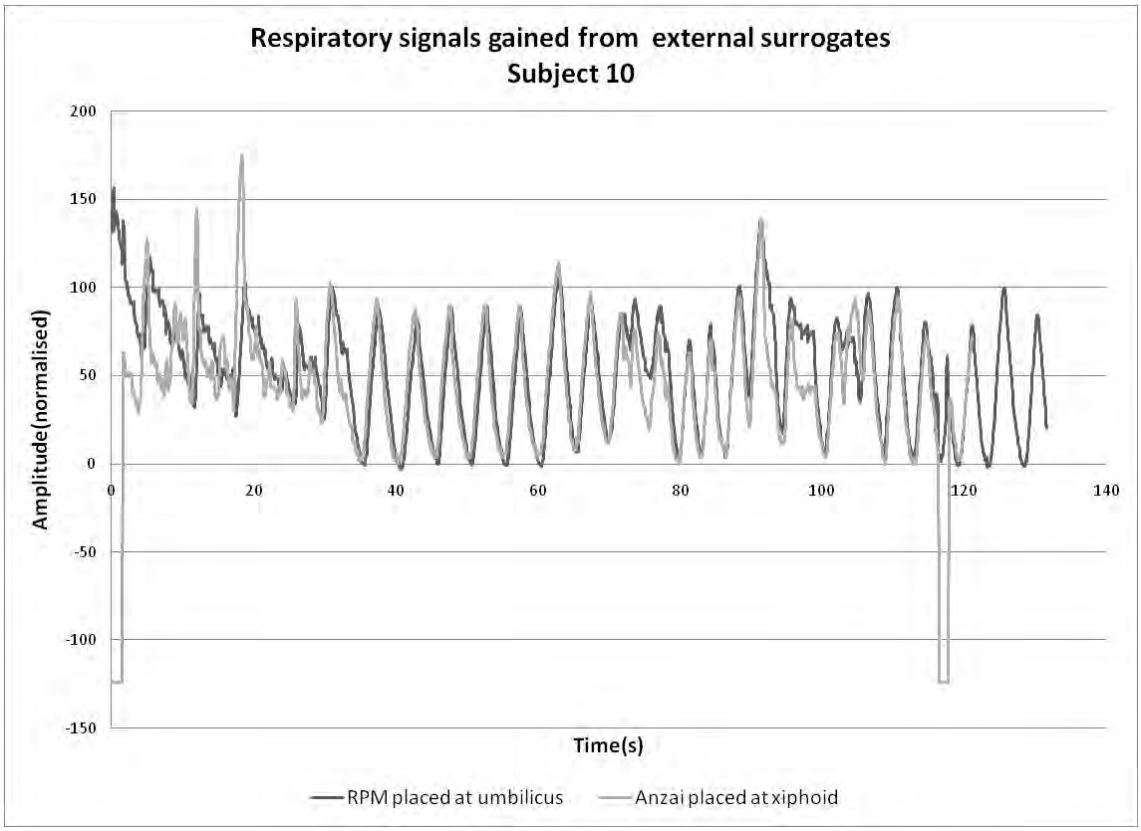


Figure A111: Respiratory signals gained using RPM marker positioned at the umbilicus and Anzai belt positioned at xiphoid for subject 10.

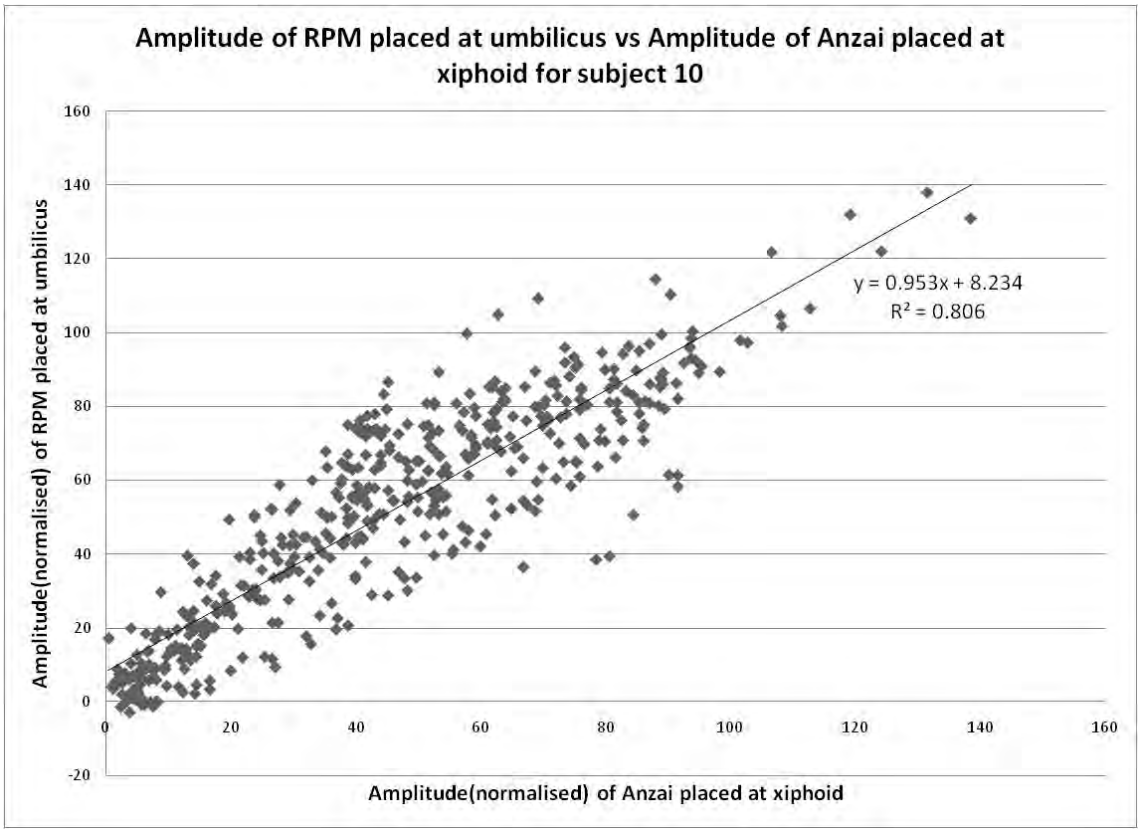


Figure A112: Determination of coefficient of determination for RPM positioned at the umbilicus and Anzai positioned at xiphoid, subject 10.

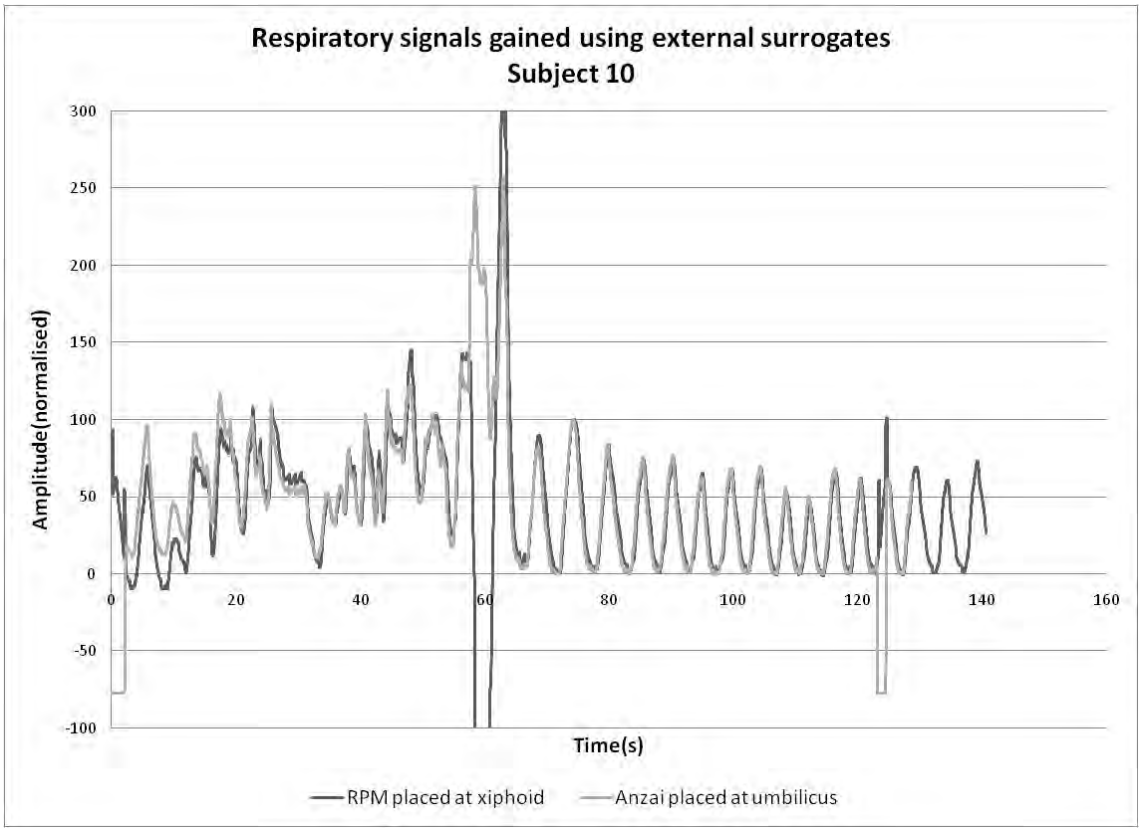


Figure A113: Respiratory signals gained using RPM marker positioned at the xiphoid and Anzai belt positioned at umbilicus for subject 10.

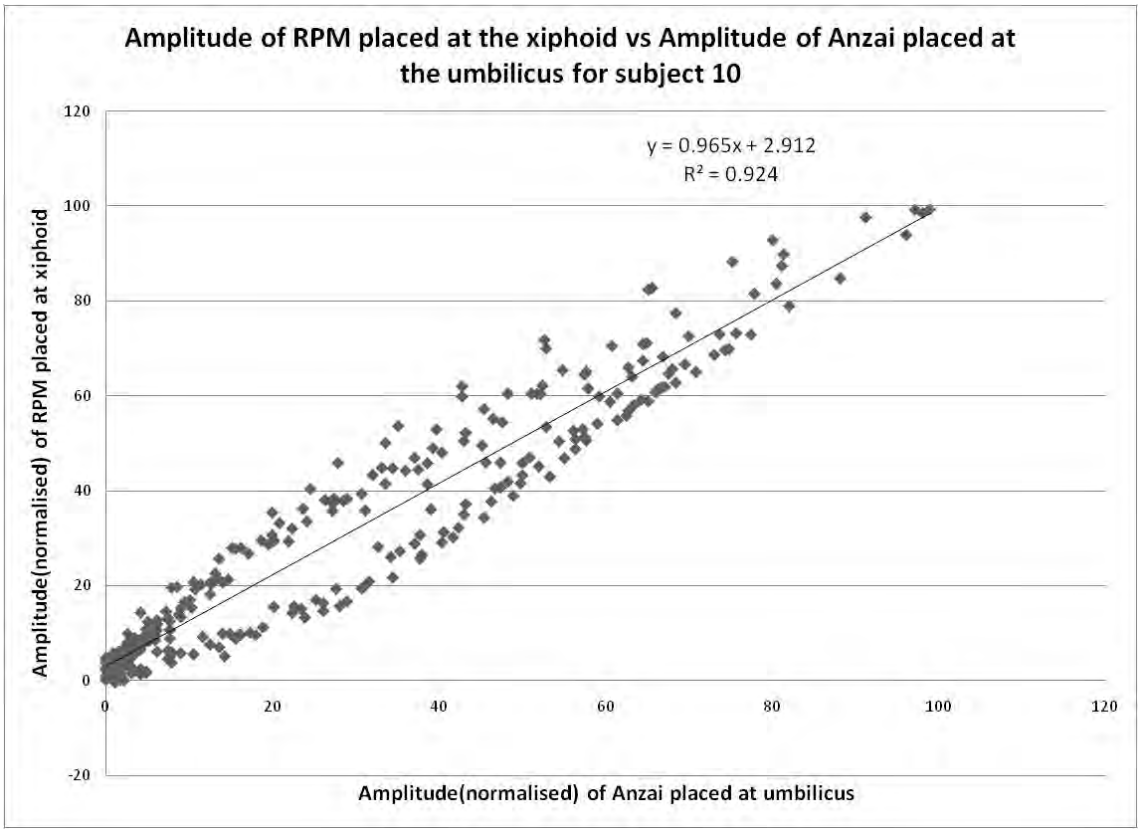


Figure A114: Determination of coefficient of determination for RPM positioned at the xiphoid and Anzai positioned at umbilicus, subject 10.

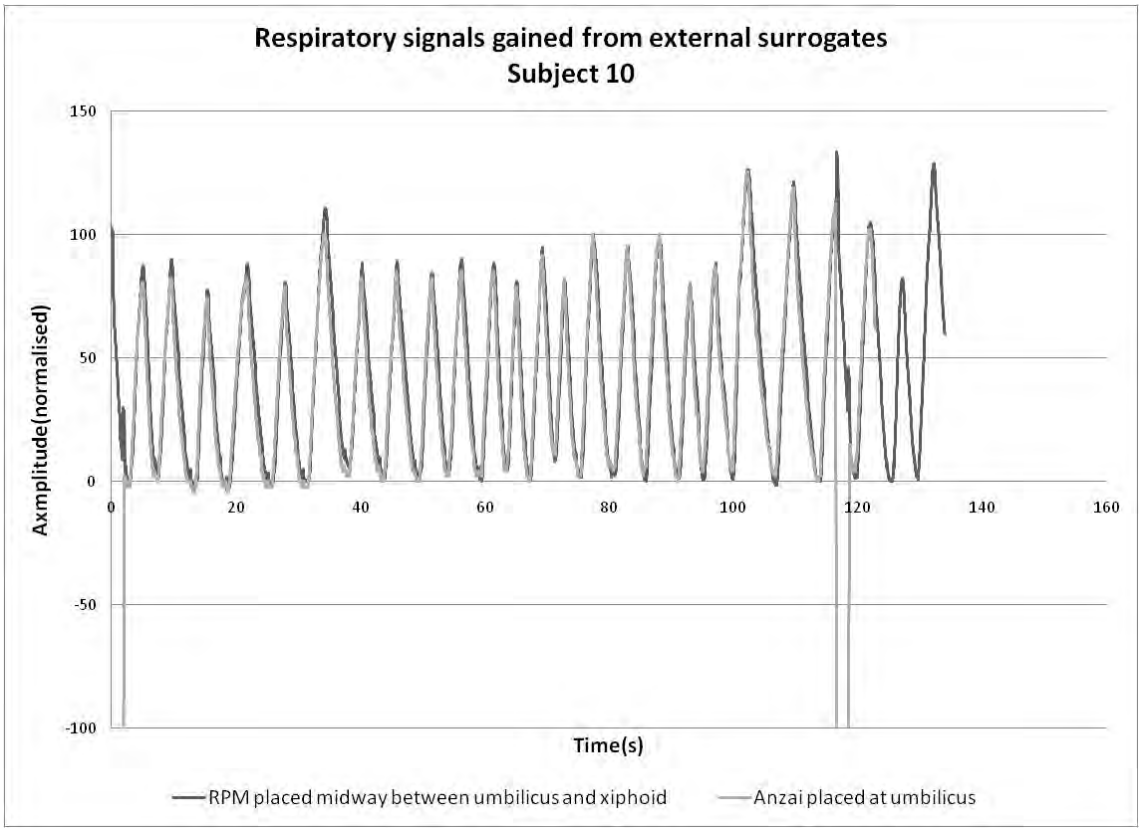


Figure A115: Respiratory signals gained using RPM marker positioned midway between xiphoid and umbilicus and Anzai belt positioned at umbilicus for subject 10.

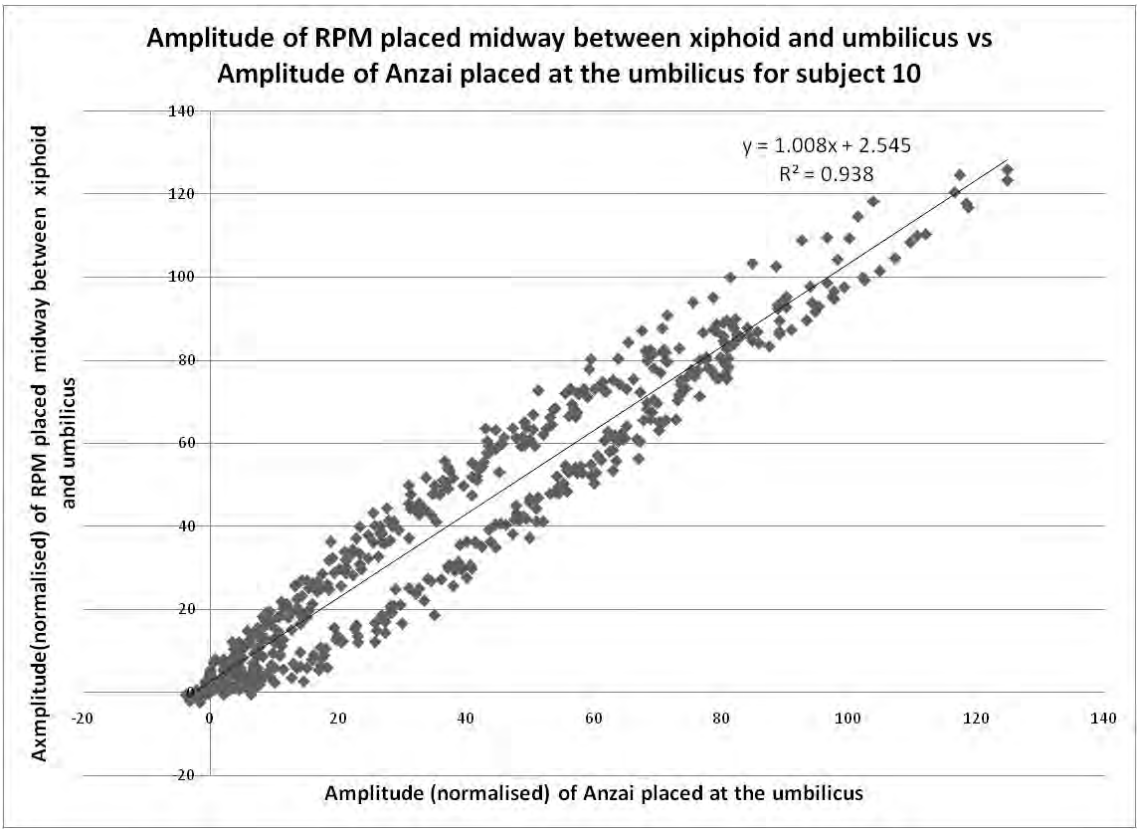


Figure A116: Determination of coefficient of determination for RPM positioned midway between xiphoid and umbilicus and Anzai positioned at umbilicus, subject 10.

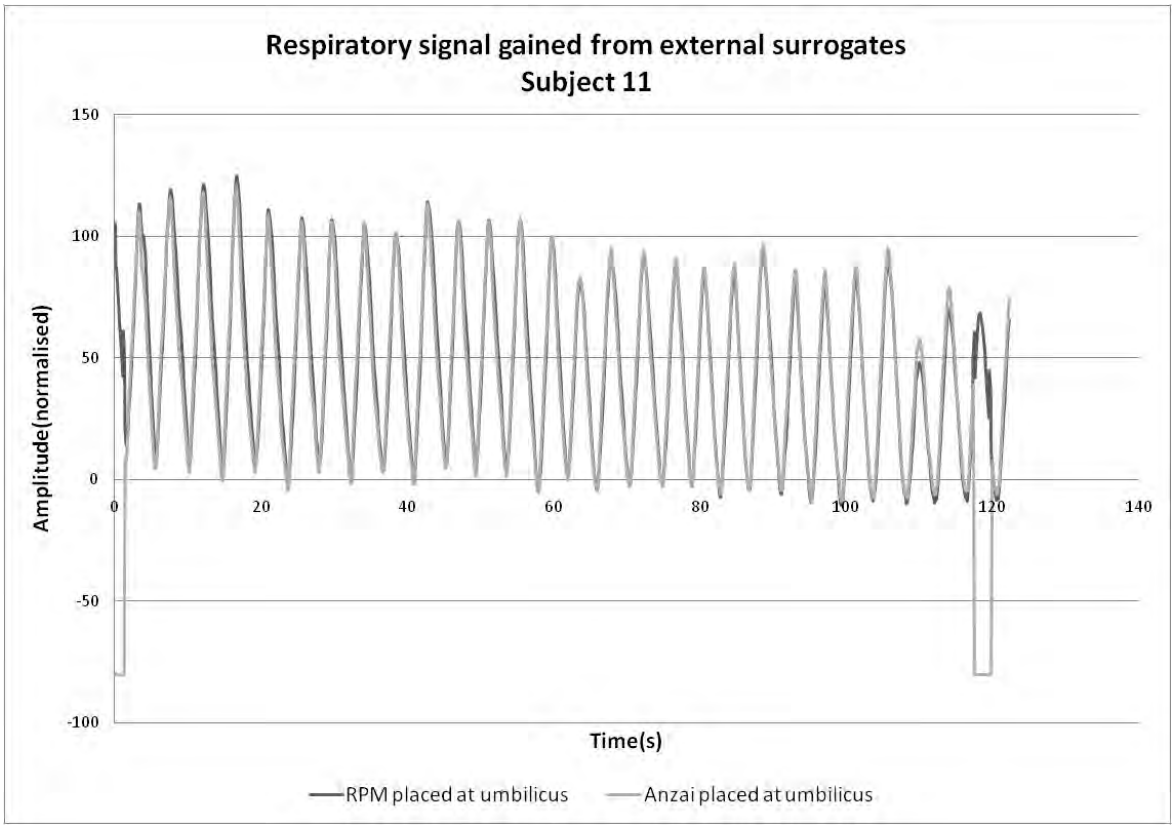


Figure A117: Respiratory signals gained using both RPM marker and Anzai belt positioned at umbilicus for subject 11.

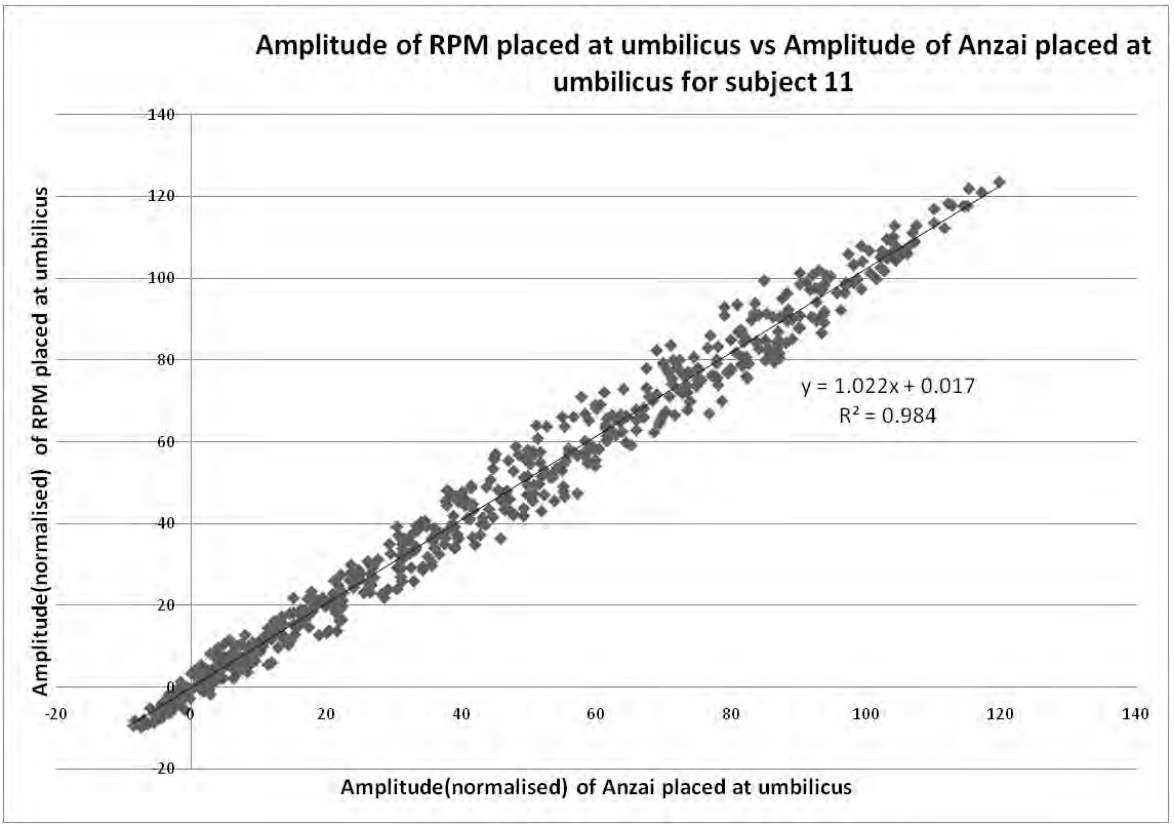


Figure A118: Determination of coefficient of determination for both RPM and Anzai positioned at umbilicus, subject 11.

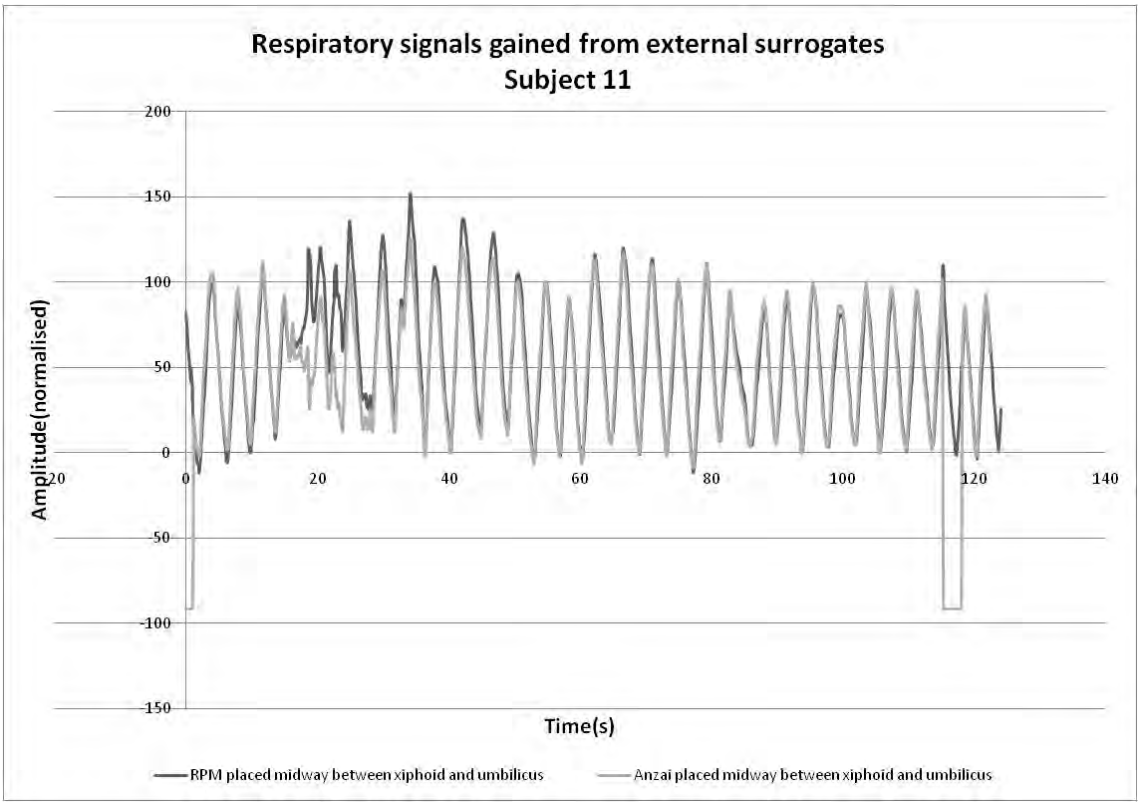


Figure A119: Respiratory signals gained using both RPM marker and Anzai belt positioned midway between umbilicus and xiphoid for subject 11.

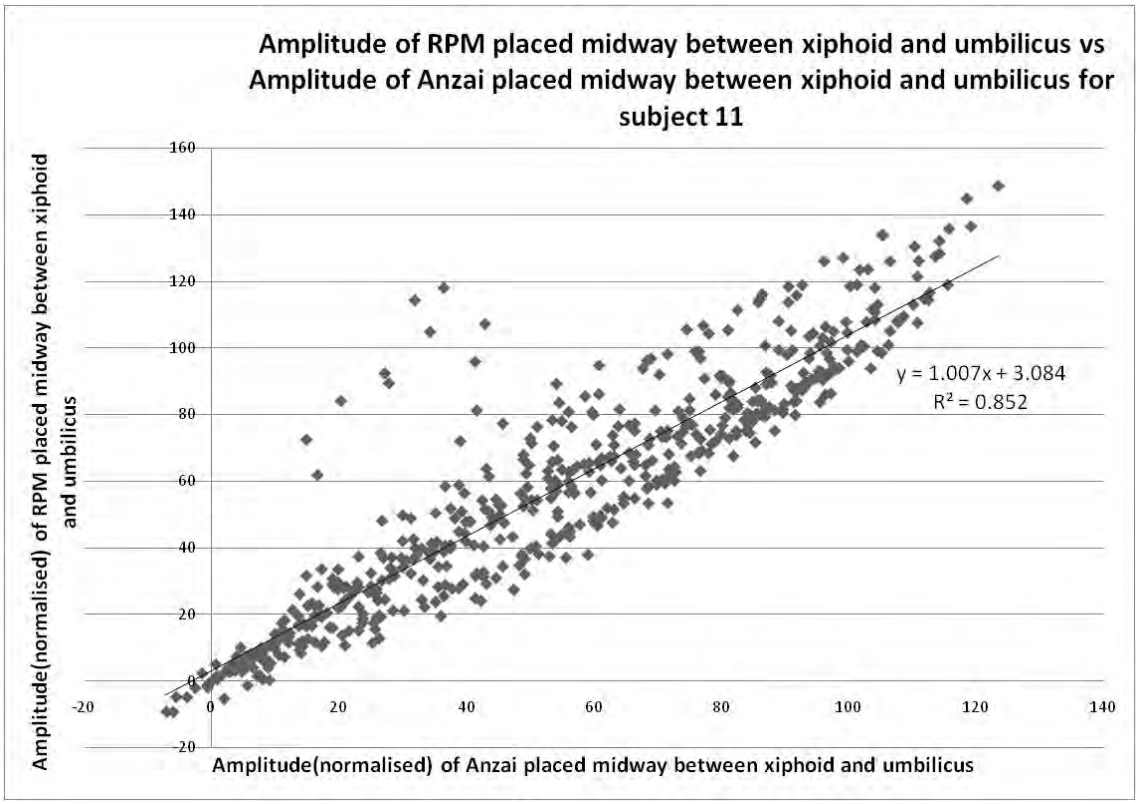


Figure A120: Determination of coefficient of determination for both RPM and Anzai positioned midway between xiphoid and umbilicus, subject 11.

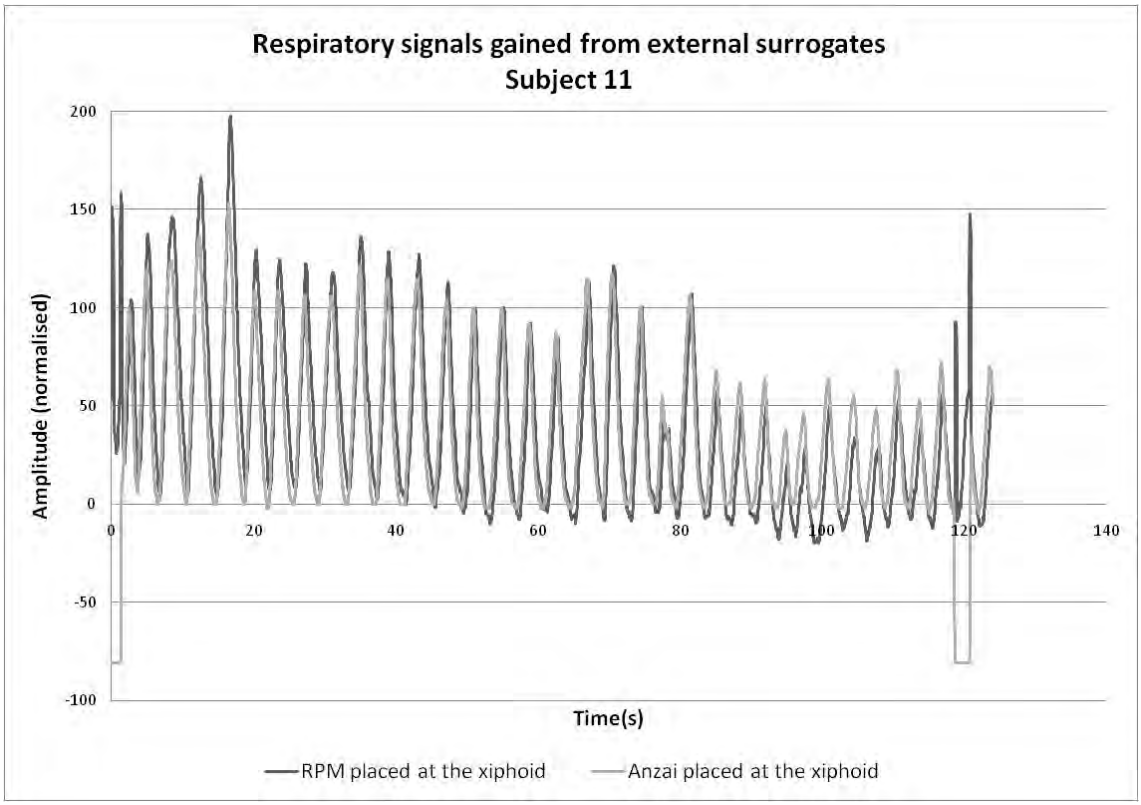


Figure A121: Respiratory signals gained using both RPM marker and Anzai belt positioned at xiphoid for subject 11.

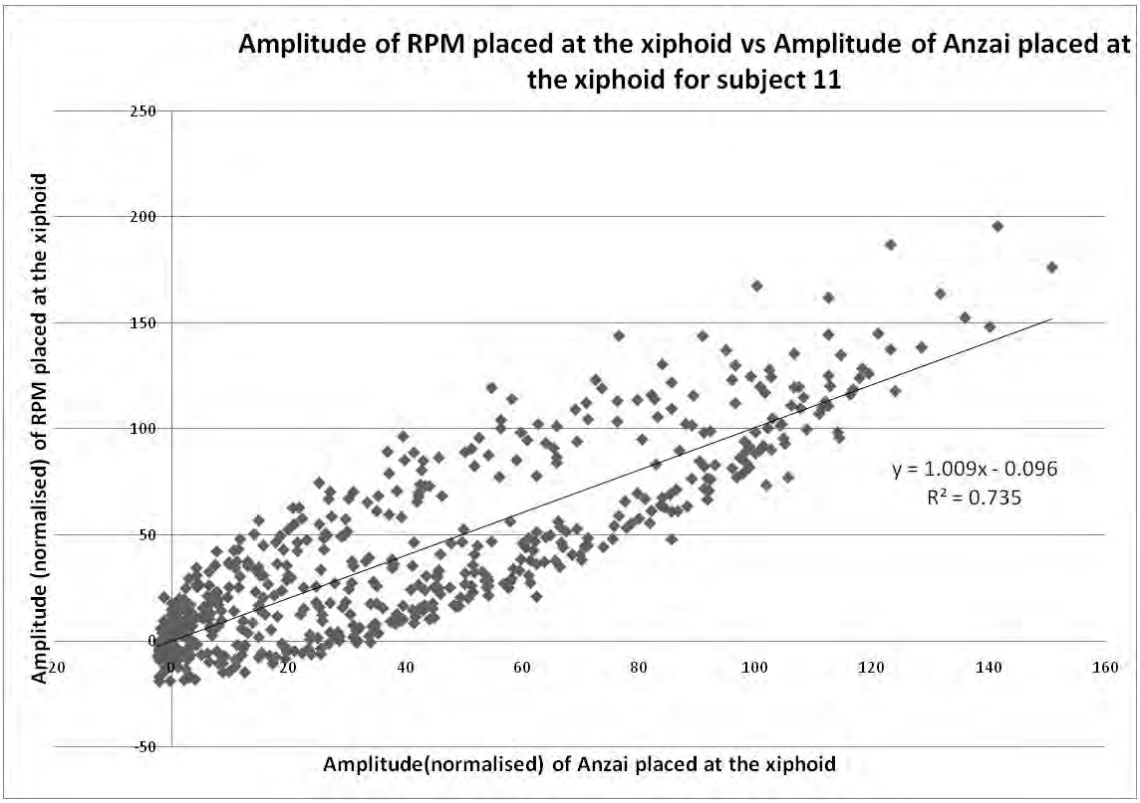


Figure A122: Determination of coefficient of determination for both RPM and Anzai positioned at xiphoid, subject 11.

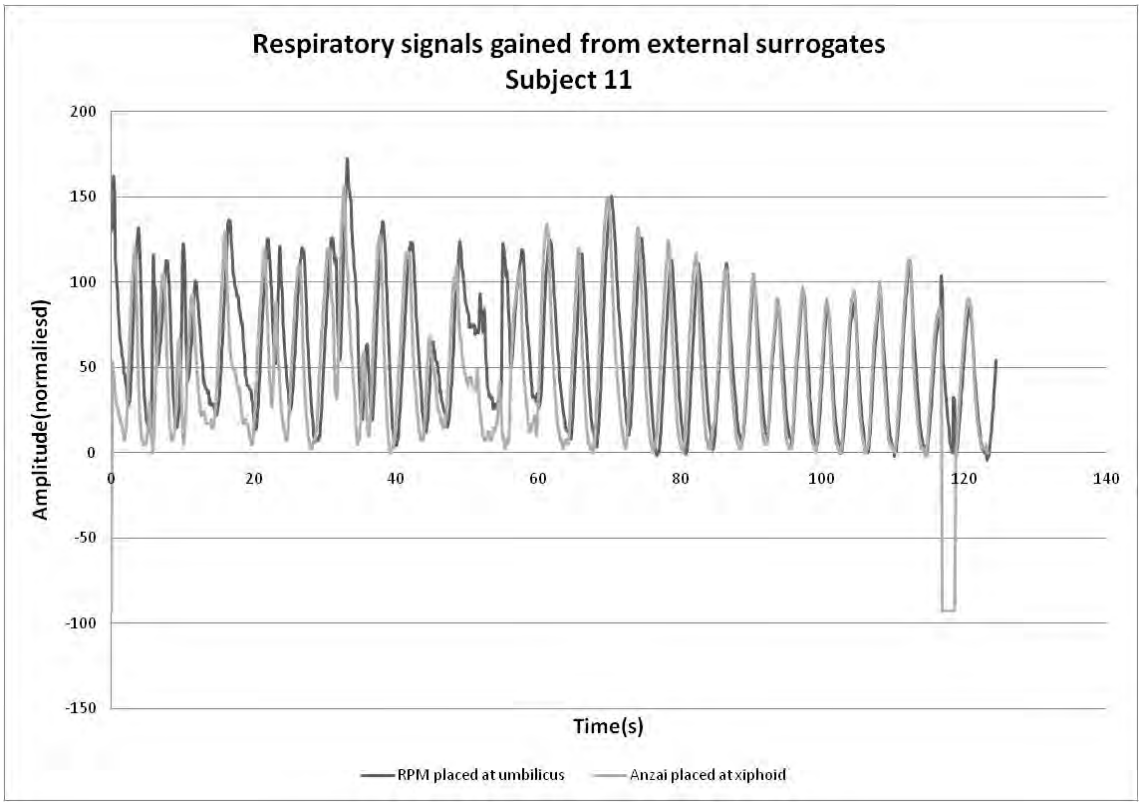


Figure A123: Respiratory signals gained using RPM marker positioned at the umbilicus and Anzai belt positioned at xiphoid for subject 11.

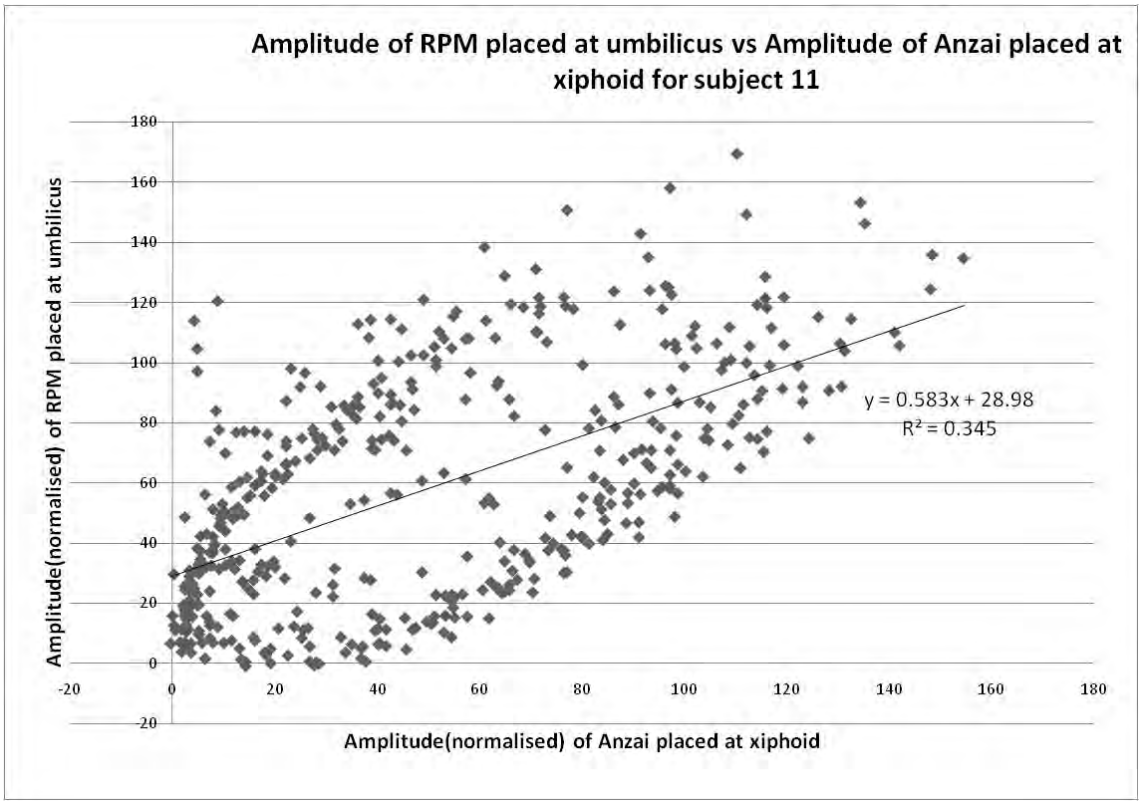


Figure A124: Determination of coefficient of determination for RPM positioned at the umbilicus and Anzai positioned at xiphoid, subject 11.

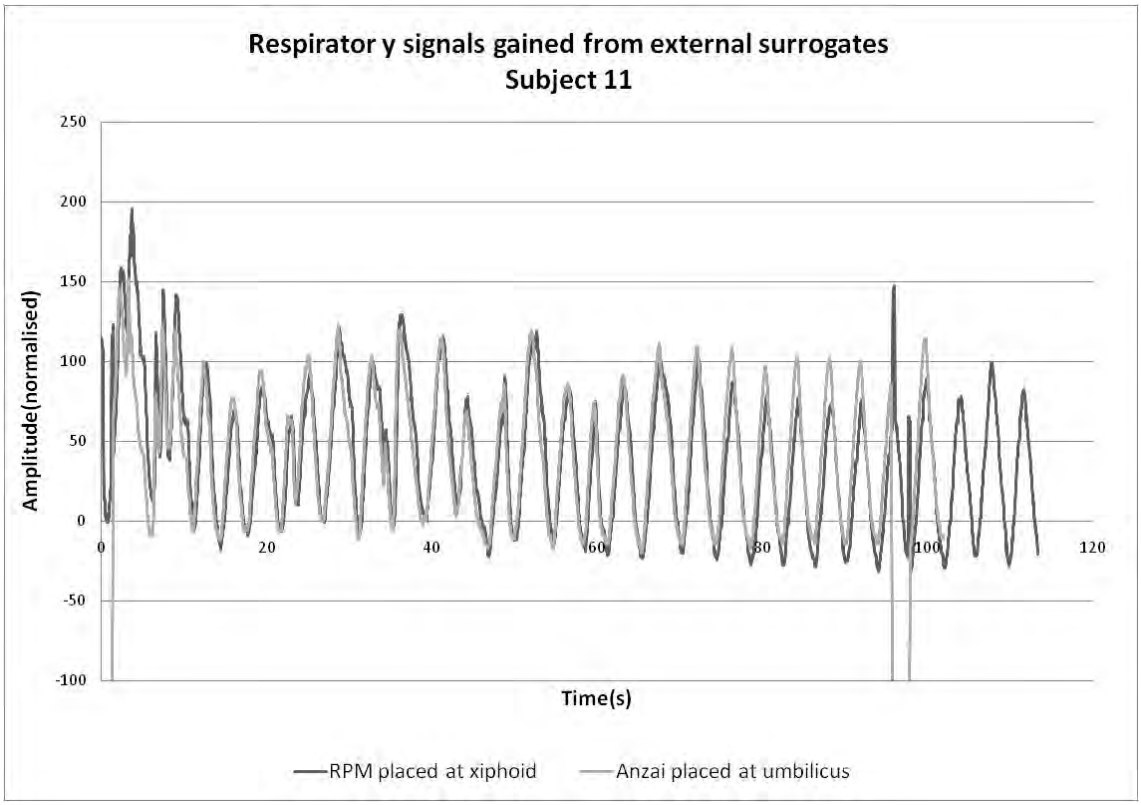


Figure A125: Respiratory signals gained using RPM marker positioned at the xiphoid and Anzai belt positioned at umbilicus for subject 11.

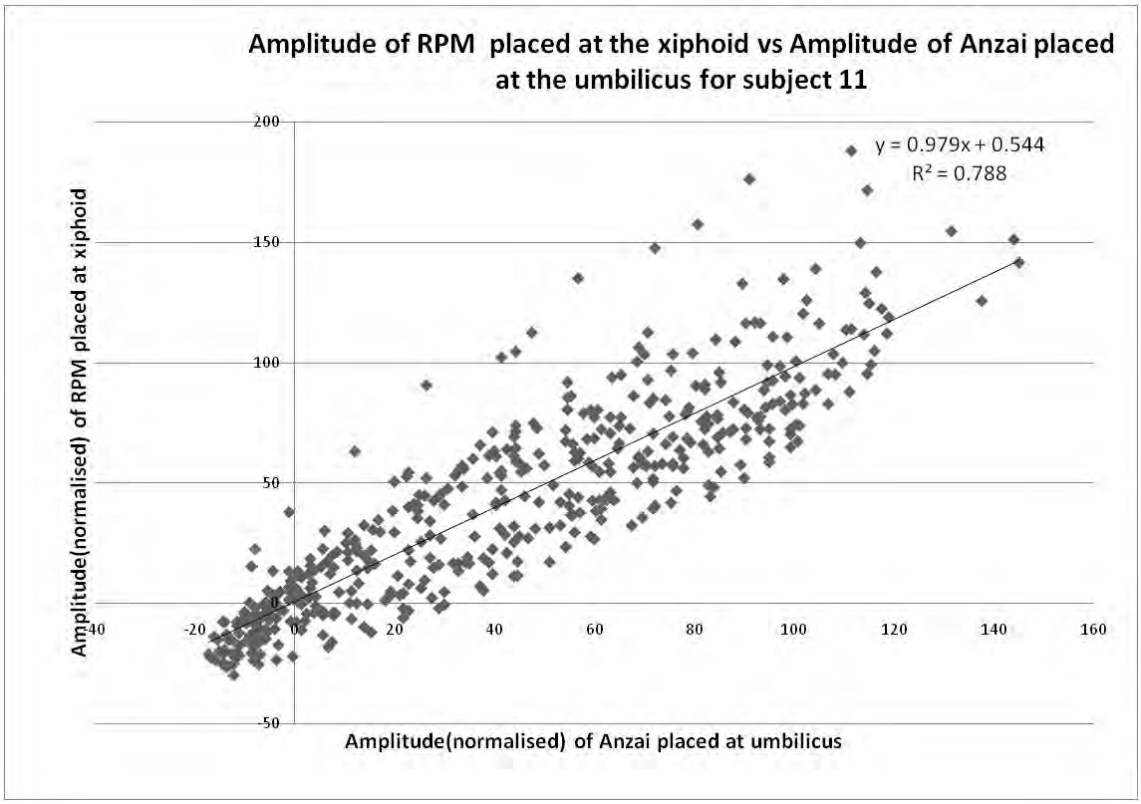


Figure A126: Determination of coefficient of determination for RPM positioned at the xiphoid and Anzai positioned at umbilicus, subject 11.

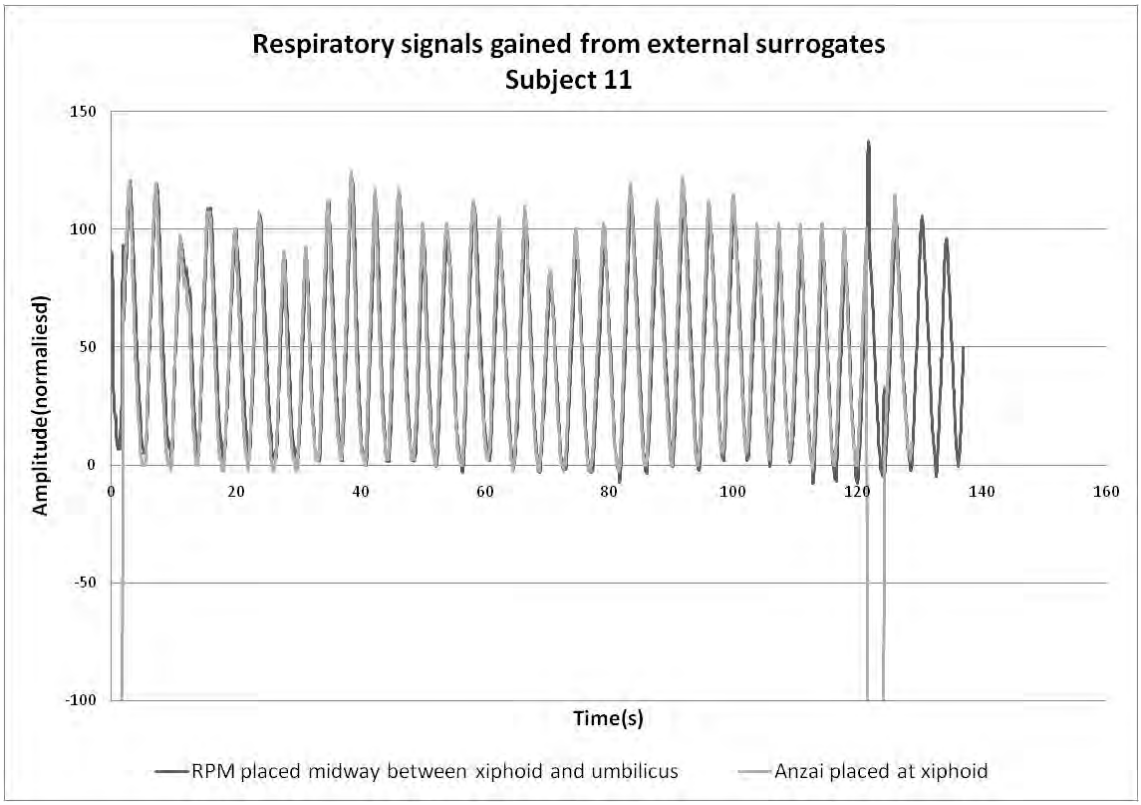


Figure A127: Respiratory signals gained using RPM marker positioned midway between xiphoid and umbilicus and Anzai belt positioned at umbilicus for subject 11.

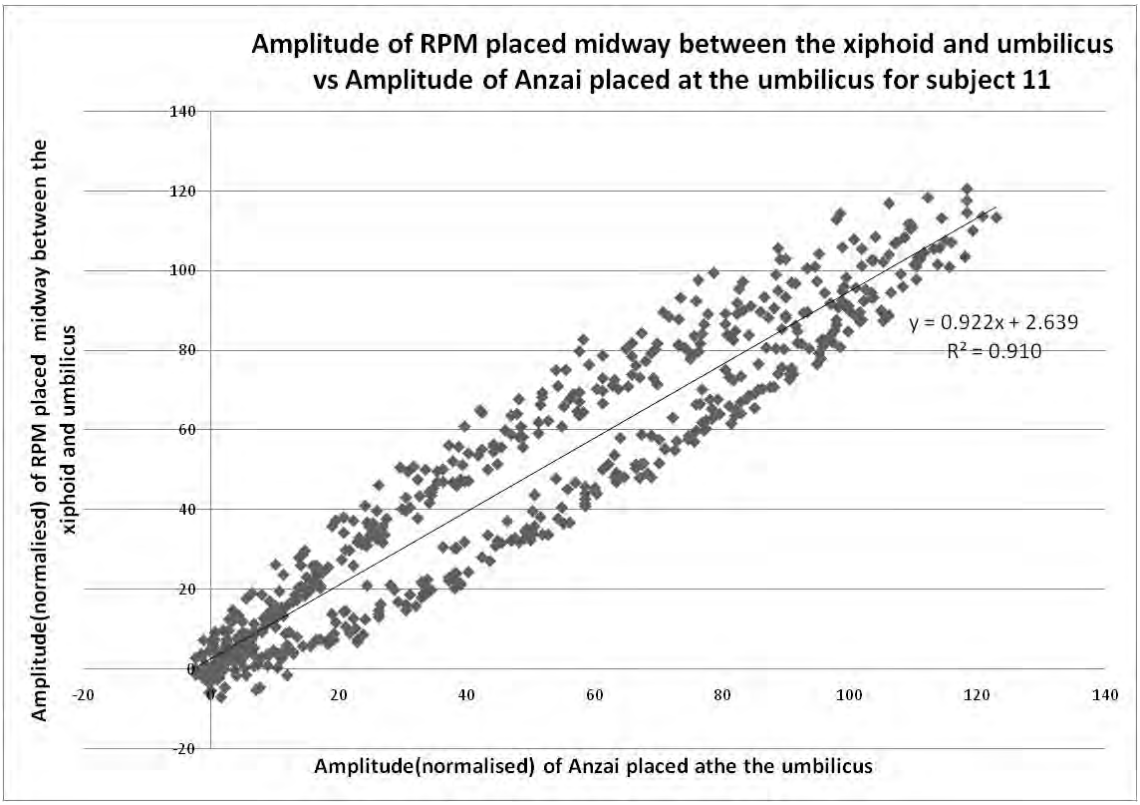


Figure A128: Determination of coefficient of determination for RPM positioned midway between xiphoid and umbilicus and Anzai positioned at umbilicus, subject 11.

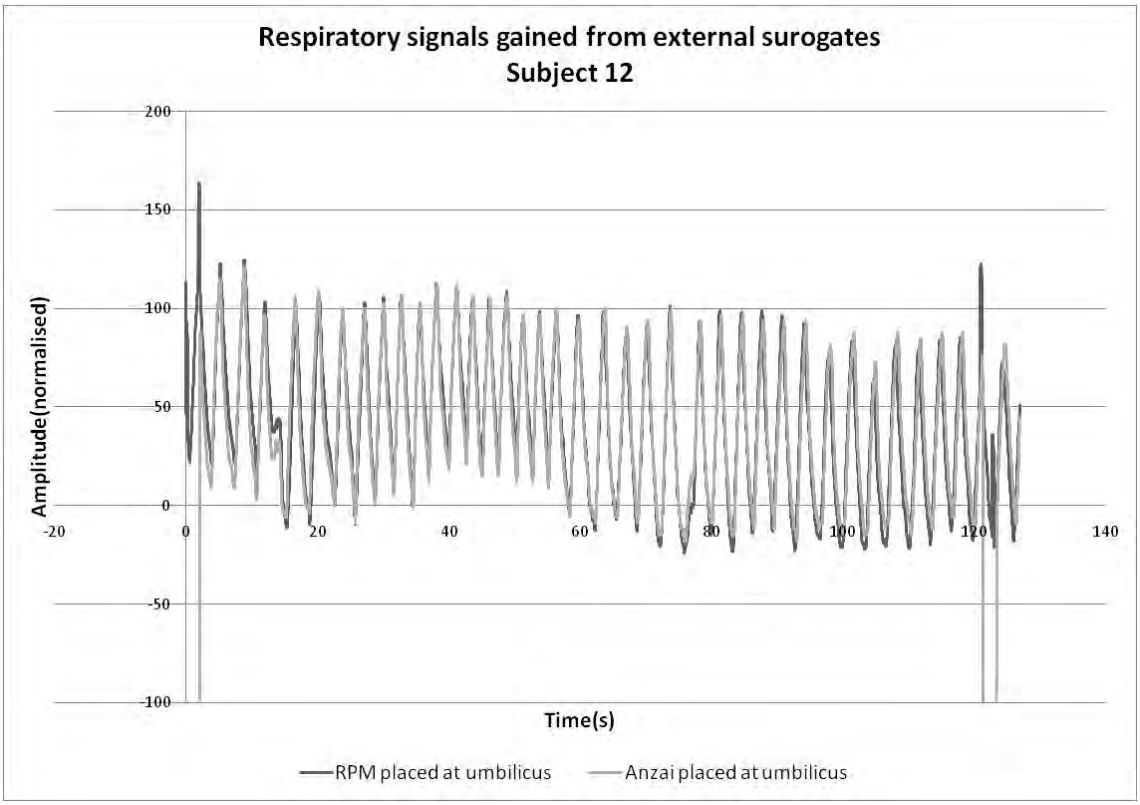


Figure A129: Respiratory signals gained using both RPM marker and Anzai belt positioned at umbilicus for subject 12.

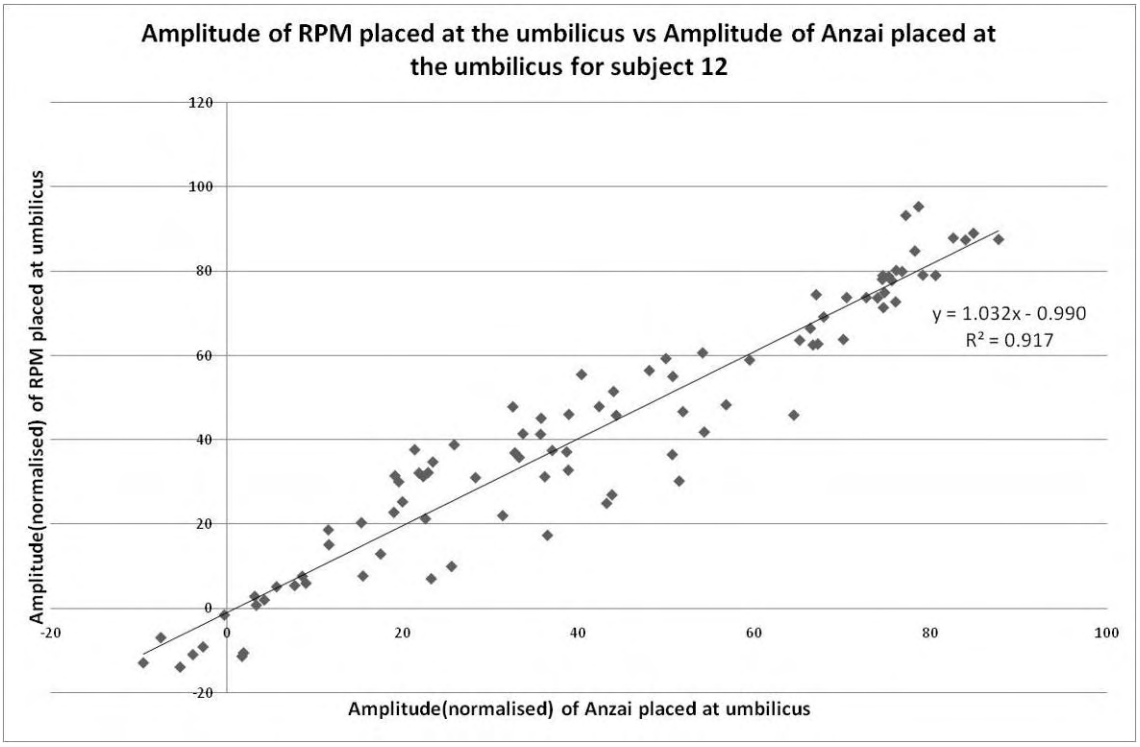


Figure A130: Determination of coefficient of determination for both RPM and Anzai positioned at umbilicus, subject 12.

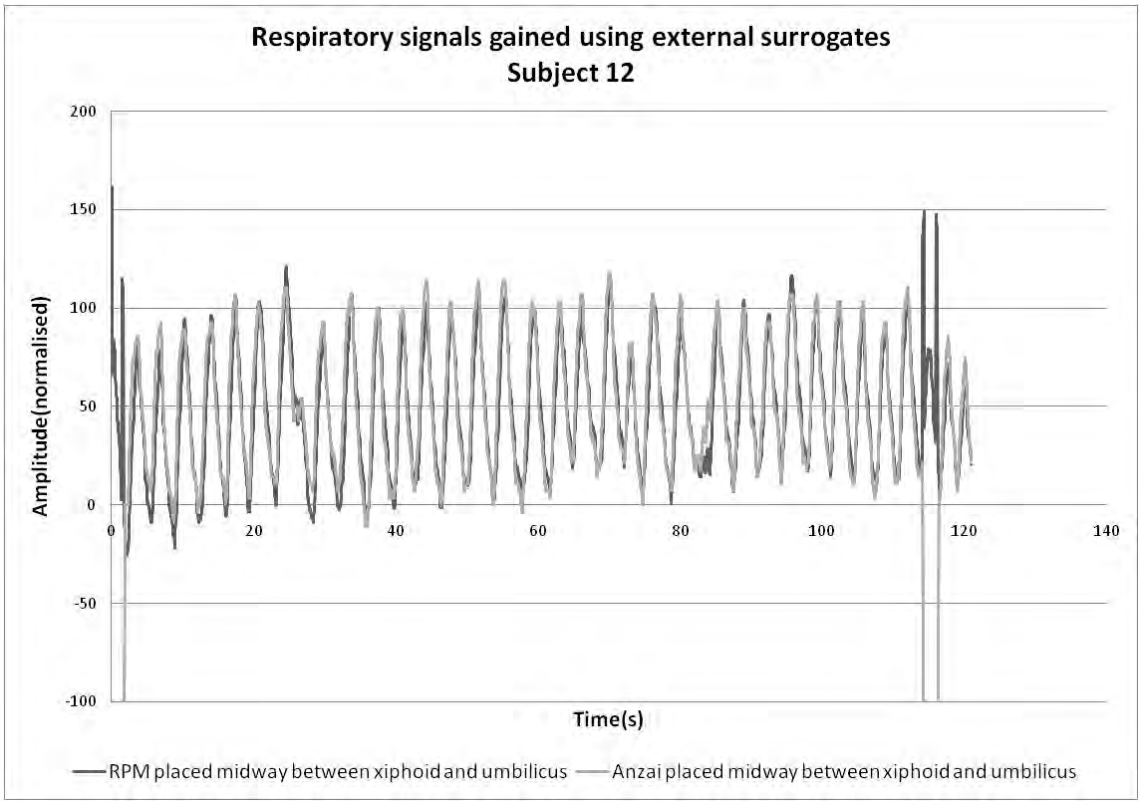


Figure A131: Respiratory signals gained using both RPM marker and Anzai belt positioned midway between umbilicus and xiphoid for subject 12.

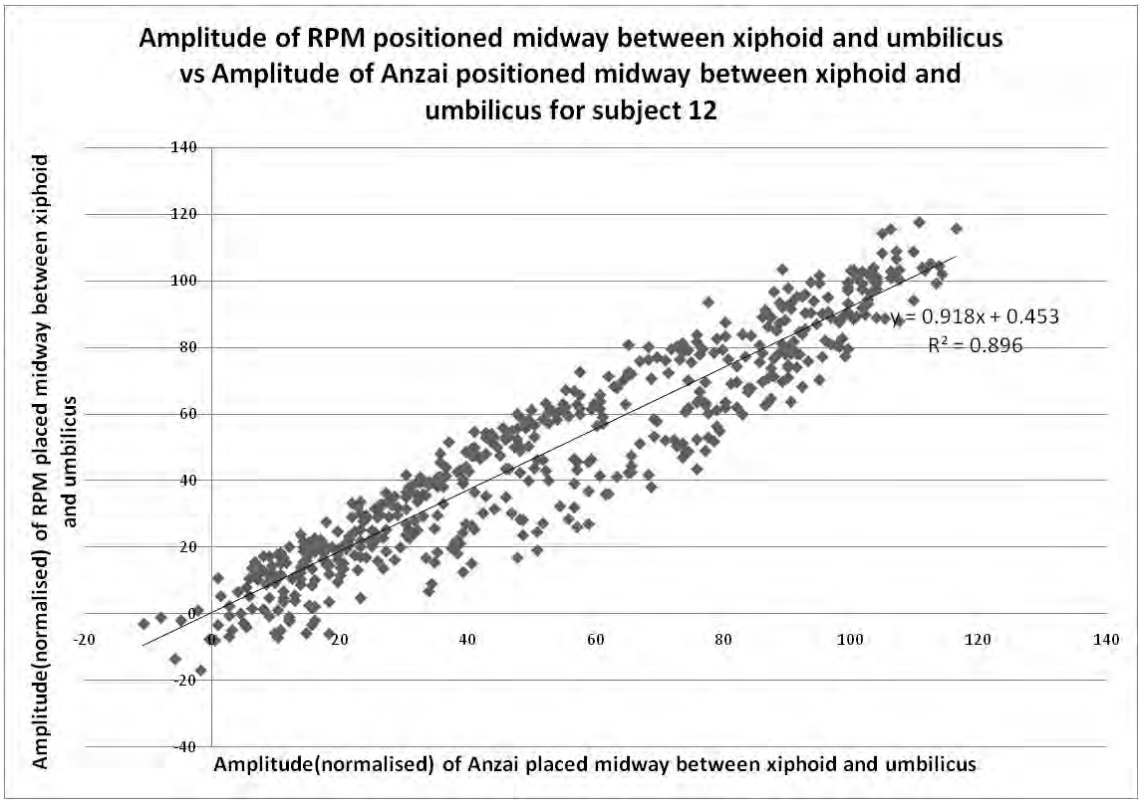


Figure A132: Determination of coefficient of determination for both RPM and Anzai positioned midway between xiphoid and umbilicus, subject 12.

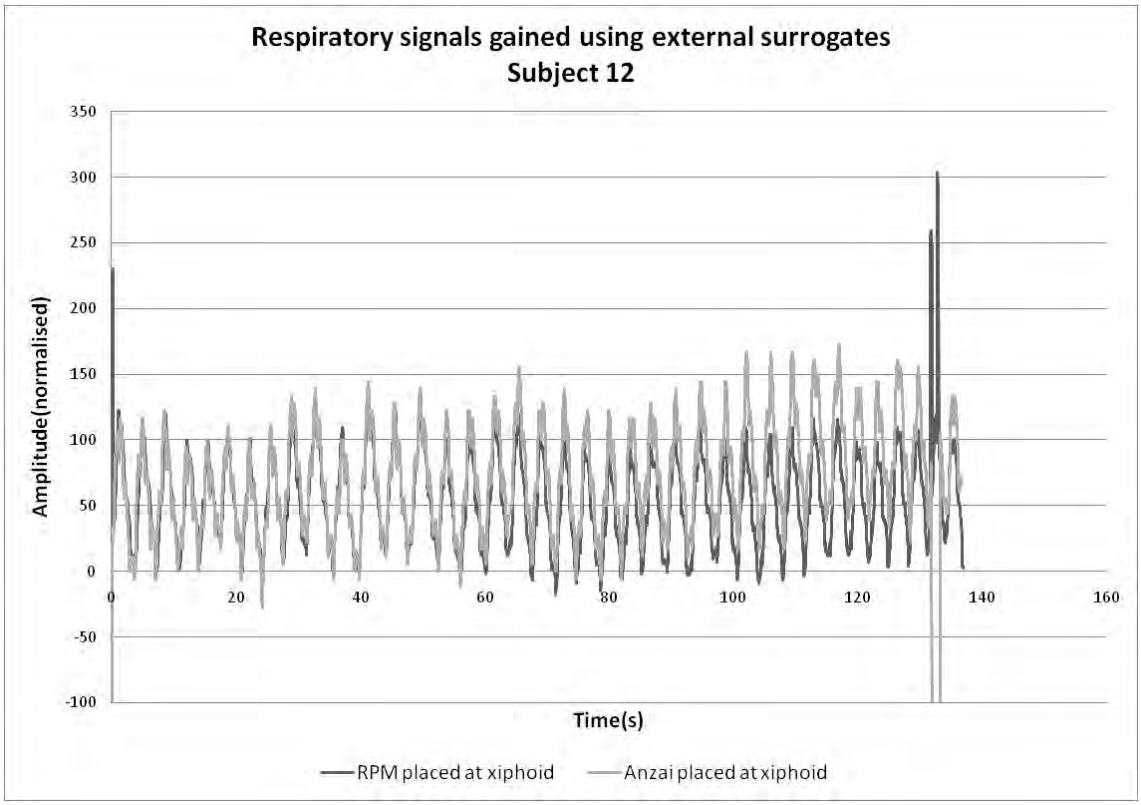


Figure A133: Respiratory signals gained using RPM marker positioned at the umbilicus and Anzai belt positioned at xiphoid for subject 12.

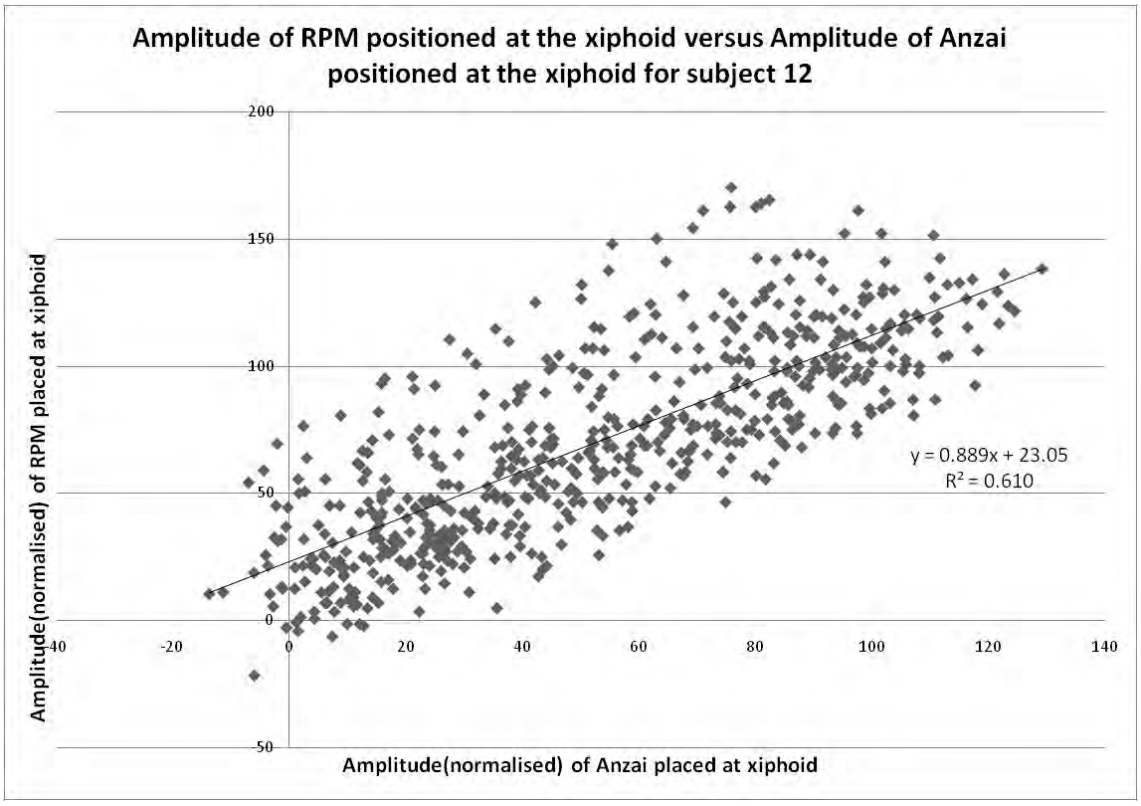


Figure A134: Determination of coefficient of determination for both RPM and Anzai positioned at xiphoid, subject 12.

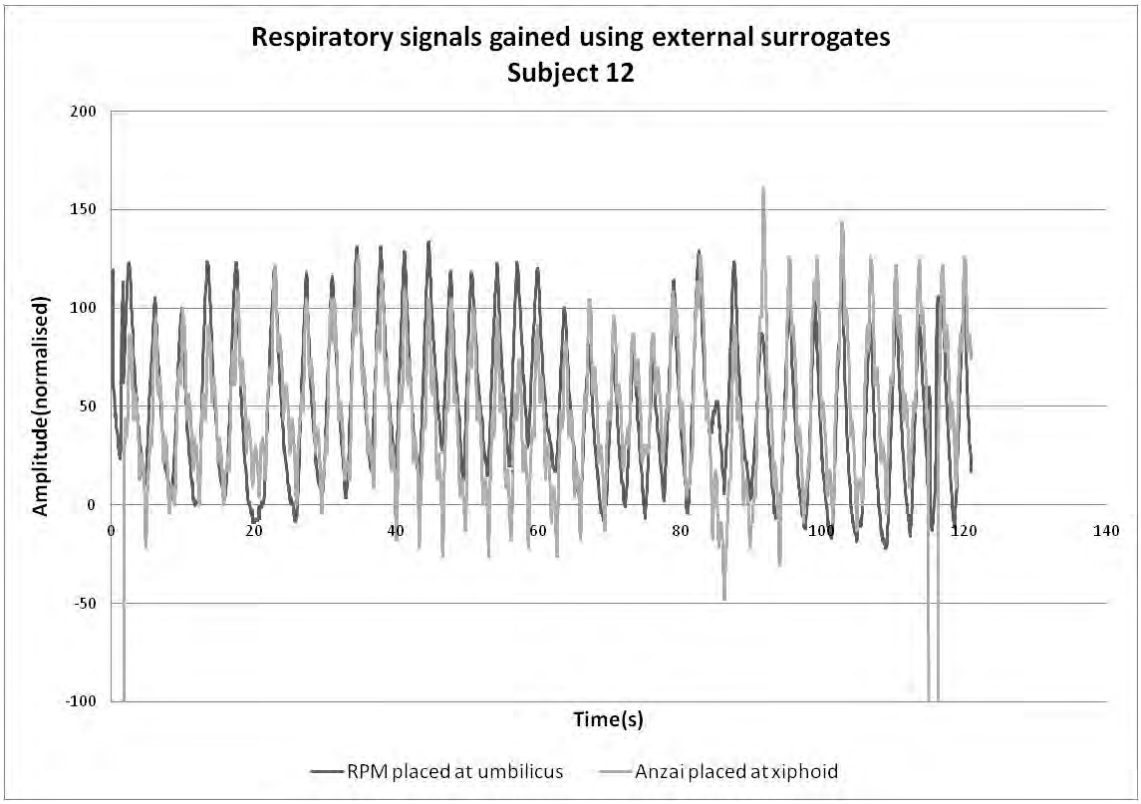


Figure A135: Respiratory signals gained using RPM marker positioned at the umbilicus and Anzai belt positioned at xiphoid for subject 12.

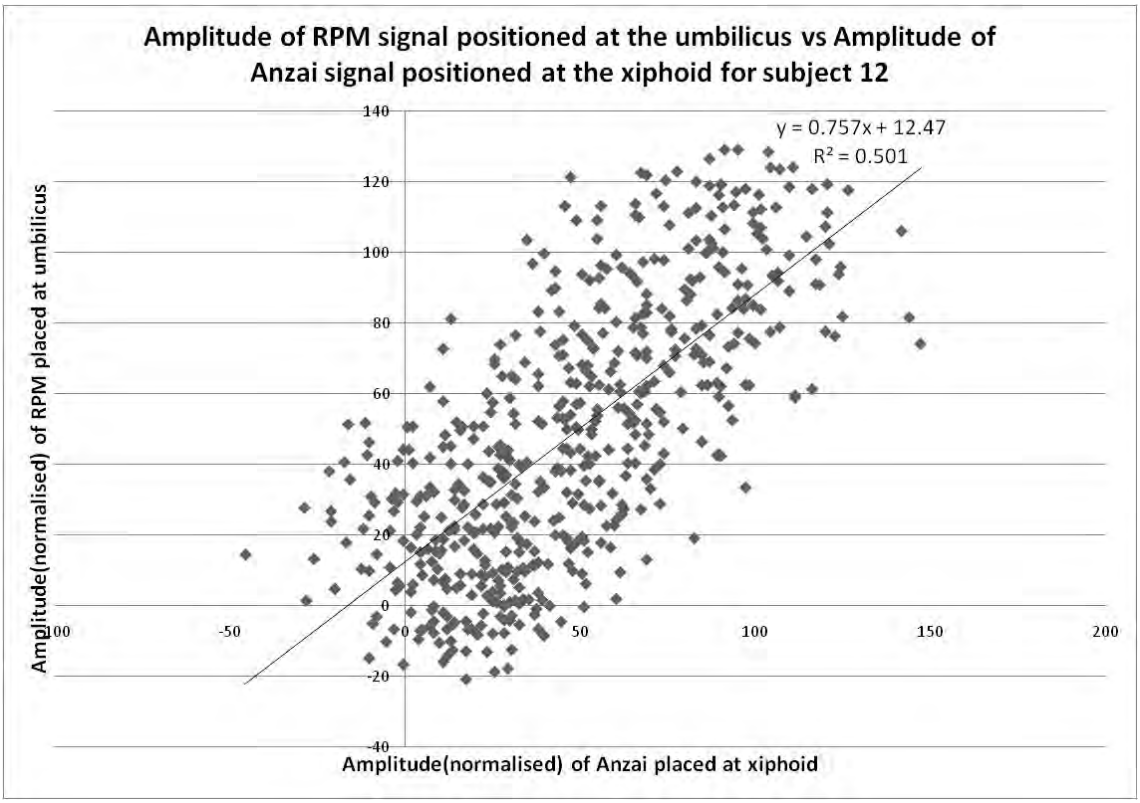


Figure A136: Determination of coefficient of determination for RPM positioned at the umbilicus and Anzai positioned at xiphoid, subject 12.

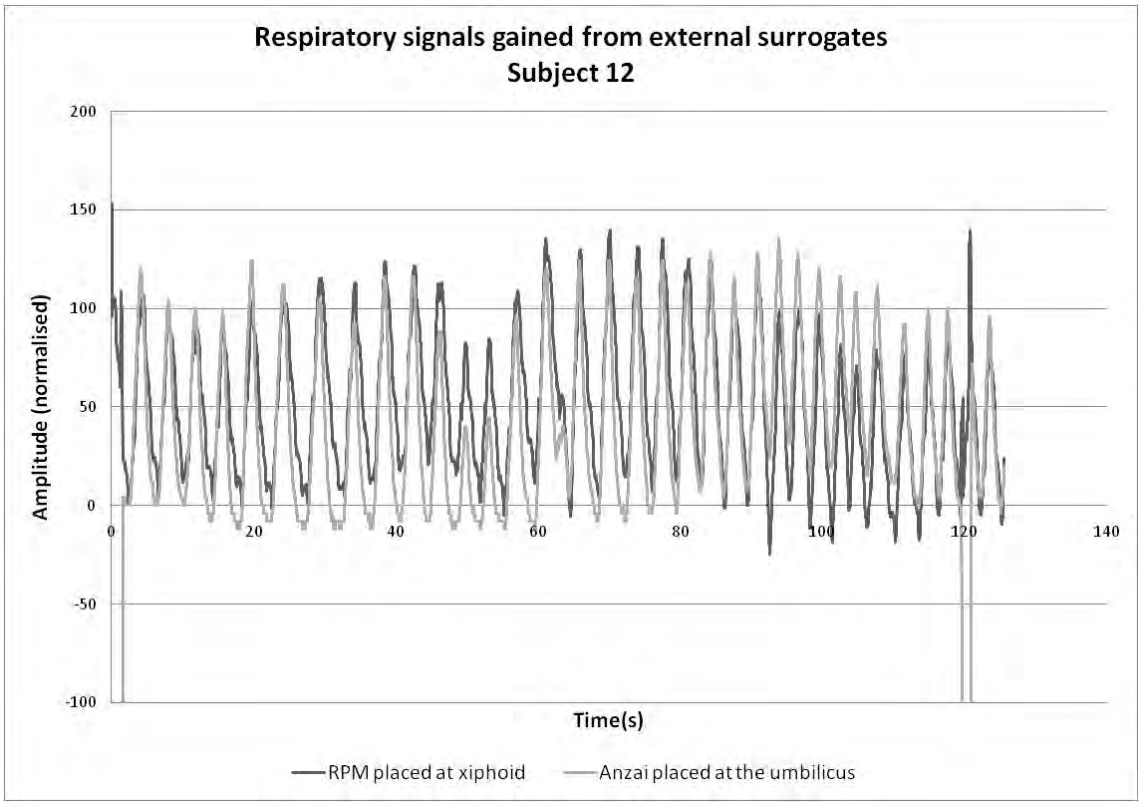


Figure A137: Respiratory signals gained using RPM marker positioned at the xiphoid and Anzai belt positioned at umbilicus for subject 12.

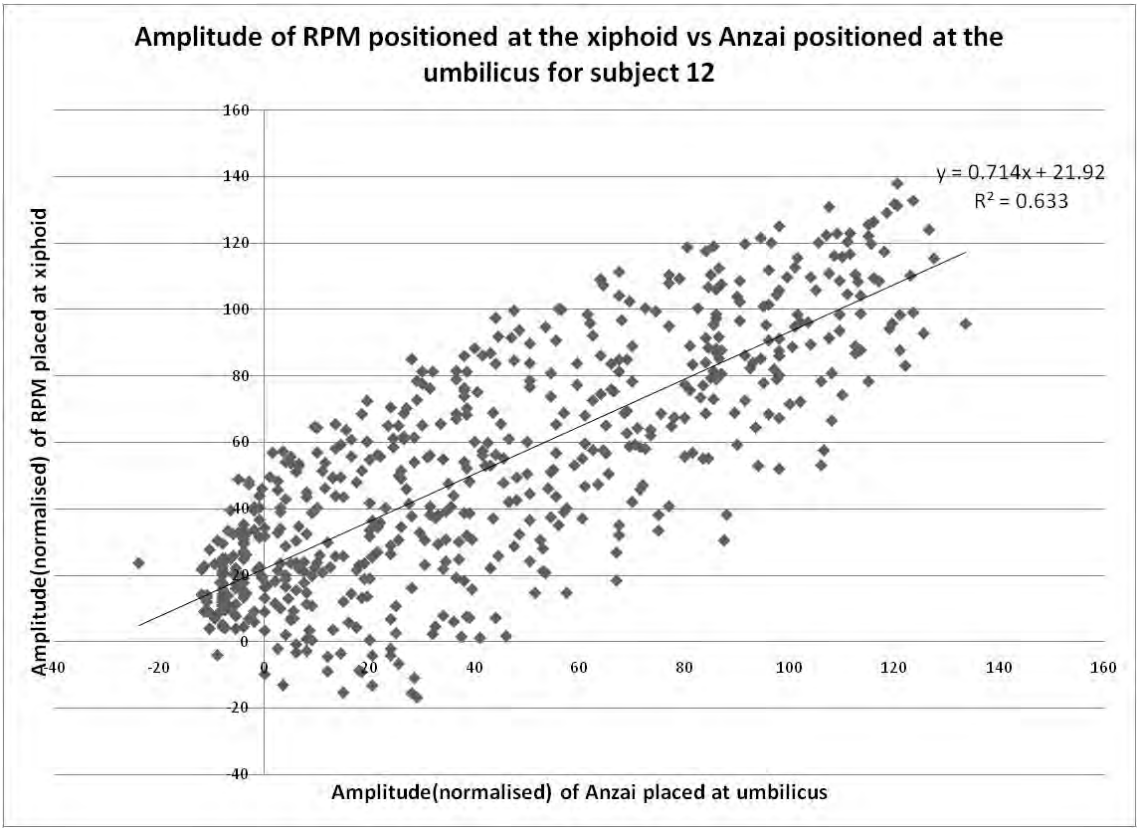


Figure A138: Determination of coefficient of determination for RPM positioned at the xiphoid and Anzai positioned at umbilicus, subject 12.

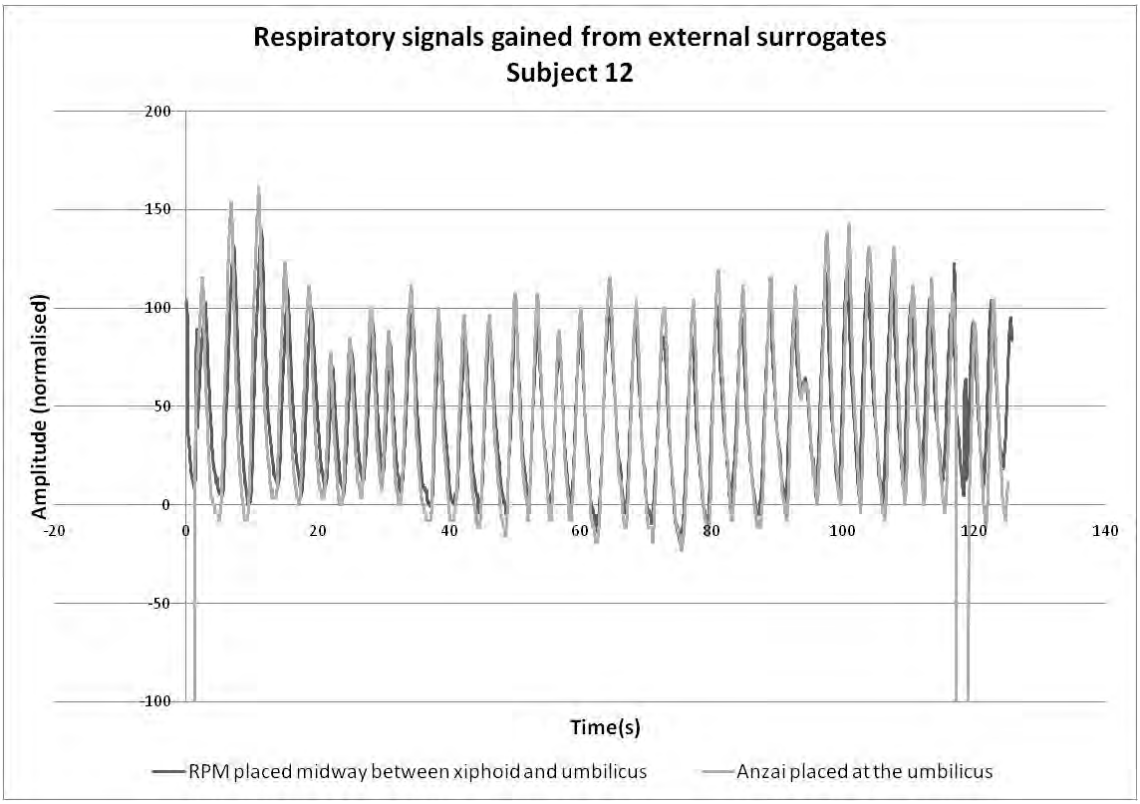


Figure A139: Respiratory signals gained using RPM marker positioned midway between xiphoid and umbilicus and Anzai belt positioned at umbilicus for subject 12.

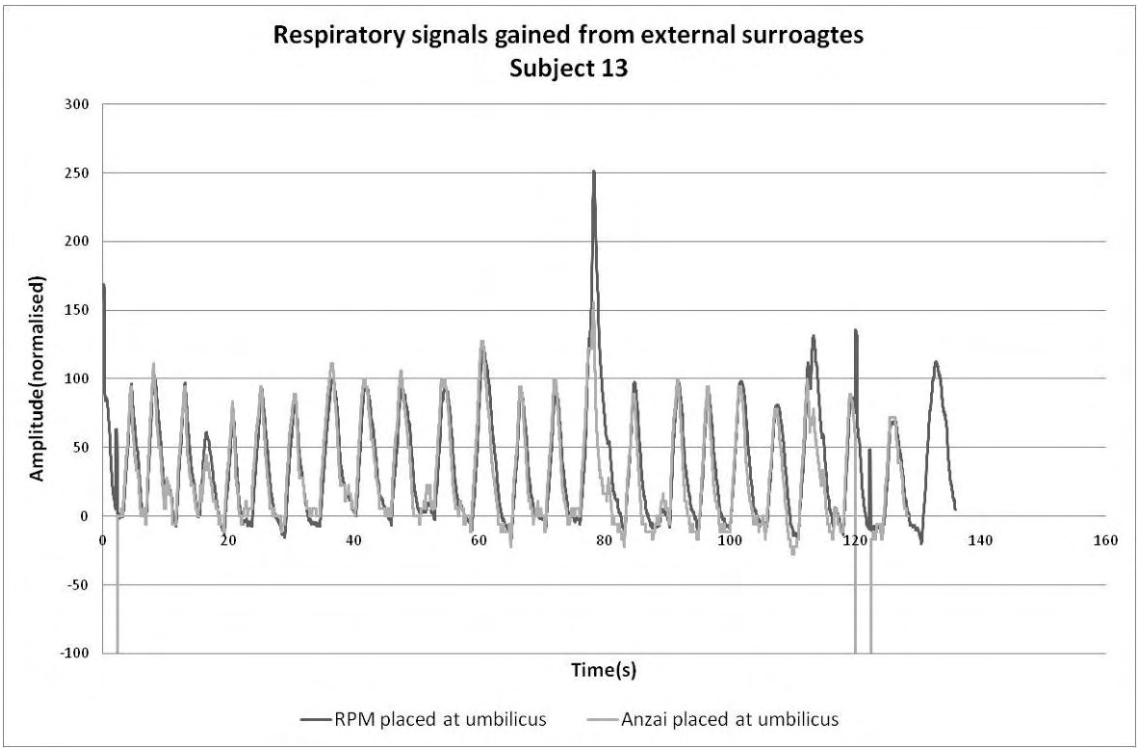


Figure A140: Respiratory signals gained using both RPM marker and Anzai belt positioned at umbilicus for subject 13.

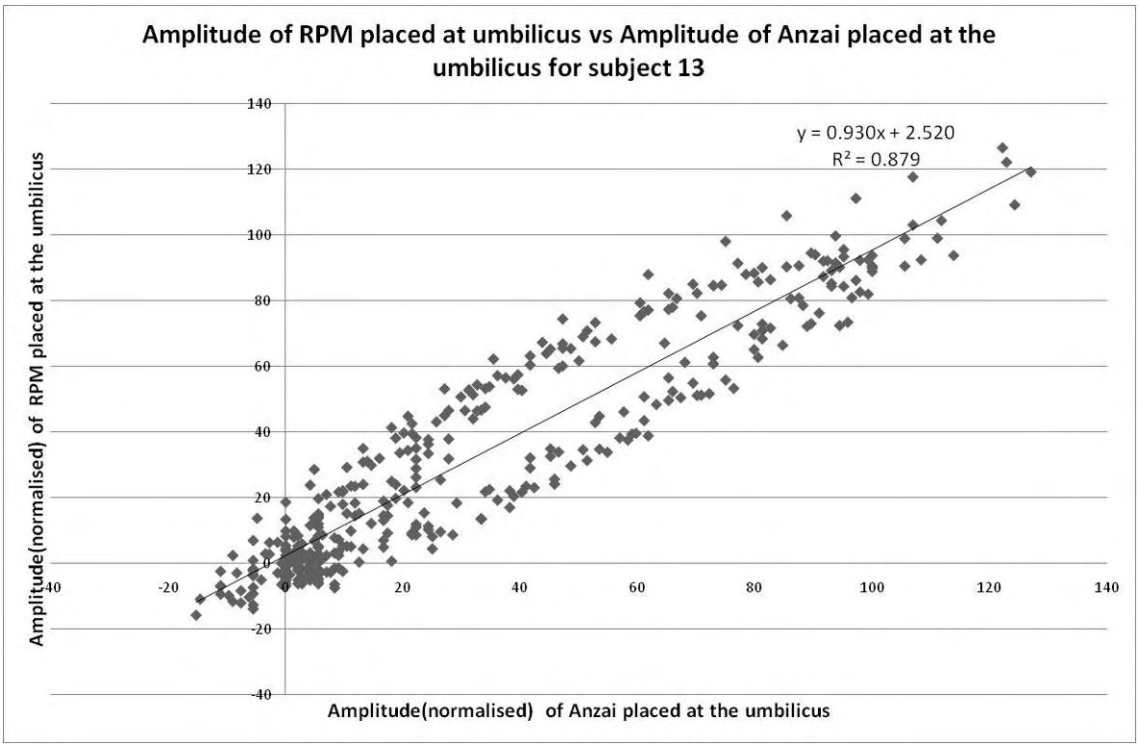


Figure A141: Determination of coefficient of determination for both RPM and Anzai positioned at umbilicus, subject 13.

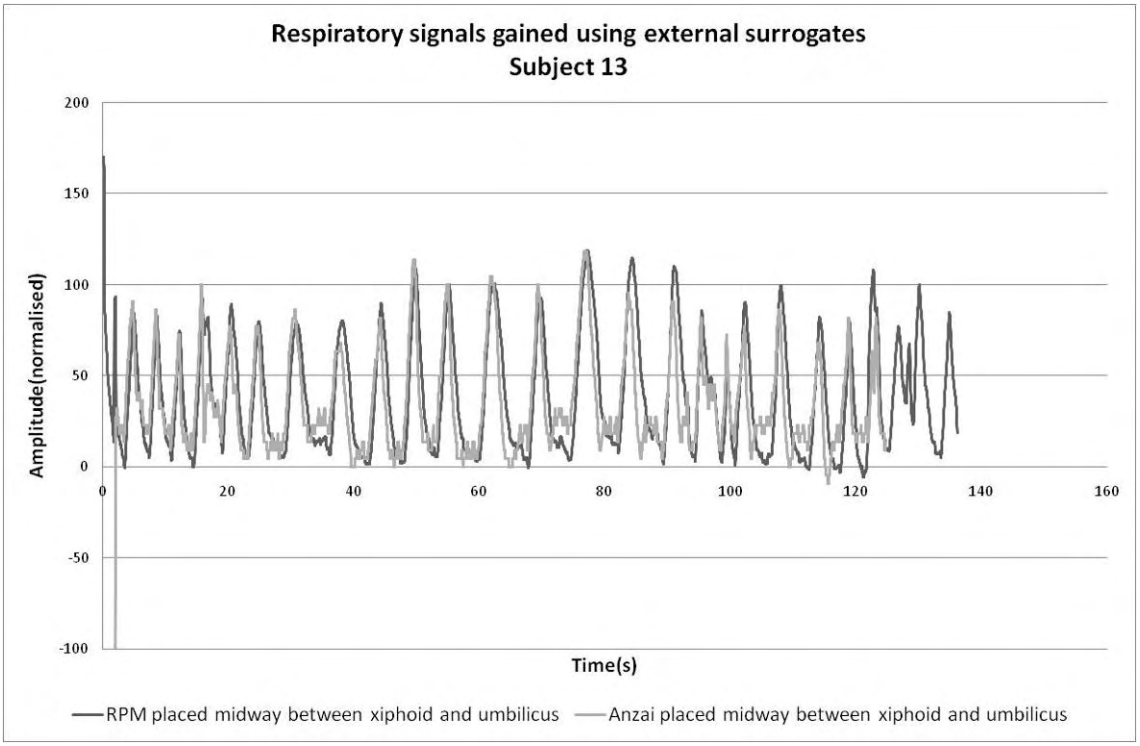


Figure A142: Respiratory signals gained using both RPM marker and Anzai belt positioned midway between umbilicus and xiphoid for subject 13.

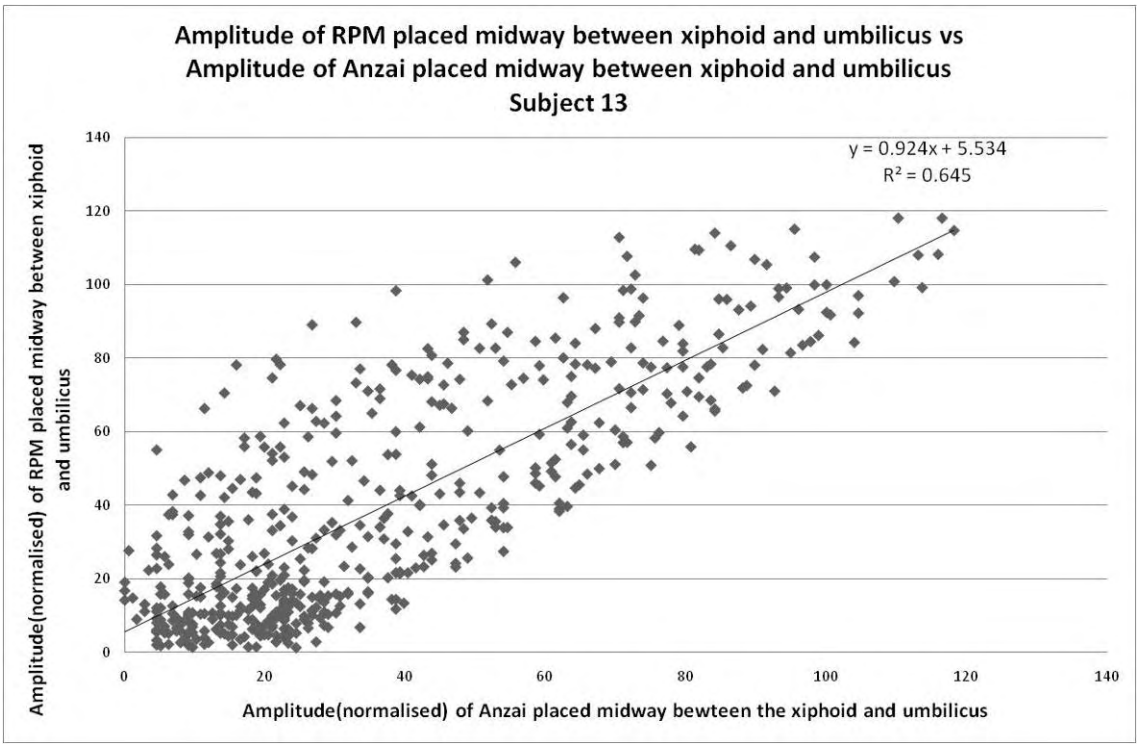


Figure A143: Determination of coefficient of determination for both RPM and Anzai positioned midway between xiphoid and umbilicus, subject 13.

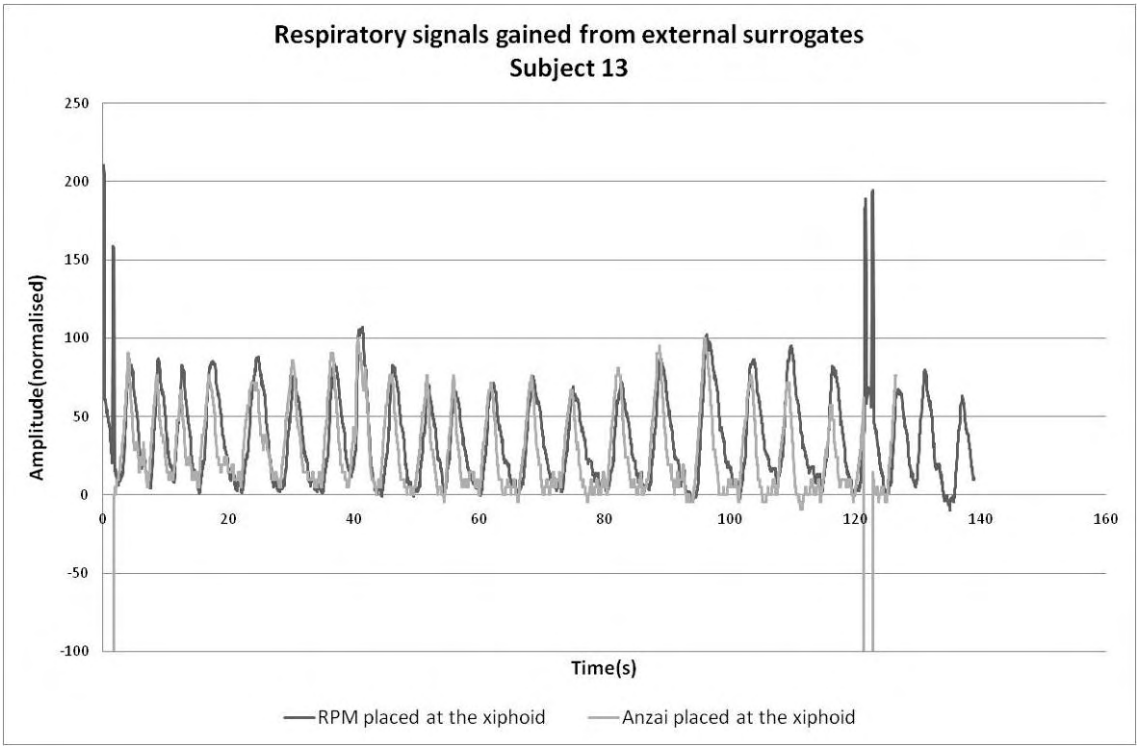


Figure A144: Respiratory signals gained using both RPM marker and Anzai belt positioned at xiphoid for subject 13.

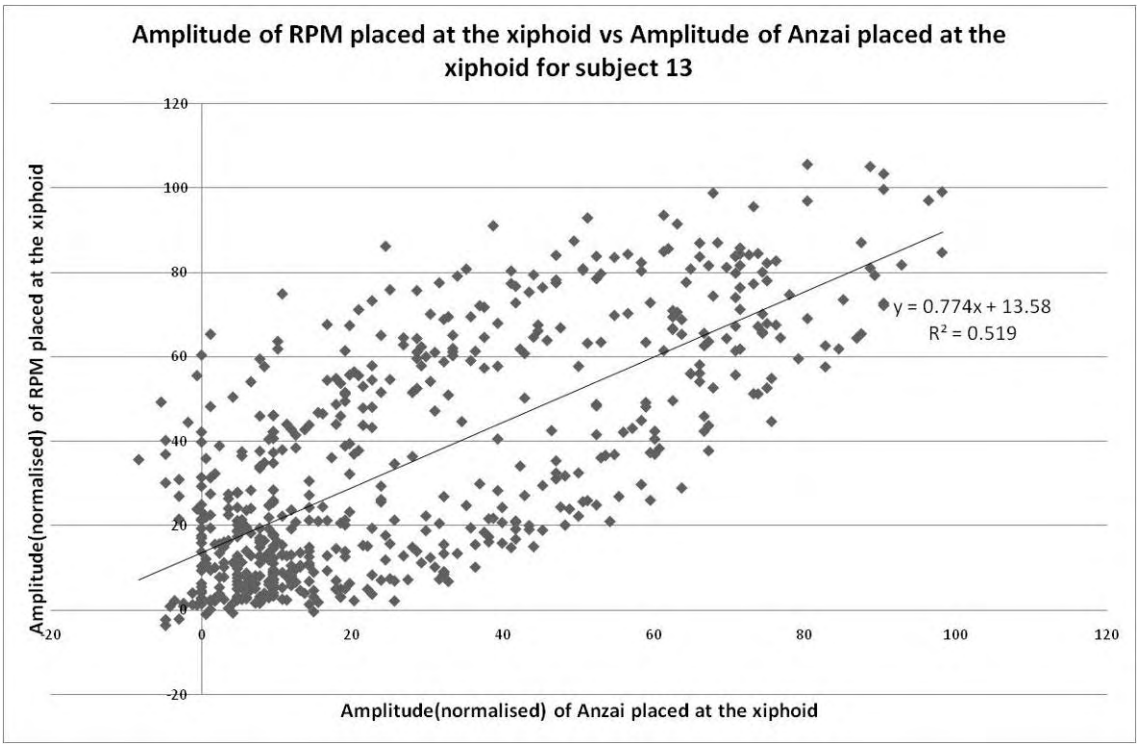


Figure A145: Determination of coefficient of determination for both RPM and Anzai positioned at xiphoid, subject 13

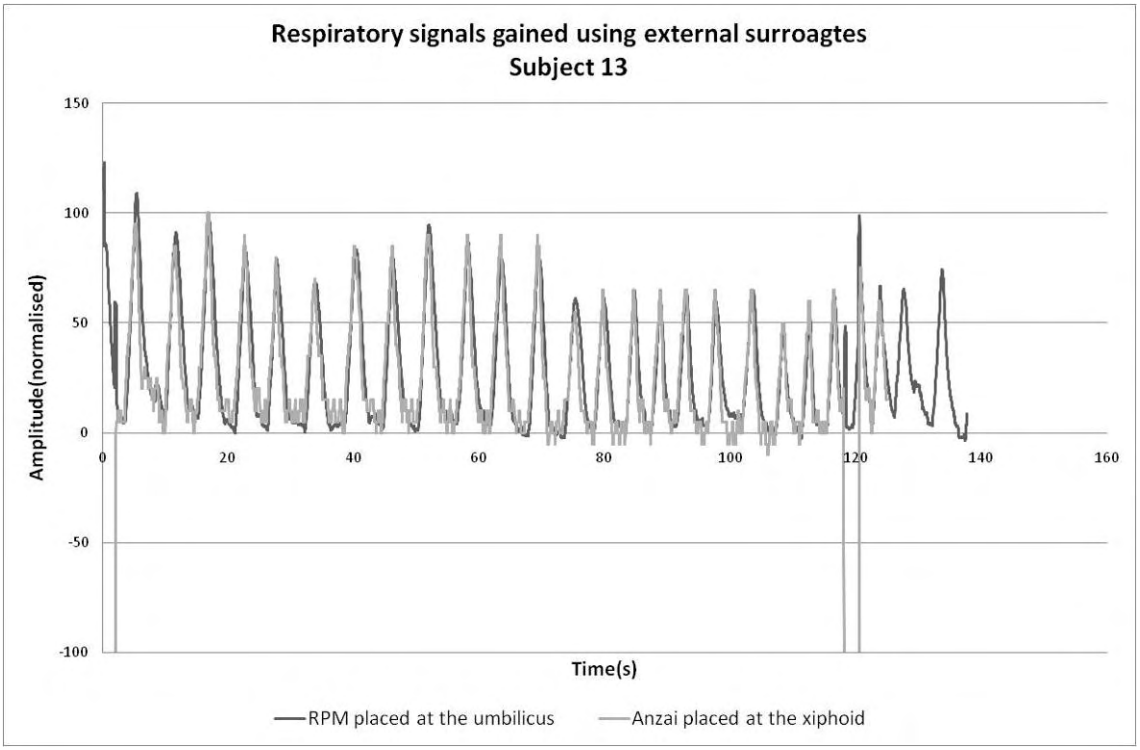


Figure A146: Respiratory signals gained using RPM marker positioned at the umbilicus and Anzai belt positioned at xiphoid for subject 13.

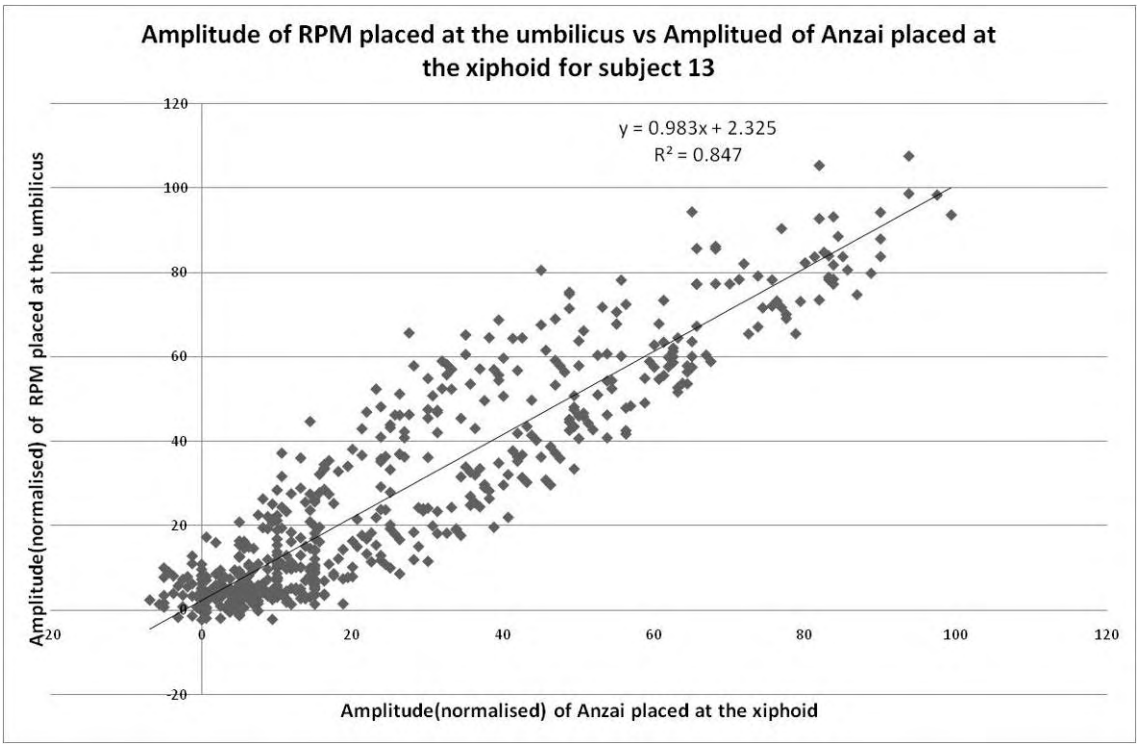


Figure A147: Determination of coefficient of determination for RPM positioned at the umbilicus and Anzai positioned at xiphoid, subject 13.

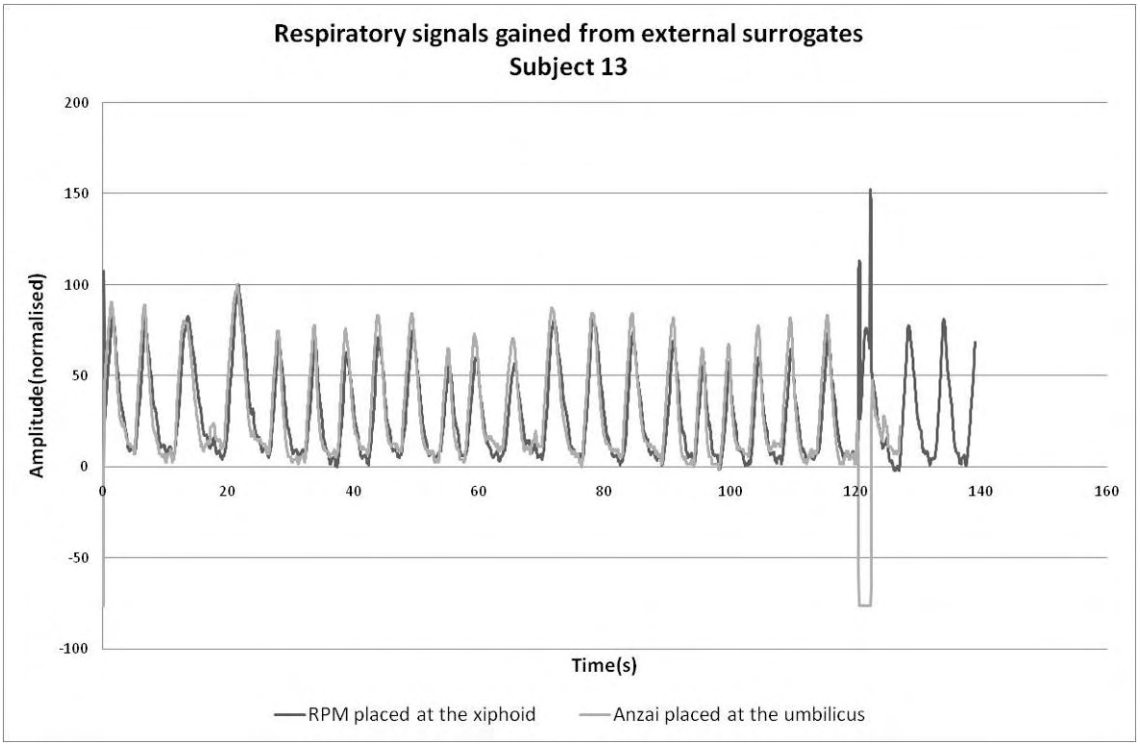


Figure A148: Respiratory signals gained using RPM marker positioned at the xiphoid and Anzai belt positioned at umbilicus for subject 13.

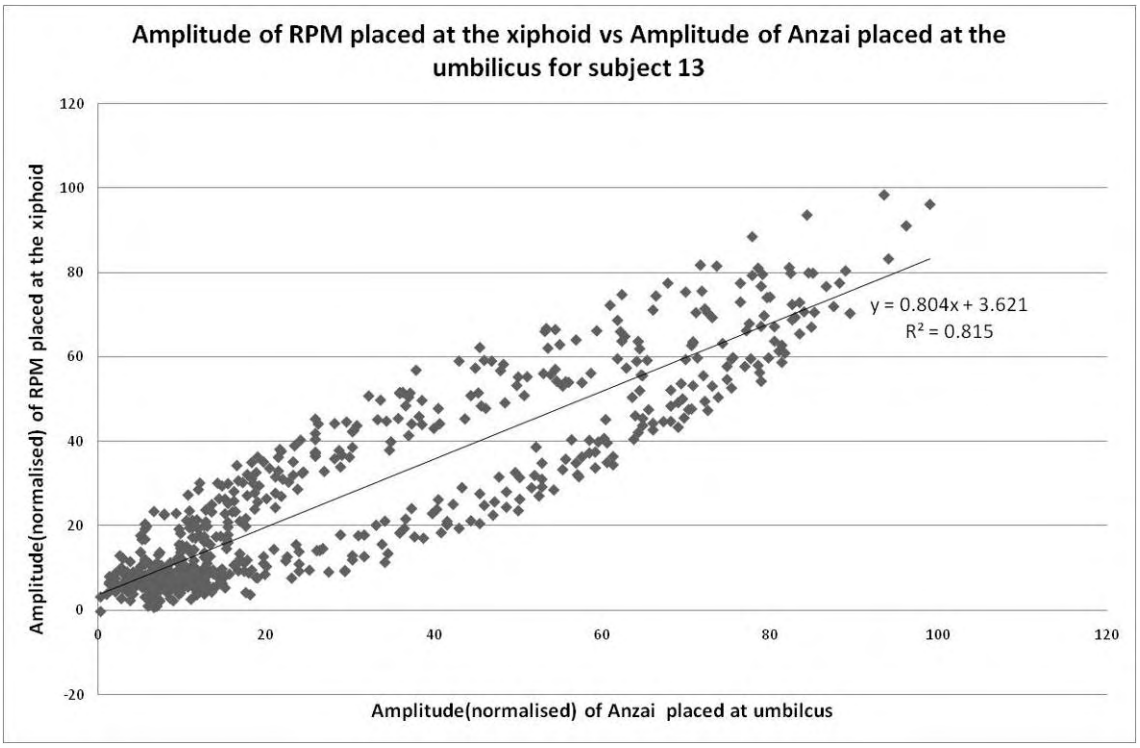


Figure A149: Determination of coefficient of determination for RPM positioned at the xiphoid and Anzai positioned at umbilicus, subject 13.

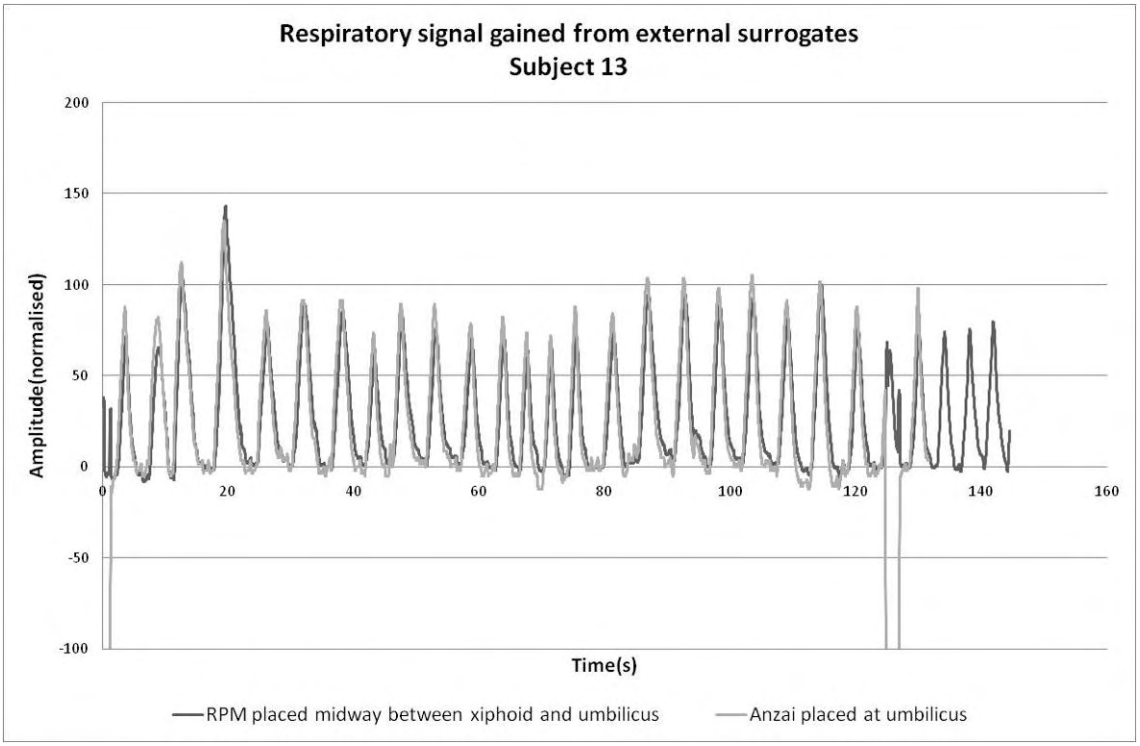


Figure A150: Respiratory signals gained using RPM marker positioned midway between xiphoid and umbilicus and Anzai belt positioned at umbilicus for subject 13.

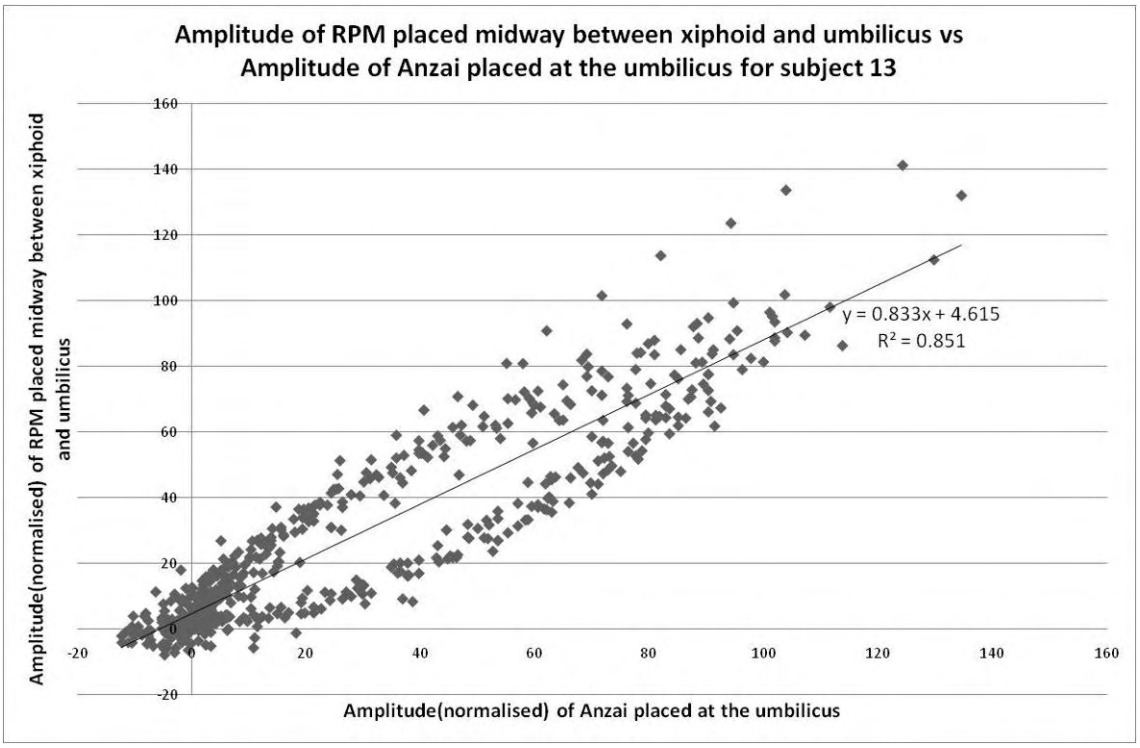


Figure A151: Determination of coefficient of determination for RPM positioned midway between xiphoid and umbilicus and Anzai positioned at umbilicus, subject 13.

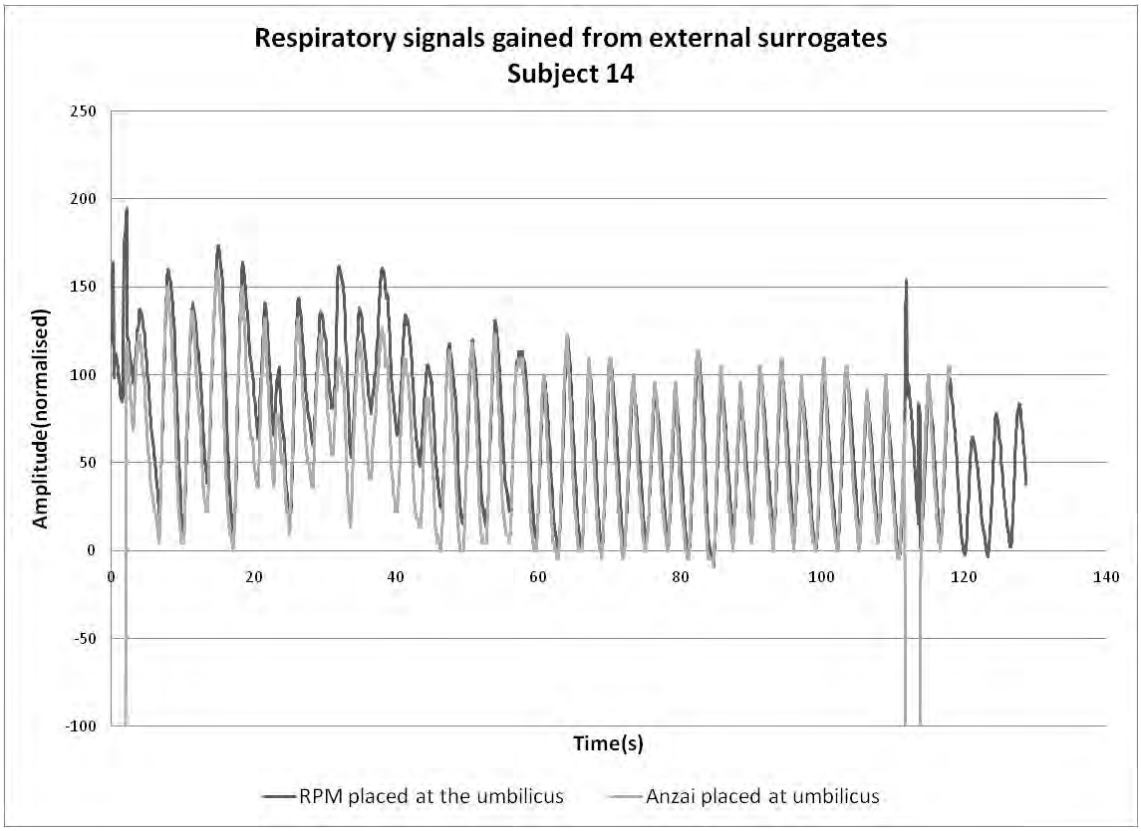


Figure A152: Respiratory signals gained using both RPM marker and Anzai belt positioned at umbilicus for subject 14.

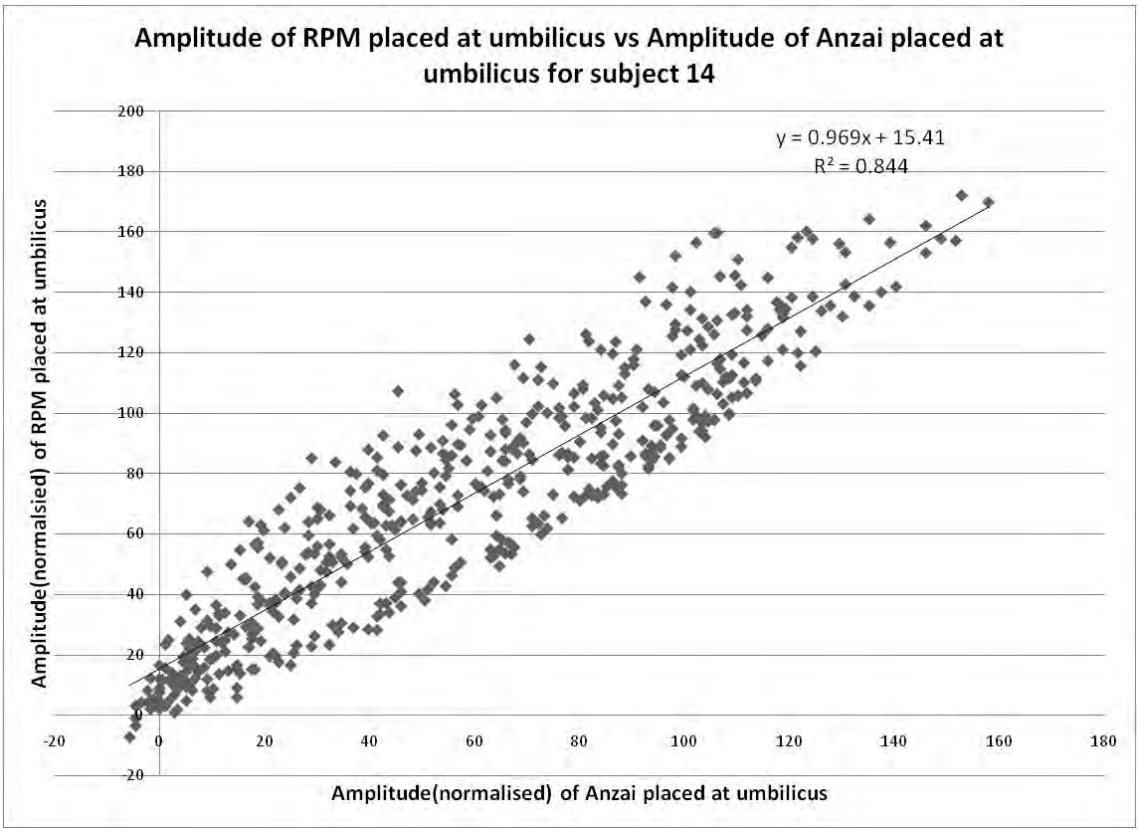


Figure A153: Determination of coefficient of determination for both RPM and Anzai positioned at umbilicus, subject 14.

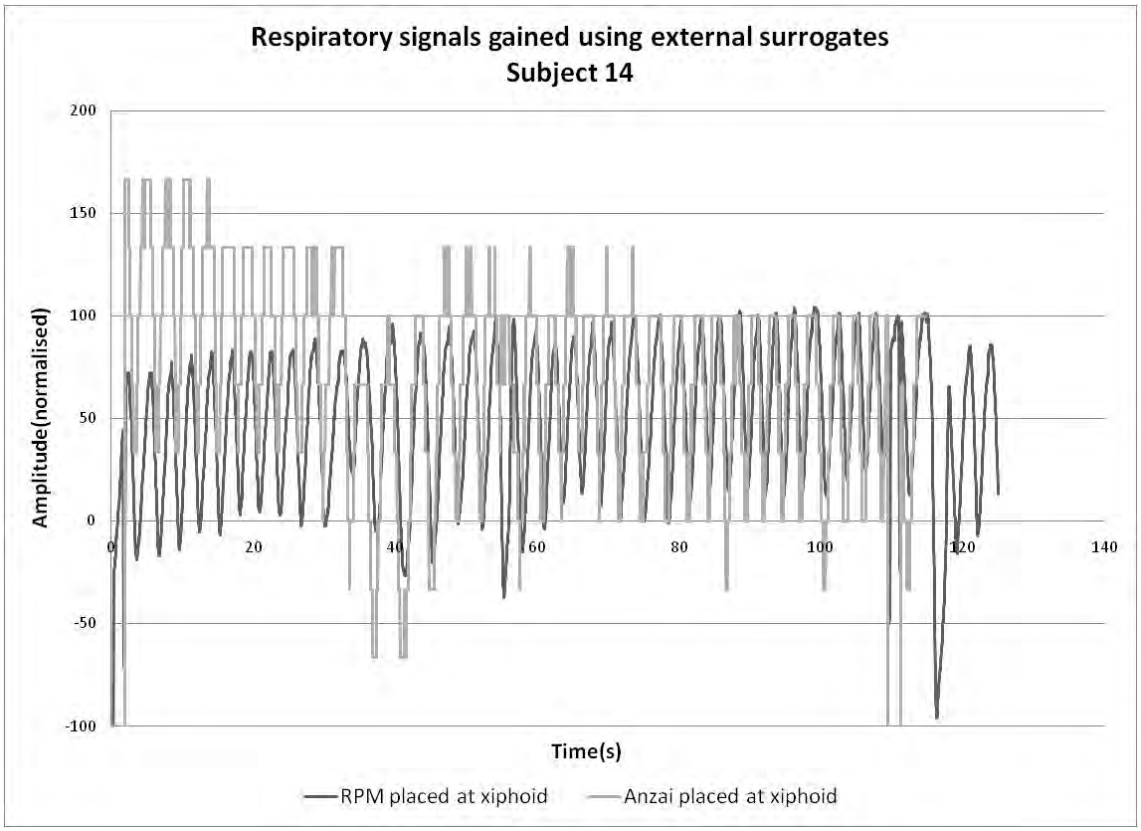


Figure A154: Respiratory signals gained using both RPM marker and Anzai belt positioned at xiphoid for subject 14.

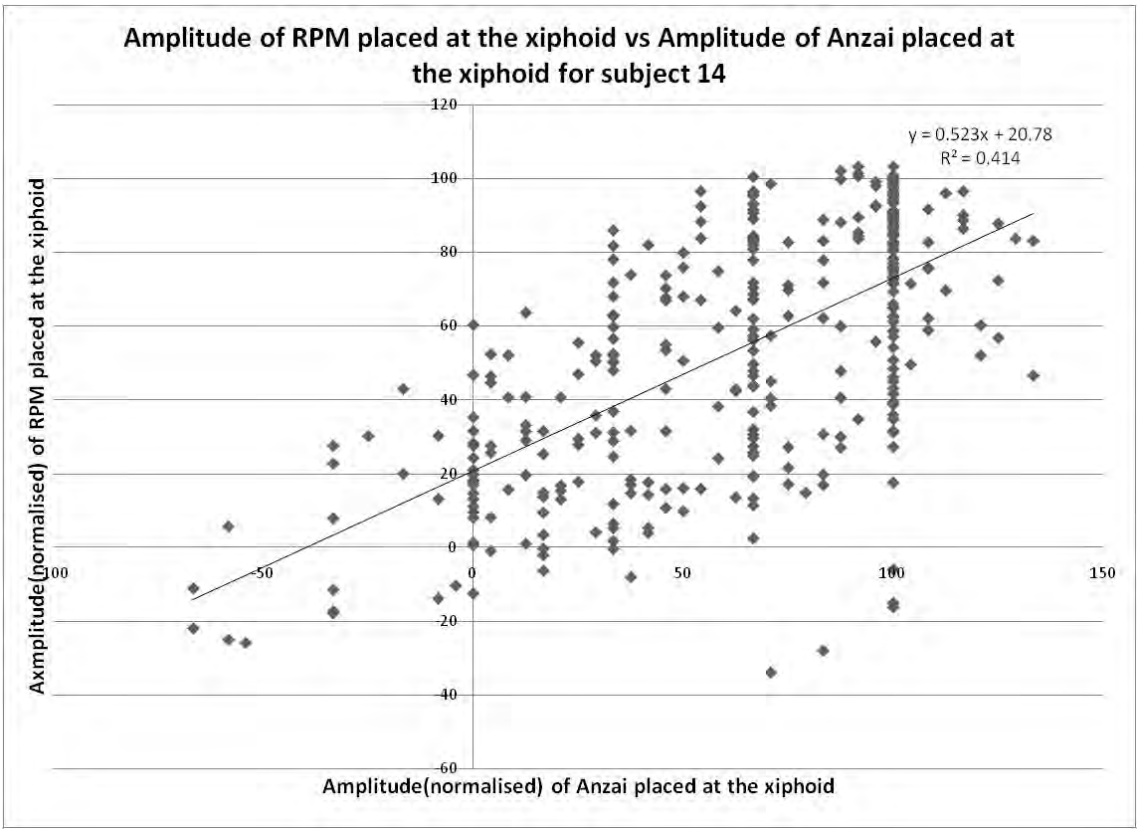


Figure A155: Determination of coefficient of determination for both RPM and Anzai positioned at xiphoid, subject 14.

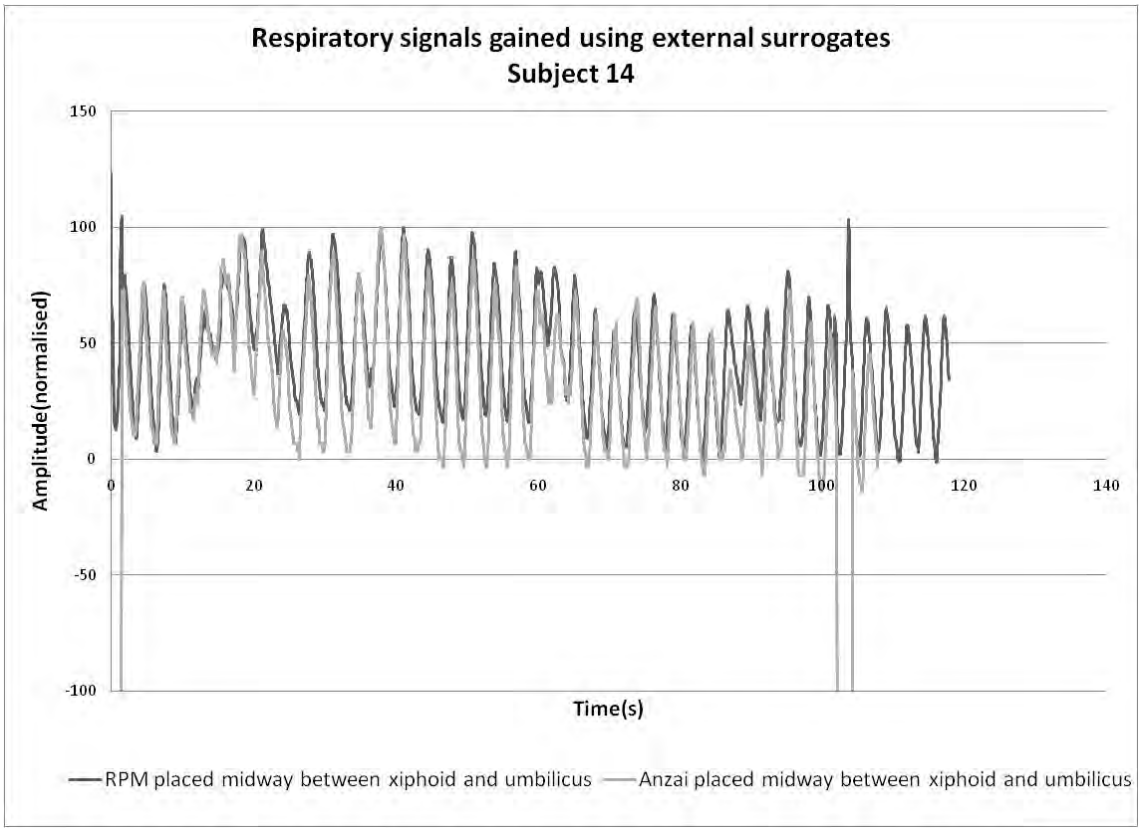


Figure A156: Respiratory signals gained using both RPM marker and Anzai belt positioned midway between umbilicus and xiphoid for subject 14.

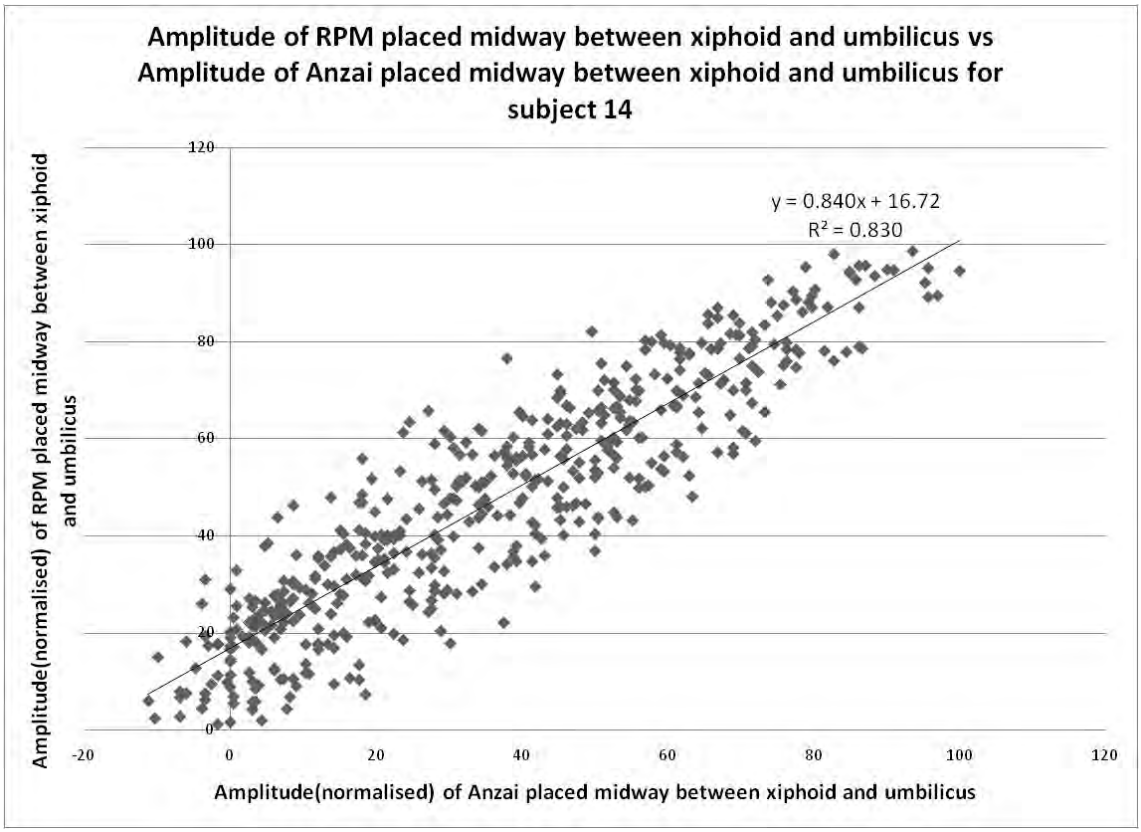


Figure A157: Determination of coefficient of determination for both RPM and Anzai positioned midway between xiphoid and umbilicus, subject 14.

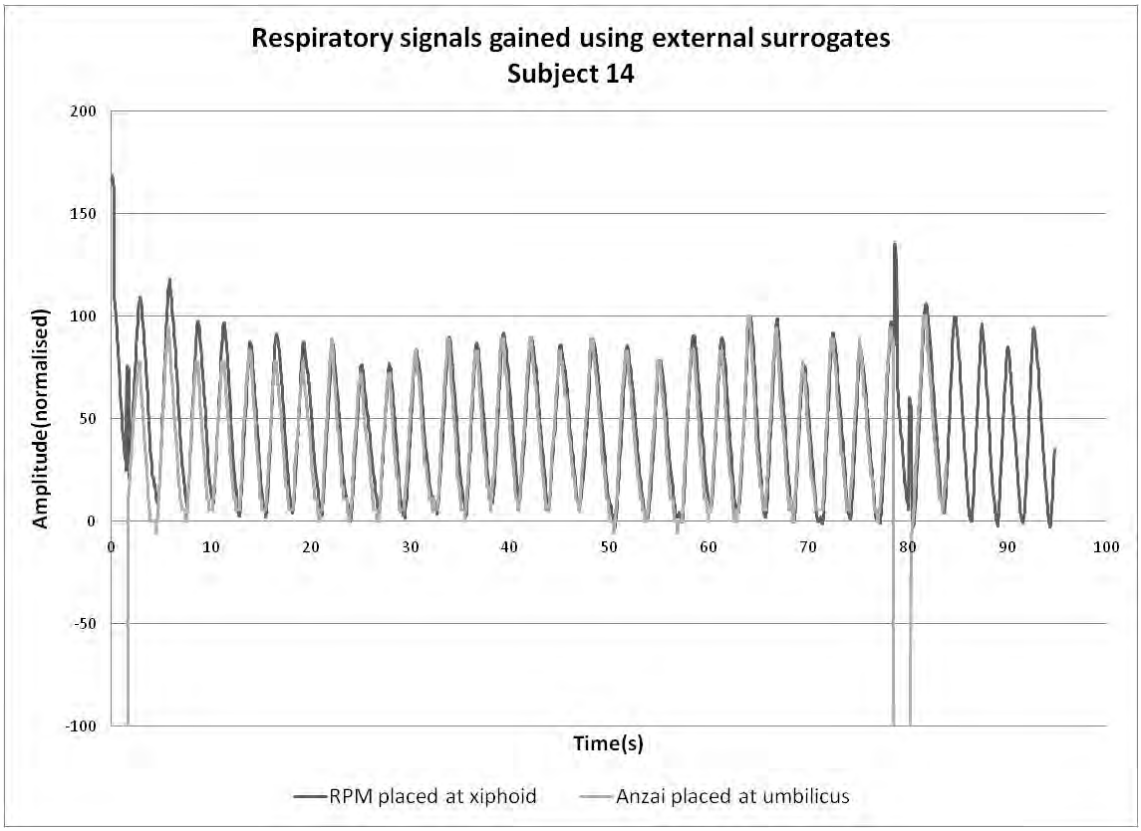


Figure A158: Respiratory signals gained using RPM marker positioned at the xiphoid and Anzai belt positioned at umbilicus for subject 14.

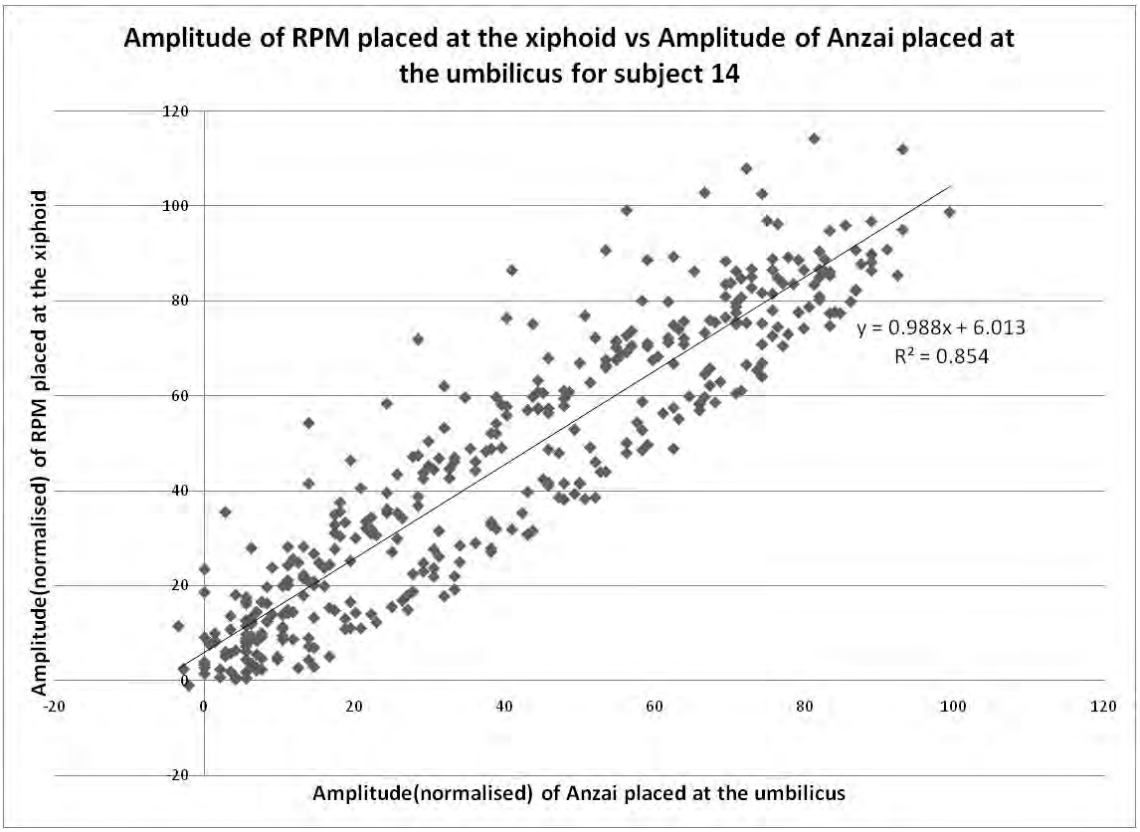


Figure A159: Determination of coefficient of determination for RPM positioned at the xiphoid and Anzai positioned at umbilicus, subject 14.

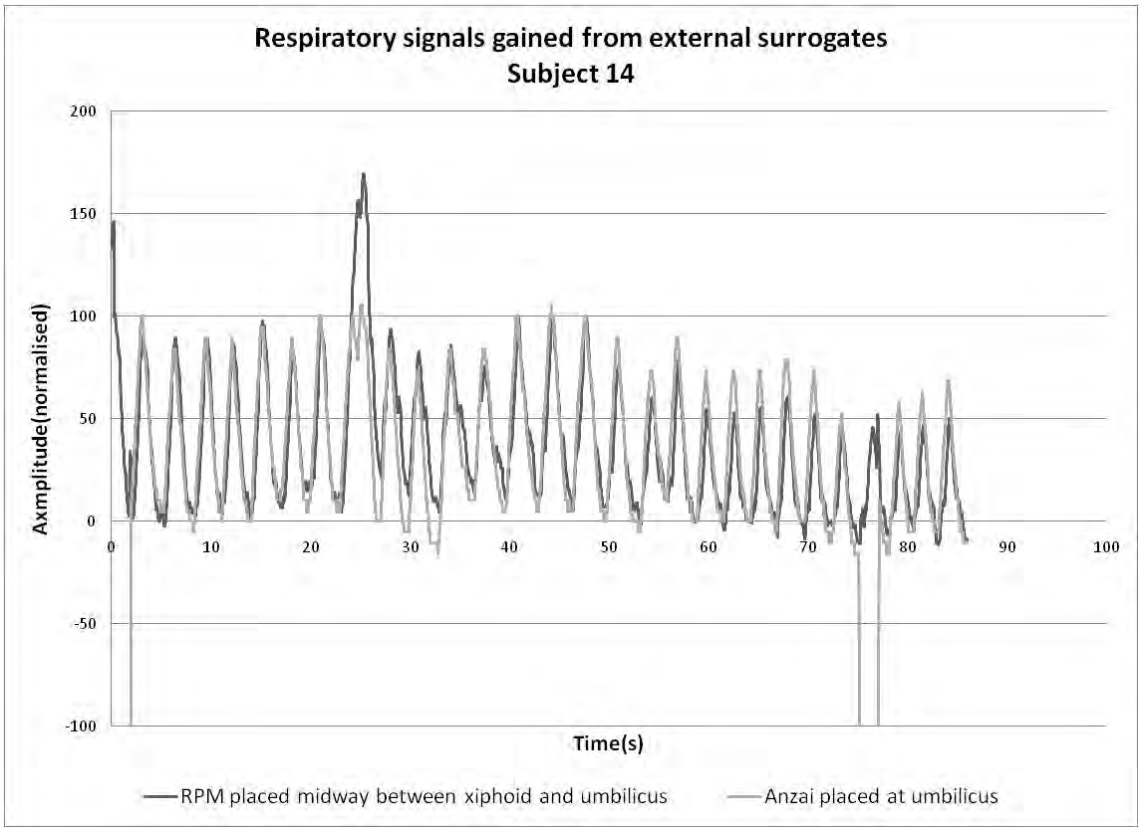


Figure A160: Respiratory signals gained using RPM marker positioned midway between xiphoid and umbilicus and Anzai belt positioned at umbilicus for subject 14.

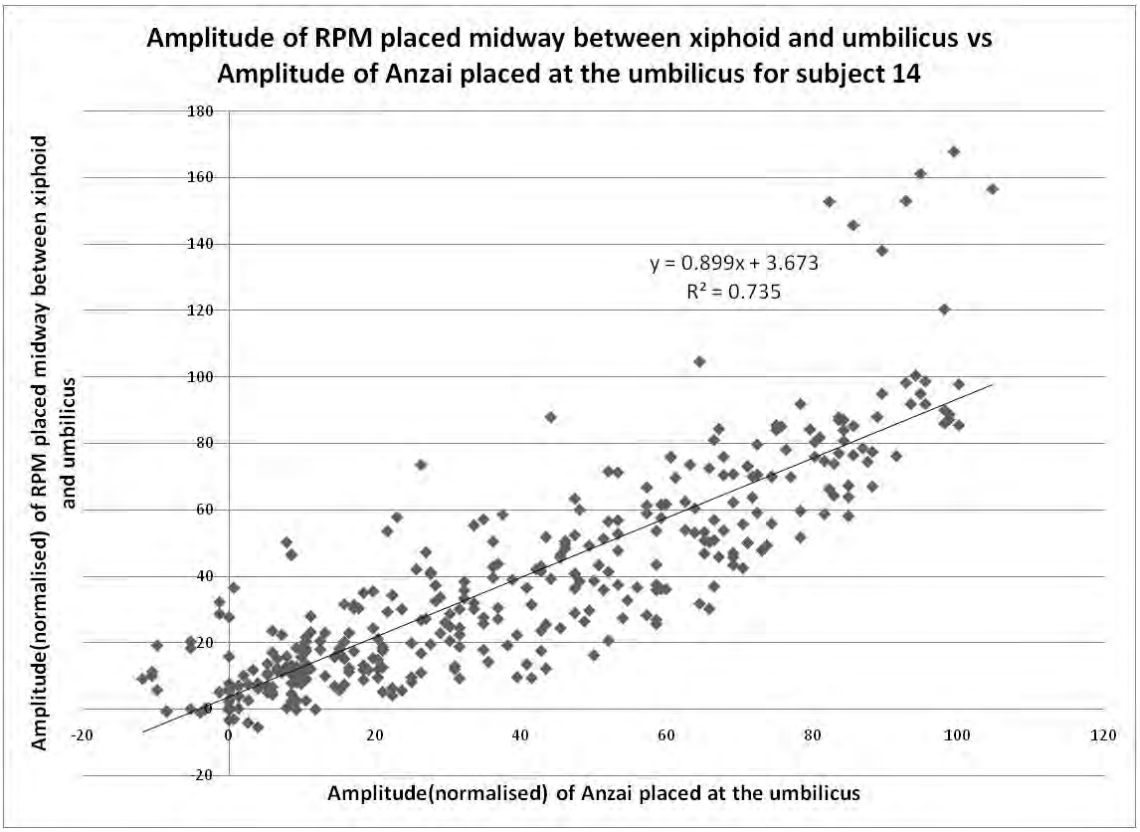


Figure A161: Determination of coefficient of determination for RPM positioned midway between xiphoid and umbilicus and Anzai positioned at umbilicus, subject 14.

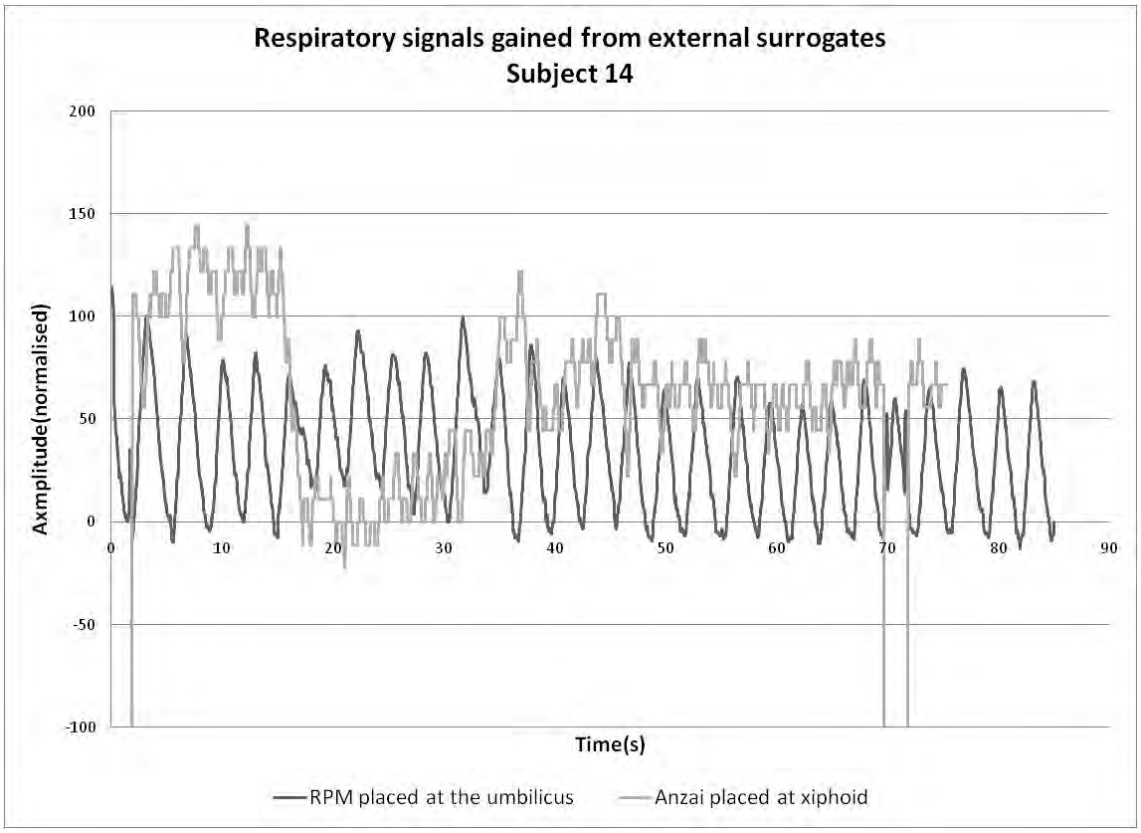


Figure A162: Respiratory signals gained using RPM marker positioned at the umbilicus and Anzai belt positioned at xiphoid for subject 14.

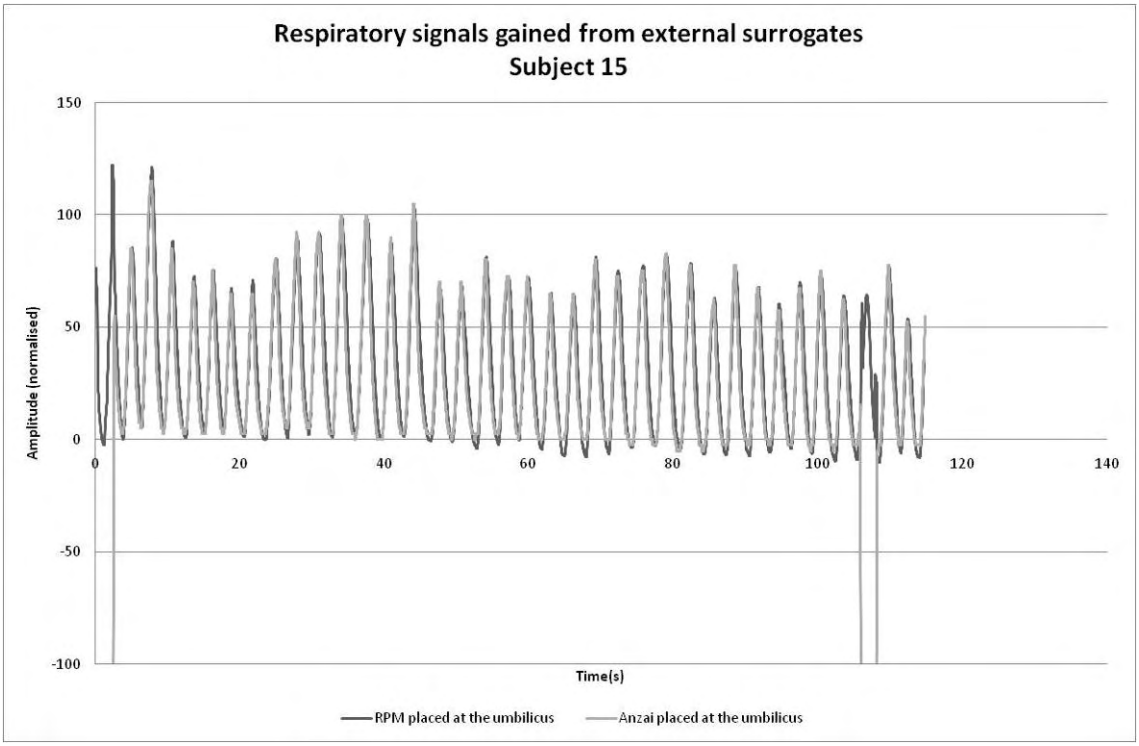


Figure A163: Respiratory signals gained using both RPM marker and Anzai belt positioned at umbilicus for subject

15.

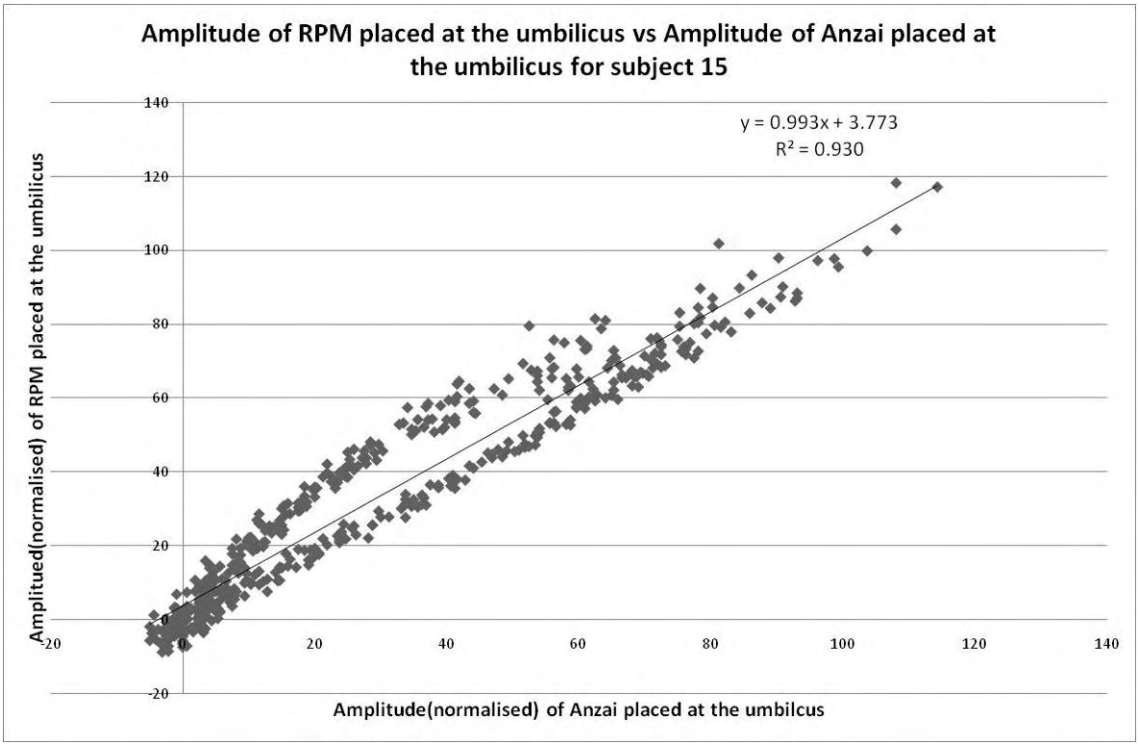


Figure A164: Determination of coefficient of determination for both RPM and Anzai positioned at umbilicus, subject 15.

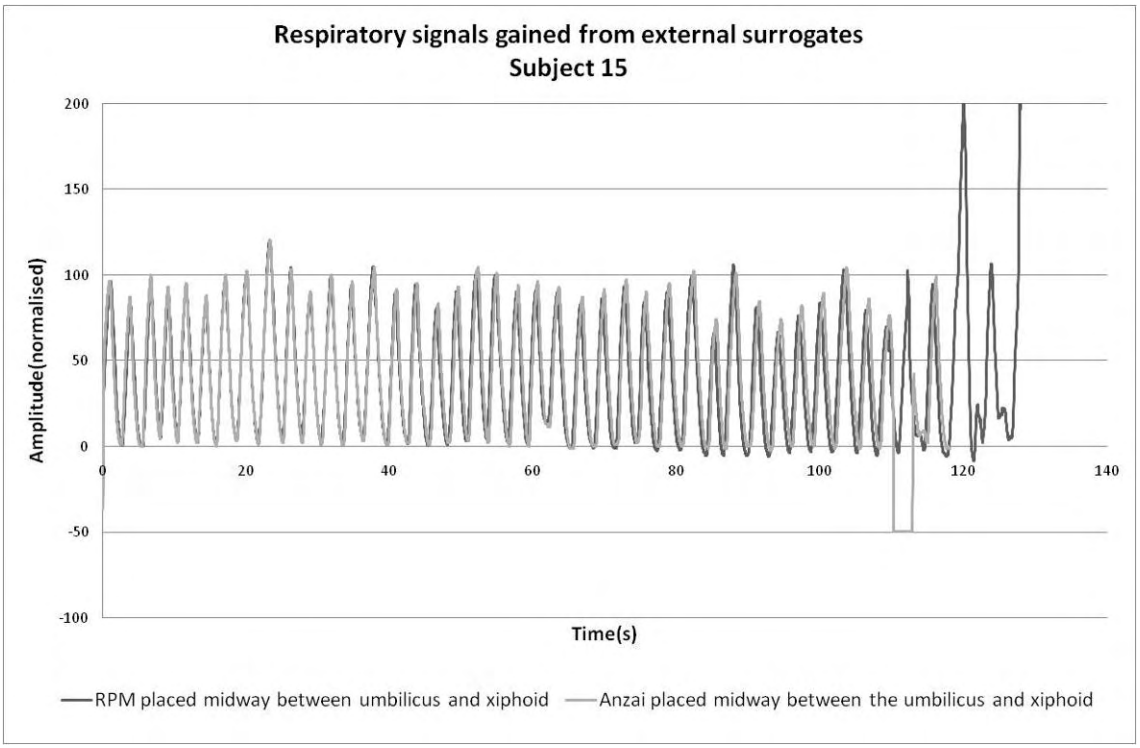


Figure A165: Respiratory signals gained using both RPM marker and Anzai belt positioned midway between umbilicus and xiphoid for subject 15.

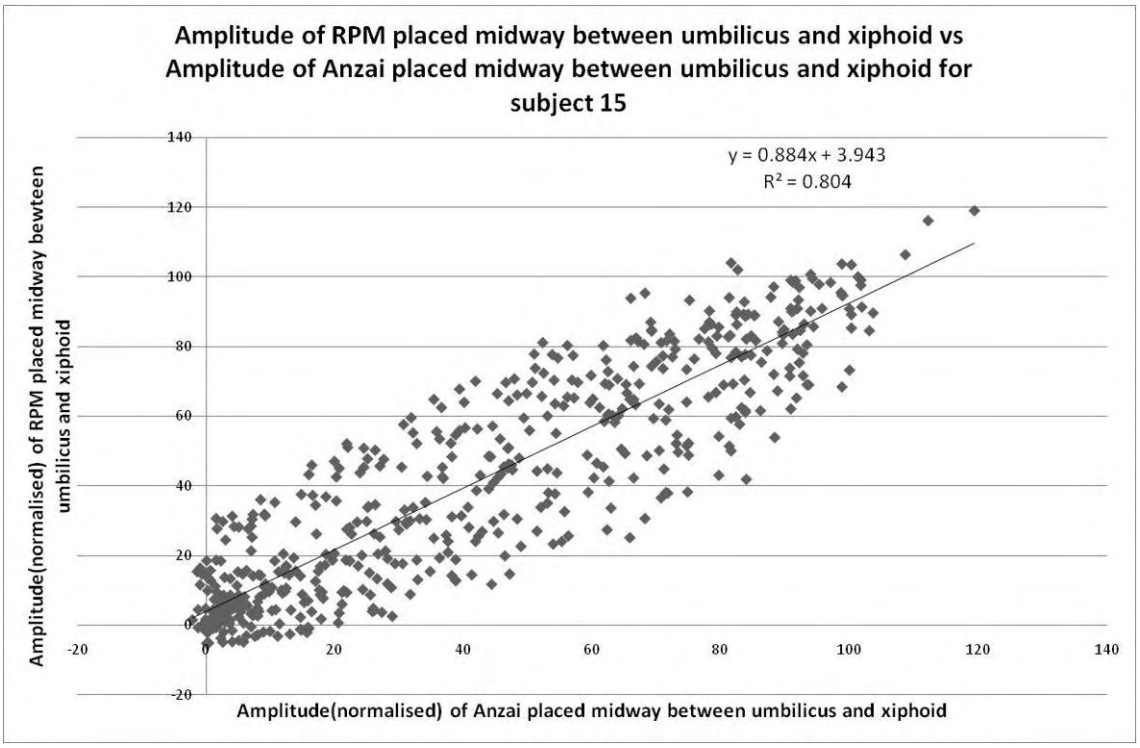


Figure A166: Determination of coefficient of determination for both RPM and Anzai positioned midway between xiphoid and umbilicus, subject 15.

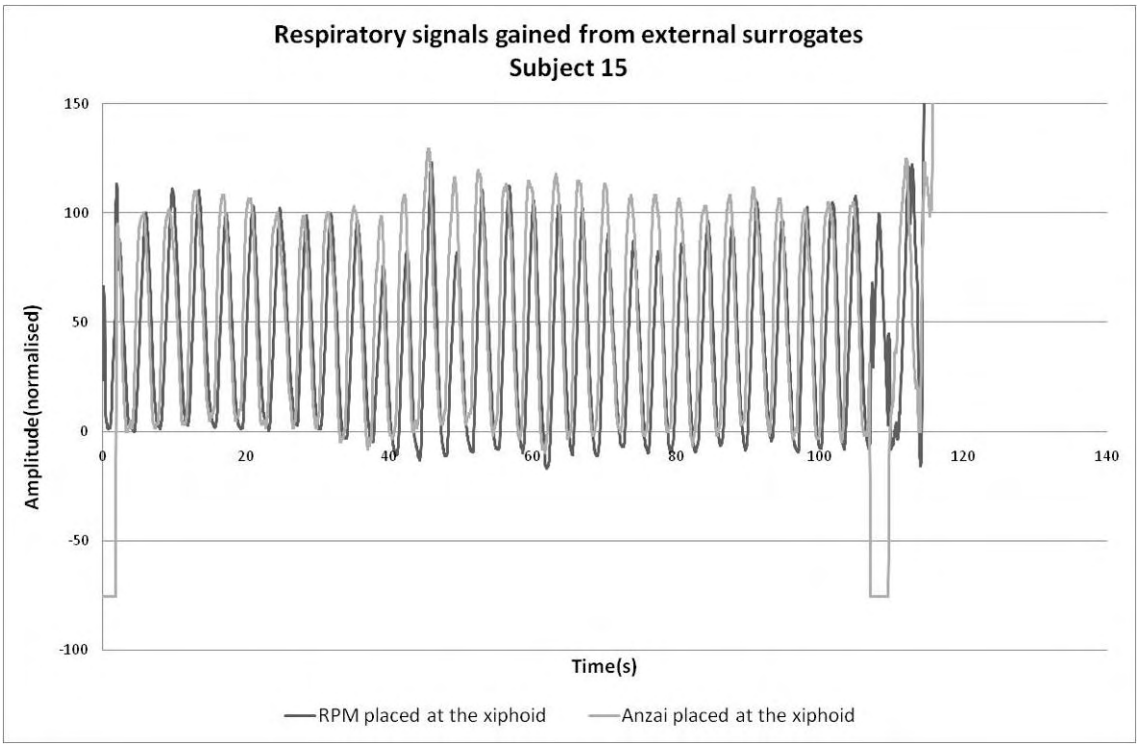


Figure A167: Respiratory signals gained using both RPM marker and Anzai belt positioned at xiphoid for subject 15.

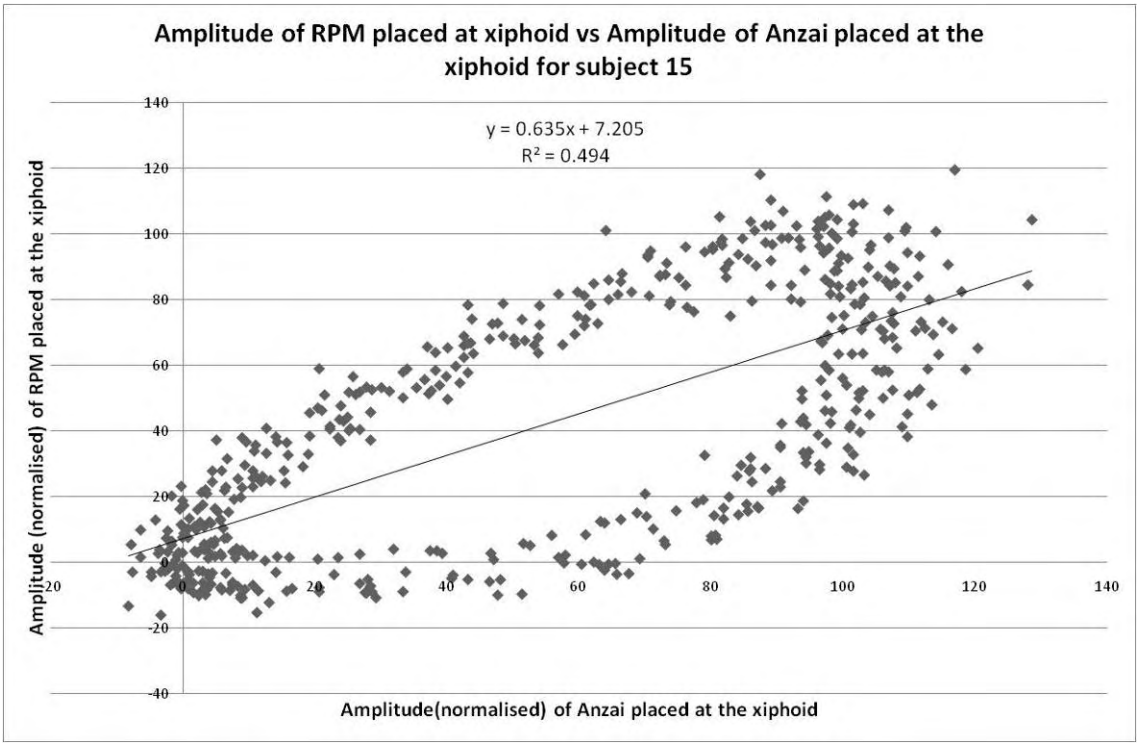


Figure A168: Determination of coefficient of determination for both RPM and Anzai positioned at xiphoid, subject 15.

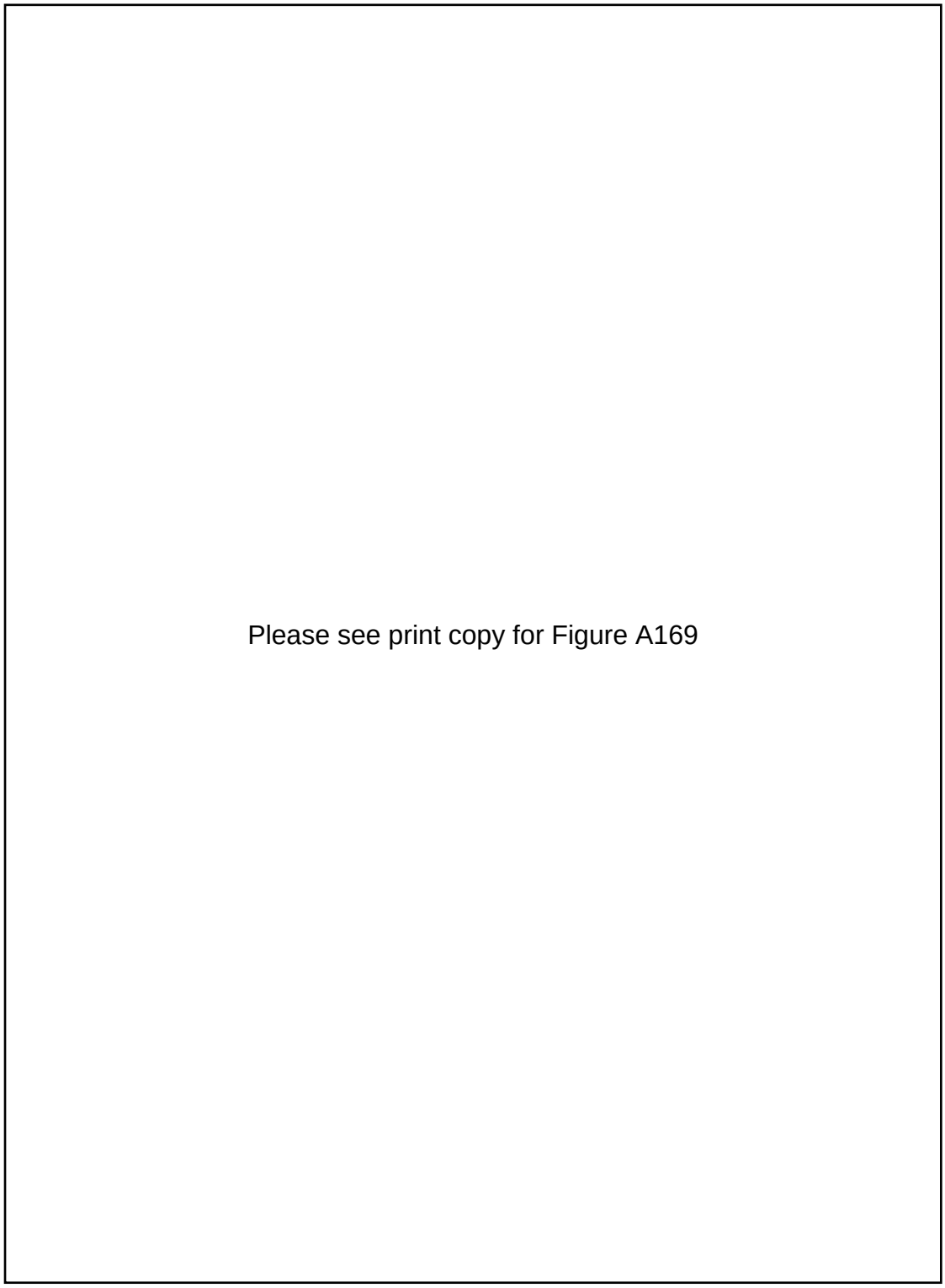


Figure A169: Human research ethics approval for comparison of respiratory signals obtained from two respiratory gating systems: the RPM system and the Anzai AZ-733V gating system.